

Innovative Lightweight Steel (LWS) System braced with Ultra-High Strength (UHS) Steel Bars

by Alessia Campiche



Department of Structures for Engineering and
Architecture

University of Naples “Federico II”

Supervisor: Professor Raffaele Landolfo

Co-supervisor: Dr. Luigi Fiorino

La borsa di dottorato è stata cofinanziata con risorse del
Programma Operativo Nazionale Ricerca e Innovazione 2014-2020 (CCI 2014IT16M2OP005),
Fondo Sociale Europeo, Azione 1.1 “Dottorati Innovativi con caratterizzazione Industriale”



UNIONE EUROPEA
Fondo Sociale Europeo



Ministero dell'Università
e della Ricerca



PON
RICERCA
E INNOVAZIONE

Innovative Lightweight Steel System braced with UHS Steel Bars

To my greatest love

ABSTRACT

The main scope of this thesis was the development of innovative solutions for lightweight steel construction with higher structural, thermal, and environmental performances, in the framework of the Italian project “ECCELSA”. To this aim a new load force resisting system was developed, which mainly consists of cold-formed steel frame braced by pre-tensioned ultra-high strength steel bars in “V” configuration. To complete the system ad hoc pre-tensioning devices and hold-down devices were designed.

Moreover, two solutions for the building envelope, which minimize the thermal bridges in the innovative system were developed and thermal performances were evaluated through the simulation in COMSOL software. The energy demand of a prototype building, considering both solutions for the building envelope was calculated, by means of simulation in EnergyPlus environment.

A wide experimental campaign was carried out to study the seismic behaviour of the innovative wall system, including tensile tests on structural materials, creep tests on ultra-high strength steel, bar-nut assembly tensile tests and full-scale wall tests. The experimental tests were conducted at Laboratory of Department of Structures for Engineering and Architecture of University of Naples “Federico II”. The obtained results demonstrate a satisfactory experimental response in terms of stiffness, strength, and deformation capacity, confirming the theoretical predictions.

To prove the validity of the solutions developed and analyse the production processes and the execution phase, a prototype building was designed and erected. The design phase followed an integrated approach, thanks also to the BIM model developed.

ACKNOWLEDGEMENTS

At the end of the PhD cycle, I feel obliged to thank all those who have accompanied me on this tiring but fantastic journey.

First of all I would like to thank prof. Raffaele Landolfo, who gave me the opportunity to pursue this career and get to know the wonderful research world. In addition, I have to thank him for welcoming me into his team and being close to me more as a father than as an employer, always making me feel at home.

I would also like to thank Luigi for having been my guide over these three years, teaching me everything I know now and making me grow both professionally and personally.

Furthermore, I express my sincere thanks to my friends and colleagues Sarmad, Roberto, Aldo, Giusy, Raffaele and Gaetano for being close to me, having endured me in moments of great pressure and always supporting and consoling me in times of need.

A special thanks goes to my family, Daniela, Maurizio and Stefano for always believing in me and leaving me free to choose my life path and always supporting my choices (a part for some pressure from my mother for the “secure job”). I have to thank Nanny because, although geographically distant, he has always been close to me, showing me immense understanding and love and always indulging my whims.

Thanks to my grandparents for always being my first supporters, never letting me lack their affection and understanding, except for the delay to Sunday lunch. Thanks to my uncles, my cousins and all my relatives for their support; in particular, I would like to thank Aunt Stefy for always having been my idol and giving me, with her example, the passion for research, and Aunt Sandra for guiding and protecting me from above.

Thanks to all my friends, in particular Cristina, Francesca, Sergio, and little Riccardo, for always believing in me, even more than I believed in myself, for

Innovative Lightweight Steel System braced with UHS Steel Bars

always showing me affection and being close to me, especially when I needed more.

I'm sure I forgot someone in these few lines, but not because you are less important in my life, but only because I couldn't write more than two pages of thanks! The important thing is not to be mentioned here, but in my heart!

I owe this achievement to all of you, so I hope that, as on any occasion, they are happy as I am. I love you!

Thank you

Ad maiora!

Alessia

RINGRAZIAMENTI

A conclusione del ciclo di dottorato mi sento in dovere di ringraziare tutti coloro che mi hanno accompagnato in questo faticoso ma fantastico percorso. In primis vorrei ringraziare il prof. Raffaele Landolfo, il quale mi ha dato la possibilità di intraprendere questa carriera e conoscere il meraviglioso mondo della ricerca. Inoltre, devo ringraziarlo per avermi accolta nel suo team ed essermi stato accanto più come un padre, che come un datore di lavoro, facendomi sempre sentire a casa.

Vorrei altresì ringraziare Luigi per essere stato la mia guida in questi anni, insegnandomi tutto quello che ora so e facendomi crescere sia dal punto professionale sia personale.

Inoltre, è doveroso esprimere i miei più sinceri ringraziamenti ai miei amici e colleghi Sarmad, Roberto, Aldo, Giusy, Raffaele e Gaetano per essermi stati accanto, avermi sopportato nei momenti di forte pressione ed avermi sempre supportato e consolato nel momento del bisogno.

Un grazie speciale va alla mia famiglia, Daniela, Maurizio e Stefano per aver sempre creduto in me ed avermi lasciato libera di scegliere il mio percorso di vita ed aver sempre appoggiato le mie scelte (seppur con qualche pressione da parte di mia madre per il posto fisso). Devo ringraziare Nanny perché, seppur lontano geograficamente, mi è sempre stato vicino, mostrandomi comprensione ed amore immensi ed assecondando sempre i miei capricci.

Grazie ai miei nonni per essere stati sempre i miei primi sostenitori, non facendomi mai mancare il loro affetto e la loro comprensione, tranne per il ritardo al pranzo domenicale. Grazie ai miei zii, ai miei cugini ed a tutti i miei parenti per il loro sostegno; in particolare, vorrei ringraziare zia Stefy per essere sempre stata il mio idolo ed avermi trasmesso, con il suo esempio, la passione per la ricerca, e zia Sandra per avermi guidato e protetto dall'alto.

Innovative Lightweight Steel System braced with UHS Steel Bars

Grazie a tutti i miei amici, in particolare Cristina, Francesca, Sergio, ed il piccolo Riccardo, per aver sempre creduto in me, anche più di quanto io credessi in me stessa, per avermi mostrato sempre affetto ed essermi stati vicini, soprattutto quando ne avevo più bisogno.

Sono sicura di aver dimenticato qualcuno in queste poche righe, ma non perché siete meno importanti nella mia vita, ma solo perché non potevo scrivere più di due pagine di ringraziamenti! L'importante non è essere citati qui, ma nel mio cuore!

Questo traguardo lo devo a tutti voi, quindi spero che, come in ogni occasione, sarete felici come lo sono io. Vi voglio bene!

Grazie.

Ad maiora!

Alessia

Table of Contents

1. ABSTRACT.....	3
2. AKNOWLEDGEMENTS	4
3. RINGRAZIAMENTI.....	6
4. TABLE OF CONTENTS	8
5. LIST OF FIGURES	11
6. LIST OF TABLES	14
7. 1 INTRODUCTION.....	15
1.1 Integrated building design.....	16
1.1.1 Structural design	17
1.1.2 Thermal/Energy design.....	21
1.2 Prototyping and industry 4.0.....	24
1.3 ECCELSA project	26
8. 2 LITERATURE REVIEW	28
2.1 Dissipative and Non-dissipative strap-braced wall systems.....	29
2.2 Energy efficiency and thermal performances of LWS systems	37
2.3 Creep in UHS steel.....	40
9. 3 DESIGN OF THE INNOVATIVE WALL SYSTEM.....	42
3.1 The concept	43
3.1.1 Structural design rules and methodologies	47
3.1.2 Thermal design rules and methodologies.....	52
10. 4 EXPERIMENTAL TESTS FOR THE EVALUATION OF THE SEISMIC BEHAVIOUR OF THE INNOVATIVE WALL	55
4.1 Experimental plan.....	56

4.2	Material tests	58
4.2.1	Tensile tests on structural materials	58
4.2.2	Creep tests on UHS steel.....	62
4.3	Tests on nut-bar assemblies.....	71
4.3.1	Set-up and instrumentation	72
4.3.2	Results.....	73
4.4	Full-scale wall tests	76
4.4.1	Specimen description and test program	76
4.4.2	Set-up.....	80
4.4.3	Instrumentation	81
4.4.4	Monotonic tests.....	83
4.4.5	Reversed cyclic tests.....	89
4.4.6	Discussion of results	96
4.4.7	Experimental evaluation of behaviour factor.....	100
11.	5 THERMAL ANALYSIS OF THE BUILDING ENVELOPE SOLUTIONS AND ENERGETIC ANALYSIS OF THE PROTOTYPE BUILDING.....	102
5.1	Basics.....	103
5.2	Numerical simulation of the thermal behaviour of the innovative wall	105
5.3	Numerical simulation of the energetic behaviour of the prototype building	113
12.	6 THE PROTOTYPE BUILDING	118
6.1	Integrated design and prototyping of the building	119
6.1.1	Architectural design.....	119
6.1.2	Structural design	123
6.1.3	Building Information Modelling.....	132
6.2	Execution and erection on site.....	135
13.	7 CONCLUSIONS AND FURTHER DEVELOPMENTS.....	141

14. **REFERENCES**..... **144**

List of Figures

Figure 1-1 Integrated building design [2]	17
Figure 1-2 Typical LWS constructions for housing.....	18
Figure 1-3 LWS stick-built (a), panelised (b) and modular constructions (c)	18
Figure 1-4 Wall and floor elements	19
Figure 1-5 LFRS typologies.....	20
Figure 1-6 Temperature distribution in cold, hybrid and warm frame [6]....	22
Figure 2-1 Typical configuration of CFS strap-braced wall.....	36
Figure 3-1 The innovative wall system developed	44
Figure 3-2 Bar shape.....	44
Figure 3-3 Transversal section of stiffened box profile for tracks.....	45
Figure 3-4 Hold-down device and pre-tensioning device.....	45
Figure 3-5 Solution A for wall.....	46
Figure 3-6 Solution B for wall.....	47
Figure 3-7 Partitioning of building into 1D, 2D and 3D geometrical models	52
Figure 4-1 Tested material specimens	59
Figure 4-2 Specimens according to EN ISO 6892-1:2009 (Annex B) [52]..	60
Figure 4-3 Tests on TM1 and S3:1	61
Figure 4-4 Creep test specimens.....	63
Figure 4-5 Creep test set-up.....	65
Figure 4-6 Centesimal dial gauge	66
Figure 4-7 Ad hoc aluminium elements produced.....	68
Figure 4-8 Elongation of bar in the time due to creep phenomenon.....	70
Figure 4-9 Nut-bar assembly test specimens	72
Figure 4-10 Bar-nut assembly test set-up	73

Innovative Lightweight Steel System braced with UHS Steel Bars

Figure 4-11 Results of bar-nut assembly tests	74
Figure 4-12 Example of test with two 12 property Class nuts.....	75
Figure 4-13 L Configuration wall tested.....	78
Figure 4-14 M Configuration wall tested.....	79
Figure 4-15 Torque wrench used for pretension.....	79
Figure 4-16 Wall test set-up.....	81
Figure 4-17 Wall test instrumentation	82
Figure 4-18 Photographs of wall test instrumentation	83
Figure 4-19 Results of M_L1 test	85
Figure 4-20 Results of M_L2 test	86
Figure 4-21 Results of M_M1 test.....	86
Figure 4-22 M_L1 test: collapse mechanism.....	87
Figure 4-23 M_L2 test: collapse mechanism.....	87
Figure 4-24 M_M1 test: collapse mechanism.....	88
Figure 4-25 Comparison among monotonic curves.....	89
Figure 4-26 CUREE cyclic protocol adopted for C_L1 and C_M1 tests	91
Figure 4-27 Cyclic response and envelope for C_L1 test.....	93
Figure 4-28 Cyclic response and envelope for C_M1 test.....	94
Figure 4-29 Comparison between cyclic tests	95
Figure 4-30 C_L1 test: collapse mechanism.....	95
Figure 4-31 C_M1 test: collapse mechanism.....	96
Figure 4-32 Comparison between M_L2 and C_L1 tests.....	99
Figure 4-33 Comparison between M_M1 and C_M1 tests.....	99
Figure 5-1 1-D linear and point thermal bridges.....	106
Figure 5-2 1D models of the wall developed.....	107
Figure 5-3 Temperature distribution in the solution A, without and with considering linear and point thermal bridges.....	109

Figure 5-4 Temperature distribution in the solution B, without and with considering linear and point thermal bridges.....	112
Figure 5-5 2D thermal bridges due to junctions	113
Figure 5-6 Developed solutions for floor and roof.....	115
Figure 5-7 Energy demand for heating and cooling	117
Figure 6-1 Renders of prototype building.....	123
Figure 6-2 Response spectra for the four limit states provided in the Italian Code	125
Figure 6-3 First floor plan.....	127
Figure 6-4 Roof trusses.....	128
Figure 6-5 Connections between truss elements.....	128
Figure 6-6 Two-storey LFRS layouts	130
Figure 6-7 Views of prototype building.....	131
Figure 6-8 BIM structural model	133
Figure 6-9 Complete BIM model developed	134
Figure 6-10 Report of execution and erection of prototype building	140

List of Tables

Table 3-1 Diagonal brace diameters and design lateral resistance for L, M and H walls.....	50
Table 3-2 Design elements obtained for L, M and H walls	51
Table 4-1 Test matrix.....	57
Table 4-2 Tensile test results	62
Table 4-3 Test matrix for the monotonic and cyclic tests on full-scale walls	80
Table 4-4 Monotonic test results.....	88
Table 4-5 General cyclic protocol.....	90
Table 4-6 Cyclic test results.....	94
Table 4-7 Test-based evaluation of behaviour factor.....	101
Table 5-1 Evaluation of U_{clear} for both solutions	104
Table 5-2 U_{clear} and the $U_{overall}$ for both A and B solutions.....	107
Table 5-3 Results of EnergyPlus simulation.....	116
Table 6-1 Parameters for the evaluation of seismic action	124

1 Introduction

The increasing market demand for high-performance and low-cost constructions oriented the choice of the last decades to a competitive and eco-friendly solution: Lightweight Steel (LWS) systems made of Cold-Formed Steel (CFS). It is now well known that LWS systems offer many advantages, associated with typical characteristics of CFS systems (e.g. lightness, high structural performance under seismic actions, simplicity of assembly and disassembly) and with dry construction (short execution times, product quality and reduction of execution times and noise on the site and minimum site waste), which made this solution really competitive. In addition, the use of recyclable materials, the flexibility of the systems and the possible reuse of elements ensures a low environmental impact. For the peculiarities of LWS constructions listed above, it is important a multi-performance design is used, which allows to guarantee good performances from the seismic, thermal/energetic, and environmental point of view.

This work of thesis is a part of an Italian Research Project, named as ECCEISA [1], in which the main aim was the development of an innovative LWS system with higher structural, energetic and environmental performances. The core of the project was the evaluation of seismic and thermal performances of a wall system braced with pre-tensioned Ultra-High-Strength (UHS) steel bars. In particular, Chapter 1 starts with a general overview on integrated building design and prototyping, applying it on the LWS systems, and it provides all the main goals and objectives of the ECCEISA project. Chapter 2 summarizes the studies available in literature on seismic behaviour of dissipative and non-dissipative strap-braced wall system, energy efficiency and thermal performances of LWS systems and creep phenomenon on UHS steel. Chapter 3 provides the details on the structural and thermal design of the innovative

wall system, starting from the choice of materials to use for structural and thermal efficiency and describing rules and methodology adopted. Chapter 4 describes the whole experimental campaign carried out to evaluate the seismic behaviour and validate the effectiveness of the innovative wall and summarizes experimental results obtained. Chapter 5 discusses the numerical simulations performed to analyse the thermal behaviour of the wall and the energetic performance of the prototype building. In Chapter 6 the report of design and the erection on site activities of the prototype building are given. Chapter 7 presents the main conclusions of the work and the possible future further developments on this topic.

1.1 Integrated building design

A joint synergy among different fields can lead the path of innovation and hence making our constructions increasingly safe, sustainable, and comfortable. This concept can be easily applied to the building design through the integrated building design. In fact, generally speaking, the integrated design is a comprehensive holistic approach to design which considers together specialisms usually considered separately, taking into account all the factors and modulations necessary to a decision-making process. Specifically, for building design, it means examining all the aspects related to the construction in each moment of its lifecycle and the consideration of end users of the building. In particular, the three key concepts are architectural, structural and energy and environmental concepts, as shown in Figure 1-1.

For the peculiarities of LWS systems, building design phase well lends itself to be integrated, guaranteeing fast and low impact constructions with high structural, energy and environmental performances.

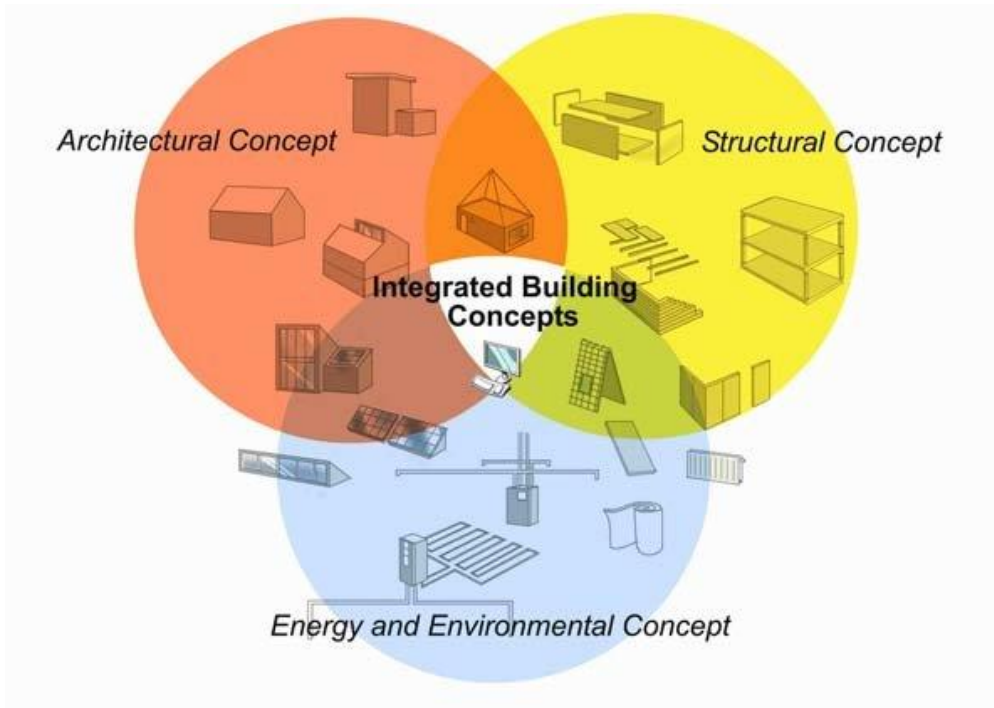


Figure 1-1 Integrated building design [2]

1.1.1 Structural design

The structural design is one of the key concepts of integrated building design. Typical LWS constructions for housing consist of a dry constructive system, in which both floors and walls are made with CFS profiles (Figure 1-2). Generally, LWS constructive systems for housing can be classified according to the level of prefabrication in stick-built (Figure 1-3a), panelised (Figure 1-3b) and modular constructions (Figure 1-3c).



Figure 1-2 Typical LWS constructions for housing



a)

b)

c)

Figure 1-3 LWS stick-built (a), panelised (b) and modular constructions (c)

The main frame of walls is composed of vertical elements, named as studs, and horizontal elements, named as tracks, whereas floor frame is generally composed of joists and tracks (Figure 1-4). Spacing between studs and joists

Innovative Lightweight Steel System braced with UHS Steel Bars

is usually in the range 300-600 mm. Dimensions and spacing of profiles change according to the intensity of gravity loads. Connections are usually made by means of self-drilling screws. Walls which have to resist only to vertical loads can be classified as gravity load resisting walls. The floors are made in a similar manner as gravity load resisting walls except they are oriented in a horizontal direction and are covered with panels or composite steel trapezoidal sheathing-concrete deck.

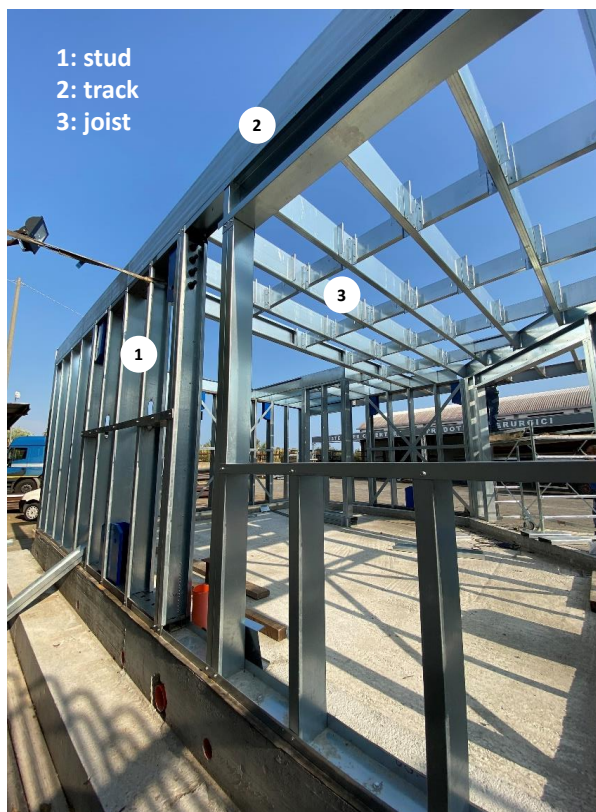


Figure 1-4 Wall and floor elements

The main lateral force resisting system (LFRS) is offered by a wall opportunely braced to resist horizontal actions (i.e. wind and earthquake loads). Bracing system can be provided by gypsum, wood-based, cement-based or other material panels (Figure 1-5a) , steel sheets (Figure 1-5b) or alternatively by steel elements, such as flat straps (Figure 1-5c). The choice of

Innovative Lightweight Steel System braced with UHS Steel Bars

the bracing leads to different wall lateral behaviours and, indeed, design approaches:

- in case of sheathing panels, the walls are defined as shear walls and the resistance is mainly provided through the interaction between the steel frame and sheathing panels (sheathing-braced design approach);
- in case of steel straps, the walls are defined as strap-braced walls and the main resistance is provided by the steel straps placed in an X configuration (“all-steel” design approach).

The LFRSs need hold down devices placed at the wall corners to transfer the uplift forces to the foundation. In addition to lateral force resisting walls, floor elements have also to provide reasonable amount of seismic resistance [3].



a) OSB panel sheathing-braced system b) Steel sheet sheathing-braced system [4] c) Strap-braced system

Figure 1-5 LFRS typologies

Therefore, once the actions have been evaluated, the structural design consists of designing the gravity resisting frame, defining steel grade, number, spacing and dimensions of CFS elements for walls and floors, and choosing the number and typology of LFRs for horizontal loads.

1.1.2 Thermal/Energy design

Thermal/Energy design has as main objective the evaluation and the optimization of thermal performance of the building, in order to increase the energy efficiency. Thermal performance stands for the ability of a building to adapt to changes in the outdoor environment, maintaining indoor thermal comfort conditions, involving as little energy demand for heating and cooling as possible. Indeed, it is vital the good design of building envelope, considering appropriate materials.

With reference to LWS systems, i.e. walls and floors, they are composed of three main material families: CFS profiles, panels, which can have or not load bearing function, and insulation materials.

Several types of panel can be used in LWS systems if it has not to work as sheathing. In the practice, for low-rise residential buildings the most common are OSB and gypsum plasterboards for the outer and inner layers of external walls, respectively. Thicker OSB panels are also used for dry floors, whereas for traditional floors a top concrete slab is provided, which could increase thermal performance and acoustic behaviour.

The most common thermal insulation material used in LWS construction is mineral wool, usually put between the steel studs, that also provides an increased fire resistance. Other types of generally employed insulation is an ETICS with expanded polystyrene, which is used continuously as the exterior thermal insulation layer, minimizing stud thermal bridges. Moreover, recent applications showed that the incorporation of vacuum insulation panels (VIPs) in ETICS can drastically reduce the thermal transmittance of a wall, reducing the effect of thermal bridges and the wall thickness [5].

According to the position of thermal insulation layer, the LWS construction element can be classified in cold, hybrid, and warm frame construction [6], if the thermal insulation is placed inside the wall between the steel studs,

distributed between the external surface and the wall cavity, or placed outside the steel framing, respectively (Figure 1-6). The best thermal performance is provided by the last solution, which is also the most expensive and thicker than the others.

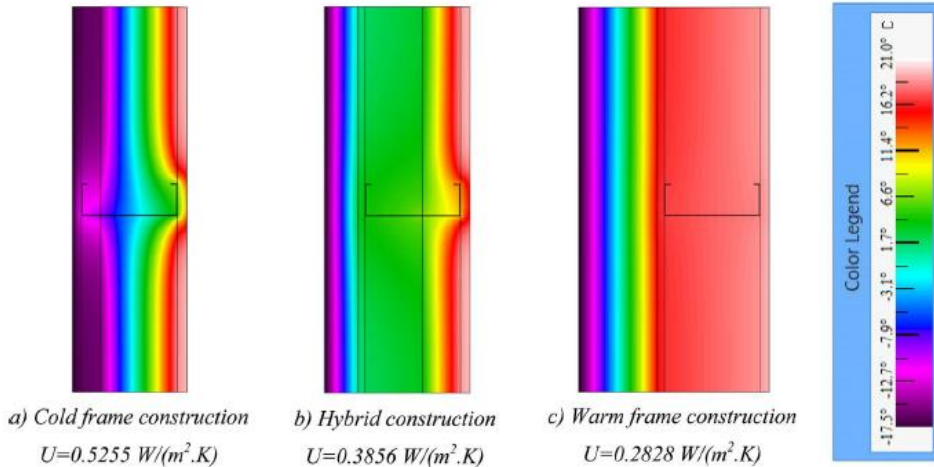


Figure 1-6 Temperature distribution in cold, hybrid and warm frame [6]

The two main problems of the LWS constructions are the presence of thermal bridges, due to steel frame, and the low thermal inertia of the system, due to the lightness. Indeed, the strategy to increase the thermal performance of LWS construction consists in the reduction of thermal bridges and the increasing the thermal inertia of the building.

Thermal bridges are zones in which the heat transfer through the building envelope increases, creating comfort problems and moisture, especially during winter. They can be reduced if some devices are adopted in the design, as using of a continuous insulation layer on the external side of the steel framing, avoiding the interruption of the insulation layers, installing windows and doors in contact with the insulation, covering junctions and studs with insulation.

Improving the thermal performance of the building envelope results in the improvement of the energy performance of buildings, obtaining long-term

Innovative Lightweight Steel System braced with UHS Steel Bars

energy efficiency, lower energy demand for heating and cooling, and higher thermal comfort conditions. Other strategy available to improve energy performance of buildings is provided by active solutions such as the use of smarter HVAC equipment.

1.2 Prototyping and industry 4.0

The advantages of the prototyping and digitalization of processes are evident, if considering the environmental performance and the development of integrated building design. This is commonly referred as industry 4.0 and it is characterized by the fusion of virtual reality and industrial production in a single system, named as cyber-physical system. The main idea of cyber-physical system is the creation of an autonomous communication between intelligent machines and storage systems, which can replicate the physical world and take decisions to modify operational strategies.

The automation of processes to produce LWS constructions can be applied specially to produce CFS elements. In this way the risk of error is reduced, productivity increases in terms of speed and efficiency, guaranteeing greater correspondence between project and product and the risk for the human life in operations is reduced.

Moreover, through the simulation of processes, it is possible to solve in advance, with a considerable saving of time and material, the problems relating to production as well as to the realization of the products or to the verification of their performance.

Thanks to the use of advanced tools, as Building Information Modelling (BIM), it is possible to take into account also this aspect in the design phase, making it as more integrated as possible.

BIM is a virtual model that allows the participation of all the players in the project, who can simultaneously control and share information related to environmental, technological, structural, architectural, and economic performance. A new frontier of design is the concept of “file to factory”, which builds a network of information using evaluation libraries, in order to create a final product, ready to be used.

Innovative Lightweight Steel System braced with UHS Steel Bars

Based on these values, LWS construction becomes more and more competitive compared to traditional construction systems, exhibiting an advantageous approach with respect to the complete production life cycle.

1.3 ECCELSA project

The University of Naples “Federico II” has started in cooperation with the Lamieredil S.p.A. Italian company a research project, funded by the Calabria region, named as ECCELSA. The main topic of the proposed project was the optimization and the improvement of LWS system performances, involving structural, thermal, and environmental aspects. In particular, it aimed to obtain increasingly safer, comfortable and eco-sustainable buildings, through advanced processes, which allow to produce high quality standards. This may also be possible thanks to advanced design tools for computational/ parametric design (BIM) and advanced tools for the control of quality and productivity, including the recent innovations related to digital fabrication in the file to factory (CAD / CAM) processes.

The main core of the ECCELSA project was the development of an innovative anti-seismic wall system, in which the frame structure is made of CFS profiles and the bracing uses the UHS steel, designed to optimize performances and production processes, through prototyping and digital fabrication. Moreover, another goal of the research project was the analysis and development of new technological solutions to improve also the thermal behaviour of the innovative wall system and the building envelope. In fact, an important part was dedicated to the analysis and selection of materials/products, generally in the form of rigid or flexible panels, more appropriate to incorporate in LWS construction elements. To validate the structural choices an extensive experimental campaign was carried out at Laboratory of Department of Engineering and Architecture of University of Naples “Federico II”, including tests on materials, nut-bar assemblies, and full-scale walls. Numerical analysis and simulations were performed in COMSOL software to evaluate the thermal performances of the developed solutions for the wall system. Moreover, to demonstrate the effectiveness of the proposed construction system, for all the

Innovative Lightweight Steel System braced with UHS Steel Bars

performance aspects (structural and thermal) and in term of simplicity of production and construction process, a prototype building, representative of residential building, was designed and erected on the Lamieredil S.p.A. ground. The energy performance of the prototype building was evaluated through numerical simulations in EnergyPlus software.

2 Literature Review

This Chapter provides the current state of the art, concerning the relevant experimental studies on LWS strap-braced wall systems, the analytical studies on the mechanical behaviour of UHS steel and the relevant studies on the thermal behaviour of CFS systems.

The experimental studies carried out around the globe for the seismic behaviour of LWS strap-braced wall systems are summarized (Section 2.1). In particular, experimental studies reviewed in this chapter includes monotonic, cyclic and shake-table tests on scaled and full-scale specimens and buildings, designed as dissipative or non-dissipative systems.

Likewise, the studies on the mechanical behaviour of UHS steel examined in this chapter includes the analysis on the time-dependent properties, and in particular the creep of the material, subjected to different temperature and load conditions (Section 2.2). Moreover, an overview of the studies on the thermal behaviour of CFS systems, including experimental tests and numerical simulations, is also provided (Section 2.3).

2.1 Dissipative and Non-dissipative strap-braced wall systems

In recent times LWS buildings, made of CFS systems, have been often preferred to traditional structures in seismic area, since they exhibited great structural performances with lower erection time and construction costs. The main lateral force resisting system (LFRS) is generally represented by shear walls, sheathed with panels or steel sheets (sheathing-braced solution), strap-braced walls or special bolted moment frames (all-steel solution) [7], which are commonly designed as energy dissipating systems, following the capacity design approach.

Focusing on strap-braced wall system, it is made of a CFS frame, in which the vertical elements are called as studs and can be internal or external (chord studs), whereas the horizontal elements are called as tracks, braced by flat straps in X configuration. The dissipative element is represented by the diagonal strap in tension, which dissipates by its yielding; the contribution given by the strap in compression is neglected, since its slenderness. Any lateral load absorbed by the strap in tension is then transmitted as axial compression force to chord studs, which are usually back-to-back lipped C-channel or box cross section, in order to avoid buckling. Unlipped U cross sections are generally employed for tracks. The connection between straps and the four corners of the wall is given by self-drilling screws and gusset plates, whereas the connection among consecutive floors and between the wall and the foundation is given by hold-down devices and shear anchors.

According to the capacity design approach, studs, tracks, gusset plates and connections have to be overstrength with respect to straps, in order to avoid brittle failures in the system and obtain the desired failure mechanism. Typical configuration of CFS strap-braced wall is shown in Figure 2-1.

Many researches have been focused on experimental characterization of strap-braced wall seismic behaviour, through static and dynamic tests on joints or

portion of LFRS [8], single, multi-bay or multi-storey LFRS [9–15] or whole building [16].

Since joints play a key role to allow the desired behaviour, the work of Casafont et al. [8], in the framework of the European research project “Seismic Design of Light-Gauge Steel Framed Buildings”, produced a set of recommendations for the seismic design of joints, through an extensive experimental activity on strap-gusset joints and lower and upper corner joints. Although the net-section failure of the diagonal strap after yielding is the only collapse mechanism accepted if rules of seismic design are followed, many different phenomena and failure modes were observed.

Recommendations were then verified by cyclic tests on two identical 1079mm × 644mm X-braced frames. In view of the results obtained, it is believed that the shear frames tested show satisfactory performance, because all the failure modes observed in the previous phases of the experimental campaign have been avoided. Furthermore, a correct development of the dissipative action of the straps has taken place. However, it should also be pointed out that local damage occurred in joints because of their semi-rigid nature. This local plasticisation in studs and gussets is common and difficult to avoid in this type of structures. For the frames tested, it specially affects lower corners, where the stiffening effect of the hold-down plates is high. In real x-braced frames, whose studs are about four times higher than the studs of the frames tested, this local plasticisation in joints will not be so relevant at too small horizontal displacements.

So the Authors [8] concluded that tested strap-braced walls performed well, since joint brittle failures were avoided. However, some plastic deformations occurred at the joint location, due to the reduced specimen dimensions.

Fülöp and Dubina [11] investigated by means of six series full-scale wall tests of monotonic and cyclic tests the lateral behaviour of different walls, which

are largely adopted in housing. Among these, one monotonic test and two cyclic tests were carried out on 3600mm × 2400mm strap-braced wall specimens. The aim was to guarantee failure of the specimen due to yielding, avoiding premature failure in end region of straps, and ensuring high level of ductility. The tests showed that, after buckling of straps in the early stage, the local deformation of the lower track followed, and the damage concentrated entirely in the corner area. After important deformation of corner there were some signs of connection elongation, and redistribution of load to the second and third stud. Although plastic elongation of the straps was observed, results showed a premature failure of the corner, due to the large deformations, so that the expected ductility and capacity were not achieved.

Moghimi and Ronagh [9] carried-out twenty cyclic tests on 2400mm × 2400mm strap-braced walls, with several different arrangements, investigating also on the presence of cladding and double-side bracing. Several factors affecting the performance of cold-formed steel frame shear wall have been considered for each arrangement. These tests showed that a strap-braced wall panel clad with gypsum board possesses a lateral load resistance capacity higher than the strap-braced wall and gypsum board clad wall put together, especially in large lateral displacements (of more than 1% inter-story drift) because the gypsum board postpones local and distortional buckling of studs and the chords' flanges. The conventional bracing type currently in practice, rendered unacceptable results. The main reason for its unsatisfactory performance is attributed to premature distortional buckling of studs at stages of the racking displacement, which causes most of the strap load to be transferred to track, bending it significantly. This causes tilting of screws which is often followed by tearing of the track or pull-out of screws from the track. After this, the strap load is transferred to the stud and a similar problem as happened to the track happens to the stud. As a result, straps do

not reach yield. Adding brackets at four corners of the wall panel improves the lateral performance. Results carried out on this last configuration showed good ductile behaviour and highly pinched hysteretic response when capacity design approach was employed. Furthermore, the presence of cladding improved the lateral performances, especially when large displacement occurred (after 1% inter-storey drift ratio), while the contribution from double-side bracing is insignificant.

Rogers and colleagues [10,12] performed experimental activities [12] and numerical analysis [10] to evaluate the seismic behaviour of strap-braced walls, estimating the seismic performance factors and validating seismic design provisions in AISI S213 [17].

In particular, in the work of Velchev et al. [12] monotonic and reversed cyclic tests were carried-out on forty-four specimens with different dimensions, ranging from 610mm × 2440mm to 2440mm × 2440mm (aspect ratio ranging from 4:1 to 1:1) in order to evaluate the influence of the wall aspect ratio on inelastic behaviour. Since capacity design principles and material requirements were considered, results showed that in the walls with aspect ratio 1:1 (2440mm) and 2:1 (1220mm), strap yielding was predominant and produced inelastic deformations. In braced walls having aspect ratios greater than 2:1, like in the 4:1 (610mm) tested walls, combined axial compression, flexure of the chord studs and only minimal strap yielding were observed. Moreover, the ductility and overstrength seismic force modification factors proposed by AISI S213 (2.0 and 1.3, respectively) were appropriate for the walls with length greater than 1220 mm.

In the work of Comeau et al. [10], the Authors applied the FEMA P695 procedure [18] to sixteen multi-storey buildings, located in Calgary, Halifax, Québec City and Vancouver for the evaluation of the seismic force modification factors. In some buildings LFRSs were designed following

capacity design approach, in others lateral system was not detailed for ductile seismic performances. The study confirmed the values of seismic force modification factors proposed in AISI S213 and the unsuitability of buildings designed without specific seismic rules in high seismic zones because of their high probability of brittle failure.

For the same purpose, Lee and Foutch [13] proposed a numerical study, based on a new procedure developed from the SAC Joint Venture, for the evaluation of seismic response modification factor of strap-braced buildings by adopting the FEMA 355F procedure [19]. In particular, single and multi-storey (from two to six storeys) Seattle buildings, chosen for this study, were designed with response modification factor equal to 2, 3 and 4 and analysed. Additionally, four and six-storey buildings with stiff and strong top storey were considered. The aim of this procedure is to reach a high level of confidence (90%) to prevent collapse. Several observations and results were obtained by the Authors. Investigating the drift capacities of all the CFSBF buildings, they found that the capacity drift limit of 0.13 was a common value for the structures analysed, so the precise determination of the drift limit is necessary. They also found that all the two-storey buildings and four- and six-storey buildings with stiff and strong top floor complied with the target confidence level of 90% also with response modification factor of 4, since the added stiffness helped to reduce the median drift demand. For the other four- and six-storey buildings, without added stiffness, also the value of 2 is appropriate so they did not reach the performance objective. So, the Authors finally stated that a response modification factor of 4 could be considered for CFSBF structural system if the top story brace has to be stiffer and stronger than the one implemented by the current design code.

In the work of Eom et al. [15] three-bay single storey strap-braced and steel-sheathed specimens were cyclically tested. Specimens had a centre-to-centre

Innovative Lightweight Steel System braced with UHS Steel Bars

height and length of 3000mm and 5713mm, respectively. Innovative corner details were used to strengthen and mitigate damage of the corner joint and increase ductility of the system. Tested specimens exhibited high deformation capacity and ductility, with a pinched hysteretic behaviour, due to premature buckling of straps and steel sheathing. The energy dissipation capacity was improved in the specimen where the beam-column joints of the boundary frame were strengthened by reducing the column section. The load-carrying capacity, stiffness and yield displacement of the framed stud walls were predicted and, in addition, recommendations for the design and particulars of the framed stud walls were provided.

Davani et al. [14] investigated the seismic damages, which occur in strap-braced structures, to define seismic performance levels by means of ten cyclic tests and numerical modelling. Three different 2400mm × 2400mm specimen configurations, differing in bracing system, were tested at the Structural Engineering Laboratory of the University of Queensland. Test results revealed that many damages occurred in specimens, i.e. strap tearing, pulling out of screws, or severe distortional buckling of studs, although only strap yielding in tension is generally considered as failure mode during design. Severe damages in connection, especially frame-to-strap connections, often happened. Adding cladding and other bracing elements improved seismic performances of strap-braced walls, increasing lateral stiffness and strength. In the work of Kim et al. [20], shake-table tests were conducted at the Tri-axial Earthquake and Shock Simulator (TESS) of the Engineer Research and Development Centre, Construction Engineering Research Laboratory (ERDC-CERL), Champaign, Illinois, on two-storey one-bay strap-braced full-scale building, which had a rectangular plan of 4400 mm and an inter-storey height of 3000mm. LFRS was composed of two 3000mm × 2800mm CFS strap-braced walls, spaced at 3900mm on centre, for each storey and 200mm

Innovative Lightweight Steel System braced with UHS Steel Bars

reinforced concrete slab diaphragm was installed at the top of each floor level. Dynamic identification and earthquake tests were conducted. Only during the earthquake test with the highest scaling factor, the yielding of straps occurred, and they showed a non-linear ductile behaviour with a highly pinched response. Moreover, also yielding of local buckling columns happened for the same intensity.

While research on energy dissipating systems have been largely spread during the last years, non-dissipating system behaviour remains almost unexplored, counting only few tests on single LFRS [21] or on whole buildings [22].

In particular, Al-Kharat and Rogers [21] evaluated the inelastic performance of CFS strap-braced walls by means of nine monotonic and seven cyclic tests on 2440mm × 2440mm specimens, with three different lateral resistances. Tested wall failure was governed by many damages to the tracks, chord studs, gusset plates, hold-downs, and the walls exhibited limited ductility. Furthermore, the seismic force modification factor was evaluated experimentally, and it was in the range of 1.72 (stronger walls) to 3.65 (weaker walls).

Gad and colleagues [22] performed quasi-static tests on 2400mm × 2400mm specimens and shake-table tests on single storey building, at the University of Melbourne. The building was the expression of typical Australian domestic construction and had plan dimensions of 2300mm × 2400mm and inter-storey height of 2400mm. No specific seismic rules were adopted for the design, except for the hold-downs, which were oversized to avoid the possibility of their failure. Shake-table tests were carried- out in different stages of construction, ranging from bare structure to construction completed with non-structural components. Test results revealed that collapse mechanism is governed by the failure of the strap braces if non-structural elements are not present. In fact, the addition of finishing materials affected the fundamental

Innovative Lightweight Steel System braced with UHS Steel Bars

vibration period, and equally the stiffness, damping ratio and loading bearing capacity.

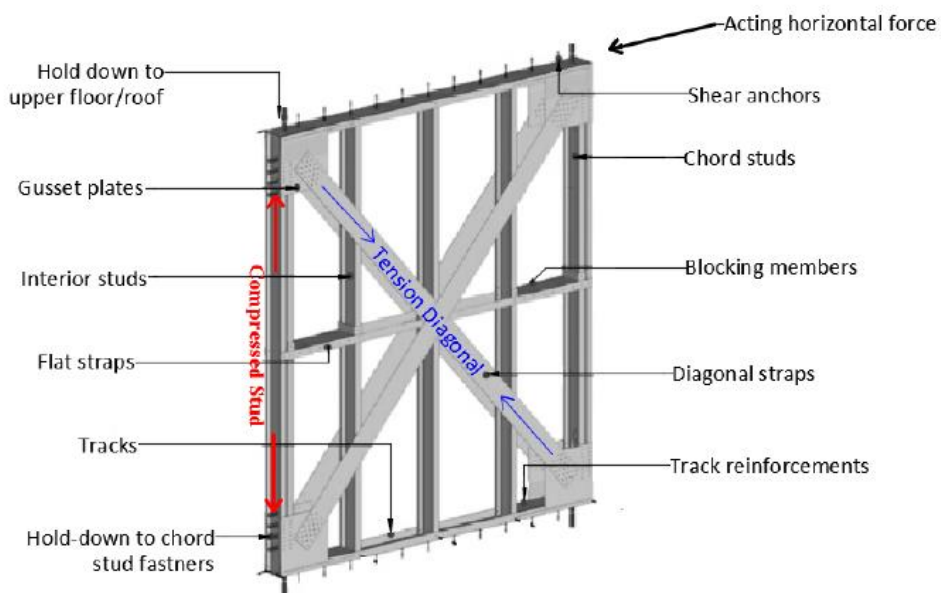


Figure 2-1 Typical configuration of CFS strap-braced wall

2.2 Energy efficiency and thermal performances of LWS systems

LWS construction shows numerous structural, architectural, and technological advantages over more traditional or heavyweight construction. However, the high thermal conductivity of steel elements and the lower thermal mass can lead to some problems, mainly summarizing in significant thermal bridges, several comfort-related problems, larger temperature fluctuations and higher energy demand for heating and cooling.

In the last decades, several researches have been devoted to the evaluation of energy efficiency and thermal performances of LWS steel construction and the solutions to improve them. Since the vital parameters to understand the thermal performance of the wall are the evaluation of thermal transmittance U-value (or equally R-value) and thermal bridges, many of them proposed the methods to evaluate it, through numerical simulations [23], experimental measurements in laboratory [24–29] or in situ [30] or combining both , whereas others proposed mitigation strategies [26,31,32] and numerical modelling of thermal bridges [33].

In fact, the U-value or equally the R-value of LWS wall can be calculated analytically through two methods: the zone method proposed by the American Society of Heating, Refrigerating and Air-Conditioning Engineers [34] and the method provided by EN ISO 6946 [35].

The first method does not take into account the influence of thermal bridges, whereas the second is not applicable for many LWS walls in which insulation layers are bridged by metallic elements.

Alternatively, in situ measurement, standardized by ISO 9869 [36] and ASTM C 1155 [37] can be used, but the evaluation of the U-value is really complicated for LWS walls.

To overcome those limitations, Kosny et al. [38] modified the zone method to take into account thermal bridges. The same Authors [23] evaluated

Innovative Lightweight Steel System braced with UHS Steel Bars

numerically R-value of walls and the zones affected by thermal bridges for several configurations, with different spacing between steel profiles and insulation layer thickness. The Authors concluded that spacing affects the R-value more when the insulation layer is thinner.

Zalewski et al. [25] quantified heat losses due to the thermal bridges for complex walls and employed IR thermography to identify them, pointing out features and limitations of that experimental method.

Gorgolewski [27] developed a simplified method to calculate U-values of LWS systems, based on similar assumptions of EN ISO 6946 [35]. The method gives an accurate estimation, also covering hybrid and cold frame LWS construction.

The group of prof. da Silva was really active in that field, classifying thermal bridges, evaluating all the geometrical parameters which affect them (i.e. space between steel frames, thickness of the steel elements, the length of the web and flanges, the cross section profile and number of steel frames), computing the temperature distribution inside different LWS walls, suggesting some strategies to reduce the effect of repeated thermal bridges and developing 3D heat transfer model [26,32].

Moreover, the Authors provided an extensive review of the energy efficiency and thermal performance of LWS construction [6].

The work of Li et al. [24] investigated, through field measurement and numerical simulation, the thermal and energy performance of LWS-bamboo wall residential building and compared it with two commonly used wall structures. The thermal and energy performance of the LWS-bamboo wall was higher than conventional walls, with an improvement of U value, resistance to outdoor air temperature fluctuation and total energy performance.

The group of prof. Founti [30] introduced two new non-destructive methods, the Representative Points Method (RPM) and the Weighted Area Method

Innovative Lightweight Steel System braced with UHS Steel Bars

(WAM), for the in-situ measurement of the overall thermal transmittance of LWS wall, considering the repeating thermal bridges due to the metal studs. The two methods can be used if the insulation is located inside the wall between the steel studs.

2.3 Creep in UHS steel

The expression Ultra-High-Strength (UHS) steels is referred to all the steels with yielding stress higher than 780 MPa. These materials are becoming more and more popular for all the applications in which high strength can be useful to obtain lighter and more effective constructions, especially in the automotive field. A big challenge is now represented using UHS steels in the construction field, in order to have safer and lighter building, taking advantage of high resistance through the reduction of cross sections. In this perspective, in the present research work the UHS steel is employed in the shape of bar as bracing for a LWS wall system. In particular, two bars in “V” configuration are used and pre-tensioned for many reasons:

1. making the system stiffer in the elastic field because both bars work in tension field;
2. allowing to bars to work both since the beginning of the load application;
3. allowing to bars to work only in tension and never in compression.

Since pre-tension is applied, creep phenomenon may spread, and the wall properties may change during the time. In fact, creep of materials is classically associated with time-dependent plasticity under a fixed stress at an elevated temperature, but for some materials it is pronounced and affects the behaviour also at the ambient temperature. In the structural engineering the experimental and numerical studies on creep of cables are quite diffused since they are used in cable-stayed bridges or in pre-stressed concrete structures [39–41].

Moreover, in the literature many researches were devoted to evaluate creep in metals and alloys (i.e. titanium alloys, stainless steels, and so on...) at elevated temperature, generally greater than half time the absolute melting temperature, and recently also at ambient temperature, but all the studies are referred to microscopic phenomenon [42–46].

Innovative Lightweight Steel System braced with UHS Steel Bars

The only study conducted on creep of UHS was the work of Liu et al. [47], in which ambient-temperature creep mechanism of ultra-high strength steel titanium alloys was investigated, considering ambient-temperature creep in several metals and alloys. Creep tests were performed at an ambient temperature under a constant stress load condition for 24 h and the Authors, analysing changes happened at microscopic level, concluded that the accumulated creep strain in a given period of time increases with increasing stress and a reduction in the hardness.

3 Design of the innovative wall system

CFS strap-braced walls are LFRS, largely used for low to mid rise LWS building and worldwide recognized as a valid alternative to traditional systems, since their good performances. To increase structural performances and design higher buildings, as requested by the Italian construction market, a new system was developed. It mainly consists of CFS framing (tracks and studs) braced by pre-tensioned UHS steel bars in “V” configuration.

This Chapter provides all the details about the design of the innovative wall system and it is articulated as follow: Sections 3.1 and 3.2 describe the structural and the insulation materials employed; Section 3.3 summarizes the innovative wall system concept, providing rules and methodologies used for structural (Section 3.3.1) and thermal design (Section 3.3.2).

3.1 The concept

The innovative wall system is mainly composed of (Figure 3-1): (1) UHS steel bracing; (2) pre-tensioning devices; (3) chord studs; (4) tracks; (5) hold-downs; (6) blocking profiles and flat straps.

The UHS steel bracing consists of two diagonal braces, which are pre-tensioned dog bone shaped round bars having thread ends to allow their connection and pre-tensioning (Figure 3-2). For the chord studs, a back-to-back C section was selected, while for tracks a stiffened box section was chosen (Figure 3-3). The pre-tensioning device is a U shape profile connected to the hold-down through a cylindrical hinge (Figure 3-4), which allows the rotation in the plane of the wall.

The main innovations of the wall system consist of the use of UHS steel bars in the construction field and the concept of bracing system; in fact, the bracing acts as an anti-seismic device, limiting the global displacement of structure in the elastic field and dissipating the seismic energy through the yielding of steel and the spreading of plastic deformations.

The global lateral behaviour of the wall can be described by three main phases: (1) initial phase, in which the system presents a linear elastic response and both diagonal bars work in elastic field, i.e. one bar (bar C) is subjected to a reduction of tensile stress, whereas in the other bar (bar T) the tensile stress increases. In this phase the stress acting in the bar C is lower than the pre-tension imposed.

(2) intermediate phase, in which the bar C does not work, i.e. for the geometry developed the bar does not work under compression, whereas the bar T works in elastic field. This phase starts when the stress acting in the bar C becomes equal to zero.

(3) final phase, in which only the bar T works in inelastic field and it is subjected to strain hardening. This phase starts when the stress acting in the

Innovative Lightweight Steel System braced with UHS Steel Bars

bar T becomes higher than the yielding stress and it ends with the tension failure of the bar, indeed the collapse of the wall. In order to guarantee the behaviour described above, the brittle failure of nut should be avoided. Indeed, choosing appropriately the number and property Class of nuts is crucial to obtain the desired response.

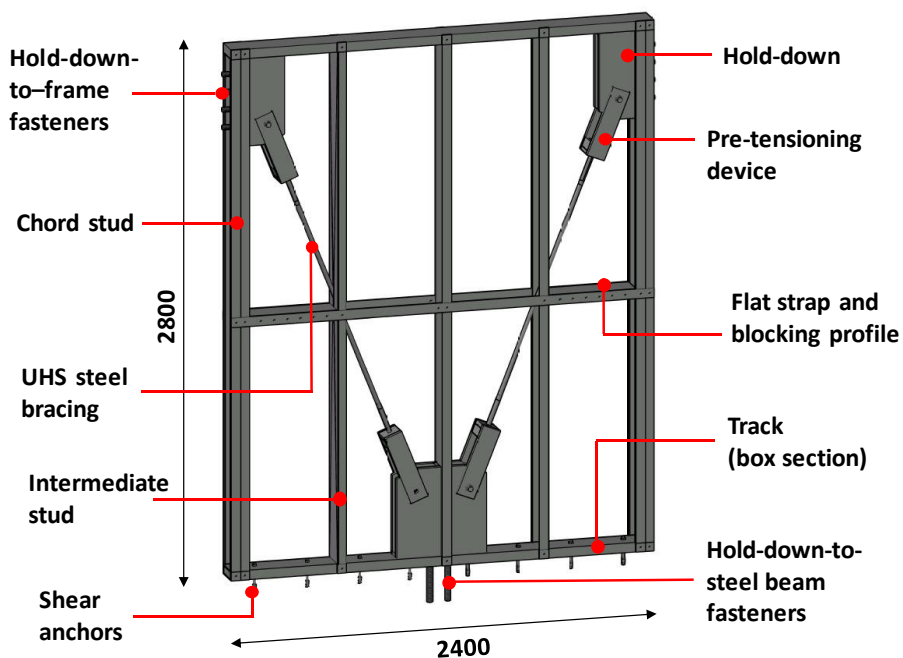


Figure 3-1 The innovative wall system developed



Figure 3-2 Bar shape



Figure 3-3 Transversal section of stiffened box profile for tracks

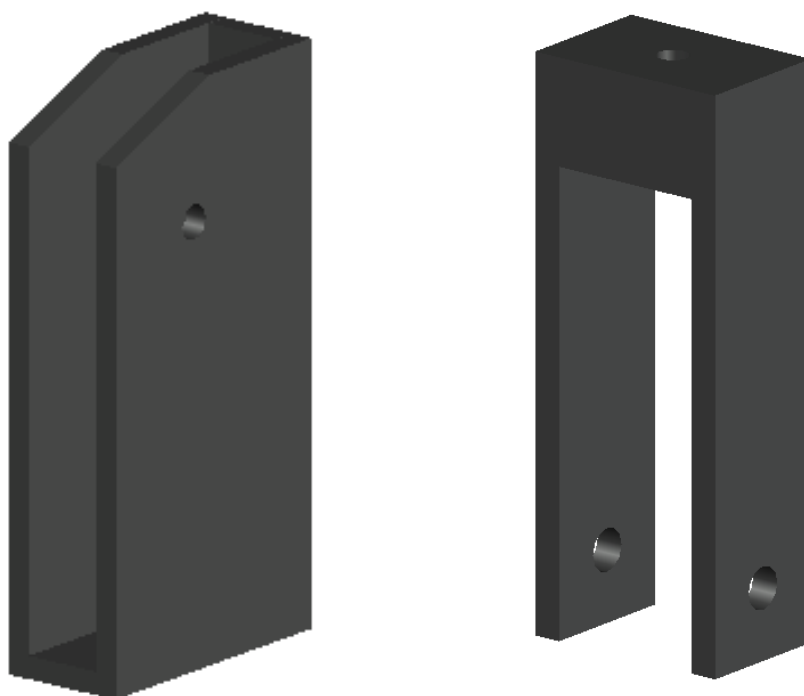


Figure 3-4 Hold-down device and pre-tensioning device

From the thermal point of view, two solutions were developed for the wall system, in which one is more traditional and less expensive (Figure 3-5), whereas the other is better performing (Figure 3-6). Both solutions are classified as warm frame construction, since the insulation layer is placed

Innovative Lightweight Steel System braced with UHS Steel Bars

outside the steel framing, in order to have the best thermal behaviour and limit thermal bridges.

In the first solution, named as A solution, the total thickness is about 315 mm, insulation is provided by mineral wool and the insulation layer thickness is 190 mm, there is an air cavity of 40 mm, finishes are traditional. The second solution, named as B solution, is a totally dry solution, in which the total thickness is about 400 mm, insulation is provided by mineral wool and the insulation layer thickness is 200 mm, there is an air cavity of 40 mm and an internal counter wall.

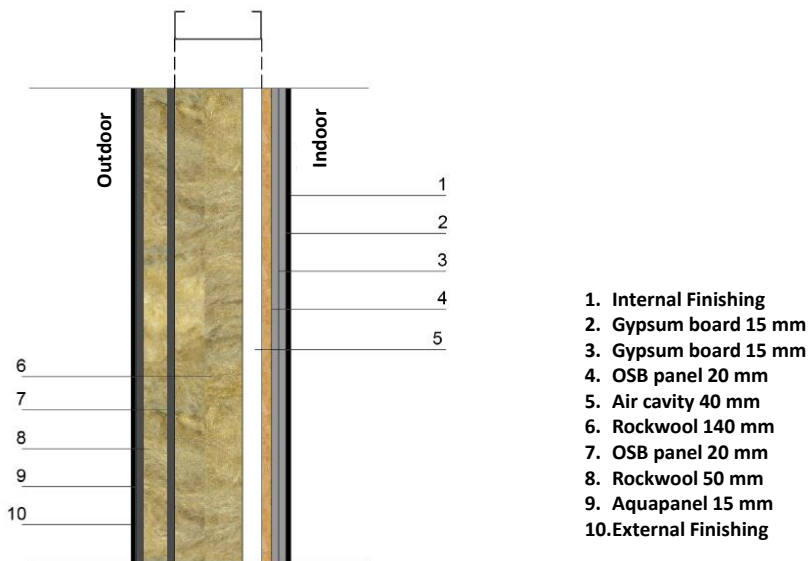


Figure 3-5 Solution A for wall

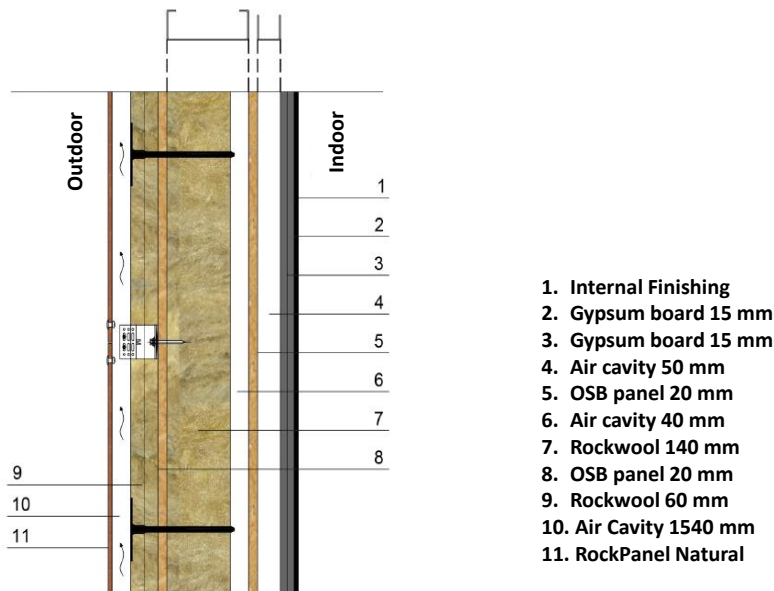


Figure 3-6 Solution B for wall

3.1.1 Structural design rules and methodologies

Different grades of steel were used for the structural elements:

- CFS members, i.e. studs, tracks, blocking and flat straps are made of S280 GD+ Z steel grade ($f_y=280$ MPa, $f_u=360$ MPa);
- devices for pre-tensioning and hold-downs are made of S355 steel grade ($f_y=355$ MPa, $f_u=470$ MPa);
- diagonal braces are made of 1300UHS steel grade ($f_y=1300$ MPa, $f_u=1450$ MPa).

In order to guarantee different lateral resistance levels, three different configurations were designed: Light wall (L), Medium wall (M), Heavy wall (H). Since the system under investigation is not covered by European building code [48,49], following the prescriptions of Italian building standards [50] for the seismic design of non-dissipative systems, which suggests a behaviour factor in the range 1.0 through 1.5, a behaviour factor equal to 1.0 was used in the design, in order to have an assumption on the safe side. On the other hand,

since the plastic behaviour of the system is matter of investigation, the walls were designed following the Capacity design approach, in order to evaluate its dissipative capacity and avoid brittle failure.

Therefore, according to Capacity design approach, diagonal braces are the dissipative elements and act as fuse of the system, in which a pre-tension is applied. Due to the geometry of the system, diagonal braces work only in tension field. Lateral capacity of the wall means the tension collapse of the diagonal brace, in correspondence to its middle zone, where bar diameter is reduced. Under this assumption both the collapse in the bar threaded area and the failure of nuts, used for pre-tension the diagonals, should be avoided.

In particular, the length of the bar with reduced diameter, l_b , is designed to allow a lateral story drift ratio of the wall equal to about 2.5%. Therefore, applying the Equation 3-1, a length of 1100 mm was chosen for light and medium walls, whereas a length of 1150 was chosen for the heavy configuration.

Equation 3-1

$$l_b \geq d_{r,lim} h / f_u \cos \alpha$$

where: $d_{r,lim}$ = minimum lateral drift ratio of the wall set equal to 2.5%; h = height of the wall; f_u = ultimate strain of the steel; α = angle of the brace with respect to horizontal.

The design yield capacity of the brace, $N_{t,Rd}$, is defined according to EN1993-1-3 [48], as shown in Equation 3-2.

Equation 3-2

$$N_{t,Rd} = A_g f_y / \gamma_{m0}$$

where A_g = gross cross-sectional area of the fuse; f_y = nominal yield strength; $\gamma_{m0} = 1.05$, partial safety factor according to the Italian building code [50].

In order to avoid the brittle failure of the threaded area, was used:

Equation 3-3

$$N_{t,Rd} \leq f_{ub} A_{res} / \gamma_{m2}$$

where f_{ub} = nominal ultimate strength of the bar, A_{res} = resistant area of the threaded bar, $\gamma_{m2} = 1.25$, partial safety factor according to the Italian building code.

Furthermore, since there are neither studies nor prescriptions available for the interaction between nuts and UHS steel bars, in order to prevent the nut failure, Equation 3-4 was applied:

Equation 3-4

$$N_{t,Rd} \leq F_{n,Rk} / \gamma_{m2}$$

where $F_{n,Rk}$ = nominal resistance of nut, provided by the manufacturer.

The design lateral resistance of the wall $H_{y,d}$ was evaluated considering the acting pre-tensioning through .

Equation 3-5

$$H_{y,d} = A_g (f_y - f_{pt}) \cos \alpha / \gamma_{m0}$$

where f_{pt} = applied pretension in the bar.

The diameter of diagonal braces, the applied pretension in the bar and the design lateral resistances for the L, M and H wall Configurations are summarized in Table 3-1.

According to capacity design approach, all non-dissipative elements of the wall systems, i.e. pre-tensioning devices, hold-downs, tracks and chord studs are designed for the expected resistance of the diagonal braces. In particular, for non-dissipative elements the design resistance R_d is evaluated according to EN1998-1 [49], with the Equation 3-6.

Equation 3-6

$$R_d \geq 1.1 \gamma_{ov} N_{t,Rd}$$

Innovative Lightweight Steel System braced with UHS Steel Bars

where R_d = resistance of the non-dissipative element; γ_{ov} = overstrength factor, set equal to 1.15; $N_{t,Rd}$ = design plastic resistance of the connected dissipative member (brace), evaluated on the basis of Equation 3-2.

The vertical and horizontal components of the brace force must be transferred through the chord stud and track elements. For the chord studs back-to-back C sections are considered to avoid buckling due to addition axial forces under the action of an earthquake. Since blocking profiles and flat straps are included at middle wall height, the chord stud unbraced length is assumed equal to a half of wall height for in-plane global buckling and equal to the wall height for out-of-plane global buckling. Studs and tracks resistance capacities are evaluated according to EN1993-1-3 [48]. Ad hoc hold-down and device for pre-tensioning are designed and their resistances are evaluated according EN1993-1-3 [48]. All the structural elements obtained from the design phase for the three wall configurations are summarized in Table 3-2.

Table 3-1 Diagonal brace diameters and design lateral resistance for L, M and H walls

Configuration	$d_i^{(1)}$ [mm]	$d_t^{(2)}$ [mm]	$d_e^{(3)}$ [mm]	f_{pt} [MPa]	$H_{y,d}^{(1)}$ [kN]
Light (L)	16	20	21	300	83
Medium (M)	19	24	26	250	117
Heavy (H)	24	30	31	250	199

d_i = minimum diameter of the bar; $^{(2)}d_t$ = diameter of threaded part, $^{(3)}d_e$ = maximum diameter of the bar

Table 3-2 Design elements obtained for L, M and H walls

L CONFIGURATION	COMPONENTS				
	Element	Section [mm]		Steel	
	Track	C152X50X35X3,5		S280GD+Z	
	Track stiffeners	U82x46x4		S280GD+Z	
	Stud	C155X50X15X3,0		S280GD+Z	
	Hold-downs	250x500x20 (longitudinal side)		S355	
		480x70x20 (transversal side)			
		250x70x20 (base)			
	U-shaped profile	375x100x20 (side)			
		125X100X25 (base)			
		110x50x20 (lateral stiffener)			
	CONNECTIONS				
	Type	Number	Class	Diameter [mm]	L [mm]
Nut	4	10	-	-	
Hold-down-stud connection	16	12.9	22	100	
Tension anchorage	4	12.9	30	120	
Shear anchorage	18	12.9	12	60	
M CONFIGURATION	COMPONENTS				
	Element	Section [mm]		Steel	
	Track	C150X50X35X4		S280GD+Z	
	Track stiffeners	U82x46x4		S280GD+Z	
	Stud	C165X50X15X4		S280GD+Z	
	Hold-downs	250x500x25 (longitudinal side)		S355	
		480x70x25 (transversal side)			
		250x70x25 (base)			
	U shaped profile	370x110x25 (side)			
		172X110X30 (base)			
		120x50x20 (lateral stiffener)			
	CONNECTIONS				
	Type	Number	Class	Diameter [mm]	L [mm]
Nut	2	12	-	-	
Hold-down-stud connection	16	12.9	22	100	
Tension anchorage	4	12.9	30	120	
Shear anchorage	18	12.9	12	60	
H CONFIGURATION	COMPONENTS				
	Element	Section [mm]		Steel	
	Track	C180X60X50X5		S280GD+Z	
	Track stiffeners	U55x80x5		S280GD+Z	
	Stud	C190X50X15X4		S280GD+Z	
	Hold-downs	250x500x30 (longitudinal side)		S355	
		470x70x30 (transversal side)			
		250x70x30 (base)			
	U shaped profile	375x100x20 (side)			
		125X100X25 (base)			
		110x50x20 (lateral stiffener)			
	CONNECTIONS				
	Type	Number	Class	Diameter [mm]	L [mm]
Nut	2	12	-	-	
Hold-down-stud connection	16	12.9	27	100	
Tension anchorage	4	12.9	32	120	
Shear anchorage	18	12.9	12	60	

3.1.2 Thermal design rules and methodologies

The two developed solutions were analysed and the thermal performance of the building envelope considering both of them, without and with thermal bridges was evaluated. According to ISO 10211:2007 [51], the analysis of the building envelope is performed considering a steady state approach, in order to take into account thermal bridges. The basic concept of the methodology is the partitioning of the envelope into three geometrical models: 1D, 2D and 3D model, as shown in Figure 3-7. The 1D geometrical model stands for the central part of the envelope assembly, while the 2D and 3D geometrical models concern the 2D junctions (geometrical linear thermal bridges) and 3D junctions (geometrical point thermal bridges) of the envelope, respectively.

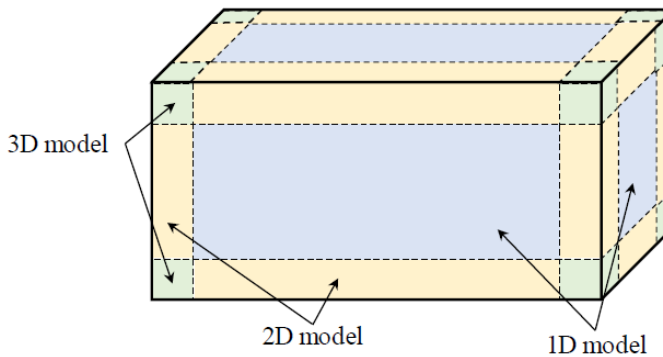


Figure 3-7 Partitioning of building into 1D, 2D and 3D geometrical models

In 1D model, the thermal performance for the central part of the envelope is assessed by means of the calculation of the thermal transmittance for the whole central surface of the element. In the case of homogenous elements (without thermal bridges), the U-value of the wall, U_{clear} , is calculated according to ISO 6946 standard [35]. In the case of LWS solutions, the studs or other structural components (i.e. hold-down, bracing,...) provide repeating thermal bridges and the thermal transmittance of the central part has to take into account them.

For this reason, the $U_{overall}$ is evaluated taking into account the effect of thermal bridges and it is calculated according to ISO 10211 [51], as described by the Equation 3-7.

Equation 3-7

$$U_{overall} = U_{clear} + \frac{\sum_{i=1}^{N_{st}} \Psi_{st}^i l_{st}^i}{A}$$

where U_{clear} is the U-value of the element without the effect of thermal bridges, calculated according to ISO 6946 standard [35], Ψ_{st} is the linear thermal transmittance of the repeating thermal bridges caused by the structure, l_{st} is the length over the which the Ψ_{st} value applies, A is the total surface of the element and N_{st} is the number of linear thermal bridges. The Ψ_{st} is calculated according to Equation 3-8.

Equation 3-8

$$\Psi_{st} = L_{1D,st} - U_{clear} \cdot l_{st}$$

where $L_{1D,st}$ is the thermal coupling coefficient, obtained from steady state 2D simulation of the examined configuration.

The non-repeating linear thermal bridges due to the junctions between two elements of the envelope are calculated by the 2D model. The linear thermal transmittance, Ψ_{2D} , is determined by the Equation 3-9.

Equation 3-9

$$\Psi_{2D} = L_{2D} - \sum_{j=1}^{N_j} U_j \cdot l_j$$

where L_{2D} is the thermal coupling coefficient, obtained from the simulation of the junction in steady state conditions, U_j is the thermal transmittance of each simulated element j of the junction and l_j is the length over which the value Ψ_{2D} applies.

The 3D model calculates the non-repeating point thermal bridges caused by the corners of the envelope, the point insulation discontinuities etc. The point thermal transmittance, χ , is calculated by the Equation 3-10.

$$\chi = L_{3D} - \sum_{i=1}^{N_i} (U_i \cdot A_i) - \sum_{j=1}^{N_j} (\Psi_j \cdot l_j)$$

where L_{3D} is the thermal coupling coefficient, obtained from a 3D simulation of the point thermal bridge separating the two environments being considered. After the calculation of all the individual thermal bridges, the equivalent thermal transmittance, $U_{eq,i}$ for each element i of the building envelope, is calculated by the Equation 3-11, taking into account all incorporating thermal bridges on the element.

$$U_{eq,1} = U_{clear,i} + \frac{\sum_k (\Psi_{st}^k \cdot l_{st}^k)}{A_i} + \frac{\sum_m (\Psi_{2D}^m \cdot l^m)}{A_i} + \frac{\sum_n \chi_n}{A_i}$$

or alternatively according to Equation 3-12.

$$U_{eq,i} = U_{clear,i} + U_{repeating,i} + U_{2D_geometrical,i} + U_{3D_geometrical}$$

where $U_{repeating}$, $U_{2D_geometrical}$ and $U_{3D_geometrical}$ are the terms for the effect of the repeating, linear and point non-repeating thermal bridges, respectively, expressed in thermal transmittance values.

The total heat flow, Φ , which passes through each configuration, is obtained by the simulation results. Hence, the 2D and 3D thermal coupling coefficients, L_{2D} and L_{3D} , are calculated by the Equation 3-13.

$$L = \frac{\Phi}{T_{in} - T_{out}}$$

where Φ is the total heat flow.

Details about the simulations to evaluate the thermal coupling coefficient and the equivalent properties are described in the Chapter 5.

4 Experimental tests for the evaluation of the seismic behaviour of the innovative wall

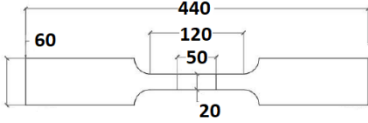
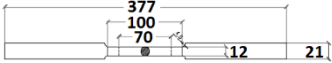
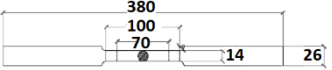
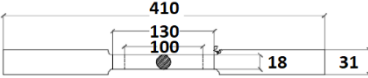

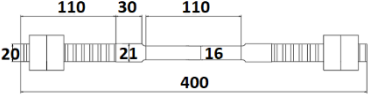
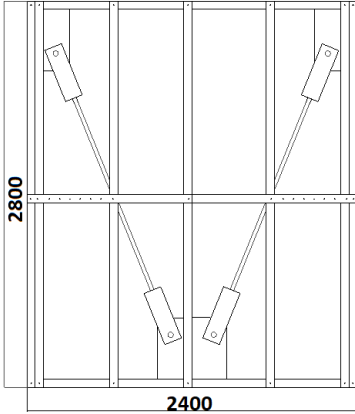
The effectiveness and the limitations of the innovative wall system were validated through an extensive experimental campaign carried out at Laboratory of the Department of Structures for Engineering and Architecture of University of Naples “Federico II”, which consisted of small-scale tests on materials and nut-bar assemblies and full-scale wall tests. In particular, Section 4.2 describes tension tests on structural materials (Section 4.2.1), and creep tests on UHS steel (Section 4.2.2), since pre-tension is applied to the bar and no information is available in literature on time-dependent behaviour of that material at ambient temperature; Section 4.3 summarizes the details about set-up (Section 4.3.1), instrumentation (Section 4.3.2) and results of tests (Section 4.3.3) carried-out on nut-bar assemblies to understand the interaction between UHS steel bar and nut and choose the nut class and number; in Section 4.4 tests on full-scale walls are presented, providing all the details about specimen (Section 4.4.1), set-up developed (Section 4.4.2), instrumentation installed (Section 4.4.3), monotonic and cyclic test performed (Sections 4.4.4 and 4.4.5). Moreover, a discussion on relevant results is provided in Section 4.4.6.

4.1 Experimental plan

The general plan for the experimental assessment of the seismic response consisted of twenty-four tension tests for the mechanical characterization of structural materials used in the wall systems, two creep tests of UHS steel, eight tension tests on bar-nut assemblies, three monotonic tests on full-scale walls (two for the light configuration and one for the medium configuration) and two cyclic tests on full-scale walls (for the light configuration and one for the medium configuration). Table 4-1 summarizes the experimental program.

Innovative Lightweight Steel System braced with UHS Steel Bars

Table 4-1 Test matrix

	Label Thickness Steel grade No. of tests	<table style="width: 100%; border-collapse: collapse;"> <tr> <td style="width: 12.5%;">S3</td> <td style="width: 12.5%;">S4</td> <td style="width: 12.5%;">S20</td> <td style="width: 12.5%;">S25</td> <td style="width: 12.5%;">S30</td> </tr> <tr> <td>3</td> <td>4</td> <td>20</td> <td>25</td> <td>30</td> </tr> <tr> <td>S280</td> <td>S280</td> <td>S355</td> <td>S355</td> <td>S355</td> </tr> <tr> <td>3</td> <td>3</td> <td>3</td> <td>3</td> <td>3</td> </tr> </table>	S3	S4	S20	S25	S30	3	4	20	25	30	S280	S280	S355	S355	S355	3	3	3	3	3
S3	S4	S20	S25	S30																		
3	4	20	25	30																		
S280	S280	S355	S355	S355																		
3	3	3	3	3																		
	Label	<table style="width: 100%; border-collapse: collapse;"> <tr> <td style="width: 33.3%;">TL</td> <td style="width: 33.3%;">TM</td> <td style="width: 33.3%;">TH</td> </tr> </table>	TL	TM	TH																	
TL	TM	TH																				
	Steel grade	<table style="width: 100%; border-collapse: collapse;"> <tr> <td style="width: 33.3%;">UHS1300</td> <td style="width: 33.3%;">UHS1300</td> <td style="width: 33.3%;">UHS1300</td> </tr> </table>	UHS1300	UHS1300	UHS1300																	
UHS1300	UHS1300	UHS1300																				
	No. of tests	<table style="width: 100%; border-collapse: collapse;"> <tr> <td style="width: 33.3%;">3</td> <td style="width: 33.3%;">3</td> <td style="width: 33.3%;">3</td> </tr> </table>	3	3	3																	
3	3	3																				
	No. of tests	<table style="width: 100%; border-collapse: collapse;"> <tr> <td style="width: 66.6%;">2</td> <td style="width: 33.3%;">2</td> </tr> </table>	2	2																		
2	2																					
	Label Nut property Class Nut number No. of tests	<table style="width: 100%; border-collapse: collapse;"> <tr> <td style="width: 33.3%;">D1-10</td> <td style="width: 33.3%;">D1-12</td> <td style="width: 33.3%;">D2-10</td> </tr> <tr> <td>10</td> <td>12</td> <td>10</td> </tr> <tr> <td></td> <td></td> <td></td> </tr> <tr> <td>1</td> <td>1</td> <td>2</td> </tr> <tr> <td>2</td> <td>3</td> <td>3</td> </tr> </table>	D1-10	D1-12	D2-10	10	12	10				1	1	2	2	3	3					
D1-10	D1-12	D2-10																				
10	12	10																				
1	1	2																				
2	3	3																				
	Label No. of monotonic tests No. of cyclic tests	<table style="width: 100%; border-collapse: collapse;"> <tr> <td style="width: 50%;">WL</td> <td style="width: 50%;">WM</td> </tr> <tr> <td>2</td> <td>1</td> </tr> <tr> <td>1</td> <td>1</td> </tr> </table>	WL	WM	2	1	1	1														
WL	WM																					
2	1																					
1	1																					

4.2 Material tests

Since the local behaviour of the used materials can affect the global behaviour of the innovative wall system and the actual properties of materials are vital to predict its experimental resistance, material tests were performed. In particular, tensile tests on structural materials (Section 4.2.1) and creep tests at ambient temperature on UHS steel bars (Section 4.2.2) were carried out and results are discussed in the following sections.

4.2.1 Tensile tests on structural materials

The tensile tests on materials were performed on all steel types and thicknesses used for structural elements of the wall, i.e. frame members (tracks and studs), diagonal bars and hold-down devices:

- Steel S280GD+Z, thickness 3.0 mm (S3);
- Steel S2800GD+Z, thickness 4.0 mm (S4);
- Steel S355, thickness 20.0 mm (S20);
- Steel S355, thickness 25.0 mm (S25);
- Steel S355, thickness 30.0 mm (S30);
- Steel UHS1300, internal diameter 12 (TL);
- Steel UHS1300, internal diameter 14 (TM);
- Steel UHS1300, internal diameter 18 (TH).

For each type and thickness of steel were performed 3 tests. All the specimens tested are reported in Figure 4-1. The specimens are in accordance to the European Standard EN ISO 6892-1:2009 (Annex B) "Metallic materials - Tensile testing - Part 1: Method of test at room temperature" [52], as shown in Figure 4-2.

Tensile tests on materials were performed by the universal testing machine MTS 810 series (UTM) to determine the engineering stress-strain response of

Innovative Lightweight Steel System braced with UHS Steel Bars

materials. The deformations were read by means of two strain gauges positioned close to the original gauge length L_0 .

Figure 4-3 shows some specimens before and after tensile test. Table 4-2 summarizes the nominal yield stress ($f_{y,n}$), nominal ultimate stress ($f_{u,n}$), experimental yield stress ($f_{y,exp}$), experimental ultimate stress ($f_{u,exp}$) and average values of experimental results. The average experimental values of the yield and ultimate stress were always equal or higher than nominal values. For steel S280GD+Z the average experimental values show an increase of the yield strength and ultimate strength respectively of 13% and 12% compared to the nominal values ($f_{y,n} = 280$ MPa and $f_{u,n} = 360$ MPa).

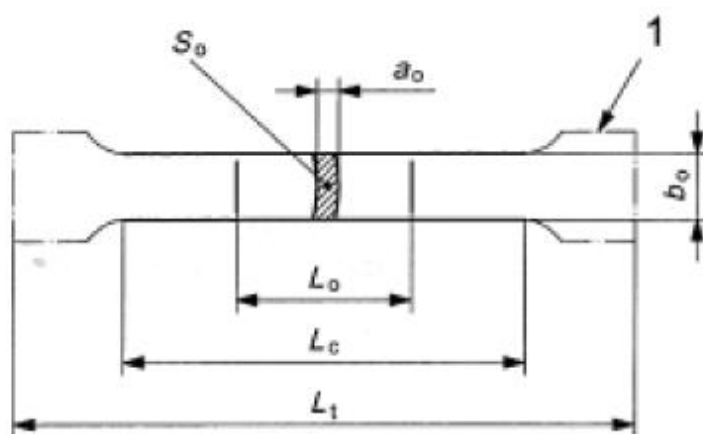
For steel S355 the average experimental values show an increase of the yield strength and ultimate strength respectively of 51% and 5% compared to the nominal values ($f_{y,n} = 355$ MPa and $f_{u,n} = 510$ MPa).

For UHS steel the average experimental values show an increase of the yield strength and ultimate strength respectively of 19% and 12% compared to the nominal values ($f_{y,n} = 1300$ MPa and $f_{u,n} = 1450$ MPa).

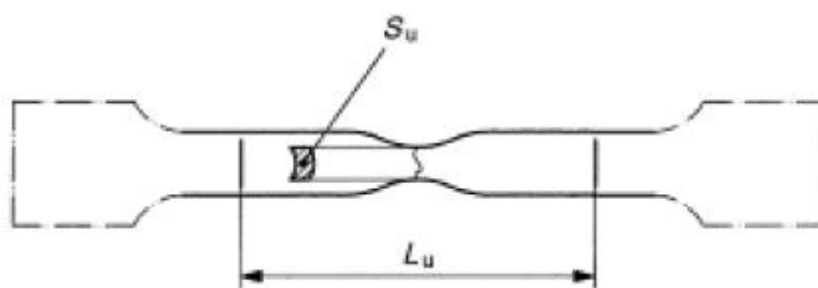
In Appendix A: "Tests on materials and components" a specific datasheet is given for each test.



Figure 4-1 Tested material specimens



a) Before testing



b) After testing

Key

- a_0 original wall thickness of a tube
- b_0 original average width of the longitudinal strip taken from a tube
- L_c parallel length
- L_0 original gauge length
- L_t total length of test piece
- L_u final gauge length after fracture
- S_0 original cross-sectional area of the parallel length
- S_u minimum cross-sectional area after fracture
- 1 gripped ends

Figure 4-2 Specimens according to EN ISO 6892-1:2009 (Annex B) [52]



a) TM1 before test



b) TM1 after test



c) S3.1 before test



d) S3.1 after test

Figure 4-3 Tests on TM1 and S3:1

Innovative Lightweight Steel System braced with UHS Steel Bars

Table 4-2 Tensile test results

Nominal values				Experimental results						
Steel grade	$f_{v,n}^a$ [MPa]	$f_{u,n}^b$ [MPa]	$f_{u,n}/f_{y,n}^a$ $f_{y,n}^a$ $f_{y,n}^a$	t- d [mm]	Label	$f_{v,exp}^c$ [MPa]	$f_{u,exp}^d$ [MPa]	$f_{y,exp}/f_{y,n}^a$ $f_{y,n}^a$ $f_{y,n}^a$	$f_{u,exp}/f_{u,n}^b$ $f_{u,n}^b$ $f_{u,n}^b$	$f_{u,exp}/f_{y,exp}^c$ $f_{y,exp}^c$ $f_{y,exp}^c$
S280GD	280	360	1.3	3	S3.1	307.2	399.9	1.10	1.11	1.30
					S3.2	307.8	400.7	1.10	1.11	1.30
					S3.3	296.7	387.3	1.06	1.08	1.31
					AV ^e	303.9	396.0	1.09	1.10	1.30
				4	S4.1	330.5	414.7	1.18	1.15	1.25
					S4.2	327.8	415.0	1.17	1.15	1.27
					S4.3	326.2	412.2	1.16	1.15	1.27
					AV ^e	328.2	414.2	1.17	1.15	1.26
S355JR	355	510	1.4	20	S20.1	357.0	561.9	1.58	1.10	1.57
					S20.2	336.4	533.3	1.50	1.05	1.59
					S20.3	339.8	533.8	1.50	1.05	1.57
					AV ^e	344.4	543.0	1.53	1.06	1.58
				25	S25.1	342.4	548.2	1.54	1.07	1.60
					S25.2	334.5	533.3	1.50	1.05	1.59
					S25.3	356.3	571.6	1.61	1.12	1.60
					AV ^e	344.4	551.1	1.55	1.08	1.60
				30	S30.1	374.0	560.8	1.58	1.10	1.50
					S30.2	414.1	620.9	1.75	1.22	1.50
					S30.3	249.2	354.5	1.00	0.70	1.42
					AV ^e	345.8	512.1	1.44	1.00	1.47
12	TL1	1236.9	1401.9	1.08	0.97	1.13				
	TL2	1630.6	2089.7	1.61	1.44	1.28				
	TL3	1424.6	1693.2	1.30	1.17	1.19				
	AV ^e	1430.7	1728.3	1.33	1.19	1.20				
14	TM1	1494.5	1734.72	1.33	1.20	1.16				
	TM2	1300.7	1548.66	1.19	1.07	1.19				
	TM3	1301.4	1505.99	1.16	1.04	1.16				
	AV ^e	1365.5	1596.46	1.23	1.10	1.17				
18	TH1	1346.4	1623.07	1.04	1.12	1.21				
	TH2	1290.0	1487.99	0.99	1.03	1.15				
	TH3	1300.0	1533.02	1.00	1.06	1.18				
	AV ^e	1312.1	1548.03	1.01	1.07	1.18				
UHS	1300	1450	1.1							

^a $f_{y,n}$: nominal yield stress;

^b $f_{u,n}$: nominal ultimate stress;

^c $f_{v,exp}$: experimental yield stress;

^d $f_{u,exp}$: experimental ultimate stress;

t: thickness

d: diameter

^e AV: average of the experimental values.

4.2.2 Creep tests on UHS steel

Since the UHS steel diagonals are pretensioned in the system, it is important to evaluate the viscous properties of material, which is still unknown from this

Innovative Lightweight Steel System braced with UHS Steel Bars

point of view, as introduced in Section 2.2. For this purpose, in the research project two creep tests in controlled temperature room were introduced. Specimens consist of two 26 mm diameter and 1200 mm long UHS steel bars with a threaded end, in order to apply the pre-tension with nuts. Both specimens were preloaded at 800 Nm, corresponding to a pre-tension of 175 kN, equal to about 50% of f_{yd} . Figure 4-4 shows the specimens used for the tests.

The room temperature was set equal to 23 degrees. The experimental tests are still on going and the measurements are under monitoring; tests will end for February 2022.

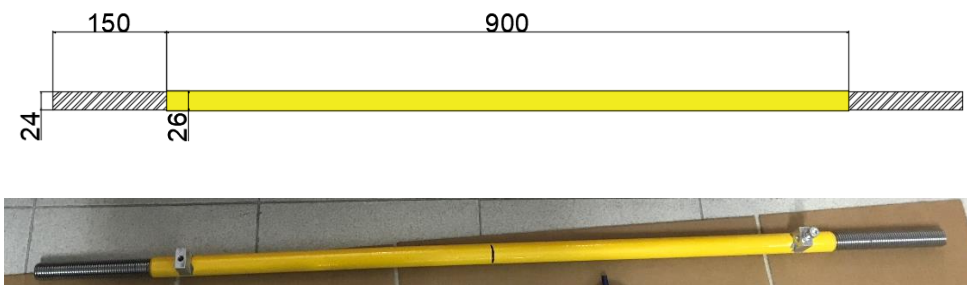


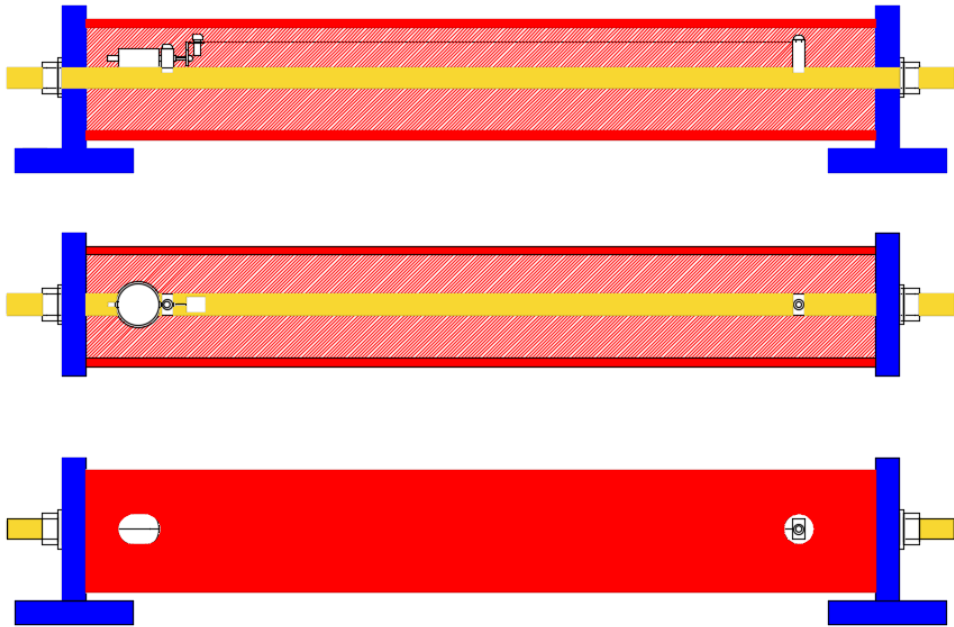
Figure 4-4 Creep test specimens

4.2.2.1 Set-up

Ad hoc set-up was designed, and it consists of a 152.4x11 mm (diameter x thickness) tubular section with opportune holes to read the measurements of instrumentation and T-shaped welded profiles. The dimensions of tubular section (i.e. diameter and thickness) and T-shaped welded profiles were designed in order to not have instability of tube, due to the compression transmitted by pre-tensioned bar, and to have an efficient restraint for the set-up. Figure 4-5 shows the set-up drawings (Figure 4-5a), the geometrical properties of tubular section and T-shaped welded profiles (Figure 4-5b) and

Innovative Lightweight Steel System braced with UHS Steel Bars

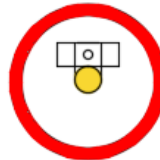
a picture of both test configurations in the controlled temperature room (Figure 4-5c).



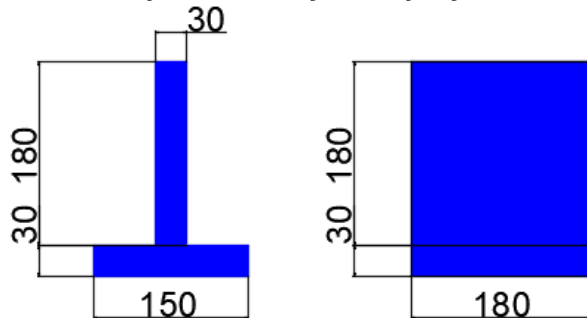
a) Drawings of set-up

Tube section properties:

- diameter 152.4 mm
- thickness 11 mm



T-shaped welded profile properties:



b) Properties of set-up components



c) Picture of both test configurations in the controlled temperature room

Figure 4-5 Creep test set-up

4.2.2.2 Instrumentation

Specimens were equipped of one centesimal dial gauge (Figure 4-6) and invar wire to measure strains during the time. Ad hoc aluminium elements were designed and produced to place the centesimal dial gauge at one end and to fix the invar wire at both ends (Figure 4-7).

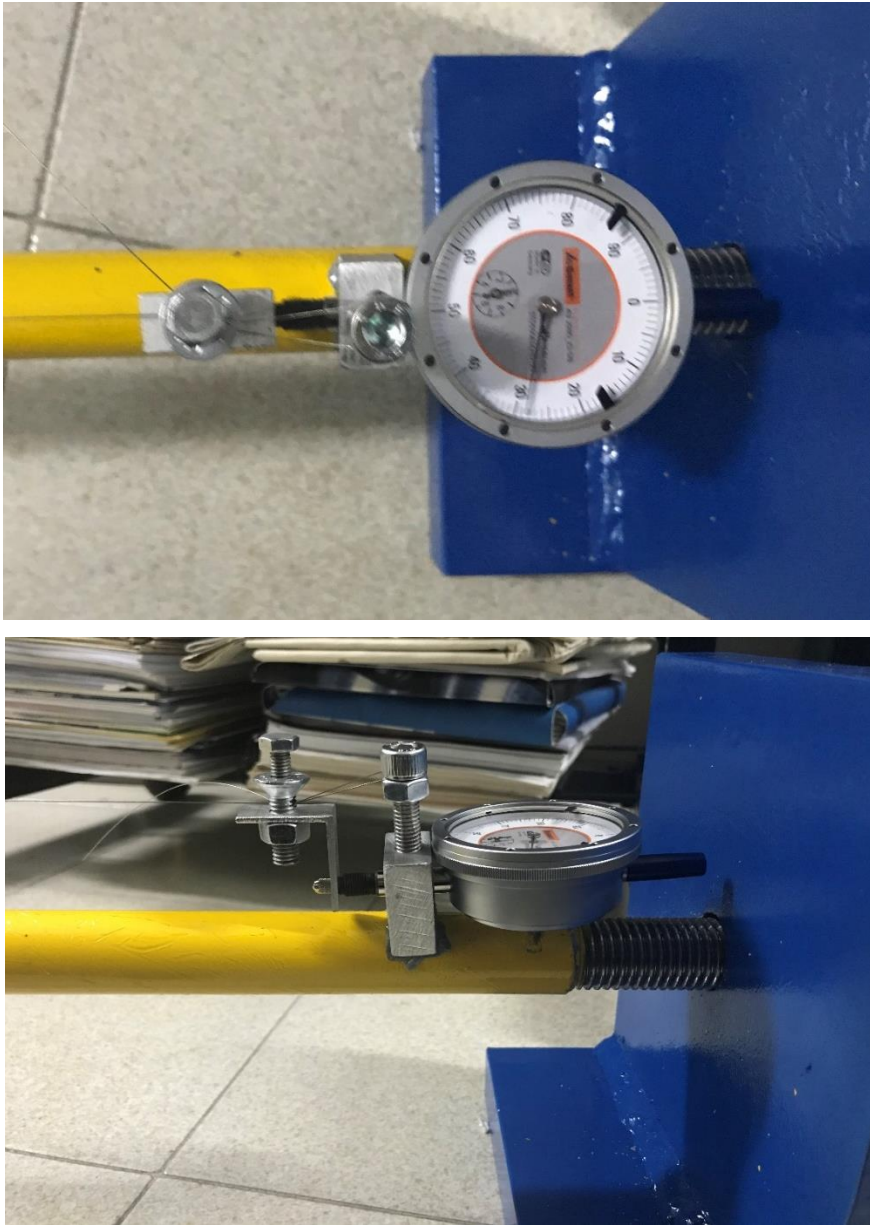
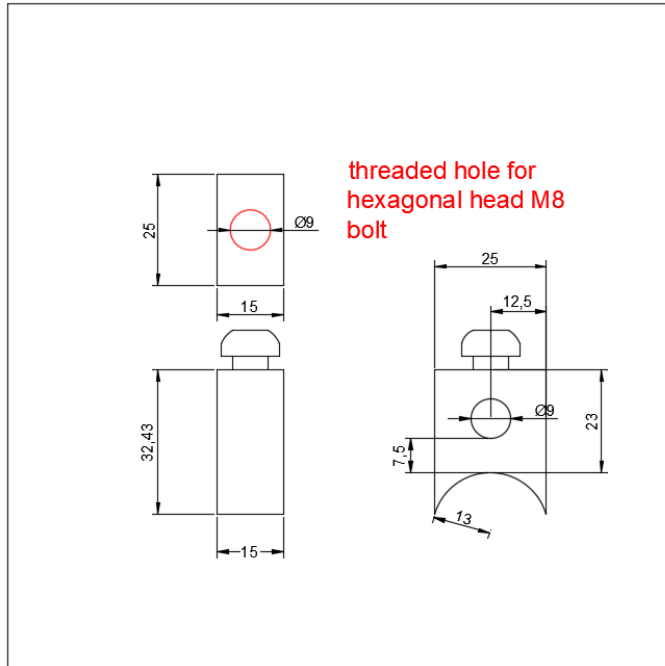
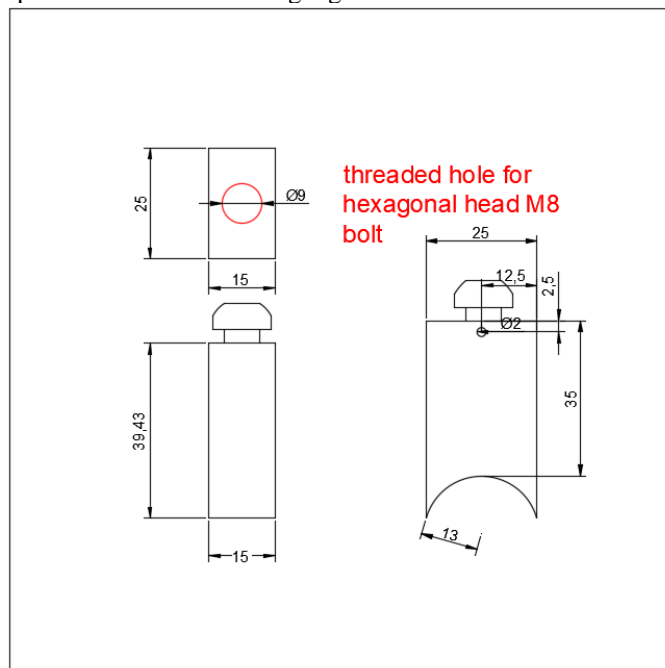


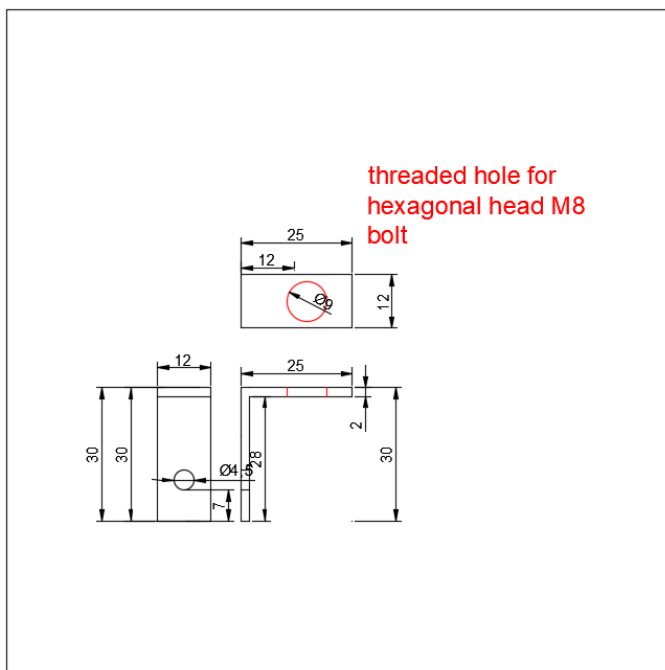
Figure 4-6 Centesimal dial gauge



a) Drawings of aluminium elements produced to place the centesimal dial gauge on the bar



b) Drawings of aluminium elements produced to fix the invar wire on the first end



c) Drawings of aluminium elements produced to fix the invar wire on the second end



d) Photograph of aluminium elements produced to fix the invar wire on the first end

Figure 4-7 Ad hoc aluminium elements produced

4.2.2.3 Results

Results are reported in Figure 4-8 in term of elongation Δl in the time t . Instrumentation in test 2 (T2) has not worked until October 2020, in which the first valid measurement was done. Until now it can be concluded that the creep phenomenon at ambient temperature is present and, after 1 year in T1 it produced a variation in tension inside the bar equal to about 6.27 kN, whereas after less than 6 months in T2 it produced a variation in tension inside the bar equal to about 2.68 kN. Moreover, from both tests it can be noted that creep started after almost 2 months. In particular, to estimate the reduction of tension in the bar, it can be used the following equations (Equation 4-1, Equation 4-2, Equation 4-3):

Equation 4-1

$$\varepsilon = \frac{\Delta l}{l}$$

where ε is the strain, Δl is the elongation produced and l is the gauge length equal to 800 mm.

Equation 4-2

$$\sigma = E\varepsilon$$

where σ is the stress acting in the bar and E the Young modulus.

Equation 4-3

$$\Delta N = \sigma A$$

where ΔN is the reduction of tension in the bar and A is the area of bar, equal to about 531 mm².

In Appendix A1.2 all the measurements and the photographic report are provided.

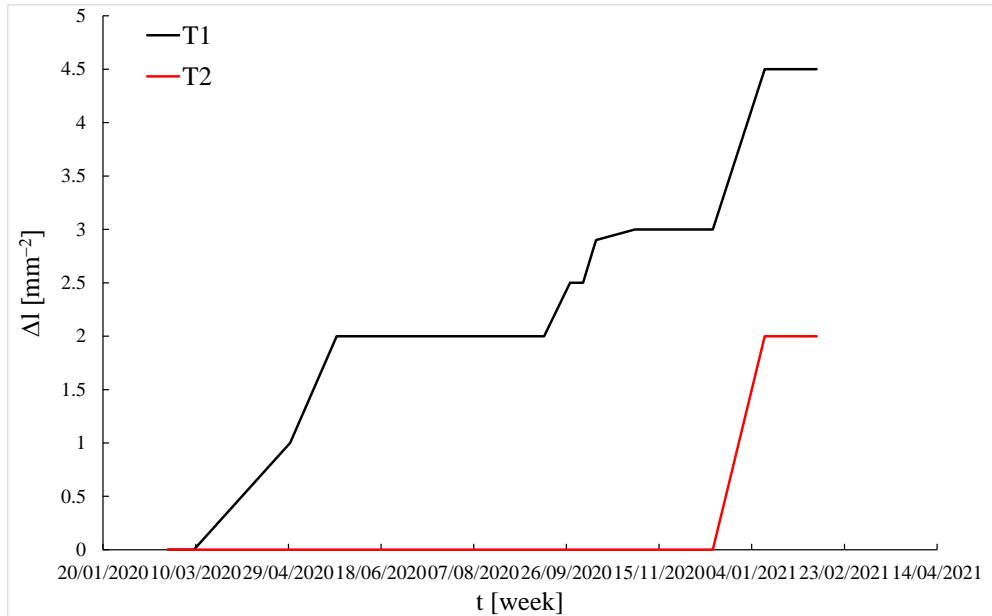


Figure 4-8 Elongation of bar in the time due to creep phenomenon

4.3 Tests on nut-bar assemblies

From the literature [53] it is well known that the nut resistance could be smaller than bolt resistance, in case of high resistance bolts. Since the assembly between nut and UHS steel bar is not codified and the behaviour of the innovative wall system can be affected by nut failure, a series of eight tests on different configurations was carried-out. In particular, the experimental tests aimed to select the nut property Class (10 or 12) and the number of nuts (1 or 2) to use, in order that the collapse mechanism of the wall consisted of the tension failure of diagonal bar in reduced section. Specimens are named as D number of nuts (D1 or D2),_ nut property Class (10 or 12),_ test number (1, 2 or 3), e.g. D1_10_1 means the test no. 1 carried out on the specimen with one nut having nut property Class equal to 10.

The tests were performed by using a UTM. In particular, specimens were subjected to imposed displacements at a rate of 0.05 mm/s without any preloading due to the tightening of nuts. The data were recorded with a sampling frequency equal to 5 Hz. In Figure 4-9 specimen types are shown.

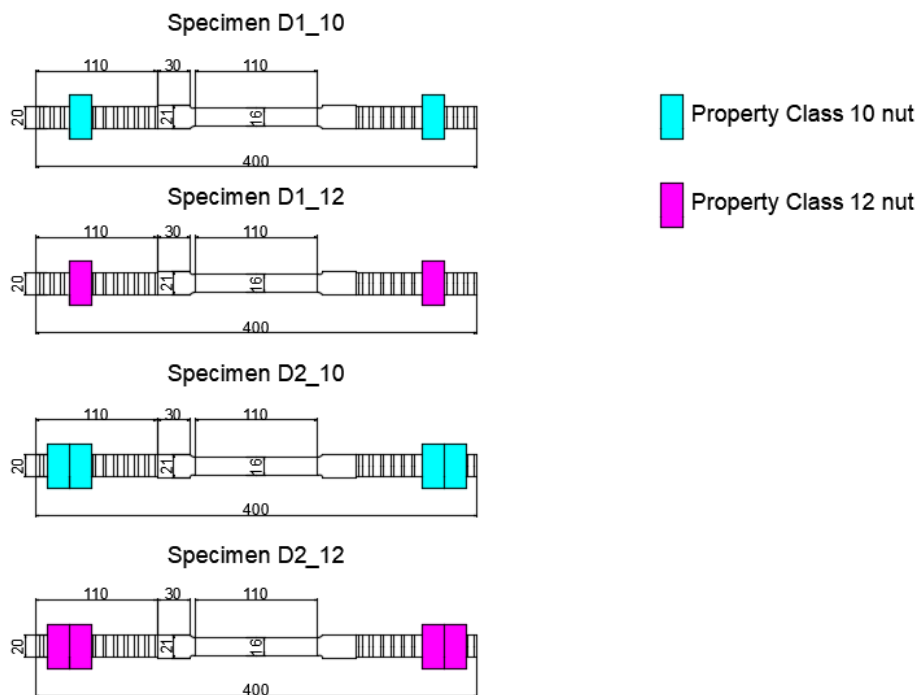


Figure 4-9 Nut-bar assembly test specimens

4.3.1 Set-up and instrumentation

Ad hoc set-up was designed for the nut-bar assembly tests and it is shown in Figure 4-10. It consists of a couple of steel casings pulled by the test machine (UTM), in which the specimen is inserted.

The plates of the casings were designed to have thickness values in order to be infinitely rigid and not deform during the tests.

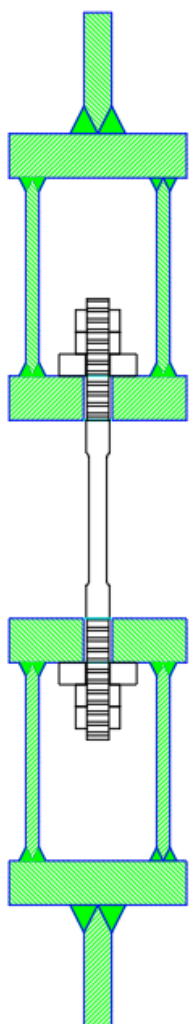


Figure 4-10 Bar-nut assembly test set-up

4.3.2 Results

Results for all the specimens in term of load vs. displacement curve are presented in Figure 4-11, where F represents the load measured, whereas δ represents the displacement imposed. According to experimental results, all assemblies with one nut having property Class equal to 10 (D1_10_1 and D1_10_2) had a brittle failure of nut and the ultimate tension resistance of bar was not achieved. Instead, for all the specimens with two nuts having property

Class equal to 10 (D2_10_1, D2_10_2 and D2_10_3) and one nut having property Class equal to 12 (D1_12_1, D_1_12_2 and D1_12_3) the tension failure of bar happened, as represented in Figure 4-12 .

Starting from results of bar-nut assembly tension tests, the use of one nut with property Class equal to 12 was selected for the walls in a first stage. However, this preliminary choice was not successful and in the first wall monotonic test (M_L1 in Section 6.1) a brittle failure of nut happened. For this reason, in all further wall tests two nuts with property Class equal to 12 were adopted.

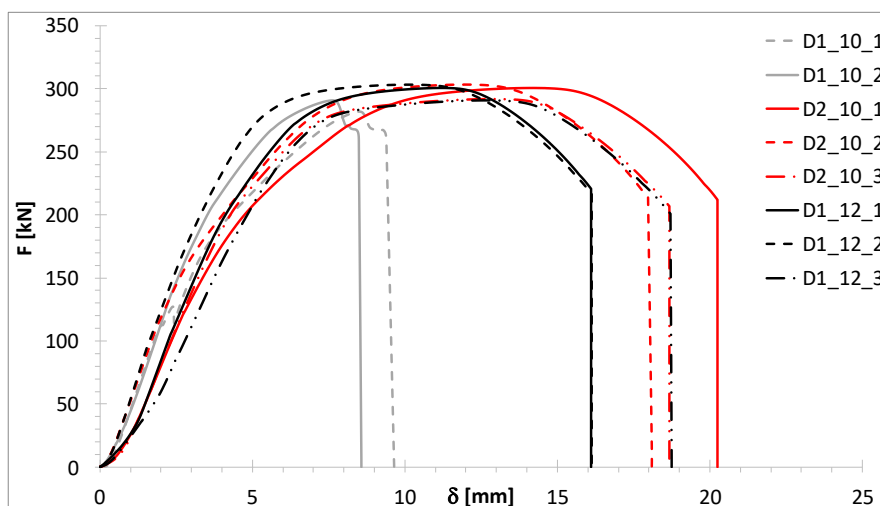


Figure 4-11 Results of bar-nut assembly tests



a) D2_12_1 before test b) D2_12_1 after test

Figure 4-12 Example of test with two 12 property Class nuts

4.4 Full-scale wall tests

The main core of the research project was the evaluation of seismic behaviour of the innovative wall system. To this purpose, five tests, including three monotonic tests and two cyclic tests, were carried out on full-scale 2400 mm long and 2800 mm high wall specimens. In this Chapter all the aspects of the full-scale wall tests are provided. In particular, Section 4.4.1 describes the specimen tested, Section 4.4.2 gives information about set-up produced for the tests, Section 4.4.3 defines the instrumentation used and its location, Section 4.4.4 and Section 4.4.5 summarize the protocols and the results of monotonic and cyclic tests, respectively, Section 4.4.6 discusses results obtained, evaluating the response, the validity and the limitations of the innovative wall system.

4.4.1 Specimen description and test program

Two configurations of the innovative wall system have been investigated, which were representative of Light (L) and Medium (M) configurations developed, as introduced in Section 3.1.1.

The label defines the specimen typology. Namely, the first letter indicates the test typology (M for monotonic test and C for reversed cyclic test), the second letter is referred to the wall specimen (L for specimen representative of Light configuration and M for specimen representative of Medium configuration) and the number represents the test number; e.g. M_L1 means the monotonic test no. 1 carried out on the specimen representative of the Light wall configuration. Specimen configurations are represented in Figure 4-13 and Figure 4-14.

In both configurations and for both protocols used, the bars were pre-tensioned before starting the test via a torque wrench, as shown in

Innovative Lightweight Steel System braced with UHS Steel Bars



Figure 4-13 L Configuration wall tested

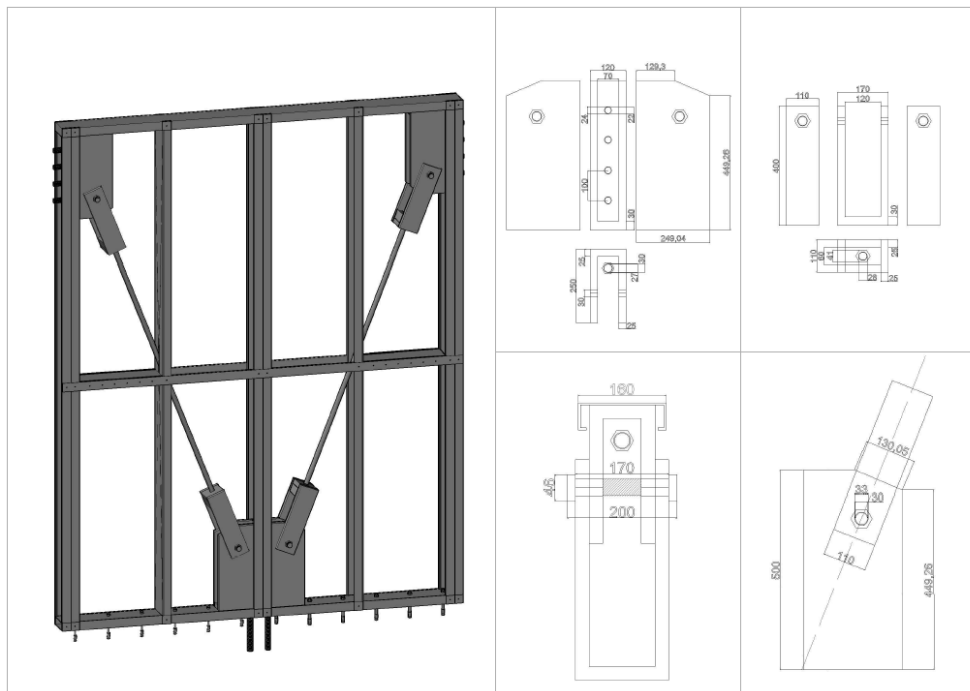




Figure 4-14 M Configuration wall tested



Figure 4-15 Torque wrench used for pretension

Table 4-3 Test matrix for the monotonic and cyclic tests on full-scale walls

Test Label	Wall type	Load Type	Protocol	Number of tests
M_L	Light	Monotonic	-	2
M_M	Medium	Monotonic	-	1
C_L	Light	Cyclic	CUREE	1
C_M	Medium	Cyclic	CUREE	1

4.4.2 Set-up

An available steel frame set-up for in-plane wall tests was modified and used for the experimental activity (Figure 4-16). The wall prototype was restrained to the laboratory strong floor by the bottom beam, which has a $300 \times 180 \times 30$ (width \times height \times thickness) rectangular hollow section. Horizontal loads were transmitted to the wall through the loading beam, which has a $200 \times 120 \times 10$ mm (width \times height \times thickness) rectangular hollow section. The out-of-plane displacements of the wall were restrained by two steel portal frames equipped with roller wheels. The tests were performed by using a hydraulic actuator having a stroke displacement of 500 mm and a load capacity of 500 kN. A sliding-hinge was placed between the loading actuator and the loading beam, in order to avoid vertical load components.

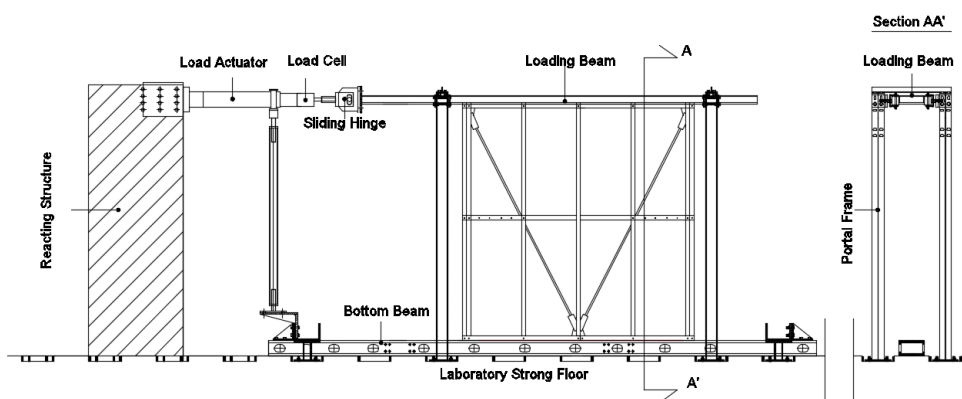




Figure 4-16 Wall test set-up

4.4.3 Instrumentation

Six LVDTs and two potentiometers were used to measure the specimen displacements. In particular, three LVDTs (L1, L2 and L3) were installed to record hold-down horizontal and vertical displacements, two LVDTs (L4 and L5) for the upper beam vertical displacements, one LVDT (L6) for wall vertical displacements and two potentiometers (P1 and P2) for wall horizontal displacements. The strains in selected points of the diagonal bars and studs were recorded by means of fourteen strain-gauges. Two strain-gauges were installed on each diagonal (SG1 and SG2 placed near the middle section, where the diameter is reduced, and SG3 and SG4 placed where the section is maximum), four strain gauges were placed on the intermediate stud in two sections (SG5 and SG6 placed on the upper section, SG7 and SG8 on the lower

Innovative Lightweight Steel System braced with UHS Steel Bars

section) and six strain gauges were placed on the right chord stud (SG9, SG10 and SG11 placed on the upper section and SG12, SG13 and SG14 placed on the lower section). The instrumentation location is shown in Figure 4-17 and some pictures are shown in Figure 4-18. A load cell was used to measure the applied loads.

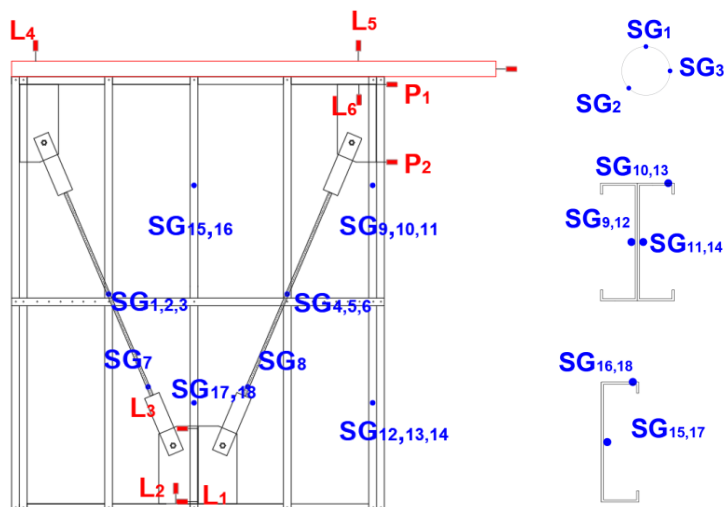


Figure 4-17 Wall test instrumentation



Figure 4-18 Photographs of wall test instrumentation

4.4.4 Monotonic tests

Monotonic tests were carried out with displacements imposed at a rate of 0.10 mm/s until the collapse of specimens occurred. The data were recorded with a sampling frequency equal to 10 Hz.

Three monotonic tests were carried out on two L and one M walls. Results for M_L1, M_L2 and C_L1 specimens are provided in Figure 4-19, Figure 4-20 and Figure 4-21, in term of load (H) vs. inter-storey drift ratio (dr) curves. The displacements used for the evaluation of inter-storey drifts were measured by potentiometer P1, whereas load was provided by load cell. Since the P1 had a damage during the M_L1 test, extrapolation of the initial data of P1 (red continuous line), also considering the displacement measurements obtained

from UTM, was considered and it is represented by the dashed curve in Figure 4-19.

Numerical values are provided in Table 4-4, according to the following parameters:

- H_0 : wall strength corresponding to the end of the Phase (1);
- H_e : wall conventional yield strength evaluated according to ECCS procedure [9];
- H_y : wall strength corresponding to the end of the Phase (2);
- H_p : maximum recorded load corresponding to the end of the Phase (3);
- d_e : yield displacement evaluated according to ECCS procedure [54];
- d_{max} : maximum displacement, evaluated in correspondence of H_p
- $d_{r,e}$: yield inter-storey drift ratio, equal to d_e/h ;
- $d_{r,max}$: maximum inter-storey drift ratio, equal to d_{max}/h ;
- k_e : initial elastic stiffness corresponding to the tangent to initial part of the response curve, equal to H_e/d_e ;
- μ : ductility, equal to the ratio between the conventional ultimate displacement and displacement at conventional elastic limit load d_{max}/d_e or equally $d_{r,max}/d_{r,e}$.

Globally, for all the specimens the monotonic response confirmed the three-phase lateral behaviour described in Chapter 3. In particular, the curves are characterized by three different branches: (1) the first linear branch with a stiffness k_e ; (2) once achieved H_0 , the second branch characterised by a linear response having a stiffness smaller than k_e ; (3) once achieved H_y , the third branch characterised by a nonlinear response.

M_L2 and M_M1 specimens showed the same collapse due to the tension failure of the bar, whereas in M_L1 specimen, during the phase (3), nut failure

happened, since only one 12 property Class nut was employed. The collapse mechanisms are provided in Figure 4-22, Figure 4-23 and Figure 4-24.

Comparing the results of two nominal identical tests, M_L1 and M_L2, can be noticed that:

- small differences in terms of H_y and H_p were revealed, equal to about 3% and 1%, respectively;
- high differences in term of inter-storey drift ratios achieved were registered, equal to about 19 and 51% for $d_{r,e}$ and $d_{r,max}$, respectively, since the M_L1 showed a brittle nut failure.

Comparison among monotonic curves is reported in Figure 4-25.

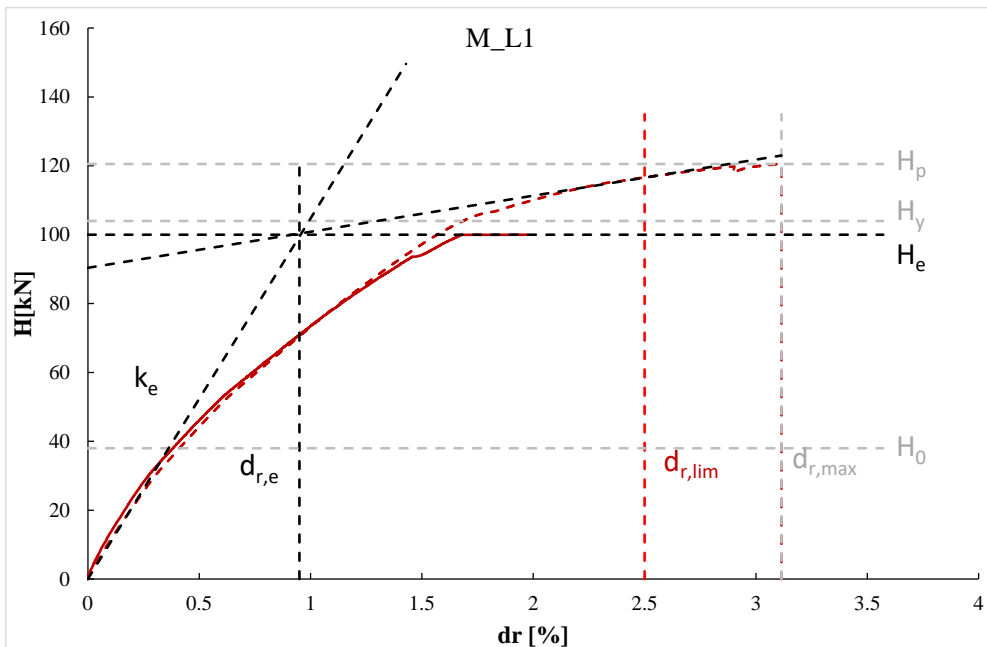


Figure 4-19 Results of M_L1 test

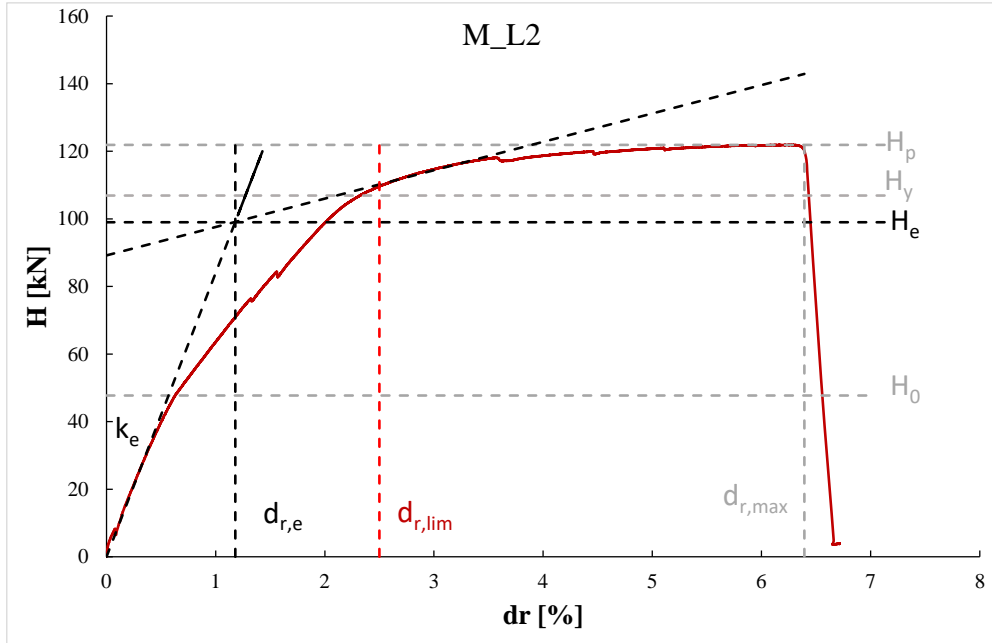


Figure 4-20 Results of M_L2 test

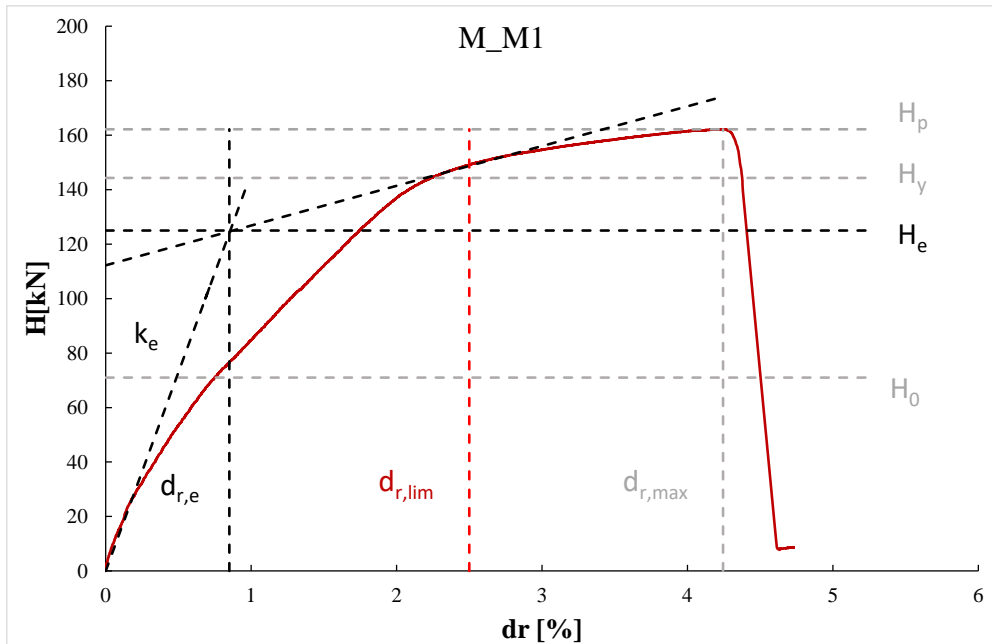


Figure 4-21 Results of M_M1 test



Figure 4-22 M_L1 test: collapse mechanism

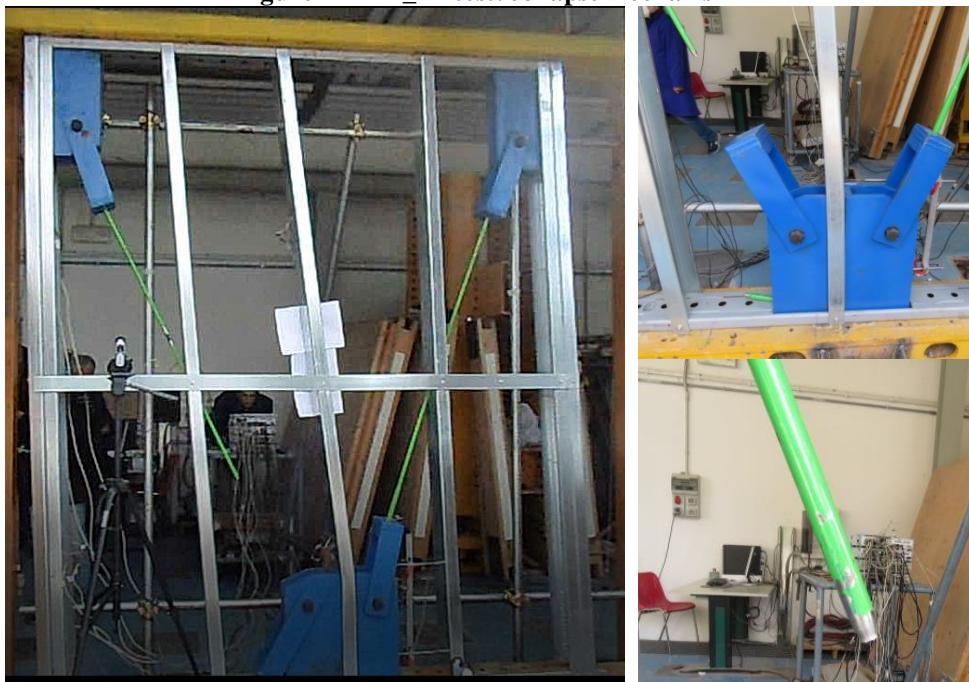


Figure 4-23 M_L2 test: collapse mechanism



Figure 4-24 M_M1 test: collapse mechanism

Table 4-4 Monotonic test results

Test	M_L1	M_L2	M_M1
H₀ [kN]	37.99	47.73	71.01
H_e [kN]	100.00	99.00	125.00
H_y [kN]	103.99	106.90	144.32
H_p [kN]	120.54	121.89	162.18
d_e [mm]	26.60	33.04	23.80
d_{max} [mm]	87.21	179.01	118.86
d_{r,e} [%]	0.95	1.18	0.85
d_{r,max} [%]	3.11	6.39	4.25
k_e [kN/mm]	3.76	3.00	5.25
μ [-]	3.28	5.42	4.99

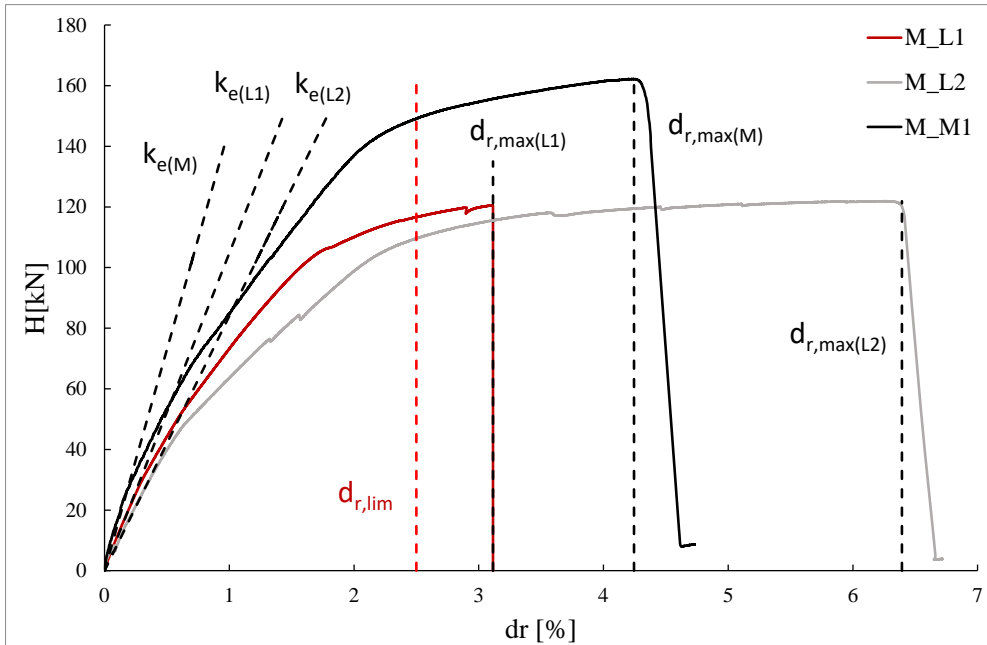


Figure 4-25 Comparison among monotonic curves

4.4.5 Reversed cyclic tests

Cyclic tests were carried out by adopting a loading protocol known as “CUREE ordinary ground motions reversed cyclic load protocol” developed for wood walls by Krawinkler et al. [55], modified according to the prescription given in Velchev et al. [12]). The cyclic loading test protocol consists of a series of stepwise increasing deformation cycles. The displacement amplitudes of each cycle D_i are defined starting from a reference deformation $\Delta = 2.667 \Delta_y$, where Δ_y is the yield displacement obtained from the nominally identical monotonic wall tests. The complete cyclic loading history for a particular wall configuration was then based upon multiples of the reference deformation, Δ . For tested walls the cyclic protocol involved displacements at three different rates (v): 1.0 mm/s, for displacements up to 0.2Δ , 2.0 mm/s for displacements in the range from 0.2Δ to Δ , and 3.0 mm/s for displacement larger than Δ . The general cyclic protocol is summarized in

Innovative Lightweight Steel System braced with UHS Steel Bars

Table 4-5. Since Δ obtained from monotonic results was not really different between L and M configuration, the same specific protocol was adopted for both C_L1 and C_M1 tests and it is shown in Figure 4-26.

Table 4-5 General cyclic protocol

No of cycles	Step i	D_i	v (mm/s)
6	1	0.05Δ	1.0
1 6	2	$D_2=0.075 \Delta$ $0.75D_2$	
1 6	3	$D_3=0.1 \Delta$ $0.75 D_3$	
1 3	4	$D_4=0.2 \Delta$ $0.75 D_4$	2.0
1 3	5	$D_5=0.3 \Delta$ $0.75 D_5$	
1 2	6	$D_6=0.4 \Delta$ $0.75 D_6$	
1 2	7	$D_7=0.7 \Delta$ $0.75 D_7$	
1 2	8	$D_8= \Delta$ $0.75 * D_8$	3.0
1 2	9	$D_9=0.5 \Delta + D_8$ $0.75 * D_9$	
1 2	n	$D_n=0.5 \Delta + D_{(n-1)}$ $0.75 D_n$	

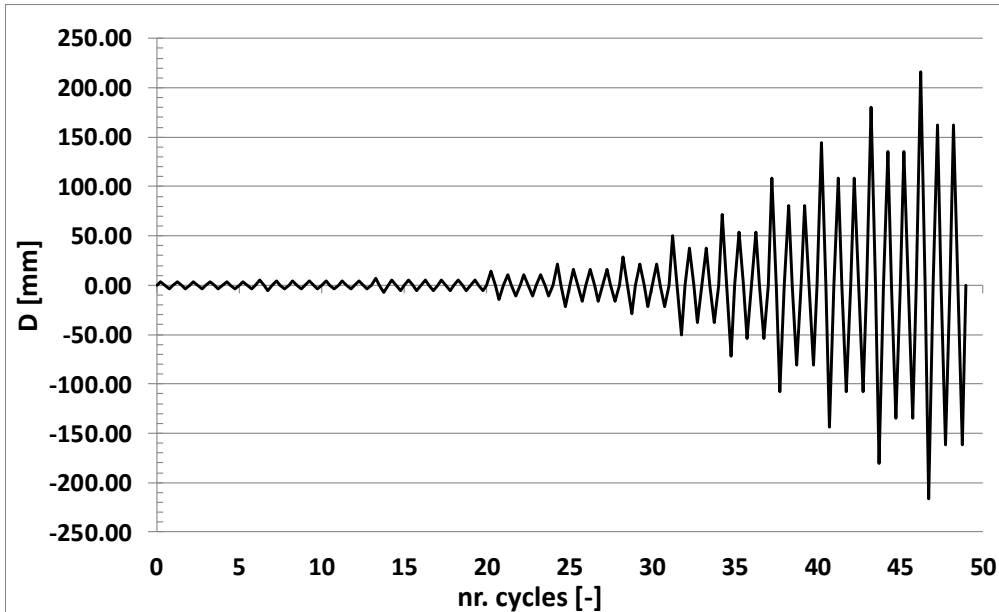


Figure 4-26 CUREE cyclic protocol adopted for C_L1 and C_M1 tests

Results of cyclic tests are described in terms of load (H) vs. inter-storey drift ratio (d_r) curve (Figure 4-27 and Figure 4-28) and according to the same parameters used for monotonic results, considering the pushing phase envelope, since in both tests walls collapse happened in pushing:

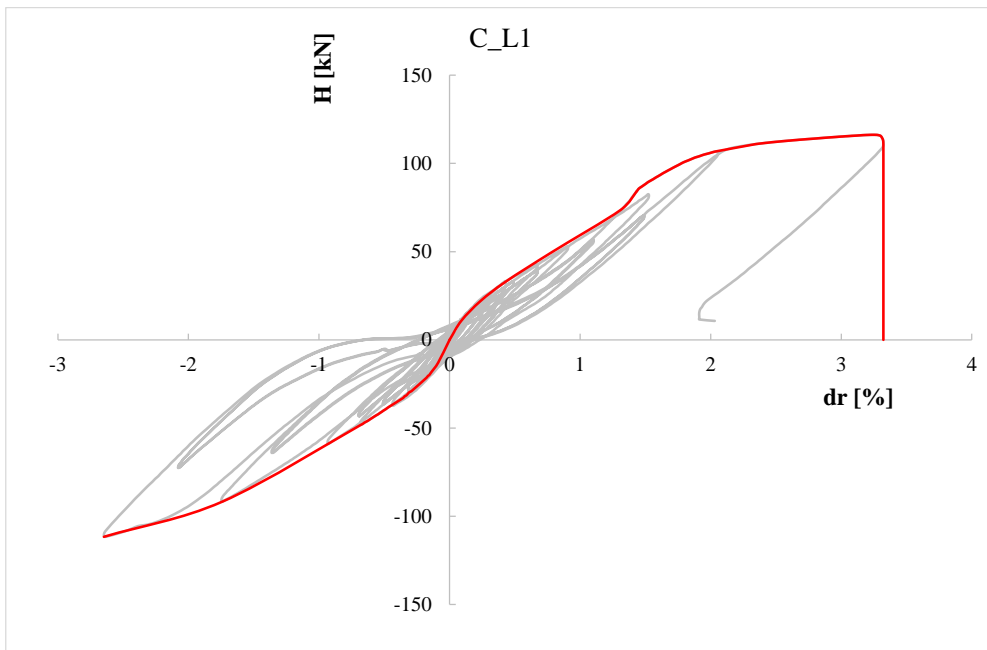
- H_0 : wall strength corresponding to the end of the Phase (1);
- H_e : wall conventional yield strength evaluated according to ECCS procedure [9];
- H_y : wall strength corresponding to the end of the Phase (2);
- H_p : maximum recorded load corresponding to the end of the Phase (3);
- d_e : yield displacement evaluated according to ECCS procedure [54];
- d_{max} : maximum displacement, evaluated in correspondence of H_p
- $d_{r,e}$: yield inter-storey drift ratio, equal to d_e/h ;
- $d_{r,max}$: maximum inter-storey drift ratio, equal to d_{max}/h ;
- k_e : initial elastic stiffness corresponding to the tangent to initial part of the response curve, equal to H_e/d_e ;

Innovative Lightweight Steel System braced with UHS Steel Bars

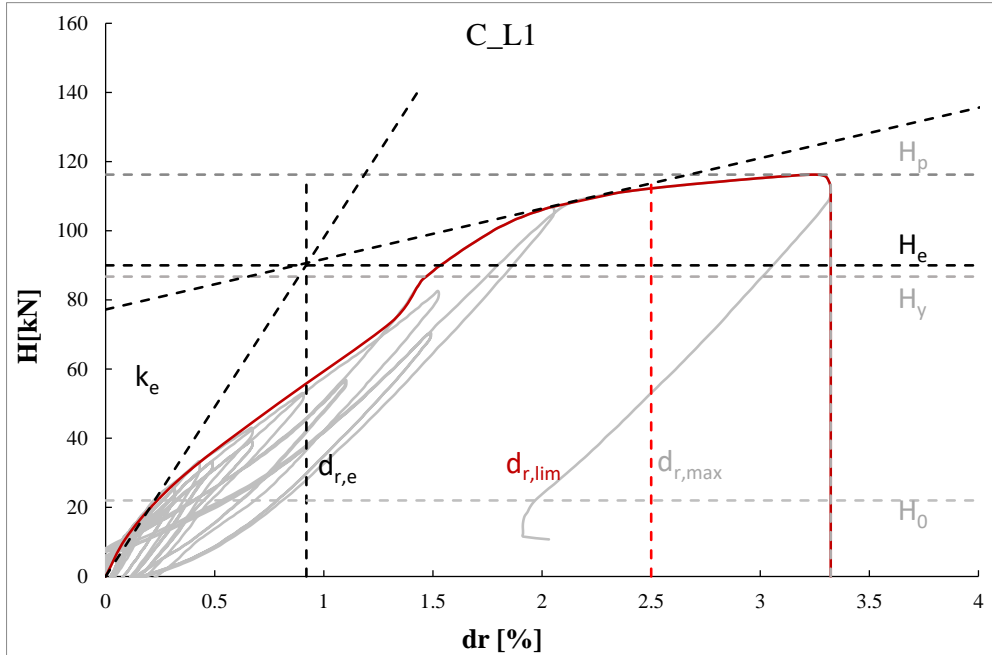
- μ : ductility, equal to the ratio between the conventional ultimate displacement and displacement at conventional elastic limit load d_{\max}/d_e or equally $d_{r,\max}/d_{r,e}$.

The cyclic curves obtained (Figure 4-27 and Figure 4-28) showed a behaviour rather symmetrical. The three-phase behaviour also characterized the cyclic response, but only in pushing. In fact, for both specimens collapse happened immediately reached the Phase (3) in pushing (positive range), whereas in pulling (negative range) the Phase (3) was not reached. Table 4-6 summarizes numerical results obtained. Comparison between the two cyclic envelopes is shown in Figure 4-29.

Both C_L1 and C_M1 specimens had the same collapse due to the tension failure of the bar, as shown in Figure 4-30 and Figure 4-31.

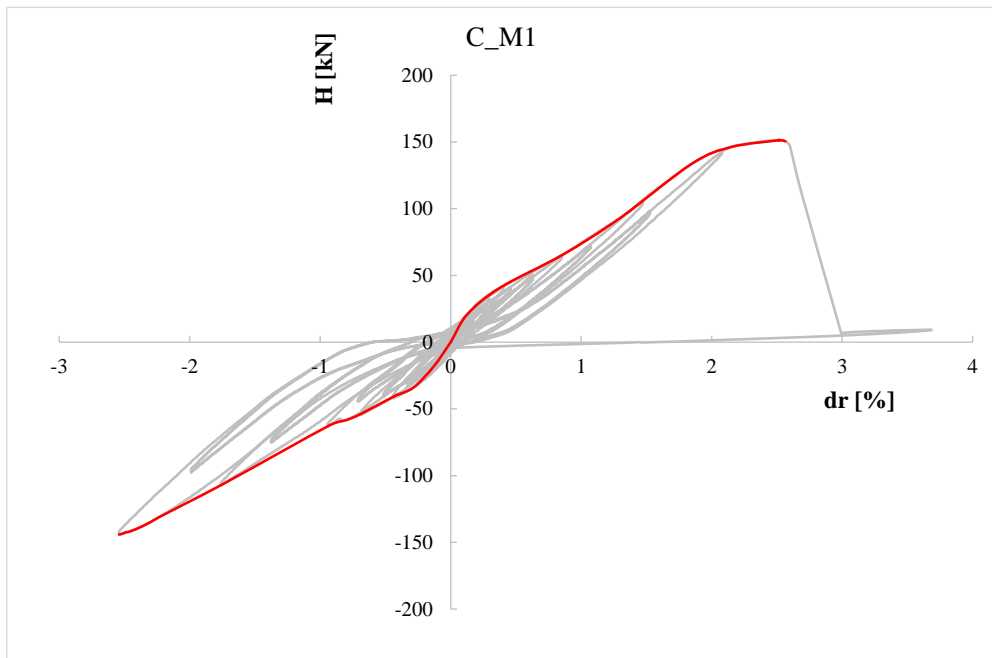


a) Cyclic response

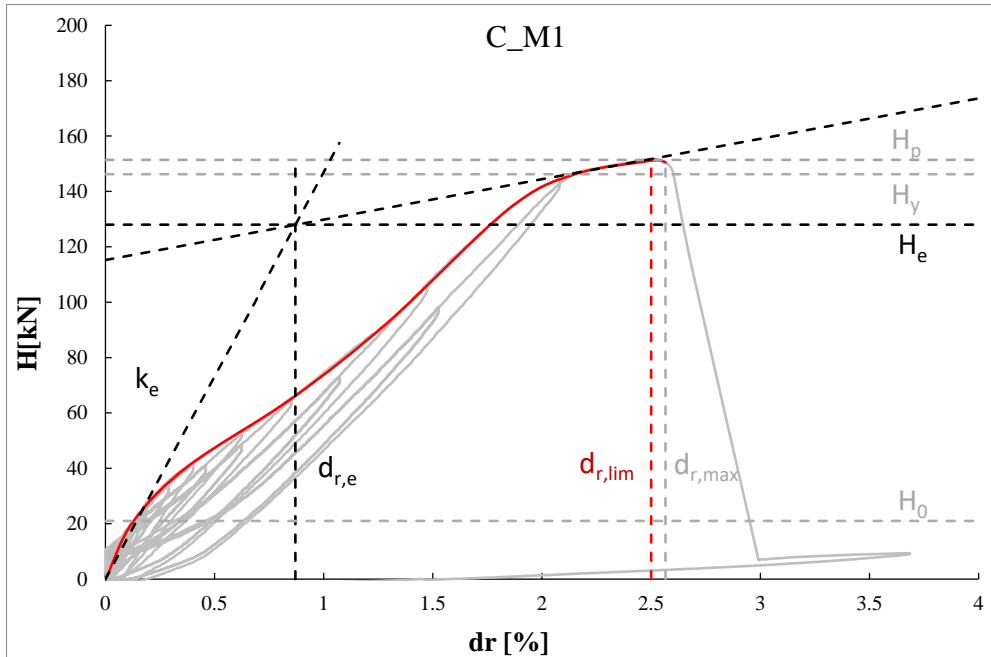


b) Pushing phase envelope

Figure 4-27 Cyclic response and envelope for C_L1 test



a) Cyclic response



b) Pushing phase envelope

Figure 4-28 Cyclic response and envelope for C_M1 test

Table 4-6 Cyclic test results

Test	C_L1	C_M1
H_0 [kN]	22.00	21.00
H_e [kN]	90.00	128.00
H_y [kN]	86.75	146.22
H_p [kN]	116.24	151.40
d_e [mm]	25.76	24.36
d_{max} [mm]	70.60	71.84
$d_{r,e}$ [%]	0.92	0.87
$d_{r,max}$ [%]	3.32	2.57
k_e [kN/mm]	3.49	5.25
μ [-]	3.61	2.95

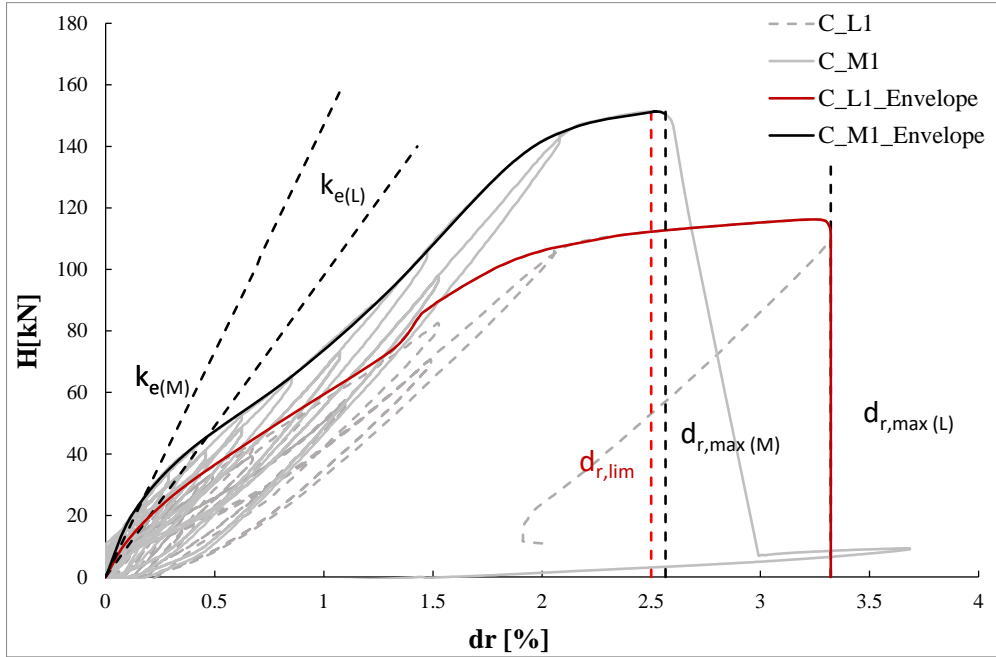


Figure 4-29 Comparison between cyclic tests



Figure 4-30 C_L1 test: collapse mechanism



Figure 4-31 C_M1 test: collapse mechanism

4.4.6 Discussion of results

The global behaviour of the innovative wall was evaluated through the measurements obtained during monotonic and cyclic tests. Thanks to potentiometers P1 and P2 the wall lateral behaviour was individuated and commented in Sections 4.4.4 and 4.4.5. More considerations can be done, if a comparison between monotonic and cyclic results of nominally identical specimens (Figure 4-32 and Figure 4-33) is conducted and, in particular, considering M_L2 and M_M1 as monotonic tests and C_L1 and C_M1 as

cyclic tests. Results of M_L1 were not considered, since it showed nut failure, instead of tension collapse of bar. It can be observed that:

- Cyclic protocol does not affect greatly the resistance of wall, in fact, monotonic and cyclic H_p difference is equal to about 5% and 7% for L and M configuration, respectively;
- Cyclic protocol greatly affects the displacement capacity of wall, indeed the ductility of wall. In fact, difference in term of $d_{r,max}$ is equal to about 92% and 65% for L and M configuration, respectively;
- Monotonic and cyclic elastic stiffness exhibited similar values for both L and M configurations (3.00 and 3.49 kN/mm for L configuration and 5.25 and 5.25 for M configuration).

The data obtained from LVDTs make possible the evaluation of hold-down stiffness and, in particular, three stiffnesses were evaluated: vertical stiffness k_v , horizontal stiffness k_h and rotational stiffness k_r . The adding source of deformability $1/k_{tot}$ produced by hold-downs was evaluated, according to Equation 4-4, and it was in the range $2-3 \times 10^{-5}$.

$$\text{Equation 4-4}$$
$$\frac{1}{k_{tot}} = \frac{1}{k_1 + k_2 + 2k_h}$$

Where k_1 and k_2 are the adding source of global stiffnesses to vertical translation and rotation offered by hold-downs and are evaluated with Equation 4-5 and Equation 4-6.

$$\text{Equation 4-5}$$

$$k_1 = \frac{k_r}{h^2}$$

$$\text{Equation 4-6}$$

$$k_2 = \frac{L^2}{h^2} k_v$$

Therefore, from the results, it can be assumed that hold-downs are rigid and offer a perfectly rigid restrain to the system.

Innovative Lightweight Steel System braced with UHS Steel Bars

Furthermore, through the local measurements given by SG, it was possible to evaluate the distribution of stresses and quantify the horizontal load absorbed by the frame and by the bracing. According to results, the contribution offered by the frame is really important, absorbing 50% of total horizontal load applied to the wall.

In the end, the experimental yield strength H_y achieved during tests was also compared with the theoretical expected wall strength $H_{y,th}$, evaluated according Equation 3-5, considering the measured average properties instead of nominal properties, and the design wall strength $H_{y,d}$ (Table 3-1 in Section 3.1.1). The comparison between $H_{y,th}$ and H_y exhibits that theoretical prevision well catches experimental values with a ratio $H_{y,th}/H_y$ in the range 0.94-1.01. The comparison between $H_{y,d}$ (Table 3-1 in Section 3.1.1) and H_y , whereas, shows that design values always underestimate the experimental values with a ratio $H_y/H_{y,d}$ in the range 1.22-1.29.

As far as inter-storey drift ratios are concerned, experimental values achieved were in the range 2.6%-6.8% and were always higher than design limit drift ratio considered (2.5%).

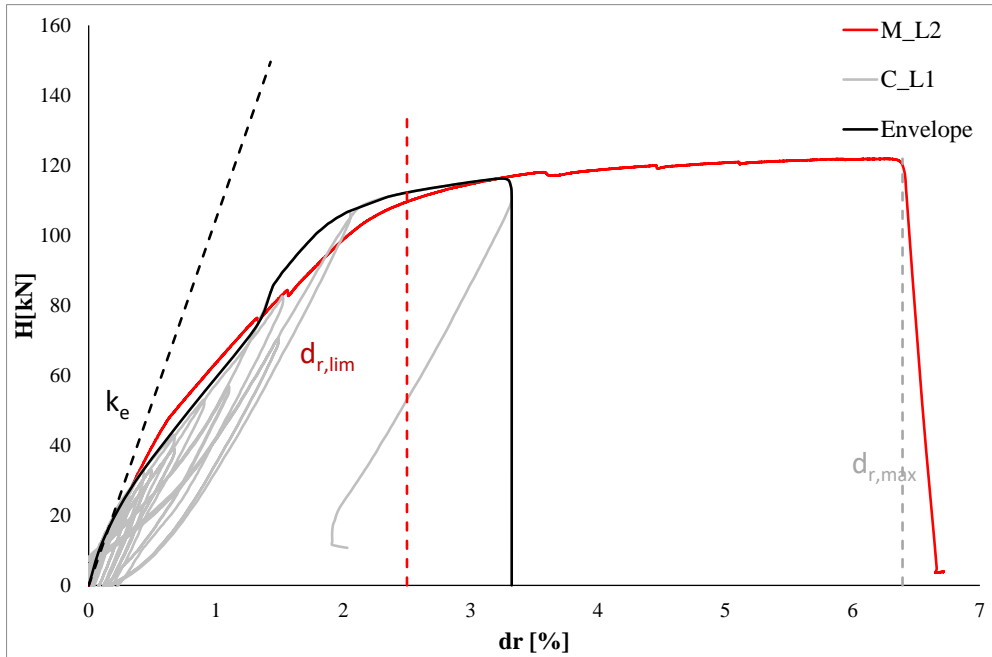


Figure 4-32 Comparison between M_L2 and C_L1 tests

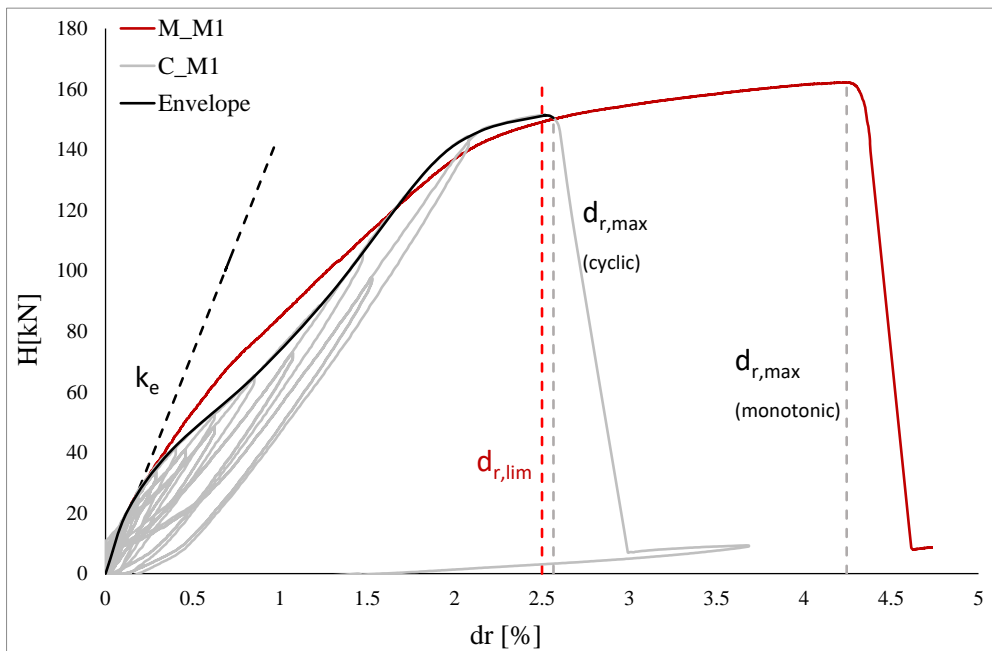


Figure 4-33 Comparison between M_M1 and C_M1 tests

4.4.7 Experimental evaluation of behaviour factor

A preliminary experimentally based evaluation of behaviour factor was conducted. The behaviour factor (q) was defined by the ductility-related (R_d) and overstrength-related (R_0) modification factors.

In particular, the ductility-related modification factor R_d represents the ability of the structural system to dissipate seismic energy, whereas the overstrength-related modification factor R_0 represents the reserve of strength of the designed structure. The behaviour factor (q) can be estimated using Equation 4-7, as given in Uang [56]:

Equation 4-7

$$q = R_d \cdot R_0$$

Since fundamental periods for this structural system is generally in the range 0.1-0.5 s, the ductility-related force modification factor R_d can be evaluated according to the principle of equal energy (Equation 4-8):

Equation 4-8

$$R_d = \sqrt{2\mu - 1}$$

where μ is the ductility.

The R_0 factor can be evaluated through the formulation provided by Mitchell et al. [57]:

Equation 4-9

$$R_0 = R_{sd} \cdot R_\phi \cdot R_{yield} \cdot R_{sh}$$

where $R_{sd} = H_c/H_d$, with H_c and H_d design wall resistance and seismic demand, respectively;

$R_\phi = H_{yn}/H_c$, with H_{yn} design resistance associated by yielding of the braces multiplied by the safety factor γ_{M0} ;

$R_{yield} = H_y/H_{yn}$, with H_y experimental yielding resistance;

$R_{sh} = H_p/H_y$, with H_p experimental wall strength.

Innovative Lightweight Steel System braced with UHS Steel Bars

In order to neglect the design overstrength, in this study the assumption of $R_{sd} = H_c/H_d = 1$ has been made. Therefore, the R_0 factor can be evaluated through Equation 4-10:

$$\text{Equation 4-10}$$
$$R_0 = \frac{H_{yn}}{H_c} \cdot \frac{H_y}{H_{yn}} \cdot \frac{H_p}{H_y} = \frac{H_p}{H_c}$$

Table 4-7 shows the values of the behaviour factors obtained by the test-based evaluation. For the cyclic tests R_0 , R_d and q were evaluated considering the average values in pushing and pulling phases. The test M_L1 was not considered since it showed a brittle premature failure. The average test-based values of behaviour factors are in the range of 3.09- 4.07 for the L Configuration and 3.67- 4.07 for the M Configuration. On the safe side, it can be concluded that a value of behaviour factor equal to 3 can be assumed for the L configuration and a value equal to 2.5 for the M Configuration.

Table 4-7 Test-based evaluation of behaviour factor

Test	M_L2	M_M1	C_L1	C_M1
μ	5,42	4,99	3,61	2,95
R_d	3,14	3,00	2,49	2,21
R_0	1,30	1,22	1,24	1,14
q	4,07	3,67	3,09	2,53

5 Thermal analysis of the building envelope solutions and energetic analysis of the prototype building

The most important strategy to reduce the building energy consumption is improving the thermal performance of the building envelope. Indeed, firstly thermal analysis of building envelope needs to be carried out, which mainly consists of the evaluation of thermal properties, considering also the thermal bridges. Then, the energy performance of the whole building may be evaluated, through numerical simulations. In this Chapter, after the introduction of basic information on the numerical simulation in COMSOL and EnergyPlus software (Section 5.1), the simulations performed on the building envelope solutions developed (Section 5.2) and the prototype building (Section 5.3) are provided, and results obtained are discussed.

5.1 Basics

As introduced in Chapter 3, the analysis of the building envelope is conducted according to ISO 10211:2007 [51], in which the steady state approach allows to calculate the equivalent thermal transmittance, taking into account all repeating and non-repeating (geometrical) thermal bridges. Since the material properties are defined, the U-value of the external wall, without taking into account the thermal bridge (U_{clear}), can be calculated according to the ISO 6946 [35]. The U_{clear} obtained for the materials used for both A and B solutions are shown in Table 5-1.

After that, it is necessary to evaluate the thermal bridges, identifying and classifying them (repeating/non-repeating and linear/point), simulate all the thermal bridge configurations by means of COMSOL software at steady state conditions and calculate the equivalent thermal transmittance, including thermal bridges. The detailed procedure to evaluate the equivalent thermal properties is provided in Section 5.3. Once equivalent thermal properties are defined, the EnergyPlus model can be built and analysed, in order to obtain the energy performance of the whole building.

Innovative Lightweight Steel System braced with UHS Steel Bars

Table 5-1 Evaluation of U_{clear} for both solutions

SOLUTION A				
Material	thickness [cm]	thermal conductivity [W/mK]	Rlayer [m²K/W]	U-clear [W/m²K]
AquaPanel	15	0.19	0.08	
Rockwool	50	0.03	1.52	
OSB panel	20	0.10	0.20	
Rockwool	140	0.03	4.24	0.15
Air Cavity	40	0.33	0.12	
OSB panel	20	0.10	0.20	
Gypsum Board	30	0.27	0.11	
SOLUTION B				
Material	thickness [cm]	thermal conductivity [W/mK]	Rlayer [m²K/W]	U-clear [W/m²K]
Rockpanel	1	0.37	0.00	
Air Cavity	40	0.33	0.12	
Rockwool	60	0.03	1.82	
OSB panel	20	0.10	0.20	
Rockwool	140	0.03	4.24	0.14
Air Cavity	40	0.33	0.12	
OSB panel	20	0.10	0.20	
Air Cavity	50	0.33	0.15	
Gypsum Board	30	0.27	0.11	

5.2 Numerical simulation of the thermal behaviour of the innovative wall

Evaluating the thermal behaviour of the innovative wall means calculating the thermal transmittance of the wall (U-value). Once known the geometry and the layers of the building envelope, the U-value of the external wall, without taking into account the thermal bridge (U_{clear}), can be easily calculated according to the ISO 6946 [35]. Although, this value is greatly affected by the presence of thermal bridges, which increases the U-value. The first step consists of the identification of 1D thermal bridges in the system, as described in ISO 10211 [51].

In the case of the innovative wall, studs are repeating thermal bridges, whereas hold-downs and pre-tension device and blocking profiles are point thermal bridges (Figure 5-1). The 1D models of the wall developed to evaluate 1D linear and point thermal bridges are shown in Figure 5-2.

As result, the total heat flow, Φ , which passes through each configuration, is obtained by the simulation. In this way, through use of Equation 3-7 (Section 3.1.2), it is possible to define the U_{overall} . Table 5-2 provides the U_{clear} and the U_{overall} for both A and B solutions. Figure 5-3 and Figure 5-4 show the temperature distribution in the solution A and B, respectively, without and with considering linear and point thermal bridges.

Innovative Lightweight Steel System braced with UHS Steel Bars

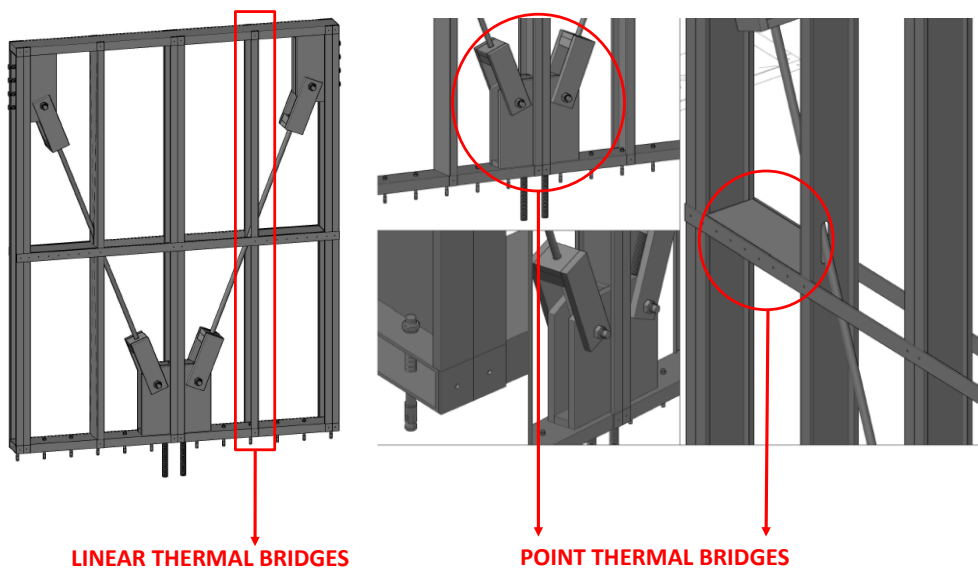
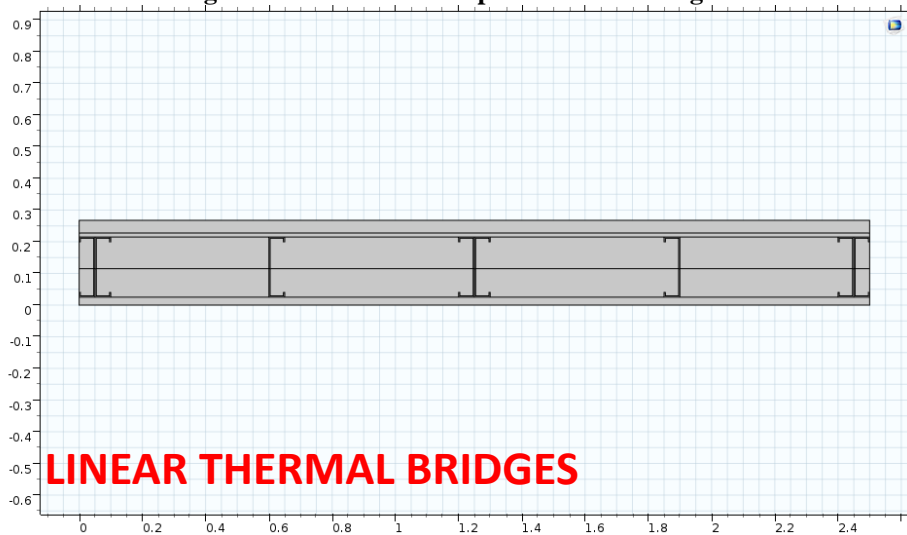


Figure 5-1 1-D linear and point thermal bridges



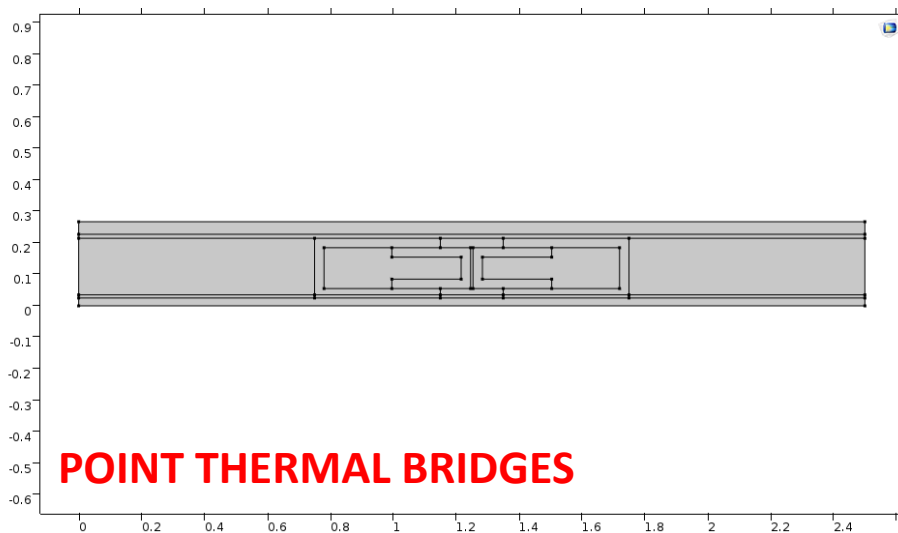
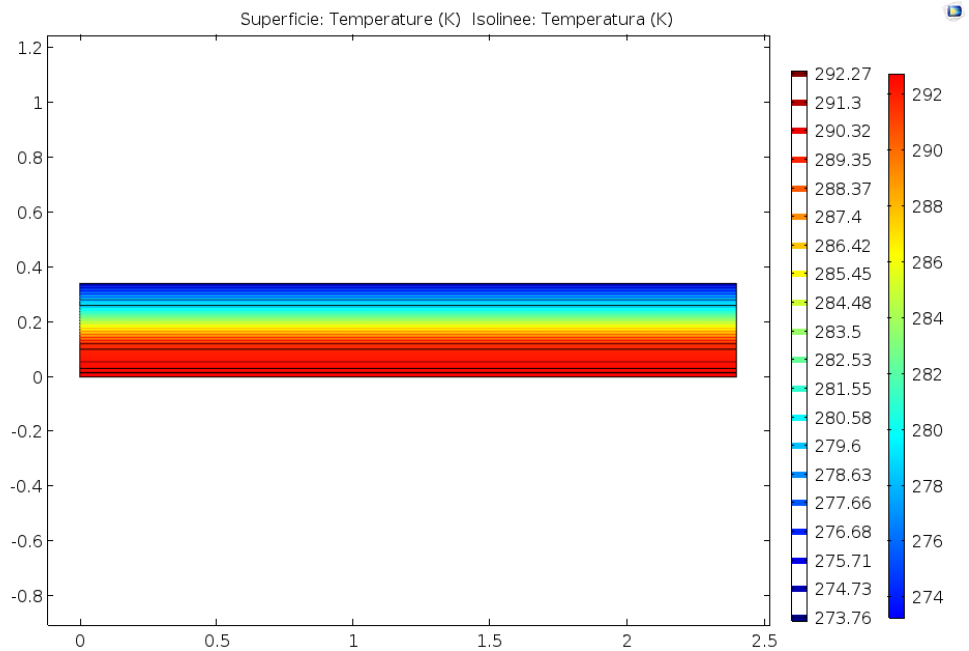


Figure 5-2 1D models of the wall developed

Table 5-2 U_{clear} and the U_{overall} for both A and B solutions

Solution [-]	U-value [W/m ² k]
A	Clear 0.15
	Overall 0.23
B	Clear 0.14
	Overall 0.21

Innovative Lightweight Steel System braced with UHS Steel Bars



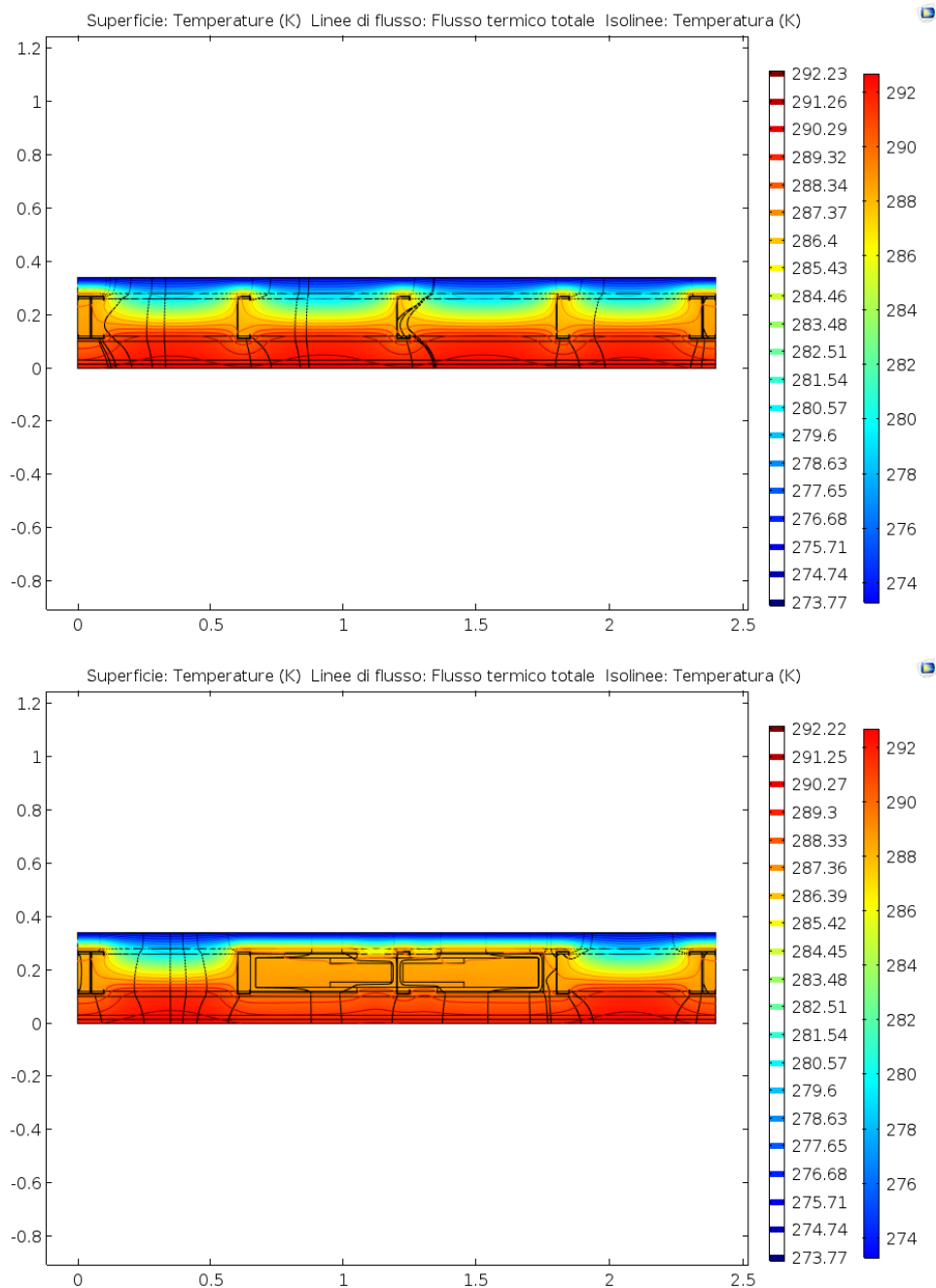
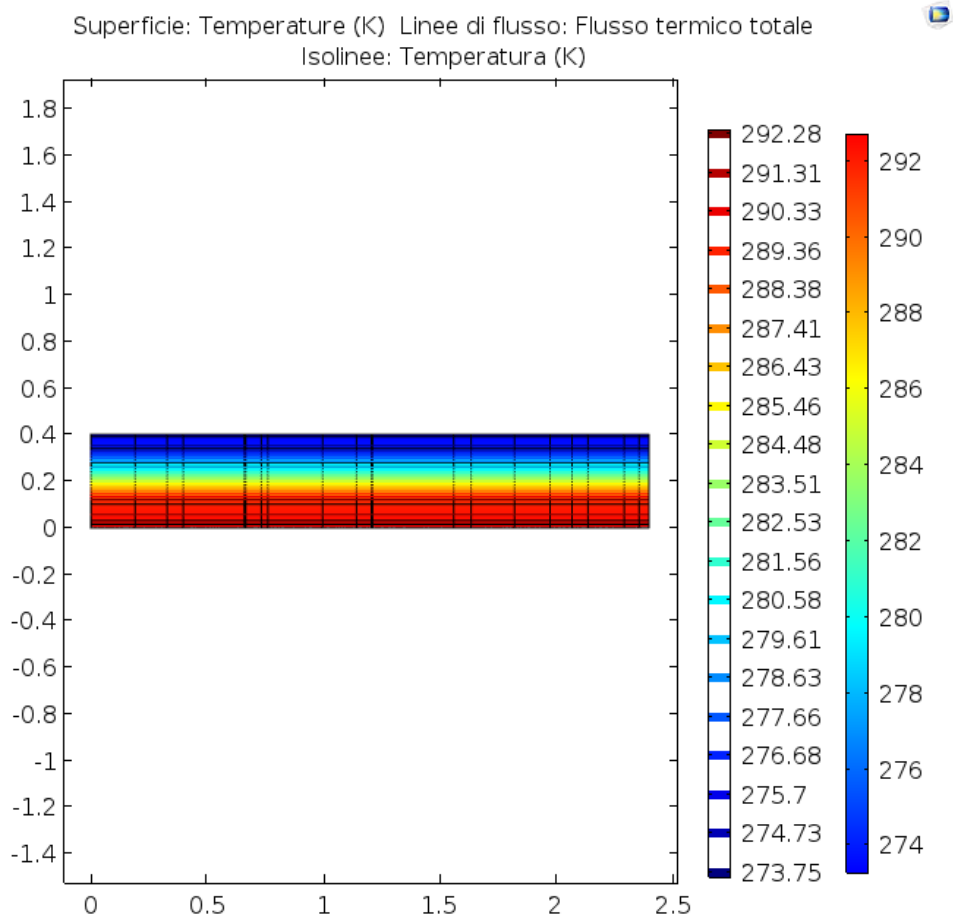
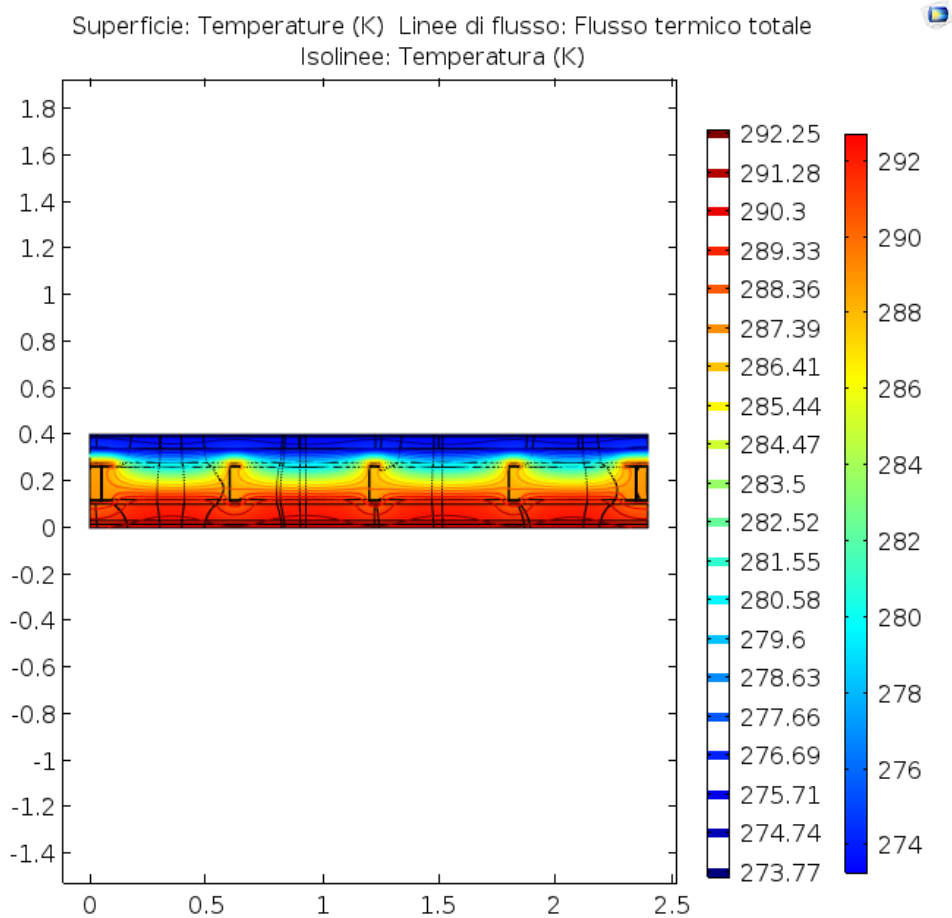


Figure 5-3 Temperature distribution in the solution A, without and with considering linear and point thermal bridges

Innovative Lightweight Steel System braced with UHS Steel Bars



Innovative Lightweight Steel System braced with UHS Steel Bars



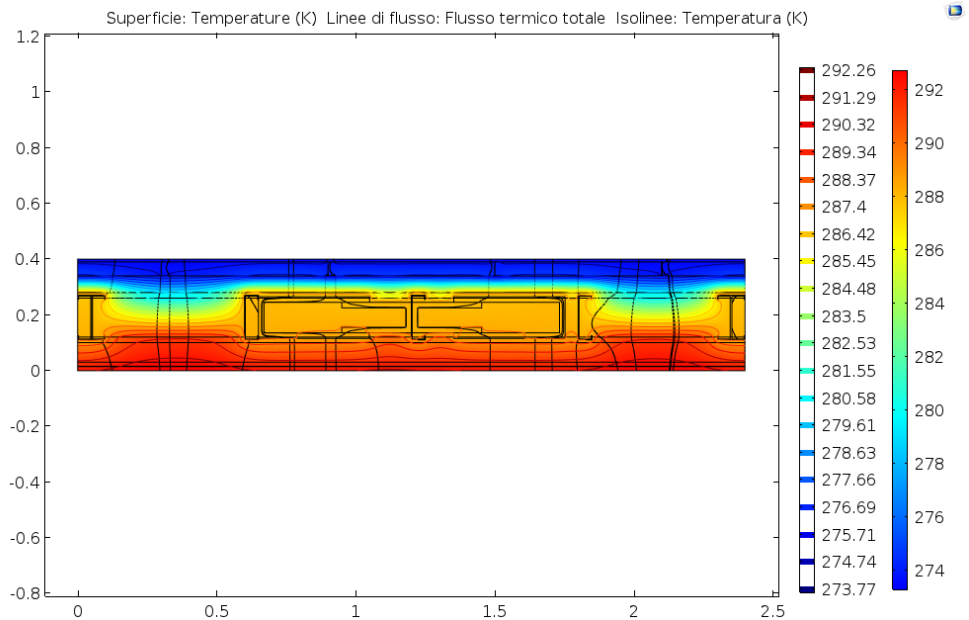


Figure 5-4 Temperature distribution in the solution B, without and with considering linear and point thermal bridges

5.3 Numerical simulation of the energetic behaviour of the prototype building

In order to simulate the energy behaviour of the prototype building, it is necessary individuating the U-value of the system, considering 1D, 2D and 3D thermal bridges, the geometry of the building, the material properties and window properties. Equally to the procedure introduced in Section 5.2, 1-D models of floor and roof were developed to calculate the U_{overall} . Moreover, 2D thermal bridges, as linear non-repeating thermal bridge due to the junction (Figure 5-5), were evaluated and modelled in COMSOL. In the same way 3D thermal bridges were individuated.

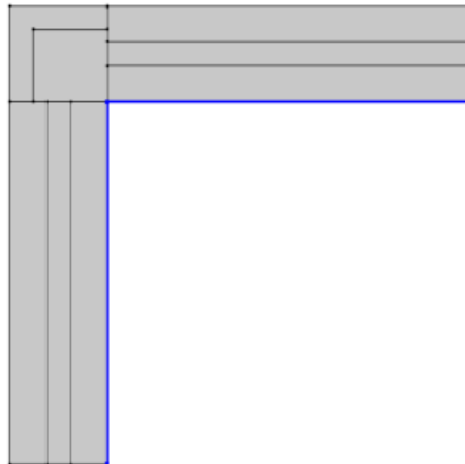


Figure 5-5 2D thermal bridges due to junctions

The geometry of the simulated building is drawn by means of the SketchUp software and imported in EnergyPlus. The roof was modelled as flat, considering the average height of the building. For walls, the two solutions (A and B solutions) developed and introduced in Section 3.1 were adopted. The stratigrafies adopted for floor and roof, instead, are represented in Figure 5-6. In all the cases the same global geometry and triple windows were considered. Starting from the material properties and the COMSOL simulation results, the equivalent thermal transmittance U_{eq} of each envelope element to upload in

the EnergyPlus model was individuated, in order to take into account the effect of all thermal bridges. The equivalent thermal resistance for every layer of each envelope element i , $R_{layer,eq,i}$ is calculated by the Equation 5-1:

$$\text{Equation 5-1}$$

$$R_{layer,eq,i} = \frac{R_{layer,clear,i}}{R_{clear,i}} \cdot R_{eq,i}$$

where $R_{layer,clear,i}$ is the clear thermal resistance of the layer of the element i (i.e. wall, floor and roof); $R_{eq,i}$ is the equivalent thermal resistance of the envelope element i evaluated with the $U_{eq,i}$; $R_{clear,i}$ is the clear thermal resistance of the envelope element i . Since the thickness d_{layer} of each layer is the same for the original and the equivalent element the equivalent thermal conductivity for each layer of the element i , $k_{layer,eq,i}$, can be calculated with Equation 5-2.

$$\text{Equation 5-2}$$

$$k_{layer,eq,i} = \frac{d_{layer,i}}{R_{clear,eq,i}}$$

Also, dynamic thermal properties of the materials were likewise modified, in order to introduce the dynamic impact of thermal bridge, due to the presence of studs. Since studs are generally placed in insulation layer or air cavity or both, only the properties of rockwool layers were modified., according to the methodology described by Gomes et. al [58]. According to this method, the equivalent density, $\rho_{MW,eq,i}$ and specific heat capacity, $C_{pMW,eq,i}$ can be calculated by Equation 5-3 and Equation 5-4:

$$\text{Equation 5-3}$$

$$\rho_{MW,eq,i} = w_{studs,i} \rho_{steel} + w_{RW,i} \rho_{RW}$$

$$\text{Equation 5-4}$$

$$C_{pMW,eq,i} = w_{studs,i} C_{p_{steel}} + w_{RW,i} C_{p_{RW}}$$

where $w_{studs,i}$ and $w_{RW,i}$ is the ratio between the studs mass and the rock wool mass for of each layer i .

Innovative Lightweight Steel System braced with UHS Steel Bars

Four simulations were performed to evaluate and quantify the influence of different envelopes and thermal bridges on the Energy Demand (ED).

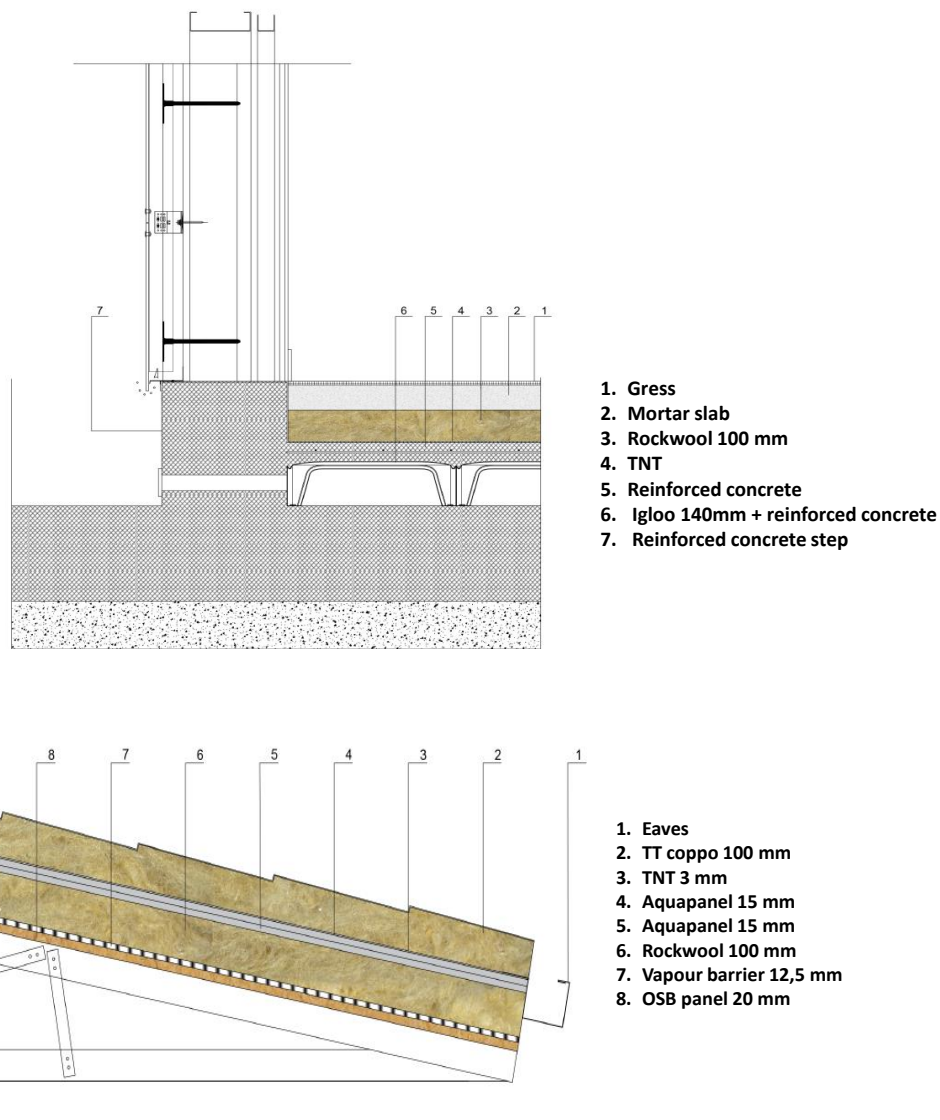


Figure 5-6 Developed solutions for floor and roof

Results are summarized in Table 5-3, which provides the influence of thermal bridges and building envelope in term of percentage increase of U-value and ED. In particular, considering the solution A, the presence of thermal bridges leads to an increase of U-value of about 52%, whereas considering the solution

Innovative Lightweight Steel System braced with UHS Steel Bars

B the increase is equal to about 50%. Moreover, considering the solution A, the presence of thermal bridges leads to an increase of ED of about 20%, whereas considering the solution B the increase is equal to about 28%.

Changing the building envelope from A to B, if considering thermal bridges, the reduction in U-value is equal to about 10%, whereas the reduction in ED is equal to about 37%. Figure 5-7 shows the ED for heating and cooling for both solutions, evaluated with U_{clear} and U_{overall} .

Table 5-3 Results of EnergyPlus simulation

Solution [-]	A		B	
	Clear	Overall	Clear	Overall
U-value [W/m²k]	0.15	0.23	0.21	0.14
U-value Increase [%]	52.71		49.91	
ED Heating [GJ]	9.52	11.2	6.16	8.09
ED Cooling [GJ]	3.39	4.24	2.67	3.22
ED total [GJ]	12.91	15.44	8.83	11.31
ED Increase [%]	19.60		28.09	

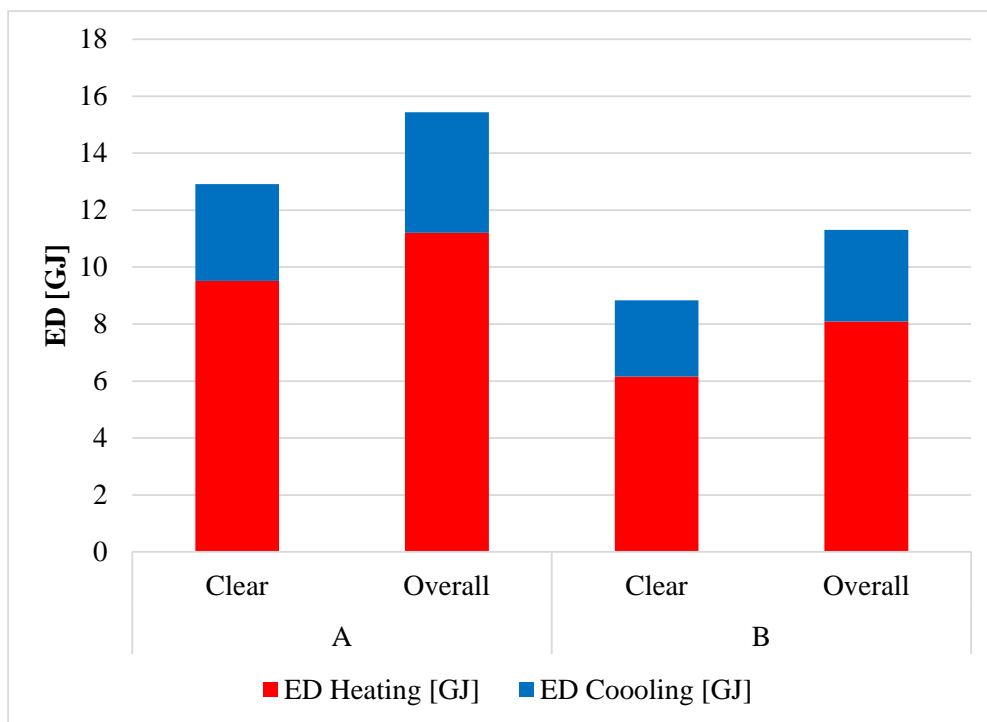


Figure 5-7 Energy demand for heating and cooling

6 The prototype building

A prototype building was designed and erected on the Company ground to prove the effectiveness of all the solutions developed and to validate the production and the erection processes. This Chapter describes the prototype building (Section 6.1), it provides detailed information on the design phase (Section 6.2), conducted following an integrated approach and taking into account also the production. It summarizes the results of the design considering architectural/technological (Section 6.2.1) and structural (Section 6.2.2) aspects and describes the BIM model developed (Section 6.2.3). Moreover, the execution and the erection phases are reported (Section 6.3).

6.1 Integrated design and prototyping of the building

To prove the effectiveness of the solutions developed in all the field considered, the design phase of prototype building followed the integrated approach, taking into account the architectural, technological and structural design and optimizing the production process, through prototyping. To this aim a BIM model of the prototype building was developed.

6.1.1 Architectural design

The prototype building represents an integrated application of different design and technological solutions, which aimed to minimize impacts, optimize the use of renewable energy sources and achieve high structural and environmental performance. The building covers an area of about 53m² and it consists of two levels. The entrance is located on the south-east side of the building in front of the factory access road. The wide openings on this side, protected by movable shielding elements in wooden slats, ensure the optimization of natural inputs and the control of solar radiation during the summer months. The north-west side presents small openings, useful for the exploitation of natural ventilation (cross-ventilation). On the inclined roof is installed 11 m² of photovoltaic panels and a mini-wind turbine. The presence on the roof of a solar chimney will increase the air circulation and will also contribute to illuminate the spaces with natural light.

The vertical envelope elements (external walls), floors, roof and windows shall ensure high performances not only relating to thermal transmittance, but above all in relation to its behaviour in terms of thermal inertia, phase shift and attenuation of the thermal wave, according to the relevant legislation.

3D representations of the prototype building are shown in Figure 6-1.

For the technological design, the study and analysis of the climatic conditions of the place where the prototype will be built, Sellia Marina (Catanzaro, South Italy), was performed and consequently solutions were chosen in order to

Innovative Lightweight Steel System braced with UHS Steel Bars

provide innovative thermal and acoustic insulation materials, such as to guarantee a remarkable thermo-acoustic comfort. As regards the opaque vertical closures, two solutions were used and analyzed, the external insulation system and the system with ventilated façade, as introduced in Chapter 3 and 5.



Innovative Lightweight Steel System braced with UHS Steel Bars



Innovative Lightweight Steel System braced with UHS Steel Bars

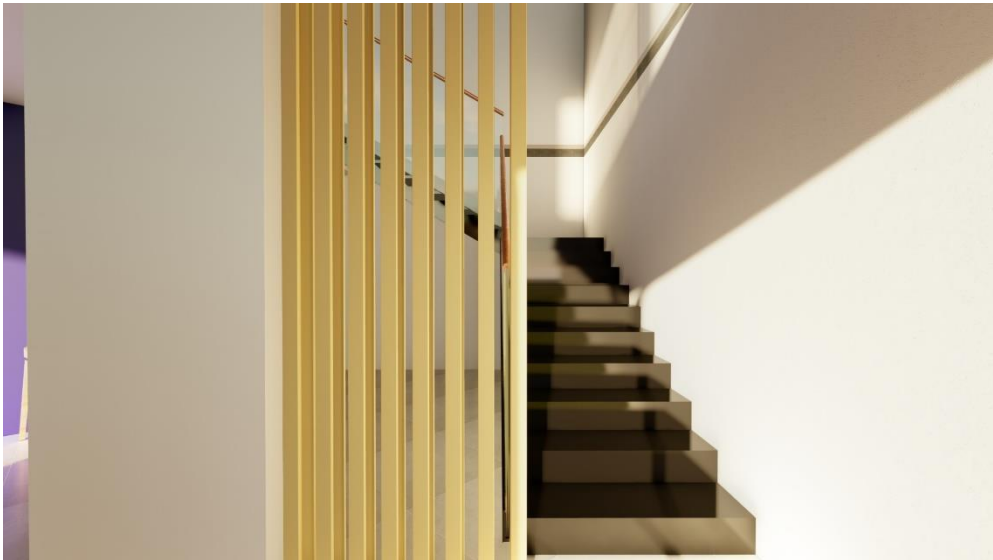




Figure 6-1 Renders of prototype building

6.1.2 Structural design

The structural design has been carried out according to Italian Codes [50] and for details not considered in this code, in accordance with Eurocode 3 [48]. From the structural point of view, the prototype building represents a LWS solution, in which the gravity frame is made of CFS profiles and LFRSs are represented by the innovative wall system developed in configuration H and L for the first and second storey, respectively.

Steel grades used for the structural elements were:

- S280 GD+ Z steel grade ($f_y=280$ MPa, $f_u=360$ MPa) for CFS members, i.e. studs, tracks, joists, blocking and flat straps;
- S355 steel grade ($f_y=355$ MPa, $f_u=470$ MPa) for pre-tensioning devices and hold-downs;
- 1300UHS steel grade ($f_y=1300$ MPa, $f_u=1450$ MPa) for diagonal braces.

The building analysed is a Class II building. The nominal life considered was 50 years, indeed the seismic action was evaluated in relation to a reference period equal to 75 years.

Innovative Lightweight Steel System braced with UHS Steel Bars

The evaluation of the actions was carried out in accordance to Italian Codes [50]. The evaluation of the permanent structural and non-structural loads was carried out on the final structural dimensions, considering the analysis of the loads. The variable loads, as prescribed by the NTC2018, have been adopted equal to 2 kN/m² for the floors and 4 kN/m² for the balconies. The wind and the snow actions has been evaluated in accordance with the indications given in the Italian Code [50].

The seismic action has been evaluated in accordance with the Italian Codes [50]. The identification of the basic seismic parameters, such as the maximum horizontal acceleration at the site a_g , the maximum value of the amplification factor of the spectrum in horizontal acceleration F_0 and the start period of the constant velocity segment of the spectrum in horizontal acceleration T_c^* for all the Limit States provided (SLO, SLD, SLV and SLC) has been conducted, starting from the latitude and longitude of the area. In particular, the definition of the basic seismic parameters was carried out by interpolating between the 4 points of the grid closest to the building reference point identified with the longitude of 16.7436 and the latitude of 38.9064, obtaining the values shown in Table 6-1.

Table 6-1 Parameters for the evaluation of seismic action

LIMIT STATE	T_R [years]	a_g [g]	F_0 [-]	T_c^* [s]
SLO	30	0.054	2.346	0.279
SLD	50	0.071	2.330	0.307
SLV	475	0.204	2.399	0.369
SLC	975	0.272	2.423	0.389

From the investigations carried out on site, it was possible to classify the foundation soil for the seismic action as Type C, according to the Italian Code, whereas the topographic category was assumed to be T1.

Thanks to the previously identified parameter it was possible to define the elastic response spectrum, reported in Figure 6-2. The behaviour factor used was equal to 1, indeed the structure was designed to remain in the elastic range due to the design seismic action.

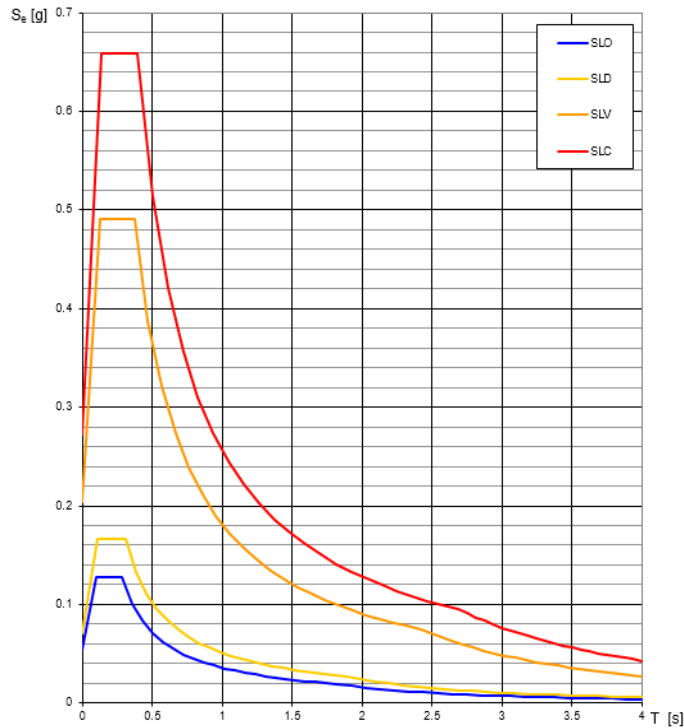


Figure 6-2 Response spectra for the four limit states provided in the Italian Code

The gravity system was composed of walls, floors and roof.

The floors were composed of joists, having a C-shaped cross section, connected to floor tracks with a U section, whose size depends on the type of joist connected. The joists have been schematized as a simply supported beam loaded by a uniformly distributed load and sized according to the maximum span of the floor equal to 6.0m. Joist spacing is equal to 600 mm.

Above the joists to complete the structural system of the floor, a corrugated trapezoidal sheathing of type A 55 / P 750 - V - HI-BOND with a thickness of

1.00 mm was used and 5cm slab of light concrete type LECA 1400 was provided.

At the Near Collapse Limit State, four checks were carried out for the joists: bending moment, shear, concentrated loads and flexural-torsional buckling. In the Serviceability Limit State, the deformability check and the vibration control check were carried out.

The evaluation of the flexural strength ($M_{c, Rd}$) was carried out, according to what is reported in EN8-Part 1-1 [49], in the middle section.

For the shear verification at the end sections, the resistance ($V_{b, Rd}$) was calculated considering the relationships reported in EN-1993- Part 1-1 [59].

The Italian standard as regards does not provide specific prescriptions for the verification of concentrated loads and it was carried out in accordance with the requirements of EN-1993-1-3 [48].

Furthermore, to avoid the possible underestimation of the deflections, for the purposes of the deformability verification the maximum deflection was evaluated considering the effects of local instability. The deflection was evaluated considering a uniform value of the moment of inertia I_{eff} , assumed on the basis of the maximum acting bending moment.

Finally, for the vibration control, the lowest natural frequency of the floor was evaluated according to Equation 6-1:

Equation 6-1

$$f = \pi^2 \sqrt{\frac{EI_{eff}}{\mu L^4}}$$

where E is the Young's modulus of steel; μ is the distributed mass acting and L is the length of the beam.

In order to satisfy the indicated checks, joist dimensions are equal to 270x60x30x3.

Innovative Lightweight Steel System braced with UHS Steel Bars

The roof is made of trusses, with a maximum span of 6m and a spacing of 600mm. Above the trusses, there is a system of purlins, with a spacing of 1.2 m, on which the roof covering rests. The purlins have been schematized as simply supported beams of span equal to the truss spacing, i.e. equal to 600mm, on which a uniformly distributed load equal to the self-weight, the weight of the roof covering and accidental overloads has been considered (exercise, snow and wind).

The purlins were designed considering the worst combination of the loads acting above the roof and a 60x40x15x1 omega section was used. In Figure 6-3 the first floor plan is shown.

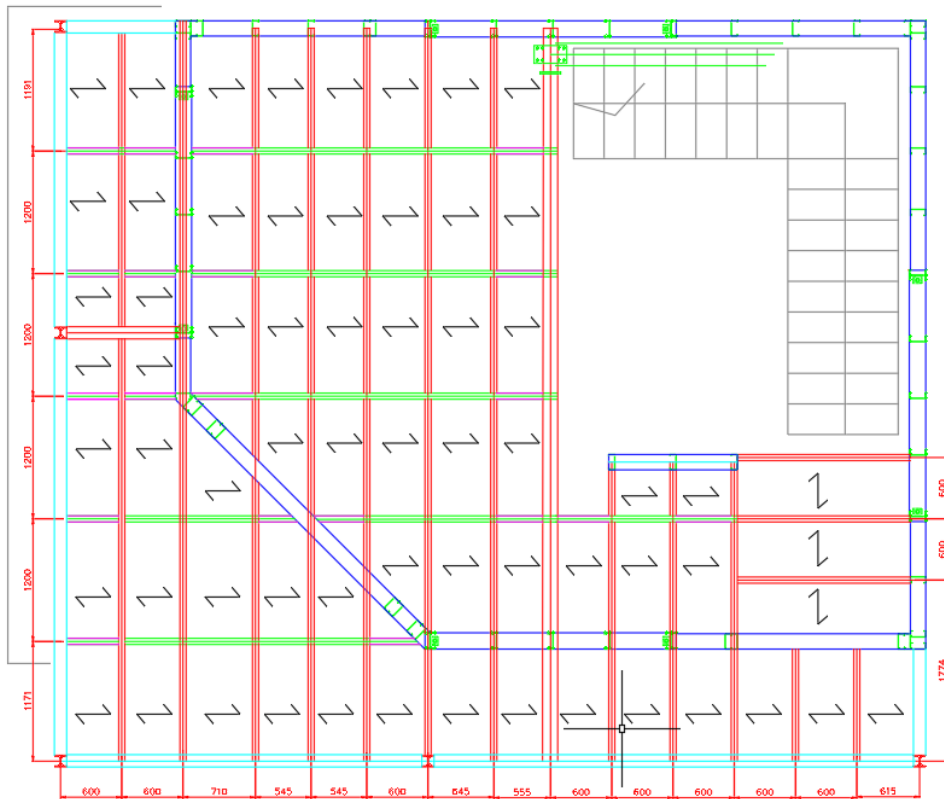


Figure 6-3 First floor plan

Innovative Lightweight Steel System braced with UHS Steel Bars

The 6.0 m span trusses are composed of 70x40x15x1.0 omega section top and bottom chords, 40x30x10x1.0 C-section diagonals and truss studs, as shown in Figure 6-4. The connection system between the various elements consists of self-drilling screws with a diameter of 6.3, arranged as shown in Figure 6-5.

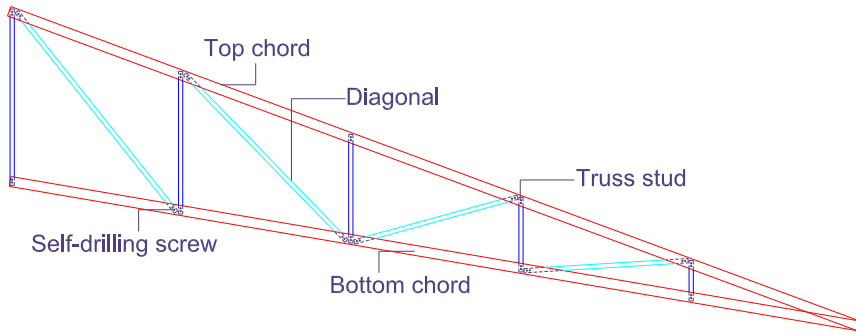


Figure 6-4 Roof trusses

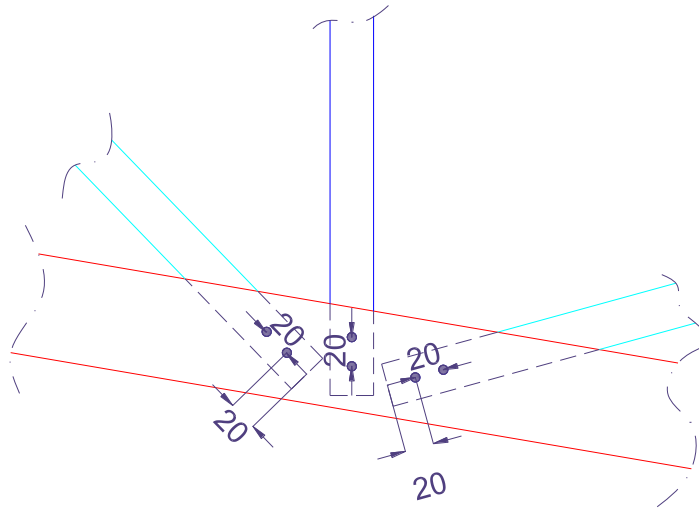


Figure 6-5 Connections between truss elements

The walls consist of a frame of studs and tracks. They have to transfer the vertical loads from the roof and floors to the foundation. The studs are loaded by floor and wind if external. Internal studs use a C-section, whereas chord studs use a back-to-back C-section.

Innovative Lightweight Steel System braced with UHS Steel Bars

At the Near Collapse Limit State checks were carried out for bending resistance and stability. The resistance check takes into account the phenomena of local and distortion instability.

For the stability check the free wavelength was set equal to the length of the profile, both for flexural deformation in plane and out of plane. In order to satisfy the resistance and stability checks a 150x60x20x1.5 C-section was adopted.

The LFRS consisted of innovative wall system developed, in which the frame was made of CFS profiles braced by pre-tensioned UHS steel bars in “V” configuration. Four walls (two for each direction) in L configuration and four walls in H configuration were used for first and second storey, respectively. Three different layouts can be used for the two-storey LFRS, as shown in Figure 6-6. The main difference among these solutions is represented by the compression force acting on the central stud if the forces in the two braces are unbalanced. In the solution a) chosen in the prototype, to withstand the unbalanced force a back-to-back C-stud was employed, instead of simple C-stud. The design of all the other elements of LFRS was performed according to the rules described in Section 3.1.1, considering the seismic action evaluated as introduced.

The foundation, which also represents the ground floor, was a reinforced concrete stiffened plate. The concrete used for foundation has a C30/37 compressive strength grade.

South-West and South-East views of prototype building are shown in Figure 6-7.

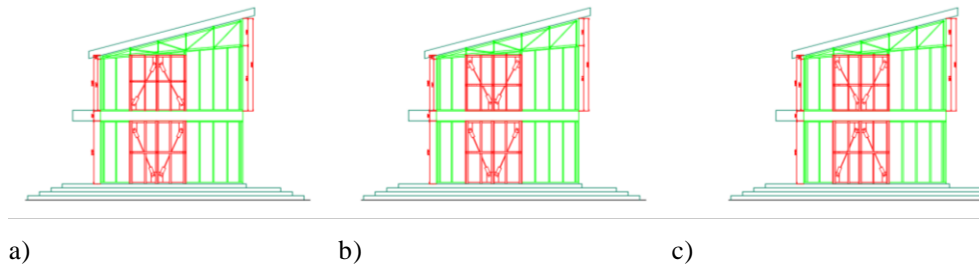
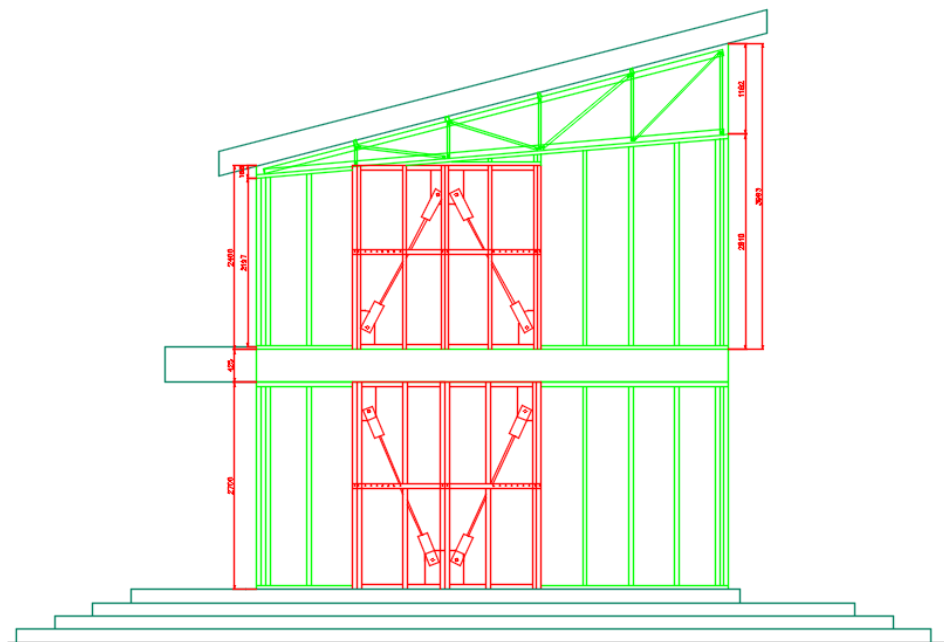
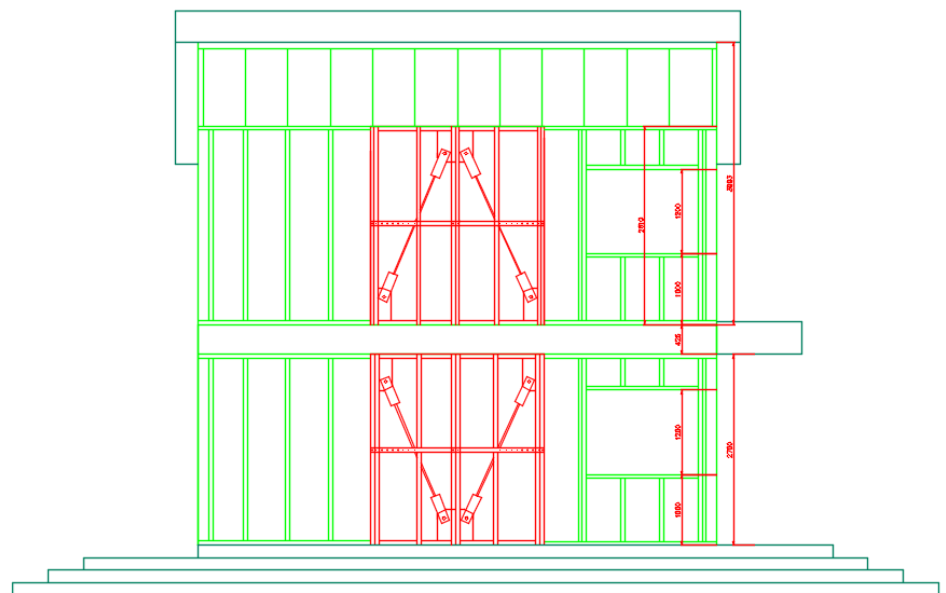


Figure 6-6 Two-storey LFRS layouts



a) South-West view



b) South-East view

Figure 6-7 Views of prototype building

6.1.3 Building Information Modelling

A BIM model of the prototype building was developed, through the Revit software. First of all, all the data were collected, starting from information such as orientation, positioning and acquisition of the plan. The BIM model was built starting from the floor plan and reproduced on Revit, in order to make the modelling mode more fluid and intuitive.

The first modelling phase was characterized by the creation of a virtual grid to define the geometry of the project, also identifying the various levels of interest with the relative heights. Subsequently, the structure of the building was reproduced, therefore all the structural elements were modelled.

All structural elements were modelled in Revit parametrically, as a new family. Figure 6-8 shows the structural part modelled in Revit.

Then, the various horizontal partitions, i.e. first level floor, second level floor and roofing floor (inclined in our case), and the opaque vertical partitions, were created, considering the two solutions developed, the external insulation system and the system with ventilated facade.

Since each building component can be represented with different levels of detail, it is possible to change and modify the structure of the desired component.

Furthermore, by accessing each single material chosen to compose the stratigraphy, Revit allows you to define the graphic representation, the graphic rendering (rendering), the physical properties and, above all, the thermal properties, fundamental since they provide a thermal resistance value, useful for energy analysis.

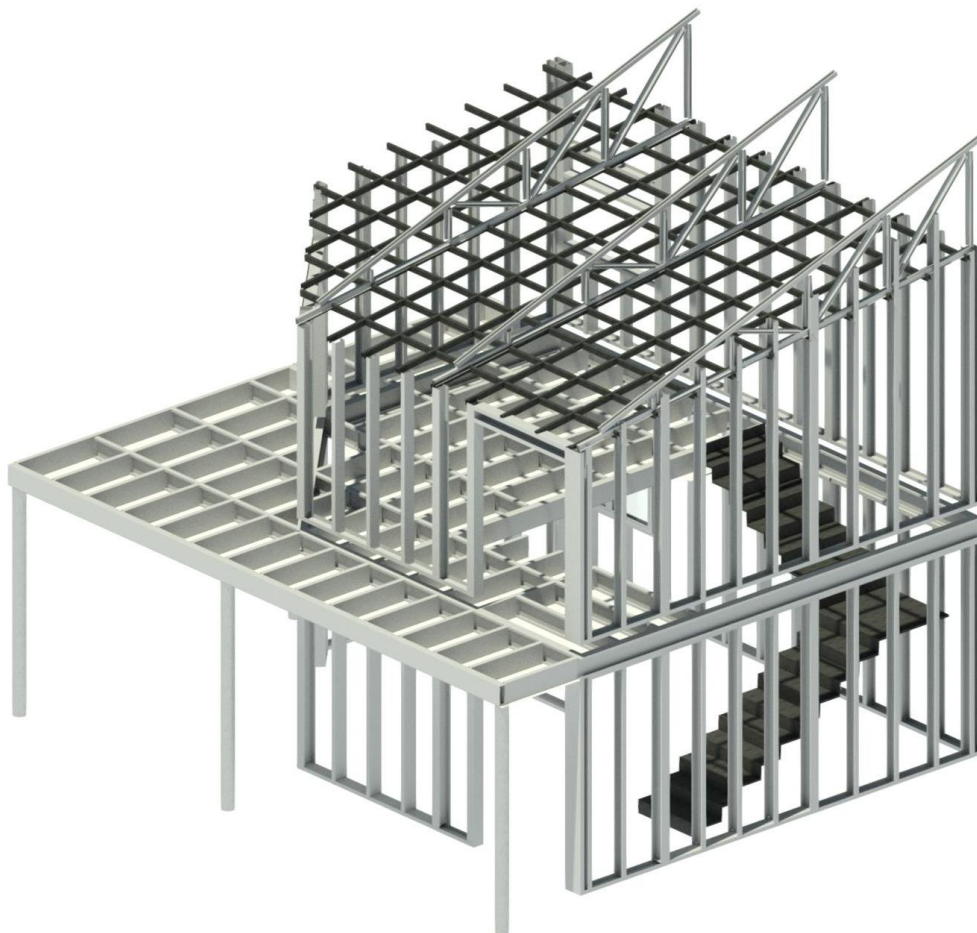


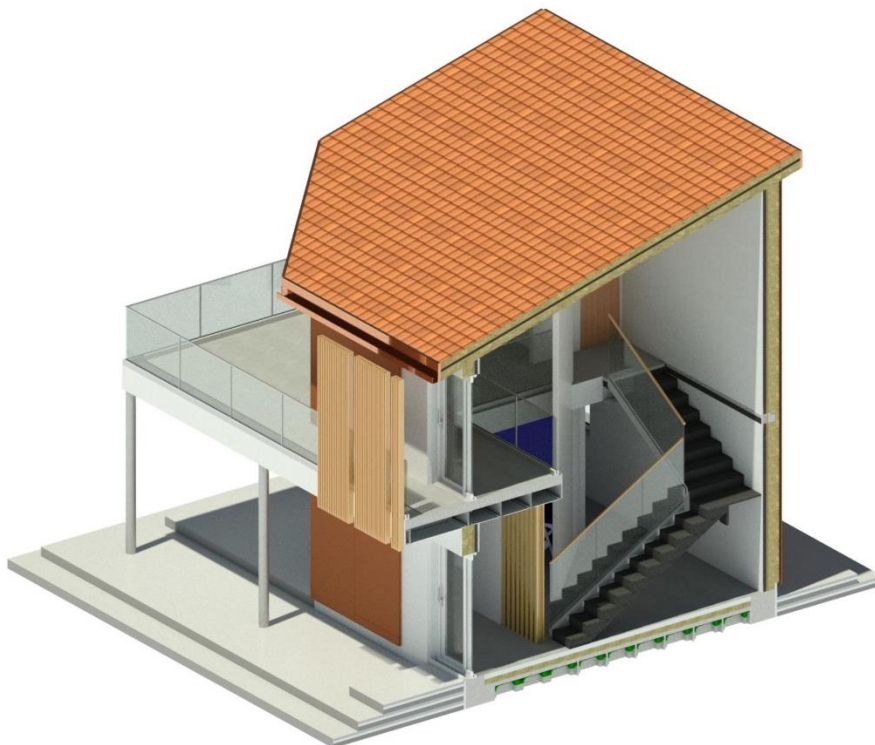
Figure 6-8 BIM structural model

The aforementioned methodology can be applied indiscriminately to any opaque component stratigraphy and therefore allows the designer, on the one hand, to obtain an optimal graphic representation and, on the other hand, to have complete control over the component in terms not only geometric, but also physical, graphical, and thermal.

In this way it is possible to manage the model in all fields such as, for example, to compute all the elements that make-up the structure or to manage the quantities of material useful for the realization of the various stratifications. Figure 6-9 shows the complete BIM model developed.



a) Complete building BIM model



b) Cut building BIM model

Figure 6-9 Complete BIM model developed

6.2 Execution and erection on site

Work began on February 2020, but it was stopped by Covid pandemic until September 2020. The structural part finished in January 2021, whereas the finishings were completed in March 2021. A complete photographic report is provided in Figure 6-10. In Appendix 3 all the drawings are provided.



a) foundation



b) LFRS and gravity frame connection



c) First storey structure

Innovative Lightweight Steel System braced with UHS Steel Bars



d) Gravity frame track-to-stud connection



e) LFRS track-to-stud connection



f) Openings

Innovative Lightweight Steel System braced with UHS Steel Bars



g) Opening details



h) Floor details

Innovative Lightweight Steel System braced with UHS Steel Bars



i) Complete first storey structure



j) Balcony detail

Innovative Lightweight Steel System braced with UHS Steel Bars



k) Different views of steel structures



l) Complete structure

Innovative Lightweight Steel System braced with UHS Steel Bars



m) Building without and with finishings



n) Complete building views

Figure 6-10 Report of execution and erection of prototype building

7 Conclusions and further developments

The increasing market demand for high-performance and low-cost constructions oriented the choice of the last decades to a competitive and eco-friendly solution. In fact, in the last decades Lightweight Steel (LWS) systems made of Cold-Formed Steel (CFS) have been often preferred to traditional structures in seismic area, since they exhibited great structural performances with lower erection time and construction costs.

The main scope of this thesis was the development of innovative solutions for LWS with higher structural, thermal and environmental performances, in the framework of the Italian project “ECCELSA”, which the University of Naples “Federico II” started in cooperation with the Lamieredil S.p.A. company.

To this end, three main objectives are pursued in this work: the development and the study of an innovative load force resisting system (wall system), the development and the analysis of innovative solutions for the building envelope and the optimization of production processes and execution phase. To this aim, an integrated design approach was used, helped by Building Information Modelling (BIM).

The innovative wall system mainly consists of CFS frame braced by pre-tensioned ultra-high strength steel bars in “V” configuration. To complete the system ad hoc pre-tensioning devices and hold-down devices were designed. In order to guarantee different lateral resistance levels, three different configurations were designed: Light wall (L), Medium wall (M), Heavy wall (H). A wide experimental program was planned and carried out to evaluate the seismic behaviour of the innovative system. It consisted of small-scale experimental tests on materials (tensile tests on structural materials and creep tests on UHS), tensile tests on bar-nut assemblies, full-scale tests on walls in light and medium configuration. In particular, were performed twenty-four

Innovative Lightweight Steel System braced with UHS Steel Bars

tension tests for the mechanical characterization of structural materials used in the wall systems, two creep tests of UHS steel, eight tension tests on bar-nut assemblies, three monotonic tests on full-scale walls (two for the light configuration and one for the medium configuration) and two cyclic tests on full-scale walls (for the light configuration and one for the medium configuration). The experimental tests were performed at the Laboratory of DIST (Department of Structures for Engineering and Architecture) of the University of Naples “Federico II”. The experimental results showed satisfactory seismic responses, in line with the theoretical previsions, if all the prescriptions are followed. In particular, if not well designed, the nut used for the bar pre-tensioning can cause a premature failure of the system and the displacement capacity is strongly reduced. The walls, in which all the design prescriptions were respected, exhibited satisfactory force and displacement capacity.

Moreover, two warm frame solutions for the building envelope were designed and analysed. The thermal bridges were individuated through the COMSOL simulations and the thermal performances of the two solutions were evaluated. The effect of the envelope and thermal bridges was analysed, quantifying the energy demand of a prototype building by means of EnergyPlus software. The more performing solution, but also the thicker and the more expensive, led to a reduction in energy demand equal to about 37%.

In the end, the effectiveness of the innovations developed, and the optimization of production processes and execution phase were proved by means of the design and erection of a prototype building on the company ground. Although BIM played a central role in speeding up manufacturing and production processes, pandemic made the erection slower.

For the future, it could be interesting testing the prototype building to evaluate the structural and thermal performances on site. Moreover, full techno-

Innovative Lightweight Steel System braced with UHS Steel Bars

economic analysis and combined LCA-resilience analysis are planned to be completed in the next future.

References

- [1] A. Campiche, Development of an innovative multi-performance system for LWS structures, in: SDSS 2019 - Int. Colloq. Stab. Ductility Steel Struct., 2019.
- [2] P. Heiselberg, Strategies for Integrative Building Design, in: Conf. “The Futur. Sustain. Built Environ. with High Perform. Energy Syst., 2016.
- [3] J. Leng, K.D. Peterman, G. Bian, S.G. Buonopane, B.W. Schafer, Modeling seismic response of a full-scale cold-formed steel-framed building, *Eng. Struct.* 153 (2017) 146–165. <https://doi.org/10.1016/j.engstruct.2017.10.008>.
- [4] N. Balh, J. Dabreo, C. Ong-Tone, K. El-Saloussy, C. Yu, C.A. Rogers, Design of steel sheathed cold-formed steel framed shear walls, *Thin-Walled Struct.* 75 (2014) 76–86. <https://doi.org/10.1016/j.tws.2013.10.023>.
- [5] I. Mandilaras, I. Atsonios, G. Zannis, M. Founti, Thermal performance of a building envelope incorporating ETICS with vacuum insulation panels and EPS, *Energy Build.* 85 (2014) 654–665. <https://doi.org/10.1016/j.enbuild.2014.06.053>.
- [6] N. Soares, P. Santos, H. Gervásio, J.J. Costa, L. Simões da Silva, Energy efficiency and thermal performance of lightweight steel-framed (LSF) construction: A review, *Renew. Sustain. Energy Rev.* 78 (2017) 194–209. <https://doi.org/10.1016/j.rser.2017.04.066>.
- [7] R. Landolfo, Lightweight steel framed systems in seismic areas: Current achievements and future challenges, *Thin-Walled Struct.* 140 (2019) 114–131. <https://doi.org/10.1016/j.tws.2019.03.039>.
- [8] M. Casafont, A. Arnedo, F. Roure, A. Rodríguez-Ferran, Experimental testing of joints for seismic design of lightweight structures. Part 3: Gussets, corner joints, x-braced frames, *Thin-Walled Struct.* 45 (2007) 637–659. <https://doi.org/10.1016/j.tws.2007.05.008>.
- [9] H. Moghimi, H.R. Ronagh, Performance of light-gauge cold-formed steel strap-braced stud walls subjected to cyclic loading, *Eng. Struct.* 31 (2009) 69–83. <https://doi.org/10.1016/j.engstruct.2008.07.016>.
- [10] G. Comeau, K. Velchev, C.A. Rogers, Development of seismic force modification factors for cold-formed steel strap braced walls, *Can. J. Civ. Eng.* 37 (2010) 236–249. <https://doi.org/10.1139/L09-153>.

- [11] L.A. Fülöp, D. Dubina, Design Criteria for Seam and Sheeting-to-Framing Connections of Cold-Formed Steel Shear Panels, *J. Struct. Eng.* 132 (2006) 582–590. [https://doi.org/10.1061/\(ASCE\)0733-9445\(2006\)132:4\(582\)](https://doi.org/10.1061/(ASCE)0733-9445(2006)132:4(582)).
- [12] K. Velchev, G. Comeau, N. Balh, C.A. Rogers, Evaluation of the AISI S213 seismic design procedures through testing of strap braced cold-formed steel walls, *Thin-Walled Struct.* 48 (2010) 846–856. <https://doi.org/10.1016/j.tws.2010.01.003>.
- [13] M.-S. Lee, D.A. Foutch, Performance evaluation of cold-formed steel braced frames designed under current U.S. seismic design code, *Int. J. Steel Struct.* 10 (2010) 305–316. <https://doi.org/10.1007/BF03215839>.
- [14] M.R. Davani, S. Hatami, A. Zare, Performance-based evaluation of strap-braced cold-formed steel frames using incremental dynamic analysis, *Steel Compos. Struct.* 21 (2016) 1369–1388. <https://doi.org/10.12989/scs.2016.21.6.1369>.
- [15] T.-S. Eom, T.-H. Ha, B.-H. Cho, T.-H. Kim, Cyclic Loading Tests on Framed Stud Walls with Strap Braces and Steel Sheathing, *J. Struct. Eng.* 141 (2015) 04014173. [https://doi.org/10.1061/\(asce\)st.1943-541x.0001133](https://doi.org/10.1061/(asce)st.1943-541x.0001133).
- [16] T.W. Kim, J. Wilcoski, D.A. Foutch, Analysis of measured and calculated response of a cold-formed steel shear panel structure, *J. Earthq. Eng.* 11 (2007) 67–85. <https://doi.org/10.1080/13632460601031862>.
- [17] A.I. and S. Institute, (AISI), AISI, AISI S213-07/S1–09, North American Standard for Cold-Formed Steel Framing – Lateral Design 2007 Edition with Supplement No. 1, Washington, D.C., 2009.
- [18] FEMA, FEMA P695: Quantification of Building Seismic Performance Factors, Washington, 749 DC, USA, 2009.
- [19] FEMA-355 F, State of the Art Report on Performance Prediction and Evaluation of Steel Moment Frame Buildings, The SAC Joint Venture for the Federal Emergency Management Agency, in: Washington, D.C., 2000.
- [20] T.W. Kim, J. Wilcoski, D.A. Foutch, M.S. Lee, Shaketable tests of a cold-formed steel shear panel, *Eng. Struct.* 28 (2006) 1462–1470. <https://doi.org/10.1016/j.engstruct.2006.01.014>.
- [21] M. Al-Kharat, C.A. Rogers, Inelastic performance of cold-formed steel strap braced walls, *J. Constr. Steel Res.* 63 (2007) 460–474. <https://doi.org/10.1016/j.jcsr.2006.06.040>.

- [22] E.F. Gad, C.F. Duffield, G.L. Hutchinson, D.S. Mansell, G. Stark, Lateral performance of cold-formed steel-framed domestic structures, *Eng. Struct.* 21 (1999) 83–95. [https://doi.org/10.1016/S0141-0296\(97\)90129-2](https://doi.org/10.1016/S0141-0296(97)90129-2).
- [23] J. Kosny, J.E. Christian, Thermal evaluation of several configurations of insulation and structural materials for some metal stud walls, *Energy Build.* 22 (1995) 157–163. [https://doi.org/10.1016/0378-7788\(94\)00913-5](https://doi.org/10.1016/0378-7788(94)00913-5).
- [24] Y. Li, J. Yao, R. Li, Z. Zhang, J. Zhang, Thermal and energy performance of a steel-bamboo composite wall structure, *Energy Build.* 156 (suppl (2017) 225–237.
- [25] L. Zalewski, S. Lassue, D. Rousse, K. Boukhalifa, Experimental and numerical characterization of thermal bridges in prefabricated building walls, *Energy Convers. Manag.* 51 (2010) 2869–2877. <https://doi.org/10.1016/j.enconman.2010.06.026>.
- [26] P. Santos, C. Martins, L.S. Da Silva, L. Bragança, Thermal performance of lightweight steel framed wall: The importance of flanking thermal losses, *J. Build. Phys.* 38 (2014) 81–98. <https://doi.org/10.1177/1744259113499212>.
- [27] M. Gorgolewski, Developing a simplified method of calculating U-values in light steel framing, *Build. Environ.* 42 (2007) 230–236. <https://doi.org/10.1016/j.buildenv.2006.07.001>.
- [28] T. Thorsell, M. Bomberg, Integrated methodology for evaluation of energy performance of the building enclosures: Part 3 - Uncertainty in thermal measurements, *J. Build. Phys.* 35 (2011) 83–96. <https://doi.org/10.1177/1744259111404381>.
- [29] M. O’Grady, A.A. Lechowska, A.M. Harte, Infrared thermography technique as an in-situ method of assessing heat loss through thermal bridging, *Energy Build.* 135 (2017) 20–32. <https://doi.org/10.1016/j.enbuild.2016.11.039>.
- [30] I.A. Atsonios, I.D. Mandilaras, D.A. Kontogeorgos, M.A. Founti, Two new methods for the in-situ measurement of the overall thermal transmittance of cold frame lightweight steel-framed walls, *Energy Build.* 170 (2018) 183–194. <https://doi.org/10.1016/j.enbuild.2018.03.069>.
- [31] T. Höglund, H. Burstrand, Slotted steel studs to reduce thermal bridges in insulated walls, *Thin-Walled Struct.* 32 (1998) 81–109. [https://doi.org/10.1016/S0263-8231\(98\)00028-7](https://doi.org/10.1016/S0263-8231(98)00028-7).

- [32] C. Martins, P. Santos, L.S. Da Silva, Lightweight steel-framed thermal bridges mitigation strategies: A parametric study, *J. Build. Phys.* 39 (2016) 342–372. <https://doi.org/10.1177/1744259115572130>.
- [33] F. Ascione, N. Bianco, F. De Rossi, G. Turni, G.P. Vanoli, Different methods for the modelling of thermal bridges into energy simulation programs: Comparisons of accuracy for flat heterogeneous roofs in Italian climates, *Appl. Energy*. 97 (2012) 405–418. <https://doi.org/10.1016/j.apenergy.2012.01.022>.
- [34] American Society of Heating, Refrigerating and Air-conditioning Engineers (ASHRAE), (1993).
- [35] EN ISO 6946:2007. Building components and building elements-thermal resistance and thermal transmittance- calculation method, (2007).
- [36] ISO 9869:1994. Thermal insulation- building elements- in-situ measurement of thermal resistance and thermal transmittance, (1994).
- [37] ASTM C1155-95. Standard practice for determining thermal resistance of building envelope components from the in-situ data, (2007).
- [38] J. Kosny, J.E. Christian, E. Barbour, J. Goodrow, M. Marietta, LABORATORY I C/ORNL 93 0235 CRADA Final Report for CRADA Number ORNL93-0235 THERMAL PERFORMANCE OF STEEL-FRAMED WALLS FOR THE UNITED STATES, (n.d.).
- [39] V. Ivanko, S. Kmet, G. Fedorko, Finite element simulation of creep of spiral strands, *Eng. Struct.* 117 (2016) 220–238. <https://doi.org/10.1016/j.engstruct.2016.02.053>.
- [40] W. Zhang, X. Yuan, L. Yang, M. Deng, Research on creep constitutive model of steel cables, *Constr. Build. Mater.* 246 (2020) 118481. <https://doi.org/10.1016/j.conbuildmat.2020.118481>.
- [41] S. Kmet, M. Mojdis, Time-dependent analysis of cable nets using a modified nonlinear force-density method and creep theory, *Comput. Struct.* 148 (2015) 45–62. <https://doi.org/10.1016/j.compstruc.2014.11.004>.
- [42] M.E. Kassner, P. Geantil, R.S. Rosen, Ambient temperature creep of type 304 stainless steel, *J. Eng. Mater. Technol. Trans. ASME*. 133 (2011) 2–7. <https://doi.org/10.1115/1.4003110>.
- [43] L. Bendersky, A. Rosen, A.K. Mukherjee, Creep and dislocation substructure, *Int. Met. Rev.* 30 (1985) 1–15. <https://doi.org/10.1179/imtr.1985.30.1.1>.

- [44] J. Hu, G. Green, S. Hogg, R. Higginson, A. Cocks, Effect of microstructure evolution on the creep properties of a polycrystalline 316H austenitic stainless steel, *Mater. Sci. Eng. A.* 772 (2020) 138787. <https://doi.org/10.1016/j.msea.2019.138787>.
- [45] R.L. Klueh, P.J. Maziasz, I.S. Kim, L. Heatherly, D.T. Hoelzer, N. Hashimoto, E.A. Kenik, K. Miyahara, Tensile and creep properties of an oxide dispersion-strengthened ferritic steel, *J. Nucl. Mater.* 307–311 (2002) 773–777. [https://doi.org/10.1016/S0022-3115\(02\)01046-2](https://doi.org/10.1016/S0022-3115(02)01046-2).
- [46] T. Matsunaga, T. Kameyama, K. Takahashi, E. Sato, Constitutive relation for ambient-temperature creep in hexagonal close-packed metals, *Mater. Trans.* 50 (2009) 2858–2864. <https://doi.org/10.2320/matertrans.M2009223>.
- [47] C. Liu, P. Liu, Z. Zhao, D.O. Northwood, Room temperature creep of a high strength steel, *Mater. Des.* 22 (2001) 325–328. [https://doi.org/10.1016/S0261-3069\(00\)00074-1](https://doi.org/10.1016/S0261-3069(00)00074-1).
- [48] CEN, EN 1993-1-3 Eurocode 3: Design of steel structures-Part 1-3: General rules-Supplementary rules for cold-formed members and sheeting, European Committee for Standardization, Brussels, 2006.
- [49] CEN, EN 1998-1 Eurocode 8: Design of Structures for earthquake resistance-Part 1: General rules, seismic actions and rules for buildings, European Committee for Standardization, Brussels, 2004.
- [50] Ministero delle Infrastrutture, D.M. 17/01/2018, Norme Tecniche per le Costruzioni, n.d.
- [51] ISO 10211:2007. Thermal bridges in building construction - heat flows and surface temperatures- detailed calculations, (2007).
- [52] European committee for standardization, UNIEN ISO 6892-1 - Metallic materials - Tensile Testing - Part 1: Method of Test at Room Temperature, (2009) 65.
- [53] M. D’Aniello, D. Cassiano, R. Landolfo, Monotonic and cyclic inelastic tensile response of European preloadable gr10.9 bolt assemblies, *J. Constr. Steel Res.* 124 (2016) 77–90. <https://doi.org/10.1016/j.jcsr.2016.05.017>.
- [54] ECCS. Recommended Testing Procedure for Assessing the Behaviour of Structural Steel Elements under Cyclic Loads, P045, ECCS Technical Committee 1 – Structural Safety and Loadings, Technical Working Group 1.3 – Seismic Design, European Convention fo, 1986.
- [55] H. Krawinkler, P. Francisco, L. Ibarra, A. Ayoub, R. Medina, CUREE

- publication No. W-02 Development of a Testing Protocol for Woodframe Structures, (2001).
- [56] C. Uang, Establishing R (or R_w) and Cd Factors for Building Seismic Provisions, *J. Struct. Eng.* 117 (1991) 19–28. [https://doi.org/10.1061/\(ASCE\)0733-9445\(1991\)117:1\(19\)](https://doi.org/10.1061/(ASCE)0733-9445(1991)117:1(19)).
- [57] D. Mitchell, R. Tremblay, E. Karacabeyli, P. Paultre, M. Saatcioglu, D.L. Anderson, Seismic force modification factors for the proposed 2005 edition of the National Building Code of Canada, *Can. J. Civ. Eng.* 30 (2003) 308–327. <https://doi.org/10.1139/102-111>.
- [58] A.P. Gomes, H.A. De Souza, A. Tribess, Impact of thermal bridging on the performance of buildings using Light Steel Framing in Brazil, *Appl. Therm. Eng.* 52 (2013) 84–89. <https://doi.org/10.1016/j.applthermaleng.2012.11.015>.
- [59] CEN, EN 1993-1-1 Eurocode 3: Design of steel structures-Part 1-1: General rules and rules for buildings, European Committee for Standardization, Brussels, 2005.

Appendix 1: Material tests

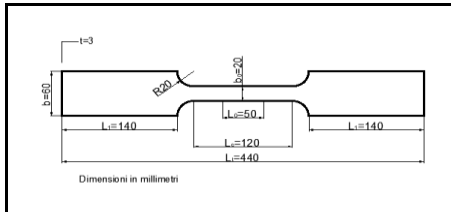
A.1.1 Tensile tests

Innovative Lightweight Steel System braced with UHS Steel Bars

TENSILE TESTS ON MATERIAL

S280gd+z

DATE	15/11/2019
TEAM LEADER	RAFFAELE LANDOLFO
RESEARCH GROUP	LUIGI FIORINO
	ALESSIA CAMPICHE
	SARMAD SHAKEEL
STUDENT	FERDINANDO NACLERIO

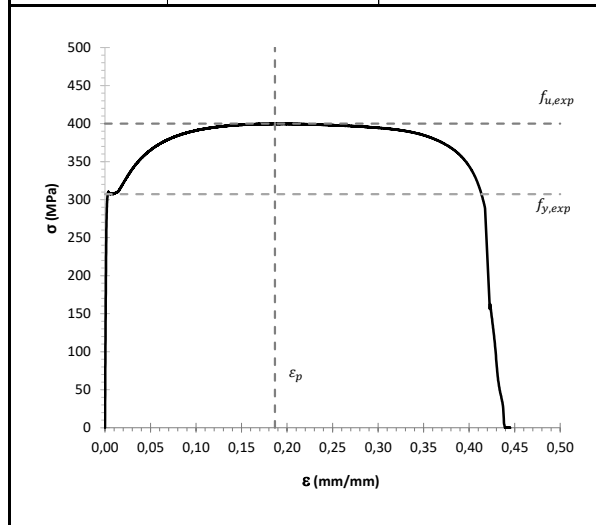


SPECIMEN DATA		
LABEL	S3_1	
COIL DATA	Type	S280gd+z
	Production factory	Lamieredil S.P.A
	Coil type	
	Production Date	
	Thickness (mm)	3,00
SAMPLE DATA-measured values	Original gauge length L_0 (mm)	50
	Width b_0 (mm)	20,00
	Thickness t_0 (mm)	3,00
	Cross section area (mm ²)	60,00



TEST DATA		
TEST PARAMETERS	Displacement rate (mm/s)	0,05
	Frequency (Hz)	5
	Test time (s)	456,64

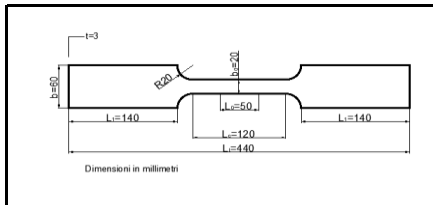
TEST RESULTS		
PRODUCTION VALUES	Yield strength R_p (Mpa)	280,00
	Tensile strength R_m (MPa)	360,00
RESULT VALUES	Yield strength f_y (Mpa)	307,18
	Tensile strength f_u (MPa)	399,93
	Last strain ϵ_u (mm/mm)	0,40
	Peak strain ϵ_p (mm/mm)	0,19
Modulus of elasticity E (Mpa)	207251	
TEST OUTCOME	Breaking	inside L_0



TENSILE TESTS STEEL MATERIAL

S280gz+z

DATE	17/11/2019
TEAM LEADER	RAFFAELE LANDOLFO
RESEARCH GROUP	LUIGI FIORINO ALESSIA CAMPICHE SARMAD SHAKEEL
STUDENT	FERDINANDO NACLERIO

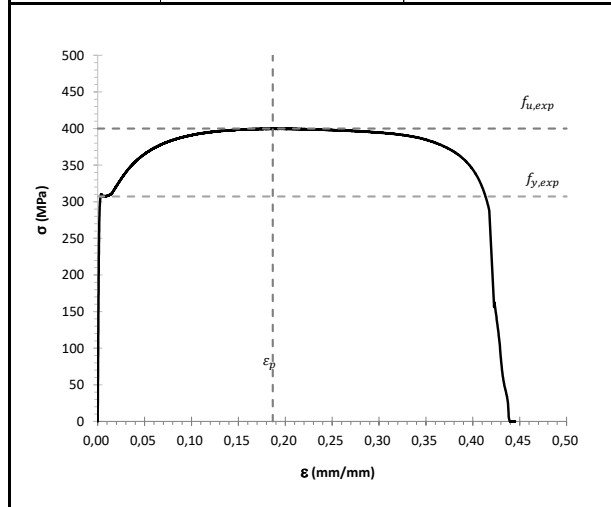


SPECIMEN DATA		
LABEL	S3_2	
COIL DATA	Type	S280gd+z
	Production factory	Lamieredil S.P.A
	Coil type	
	Production Date	
	Thickness (mm)	3,00
SAMPLE DATA-measured values	Original gauge length L_o (mm)	50
	Width b_o (mm)	20,00
	Thickness t_o (mm)	3,00
	Cross section area (mm ²)	60,00



TEST DATA		
TEST PARAMETERS	Displacement rate (mm/s)	0,05
	Frequency (Hz)	5
	Test time (s)	363,08

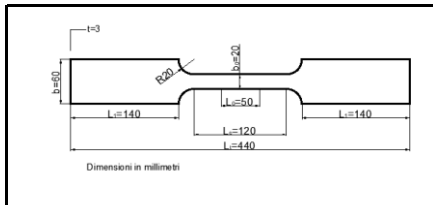
TEST RESULTS		
PRODUCTION VALUES	Yield strength R_e (Mpa)	280,00
	Tensile strength R_m (MPa)	360,00
RESULT VALUES	Yield strength f_y (Mpa)	307,84
	Last strain ϵ_w (mm/mm)	0,40
	Tensile strength f_u (MPa)	400,70
	Peak strain ϵ_p (mm/mm)	0,19
	Modulus of elasticity E (Mpa)	212695,66
TEST OUTCOME	Breaking	inside L_o



TENSILE TESTS ON STEEL MATERIAL

S280gd+z

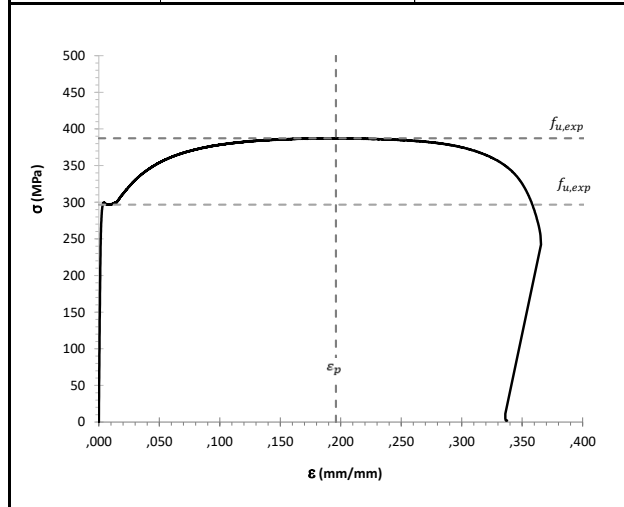
DATE	17/02/2014
TEAM LEADER	RAFFAELE LANDOLFO
RESEARCH GROUP	LUIGI FIORINO ALESSIA CAMPICHE SARMAD SHAKEEL
STUDENT	FERDINANDO NACLERIO



SPECIMEN DATA		
LABEL	S3_3	
COIL DATA	Type	S280gd+z
	Production factory	Lamieredil S.P.A.
	Coil type	
	Production Date	
	Thickness (mm)	3,00
SAMPLE DATA-measured values	Original gauge length L_o (mm)	50
	Width b_o (mm)	20,00
	Thickness t_o (mm)	3,00
	Cross section area (mm ²)	60,00

TEST DATA		
TEST PARAMETERS	Displacement rate (mm/s)	0,05
	Frequency (Hz)	5
	Test time (s)	314,06

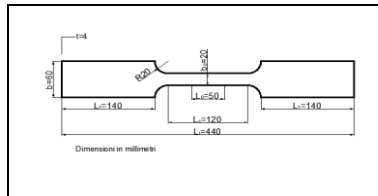
TEST RESULTS		
PRODUCTION VALUES	Yield strength R_e (Mpa)	280,00
	Tensile strength R_m (MPa)	360,00
RESULT VALUES	Yield strength f_y (Mpa)	296,68
	Tensile strength f_u (MPa)	387,29
	Last strain ϵ_u (mm/mm)	0,40
	Peak strain ϵ_p (mm/mm)	0,20
	Modulus of elasticity E (Mpa)	200354,05
TEST OUTCOME	Breaking	inside L_o



TENSILE TESTS ON STEEL MATERIAL

S280gd+z

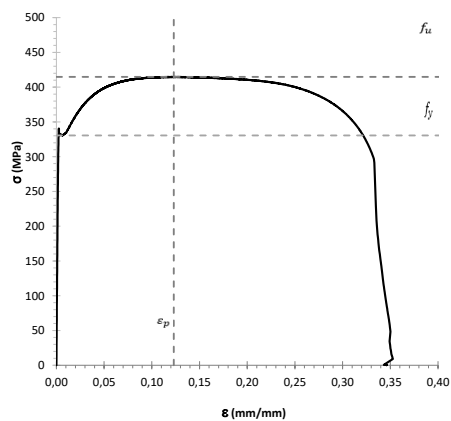
DATE	17/11/2019
TEAM LEADER	RAFFAELE LANDOLFO
RESEARCH GROUP	LUIGI FIORINO ALESSIA CAMPICHE SARMAD SHAKEEL
STUDENT	FERDINANDO NACLERIO



SPECIMEN DATA		
LABEL	S4_1	
COIL DATA	Type	280gd+z
	Production factory	Lamieredil S.P.A
	Coil type	
	Production Date	
	Thickness (mm)	4,00
SAMPLE DATA-measured values	Original gauge length L_0 (mm)	50
	Width b_0 (mm)	20,00
	Thickness t_0 (mm)	4,00
	Cross section area (mm^2)	80,00

TEST DATA		
TEST PARAMETERS	Displacement rate (mm/s)	0,05
	Frequency (Hz)	5
	Test time (s)	288,66

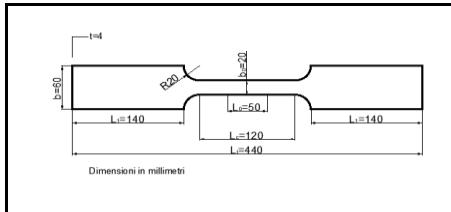
TEST RESULTS		
PRODUCTION VALUES	Yield strength R_e (Mpa)	280,00
	Tensile strength R_m (MPa)	360,00
RESULT VALUES	Yield strength f_y (Mpa)	330,54
	Tensile strength f_u (MPa)	414,75
	Last strain ϵ_u (mm/mm)	0,40
	Peak strain ϵ_p (mm/mm)	0,12
	Modulus of elasticity E (Mpa)	180015,78
TEST OUTCOME	Breaking	inside L_0



TENSILE TESTS ON STEEL MATERIAL

S280gd+z

DATE	17/11/2019
TEAM LEADER	RAFFAELE LANDOLFO
RESEARCH GROUP	LUGI FIORINO
	ALESSIA CAMPICHE
	SARMAD SHAKEEL
STUDENT	FERDINANDO NACLERIO

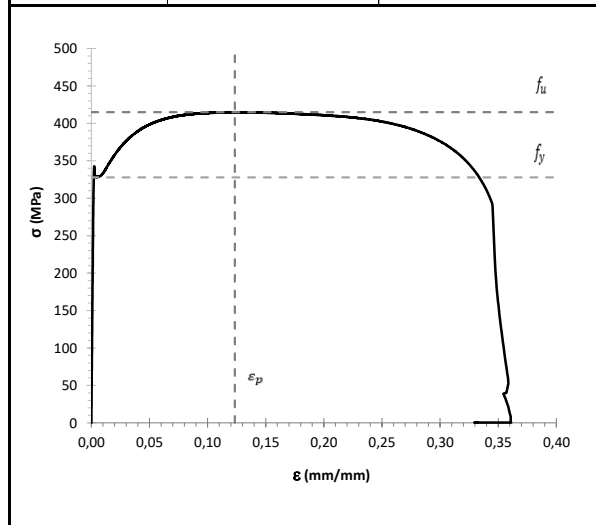


SPECIMEN DATA		
LABEL	S4_2	
COIL DATA	Type	S280gd+z
	Production factory	Lamieredil S.P.A
	Coil type	
	Production Date	
	Thickness (mm)	4,00
SAMPLE DATA-measured values	Original gauge length L_0 (mm)	50
	Width b_0 (mm)	20,00
	Thickness t_0 (mm)	4,00
	Cross section area (mm ²)	80,00



TEST DATA		
TEST PARAMETERS	Displacement rate (mm/s)	0,05
	Frequency (Hz)	5
	Test time (s)	288,66

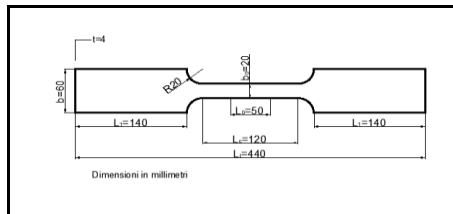
TEST RESULTS		
PRODUCTION VALUES	Yield strength R_e (Mpa)	280,00
	Tensile strength R_m (MPa)	360,00
RESULT VALUES	Yield strength f_y (Mpa)	327,81
	Tensile strength f_u (MPa)	414,98
	Last strain ϵ_u (mm/mm)	0,40
	Peak strain ϵ_p (mm/mm)	0,12
	Modulus of elasticity E (Mpa)	198408,87
TEST OUTCOME	Breaking	inside L_0



TENSILE TESTS ON STEEL MATERIAL

S280gd+z

DATE	17/11/2019
TEAM LEADER	RAFFAELE LANDOLFO
RESEARCH GROUP	LUIGI FIORINO
	ALESSIA CAMPICHE
	SARMAD SHAKEEL
STUDENT	FERDINANDO NACLERIO

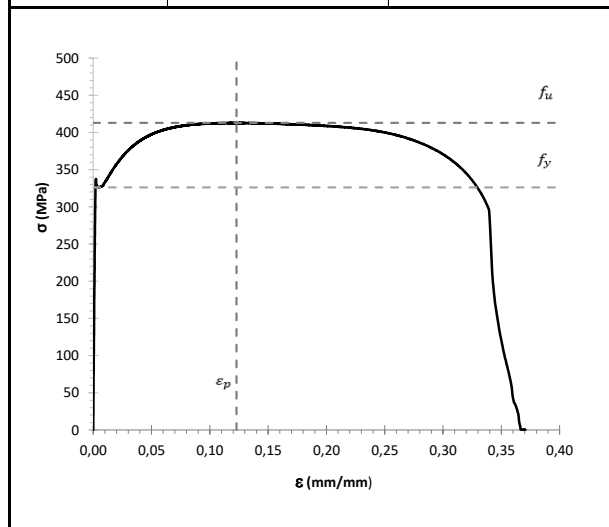


SPECIMEN DATA		
LABEL	S4_2	
COIL DATA	Type	S280gd+z
	Production factory	Lamieredil S.P.A
	Coil type	
	Production Date	
	Thickness (mm)	4,00
SAMPLE DATA-measured values	Original gauge length L_o (mm)	50
	Width b_o (mm)	20,00
	Thickness t_o (mm)	4,00
	Cross section area (mm ²)	80,00



TEST DATA		
TEST PARAMETERS	Displacement rate (mm/s)	0,05
	Frequency (Hz)	5
	Test time (s)	288,66

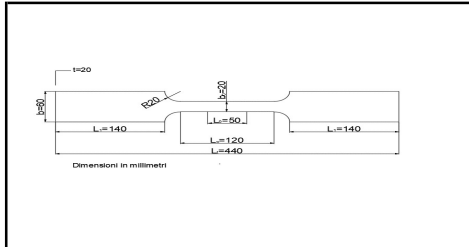
TEST RESULTS		
PRODUCTION VALUES	Yield strength R_e (Mpa)	280,00
	Tensile strength R_m (MPa)	360,00
RESULT VALUES	Yield strength f_y (Mpa)	326,18
	Tensile strength f_u (MPa)	412,92
	Last strain ϵ_u (mm/mm)	0,40
	Peak strain ϵ_p (mm/mm)	0,12
	Modulus of elasticity E (Mpa)	217438,44
TEST OUTCOME	Breaking	inside L_o



TENSILE TESTS ON STEEL MATERIAL

S355jr

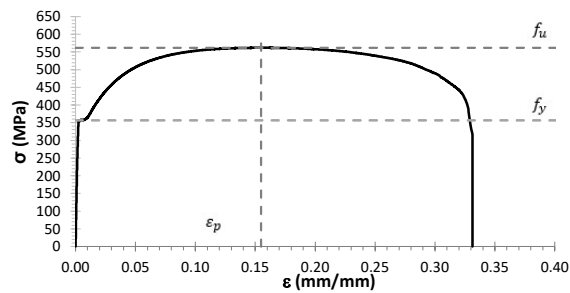
DATE	17/11/2019
TEAM LEADER	RAFFAELE LANDOLFO
RESEARCH GROUP	LUIGI FIORINO
	ALESSIA CAMPICHE
	SARMAD SHAKEEL
STUDENT	FERDINANDO NACLERIO



SPECIMEN DATA		
LABEL	S20_1	
COIL DATA	Type	S355jr
	Production factory	Lamieredil S.P.A
	Coil type	
	Production Date	
SAMPLE DATA-measured values	Thickness (mm)	20.00
	Original gauge length L_0 (mm)	50
	Width b_0 (mm)	20.00
	Thickness t_0 (mm)	20.00
	Cross section area (mm ²)	400.00

TEST DATA		
TEST PARAMETERS	Displacement rate (mm/s)	0.05
	Frequency (Hz)	5
	Test time (s)	288.66

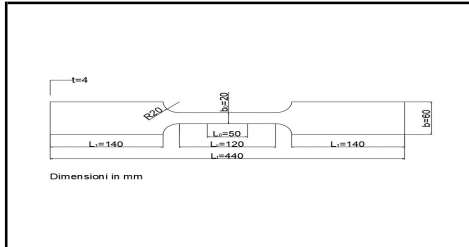
TEST RESULTS		
PRODUCTION VALUES	Yield strength R_e (Mpa)	355.00
	Tensile strength R_m (MPa)	510.00
RESULT VALUES	Yield strength f_y (Mpa)	356.98
	Tensile strength f_u (MPa)	561.91
	Last strain ϵ_u (mm/mm)	0.40
	Peak strain ϵ_p (mm/mm)	0.15
	Modulus of elasticity E (Mpa)	217438.44
TEST OUTCOME	Breaking	all'interno di L_0



TENSILE TESTS ON STEEL MATERIAL

S355jr

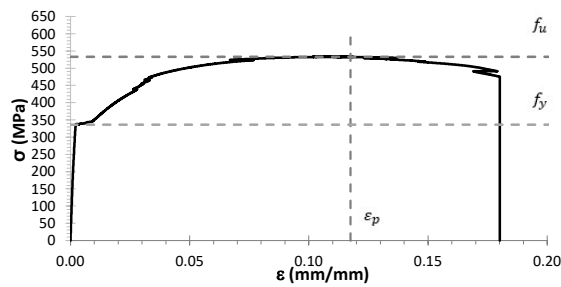
DATE	17/11/2019
TEAM LEADER	RAFFAELE LANDOLFO
RESEARCH GROUP	LUIGI FIORINO
	ALESSIA CAMPICHE
	SARMAD SHAKEEL
STUDENT	FERDINANDO NACLERIO



SPECIMEN DATA		
LABEL	S20_2	
COIL DATA	Type	S355jr
	Production factory	Lamieredil S.P.A
	Coil type	
	Production Date	
SAMPLE DATA-measured values	Thickness (mm)	20.00
	Original gauge length L_0 (mm)	50
	Width b_0 (mm)	21.00
	Thickness t_0 (mm)	20.00
	Cross section area (mm ²)	420.00

TEST DATA		
TEST PARAMETERS	Displacement rate (mm/s)	0.05
	Frequency (Hz)	5
	Test time (s)	288.66

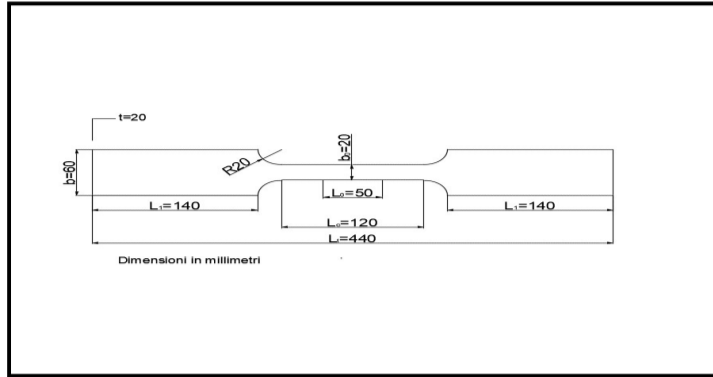
TEST RESULTS		
PRODUCTION VALUES	Yield strength R_e (Mpa)	355.00
	Tensile strength R_m (MPa)	510.00
RESULT VALUES	Yield strength f_y (Mpa)	336.43
	Tensile strength f_u (MPa)	533.31
	Last strain ϵ_u (mm/mm)	0.40
	Peak strain ϵ_p (mm/mm)	0.12
	Modulus of elasticity E (Mpa)	212711.81
TEST OUTCOME	Breaking	all'interno di L_0



TENSILE TESTS STEEL MATERIAL

S355jr

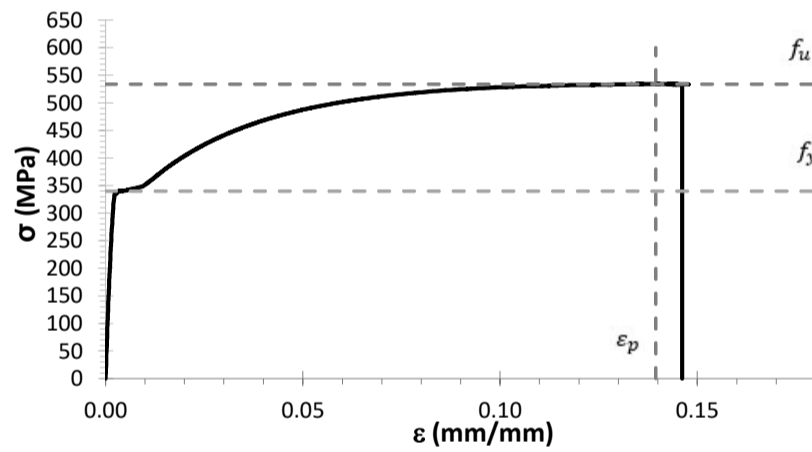
DATE	17/11/2019
TEAM LEADER	RAFFAELE LANDOLFO
RESEARCH GROUP	LUIGI FIORINO ALESSIA CAMPICHE SARMAD SHAKEEL
STUDENT	FERDINANDO NACLERIO



SPECIMEN DATA		
LABEL		
COIL DATA	Type	S355jr
	Production factory	Lamieredil S.P.A
	Coil type	
	Production Date	
	Thickness (mm)	25.00
SAMPLE DATA-measured values	Original gauge length L_0 (mm)	50
	Width b_0 (mm)	21.00
	Thickness t_0 (mm)	20.00
	Cross section area (mm ²)	420.00

TEST DATA		
TEST PARAMETERS	Displacement rate (mm/s)	0.05
	Frequency (Hz)	5
	Test time (s)	409.78

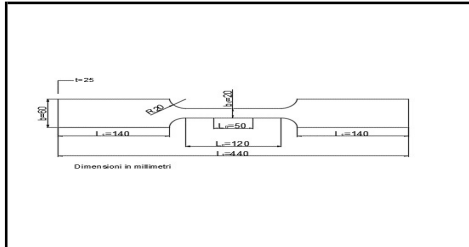
TEST RESULTS		
PRODUCTION VALUES	Yield strength R_e (Mpa)	355.00
	Tensile strength R_m (MPa)	510.00
RESULT VALUES	Yield strength f_y (Mpa)	339.85
	Tensile strength f_u (MPa)	533.83
	Last strain ϵ_u (mm/mm)	0.20
	Peak strain ϵ_p (mm/mm)	0.14
	Modulus of elasticity E (Mpa)	221304.75
TEST OUTCOME	Breaking	inside L_0



TENSILE TESTS STEEL MATERIAL

S355jr

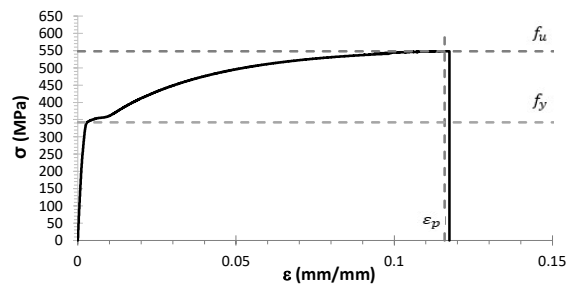
DATE	17/11/2019
TEAM LEADER	RAFFAELE LANDOLFO
RESEARCH GROUP	LUIGI FIORINO
	ALESSIA CAMPICHE
	SARMAD SHAKEEL
STUDENT	FERDINANDO NACLERIO



SPECIMEN DATA		
LABEL	Type	S355jr
COIL DATA	Production factory	Lamieredil S.P.A
	Coil type	
	Production Date	
	Thickness (mm)	25.00
SAMPLE DATA-measured values	Original gauge length L_0 (mm)	50
	Width b_0 (mm)	20.00
	Thickness t_0 (mm)	25.00
	Cross section area (mm ²)	500.00

TEST DATA		
TEST PARAMETERS	Displacement rate (mm/s)	0.05
	Frequency (Hz)	5
	Test time (s)	361.79

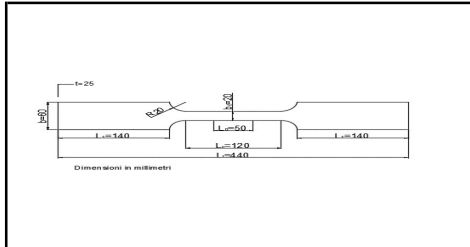
TEST RESULTS		
PRODUCTION VALUES	Yield strength R_e (Mpa)	355.00
	Tensile strength R_m (MPa)	510.00
RESULT VALUES	Yield strength f_y (Mpa)	342.37
	Tensile strength f_u (MPa)	548.19
	Last strain ϵ_u (mm/mm)	0.20
	Peak strain ϵ_p (mm/mm)	0.12
TEST OUTCOME	Modulus of elasticity E (Mpa)	211113.92
	Breaking	inside L_0



TENSILE TESTS STEEL MATERIAL

S355jr

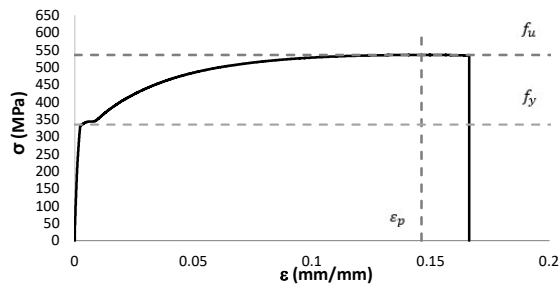
DATE	17/11/2019
TEAM LEADER	RAFFAELE LANDOLFO
RESEARCH GROUP	LUIGI FIORINO
	ALESSIA CAMPICHE
	SARMAD SHAKEEL
STUDENT	FERDINANDO NACLERIO



SPECIMEN DATA		
LABEL	S25_2	
COIL DATA	Type	S355jr
	Production factory	Lamieredil S.P.A
	Coil type	
	Production Date	
SAMPLE DATA-measured values	Thickness (mm)	25.00
	Original gauge length L_0 (mm)	50
	Width b_0 (mm)	20.00
	Thickness t_0 (mm)	25.00
	Cross section area (mm ²)	500.00

TEST DATA		
TEST PARAMETERS	Displacement rate (mm/s)	0.05
	Frequency (Hz)	5
	Test time (s)	412.25

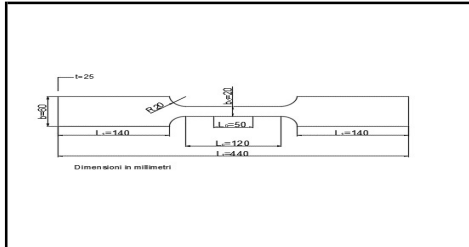
TEST RESULTS		
PRODUCTION VALUES	Yield strength R_e (Mpa)	355.00
	Tensile strength R_m (MPa)	510.00
RESULT VALUES	Yield strength f_y (Mpa)	334.48
	Tensile strength f_u (MPa)	535.35
	Last strain ϵ_u (mm/mm)	0.20
	Peak strain ϵ_p (mm/mm)	0.15
TEST OUTCOME	Modulus of elasticity E (Mpa)	332699.52
	Breaking	inside L_0



TENSILE TESTS STEEL MATERIAL

S355jr

DATE	17/11/2019
TEAM LEADER	RAFFAELE LANDOLFO
RESEARCH GROUP	LUIGI FIORINO
	ALESSIA CAMPICHE
	SARMAD SHAKEEL
STUDENT	FERDINANDO NACLERIO



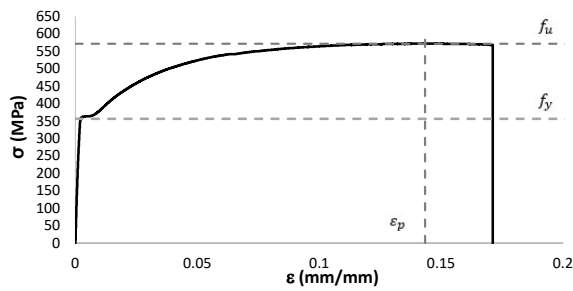
SPECIMEN DATA		
LABEL	S25_3	
COIL DATA	Type	S355jr
	Production factory	Lamieredil S.P.A
	Coil type	
	Production Date	
SAMPLE DATA-measured values	Thickness (mm)	25.00
	Original gauge length L_0 (mm)	50
	Width b_0 (mm)	19.00
	Thickness t_0 (mm)	25.00
	Cross section area (mm ²)	475.00

TEST DATA

TEST PARAMETERS		
	Displacement rate (mm/s)	0.05
	Frequency (Hz)	5
	Test time (s)	427.88

TEST RESULTS

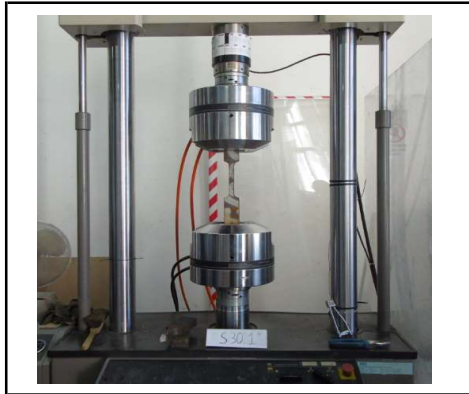
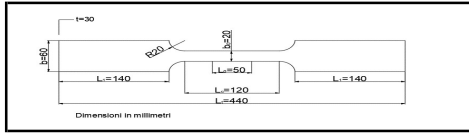
PRODUCTION VALUES		
	Yield strength R_e (Mpa)	355.00
	Tensile strength R_m (MPa)	510.00
RESULT VALUES	Yield strength f_y (Mpa)	356.26
	Tensile strength f_u (MPa)	571.63
	Last strain ϵ_u (mm/mm)	0.20
	Peak strain ϵ_p (mm/mm)	0.14
	Modulus of elasticity E (Mpa)	244858.88
TEST OUTCOME	Breaking	inside L_0



TENSILE TESTS STEEL MATERIAL

S355jr

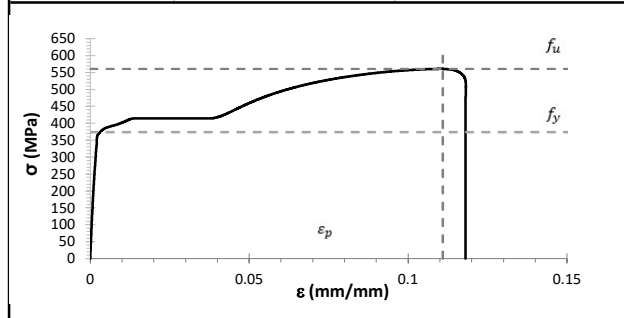
DATE	17/11/2019
TEAM LEADER	RAFFAELE LANDOLFO
RESEARCH GROUP	LUIGI FIORINO
	ALESSIA CAMPICHE
	SARMAD SHAKEEL
STUDENT	FERDINANDO NACLERIO



SPECIMEN DATA		
LABEL	S30_1	
COIL DATA	Type	S355jr
	Production factory	Lamieredil S.P.A
	Coil type	
	Production Date	
SAMPLE DATA-measured values	Thickness (mm)	30.00
	Original gauge length L_0 (mm)	50
	Width b_0 (mm)	19.00
	Thickness t_0 (mm)	30.00
	Cross section area (mm ²)	570.00

TEST DATA		
TEST PARAMETERS	Displacement rate (mm/s)	0.05
	Frequency (Hz)	5
	Test time (s)	235.45

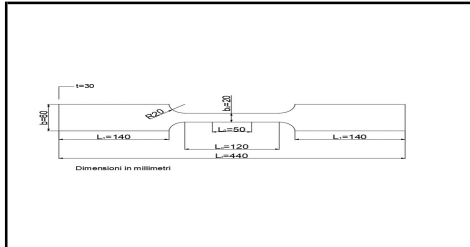
TEST RESULTS		
PRODUCTION VALUES	Yield strength R_e (Mpa)	355.00
	Tensile strength R_m (MPa)	510.00
RESULT VALUES	Yield strength f_y (Mpa)	374.02
	Tensile strength f_u (MPa)	560.79
	Last strain ϵ_u (mm/mm)	0.20
	Peak strain ϵ_p (mm/mm)	0.11
	Modulus of elasticity E (Mpa)	235034.31
TEST OUTCOME	Breaking	inside L_0



TENSILE TESTS STEEL MATERIAL

S355jr

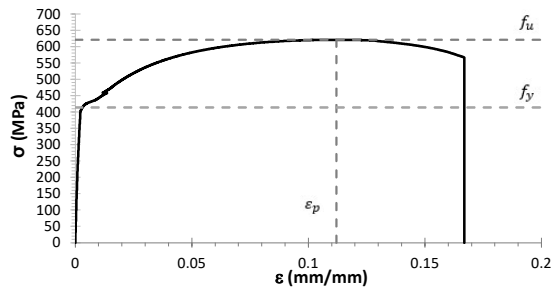
DATE	17/11/2019
TEAM LEADER	RAFFAELE LANDOLFO
RESEARCH GROUP	LUIGI FIORINO
	ALESSIA CAMPICHE
	SARMAD SHAKEEL
STUDENT	FERDINANDO NACLERIO



SPECIMEN DATA		
LABEL	S30_2	
COIL DATA	Type	S355jr
	Production factory	Lamieredil S.P.A
	Coil type	
	Production Date	
SAMPLE DATA-measured values	Thickness (mm)	30.00
	Original gauge length L_0 (mm)	50
	Width b_0 (mm)	17.00
	Thickness t_0 (mm)	30.00
	Cross section area (mm ²)	510.00

TEST DATA		
TEST PARAMETERS	Displacement rate (mm/s)	0.05
	Frequency (Hz)	5
	Test time (s)	235.28

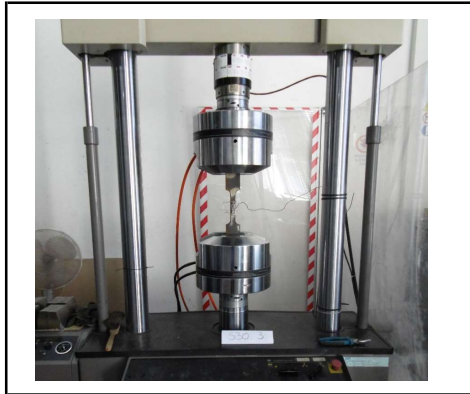
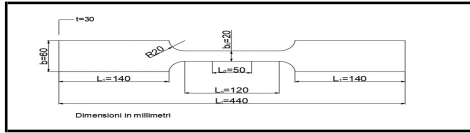
TEST RESULTS		
PRODUCTION VALUES	Yield strength R_e (Mpa)	355.00
	Tensile strength R_m (MPa)	510.00
RESULT VALUES	Yield strength f_y (Mpa)	414.10
	Tensile strength f_u (MPa)	620.95
	Last strain ϵ_u (mm/mm)	0.20
	Peak strain ϵ_p (mm/mm)	0.11
	Modulus of elasticity E (Mpa)	251373.01
TEST OUTCOME	Breaking	inside L_0



TENSILE TESTS STEEL MATERIAL

S355jr

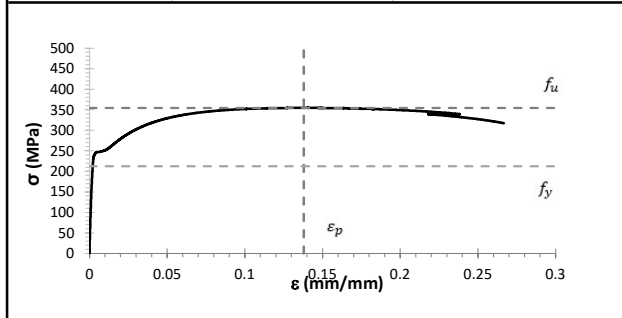
DATE	17/11/2019
TEAM LEADER	RAFFAELE LANDOLFO
RESEARCH GROUP	LUIGI FIORINO
	ALESSIA CAMPICHE
	SARMAD SHAKEEL
STUDENT	FERDINANDO NACLERIO



SPECIMEN DATA		
LABEL	S30_3	
COIL DATA	Type	S355jr
	Production factory	Lamieredil S.P.A
	Coil type	
	Production Date	
SAMPLE DATA-measured values	Thickness (mm)	30.00
	Original gauge length L_0 (mm)	50
	Width b_0 (mm)	21.00
	Thickness t_0 (mm)	30.00
	Cross section area (mm ²)	630.00

TEST DATA		
TEST PARAMETERS	Displacement rate (mm/s)	0.05
	Frequency (Hz)	5
	Test time (s)	415.19

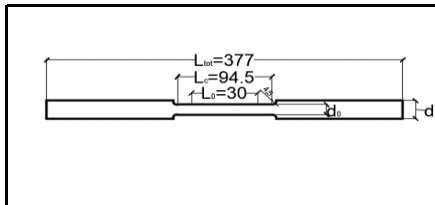
TEST RESULTS		
PRODUCTION VALUES	Yield strength R_e (Mpa)	355.00
	Tensile strength R_m (MPa)	510.00
RESULT VALUES	Yield strength f_y (Mpa)	212.57
	Tensile strength f_u (MPa)	354.50
	Last strain ϵ_u (mm/mm)	0.20
	Peak strain ϵ_p (mm/mm)	0.14
	Modulus of elasticity E (Mpa)	151744.88
TEST OUTCOME	Breaking	inside L_0



TENSILE TESTS ON STEEL MATERIAL

UHSS1300

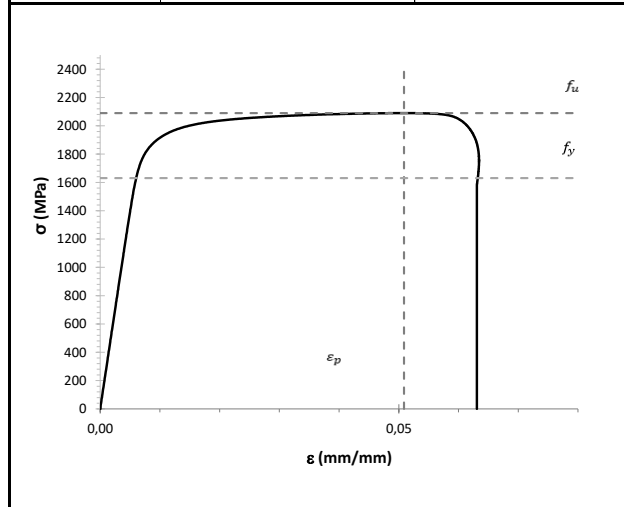
DATE	17/02/2014
TEAM LEADER	RAFFAELE LANDOLFO
RESEARCH GROUP	LUIGI FIORINO
	ALESSIA CAMPICHE
	SARMAD SHAKEEL
STUDENT	FERDINANDO NACLERIO



SPECIMEN DATA		
LABEL	L1	
COIL DATA	Type	UHSS1300
	Production factory	Lamieredil S.P.A
	Coil type	
	Production Date	
	Thickness (mm)	12,00
SAMPLE DATA-measured values	Original gauge length L_0 (mm)	30
	Width b_0 (mm)	21,00
	Thickness t_0 (mm)	9,50
	Cross section area (mm ²)	80,12

TEST DATA		
TEST PARAMETERS	Displacement rate (mm/s)	0,05
	Frequency (Hz)	5
	Test time (s)	197,24

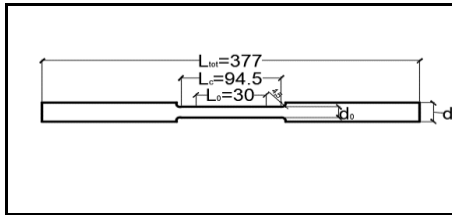
TEST RESULTS		
PRODUCTION VALUES	Yield strength R_e (Mpa)	1300,00
	Tensile strength R_m (MPa)	1450,00
RESULT VALUES	Yield strength f_y (Mpa)	1630,57
	Tensile strength f_u (MPa)	2089,71
	Last strain ϵ_u (mm/mm)	0,67
	Peak strain ϵ_p (mm/mm)	0,05
	Modulus of elasticity E (Mpa)	283651,12
TEST OUTCOME	Breaking	inside L_0



TENSILE TESTS ON STEEL MATERIAL

UHSS1300

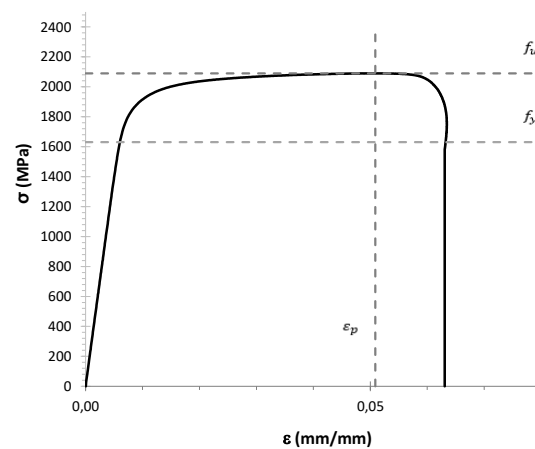
DATE	17/02/2014
TEAM LEADER	RAFFAELE LANDOLFO
RESEARCH GROUP	LUIGI FIORINO
	ALESSIA CAMPICHE
	SARMAD SHAKEEL
STUDENT	FERDINANDO NACLERIO



SPECIMEN DATA		
LABEL	L2	
COIL DATA	Type	UHSS1300
	Production factory	Lamieredil S.P.A
	Coil type	
	Production Date	
	Diameter (mm)	12,00
SAMPLE DATA-measured values	Original gauge length L_0 (mm)	30
	Diameter d (mm)	21,00
	Diameter d_0 (mm)	9,50
	Cross section area (mm ²)	80,12

TEST DATA		
TEST PARAMETERS	Displacement rate (mm/s)	0,05
	Frequency (Hz)	5
	Test time (s)	104,23

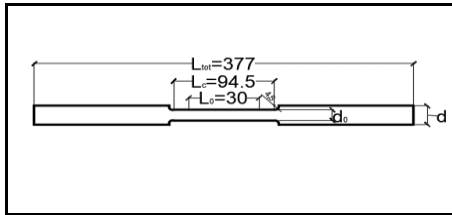
TEST RESULTS		
PRODUCTION VALUES	Yield strength R_p (Mpa)	1300,00
	Tensile strength R_m (MPa)	1450,00
RESULT VALUES	Yield strength f_y (Mpa)	1630,57
	Tensile strength f_u (MPa)	2089,71
	Last strain ϵ_u (mm/mm)	0,67
	Peak strain ϵ_p (mm/mm)	0,05
	Modulus of elasticity E (Mpa)	283651,12
TEST OUTCOME	Breaking	inside L_0



TENSILE TESTS ON STEEL MATERIAL

UHSS1300

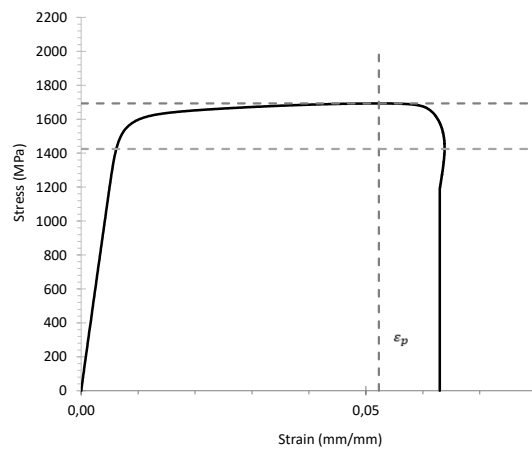
DATE	17/11/2019
TEAM LEADER	RAFFAELE LANDOLFO
RESEARCH GROUP	LUIGI FIORINO
	ALESSIA CAMPICHE
	SARMAD SHAKEEL
STUDENT	FETRDINANDO NACLERIO



SPECIMEN DATA		
LABEL	L3	
COIL DATA	Type	UHSS1300
	Production factory	Lamieredil S.P.A
	Coil type	
	Production Date	
SAMPLE DATA-measured values	Diameter (mm)	12,00
	Original gauge length L_0 (mm)	30
	Diameter d (mm)	21,00
	Diameter d_0 (mm)	11,00
	Cross section area (mm ²)	95,03

TEST DATA		
TEST PARAMETERS	Displacement rate (mm/s)	0,05
	Frequency (Hz)	5
	Test time (s)	102,45

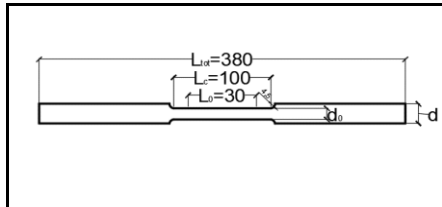
TEST RESULTS		
PRODUCTION VALUES	Yield strength R_p (Mpa)	1300,00
	Tensile strength R_m (MPa)	1450,00
RESULT VALUES	Yield strength f_y (Mpa)	1424,64
	Tensile strength f_u (MPa)	1693,20
	Last strain ϵ_u (mm/mm)	0,67
	Peak strain ϵ_p (mm/mm)	0,05
	Modulus of elasticity E (Mpa)	241825,53
TEST OUTCOME	Breaking	inside L_0



TENSILE TESTS ON STEEL MATERIAL

UHSS1300

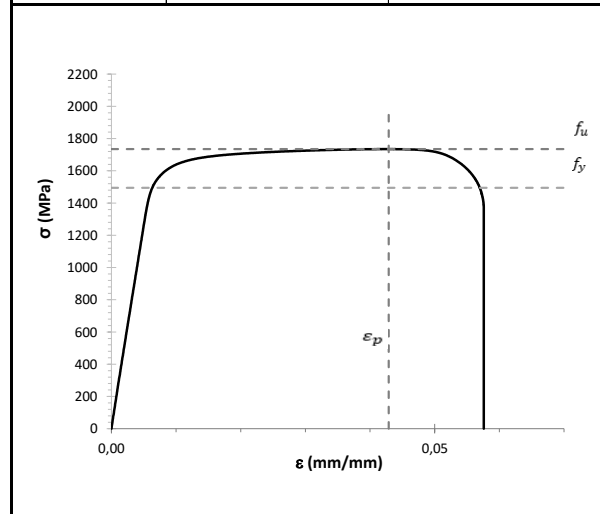
DATE	17/11/2019
TEAM LEADER	RAFFAELE LANDOLFO
RESEARCH GROUP	LUIGI FIORINO
	ALESSIA CAMPICHE
	SARMAD SHAKEEL
STUDENT	FETR DINANDO NACLERIO



SPECIMEN DATA		
LABEL	M1	
COIL DATA	Type	UHSS1300
	Production factory	Lamieredil S.P.A
	Coil type	
	Production Date	
	Diameter (mm)	14,00
SAMPLE DATA-measured values	Original gauge length L_0 (mm)	30
	Diameter d (mm)	26,00
	Diameter d_0 (mm)	13,00
	Cross section area (mm ²)	132,73

TEST DATA		
TEST PARAMETERS	Displacement rate (mm/s)	0,05
	Frequency (Hz)	5
	Test time (s)	102,45

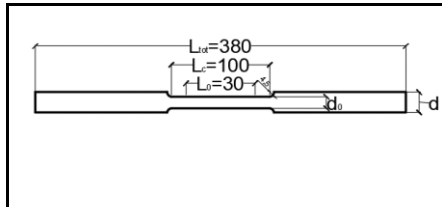
TEST RESULTS		
PRODUCTION VALUES	Yield strength R_e (Mpa)	1300,00
	Tensile strength R_m (MPa)	1450,00
RESULT VALUES	Yield strength f_y (Mpa)	1494,47
	Tensile strength f_u (MPa)	1734,72
	Last strain ϵ_w (mm/mm)	0,67
	Peak strain ϵ_p (mm/mm)	0,04
	Modulus of elasticity E (Mpa)	263508,18
TEST OUTCOME	Breaking	inside L_0



TENSILE TESTS ON STEEL MATERIAL

UHSS1300

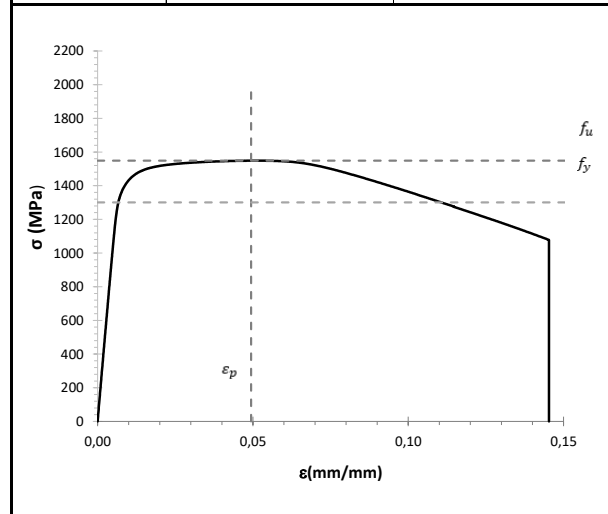
DATE	17/11/2019
TEAM LEADER	RAFFAELE LANDOLFO
RESEARCH GROUP	LUIGI FIORINO
	ALESSIA CAMPICHE
	SARMAD SHAKEEL
STUDENT	FETRINANDO NACLERIO



SPECIMEN DATA		
LABEL	M2	
COIL DATA	Type	UHSS1300
	Production factory	Lamieredil S.P.A
	Coil type	
	Production Date	
	Diameter (mm)	14,00
SAMPLE DATA-measured values	Original gauge length L_0 (mm)	30
	Diameter d (mm)	26,50
	Diameter d_0 (mm)	14,00
	Cross section area (mm ²)	153,94

TEST DATA		
TEST PARAMETERS	Displacement rate (mm/s)	0,05
	Frequency (Hz)	5
	Test time (s)	102,45

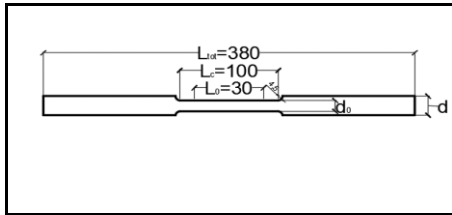
TEST RESULTS		
PRODUCTION VALUES	Yield strength R_e (Mpa)	1300,00
	Tensile strength R_m (MPa)	1450,00
RESULT VALUES	Yield strength f_y (Mpa)	1300,68
	Tensile strength f_u (MPa)	1548,67
	Last strain ϵ_u (mm/mm)	0,67
	Peak strain ϵ_p (mm/mm)	0,05
	Modulus of elasticity E (Mpa)	263508,18
TEST OUTCOME	Breaking	inside L_0



TENSILE TESTS ON STEEL MATERIAL

UHSS1300

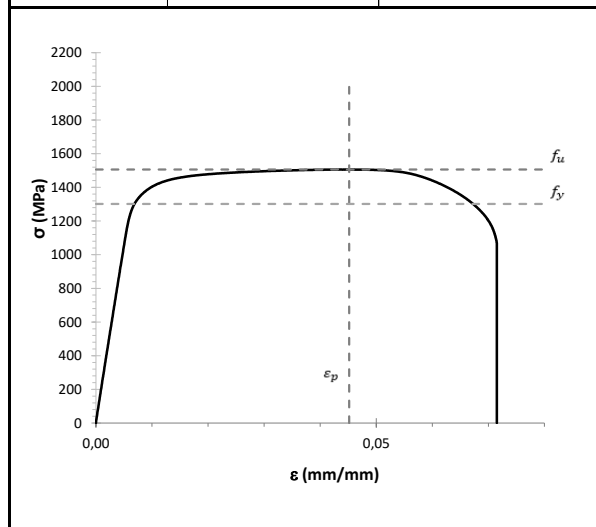
DATE	17/11/2019
TEAM LEADER	RAFFAELE LANDOLFO
RESEARCH GROUP	LUIGI FIORINO
	ALESSIA CAMPICHE
	SARMAD SHAKEEL
STUDENT	FETRDINANDO NACLERIO



SPECIMEN DATA		
LABEL	M3	
COIL DATA	Type	UHSS1300
	Production factory	Lamieredil S.P.A
	Coil type	
	Production Date	
	Diameter (mm)	14,00
SAMPLE DATA-measured values	Original gauge length L_0 (mm)	30
	Diameter d (mm)	26,50
	Diameter d_0 (mm)	14,00
	Cross section area (mm ²)	153,94

TEST DATA		
TEST PARAMETERS	Displacement rate (mm/s)	0,05
	Frequency (Hz)	5
	Test time (s)	102,45

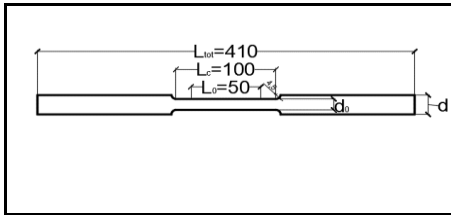
TEST RESULTS		
PRODUCTION VALUES	Yield strength R_p (Mpa)	1300,00
	Tensile strength R_m (MPa)	1450,00
RESULT VALUES	Yield strength f_y (Mpa)	1301,41
	Tensile strength f_u (MPa)	1506,00
	Last strain ϵ_u (mm/mm)	0,67
	Peak strain ϵ_p (mm/mm)	0,05
	Modulus of elasticity E (Mpa)	263508,18
TEST OUTCOME	Breaking	inside L_0



TENSILE TESTS ON STEEL MATERIAL

UHSS1300

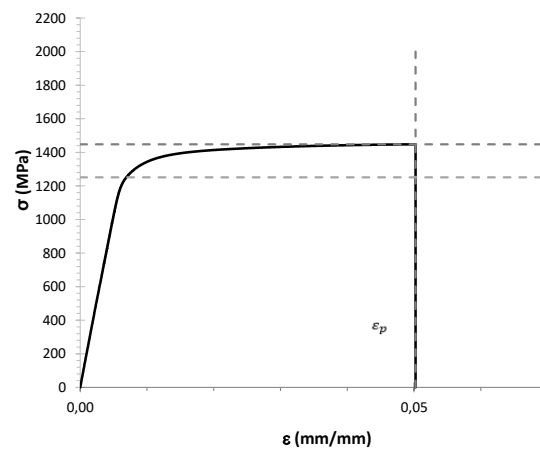
DATE	17/11/2019
TEAM LEADER	RAFFAELE LANDOLFO
RESEARCH GROUP	LUIGI FIORINO
	ALESSIA CAMPICHE
	SARMAD SHAKEEL
STUDENT	FETRDINANDO NACLERIO



SPECIMEN DATA		
LABEL	W1	
COIL DATA	Type	UHSS1300
	Production factory	Lamieredil S.P.A
	Coil type	
	Production Date	
	Diameter (mm)	18,00
SAMPLE DATA-measured values	Original gauge length L_0 (mm)	50
	Diameter d (mm)	32,00
	Diameter d_0 (mm)	18,00
	Cross section area (mm ²)	254,47

TEST DATA		
TEST PARAMETERS	Displacement rate (mm/s)	0,05
	Frequency (Hz)	5
	Test time (s)	102,45

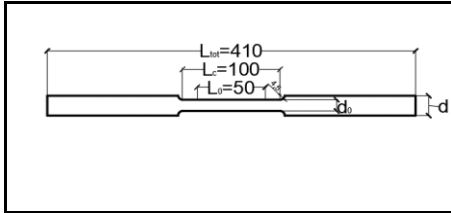
TEST RESULTS		
PRODUCTION VALUES	Yield strength R_p (Mpa)	1300,00
	Tensile strength R_m (MPa)	1450,00
RESULT VALUES	Yield strength f_y (Mpa)	1251,06
	Tensile strength f_u (MPa)	1447,74
	Last strain ϵ_u (mm/mm)	0,40
	Peak strain ϵ_p (mm/mm)	0,05
	Modulus of elasticity E (Mpa)	207060,75
TEST OUTCOME	Breaking	inside L_0



TENSILE TESTS ON STEEL MATERIAL

UHSS1300

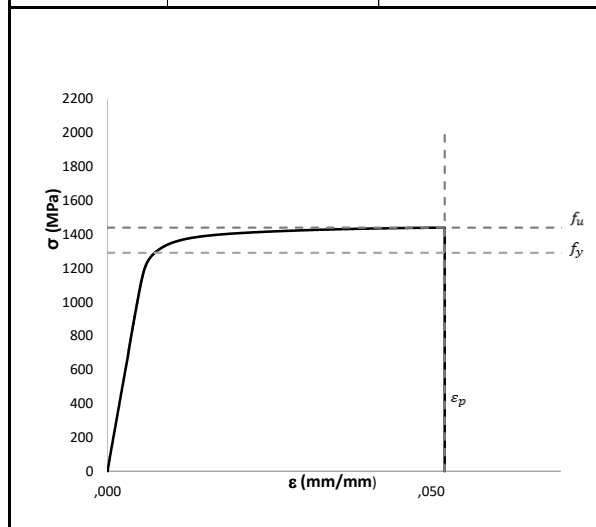
DATE	17/11/2019
TEAM LEADER	RAFFAELE LANDOLFO
RESEARCH GROUP	LUIGI FIORINO
	ALESSIA CAMPICHE
	SARMAD SHAKEEL
STUDENT	FETRDINANDO NACLERIO



SPECIMEN DATA		
LABEL	W2	
COIL DATA	Type	UHSS1300
	Production factory	Lamieredil S.P.A
	Coil type	
	Production Date	
	Diameter (mm)	18,00
SAMPLE DATA-measured values	Original gauge length L_0 (mm)	50
	Diameter d (mm)	31,50
	Diameter d_0 (mm)	18,00
	Cross section area (mm ²)	254,47

TEST DATA		
TEST PARAMETERS	Displacement rate (mm/s)	0,05
	Frequency (Hz)	5
	Test time (s)	102,45

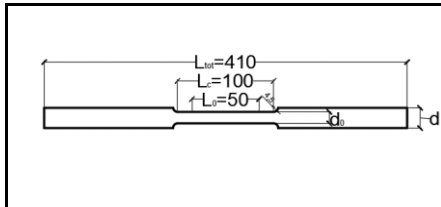
TEST RESULTS		
PRODUCTION VALUES	Yield strength R_p (Mpa)	1300,00
	Tensile strength R_m (MPa)	1450,00
RESULT VALUES	Yield strength f_y (Mpa)	1203,84
	Tensile strength f_u (MPa)	1438,80
	Last strain ϵ_u (mm/mm)	0,40
	Peak strain ϵ_p (mm/mm)	0,05
	Modulus of elasticity E (Mpa)	207060,75
TEST OUTCOME	Breaking	inside L_0



TENSILE TESTS ON STEEL MATERIAL

UHSS1300

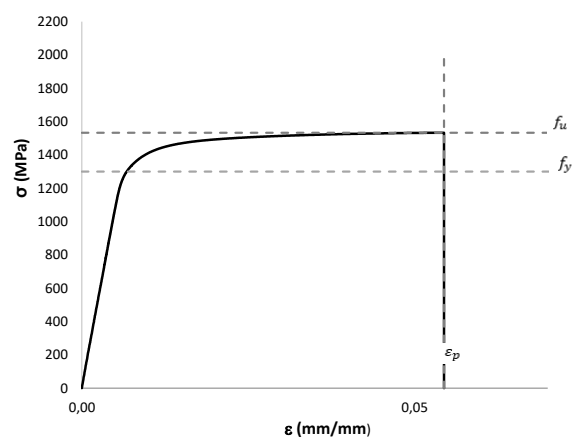
DATE	17/11/2019
TEAM LEADER	RAFFAELE LANDOLFO
RESEARCH GROUP	LUIGI FIORINO
	ALESSIA CAMPICHE
	SARMAD SHAKEEL
STUDENT	FETR DINANDO NACLERIO



SPECIMEN DATA		
LABEL	W3	
COIL DATA	Type	UHSS1300
	Production factory	Lamieredil S.P.A
	Coil type	
	Production Date	
	Diameter (mm)	18,00
SAMPLE DATA-measured values	Original gauge length L_0 (mm)	50
	Diameter d (mm)	31,50
	Diameter d_0 (mm)	17,50
	Cross section area (mm^2)	240,53

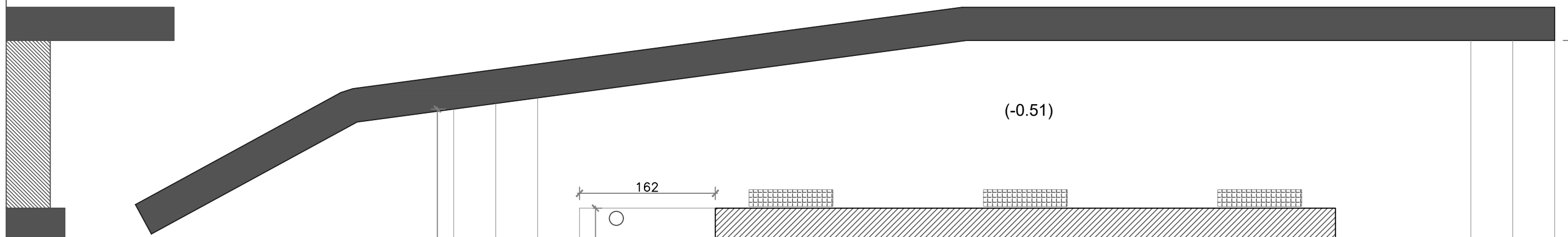
TEST DATA		
TEST PARAMETERS	Displacement rate (mm/s)	0,05
	Frequency (Hz)	5
	Test time (s)	102,45

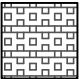
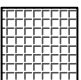
TEST RESULTS		
PRODUCTION VALUES	Yield strength R_e (Mpa)	1300,00
	Tensile strength R_m (MPa)	1450,00
RESULT VALUES	Yield strength f_y (Mpa)	1272,17
	Tensile strength f_u (MPa)	1533,02
	Last strain ϵ_w (mm/mm)	0,40
	Peak strain ϵ_p (mm/mm)	0,05
	Modulus of elasticity E (Mpa)	232167,57
TEST OUTCOME	Breaking	inside L_0

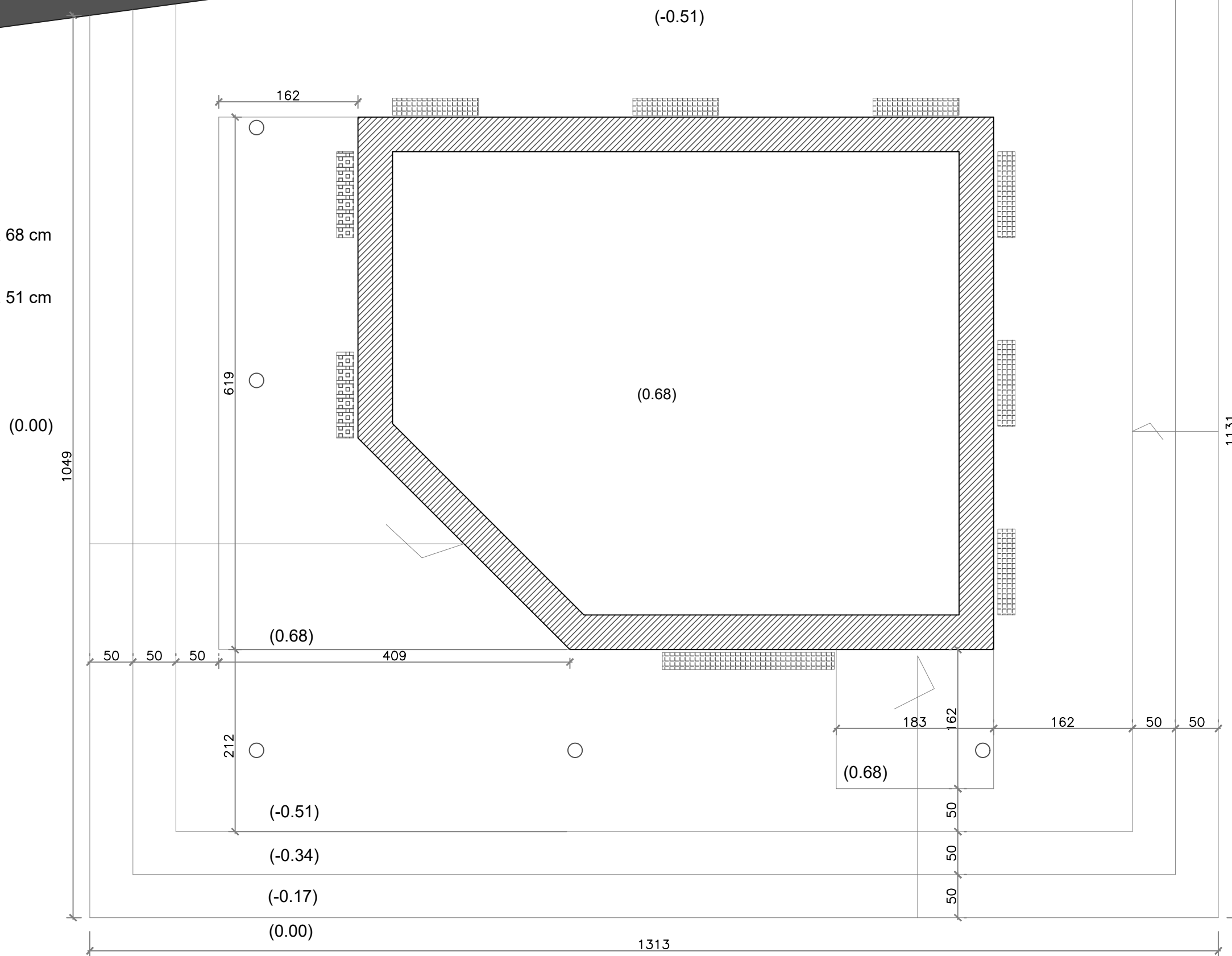


Appendix 3: Prototype drawings

A-A'



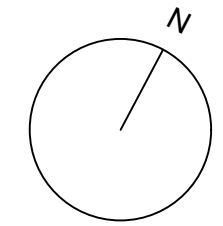
-  Canale di ventilazione quota 68 cm
-  Canale di ventilazione quota 51 cm



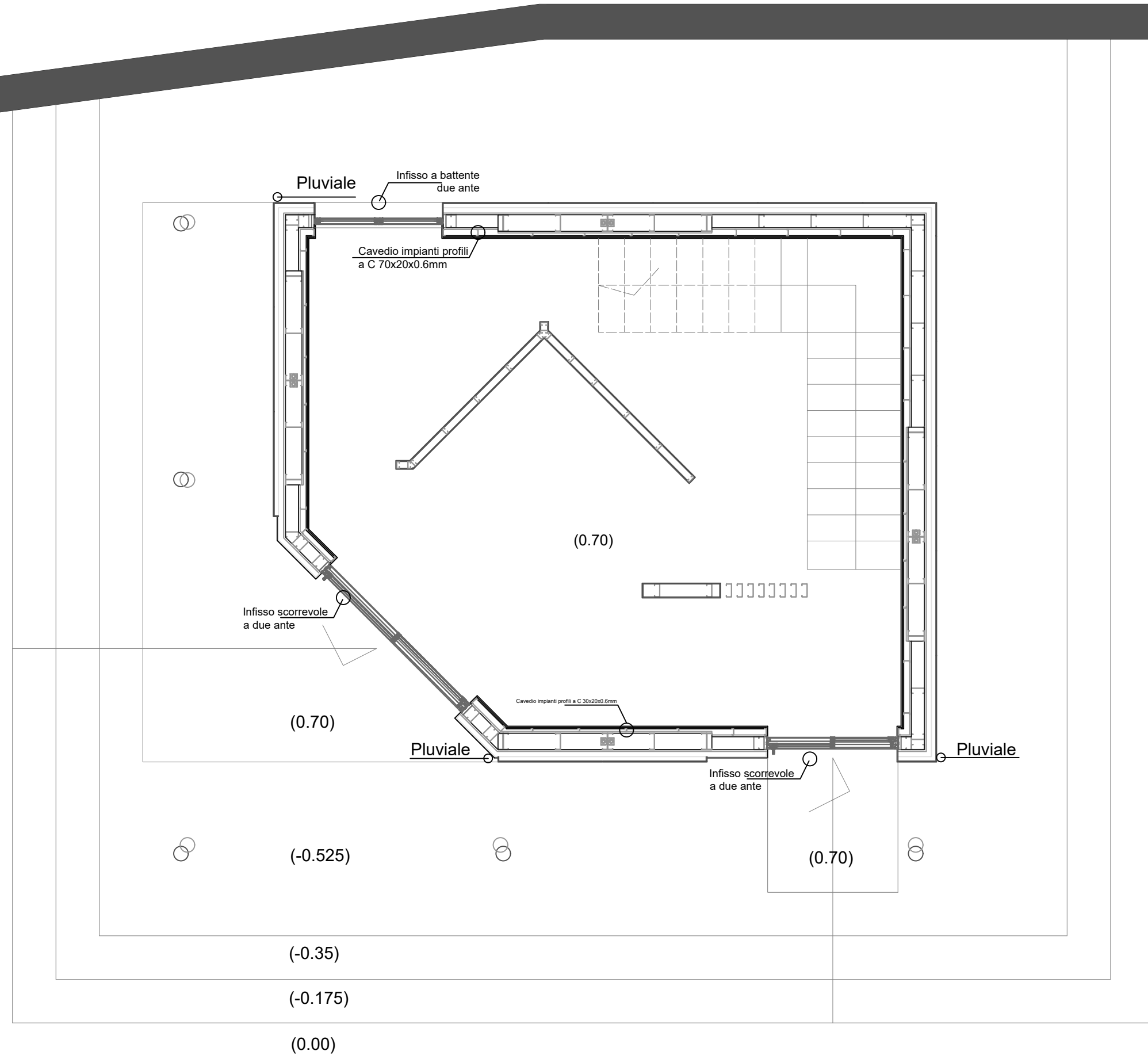
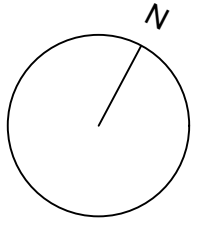
(0.00)
B-B'

B-B'

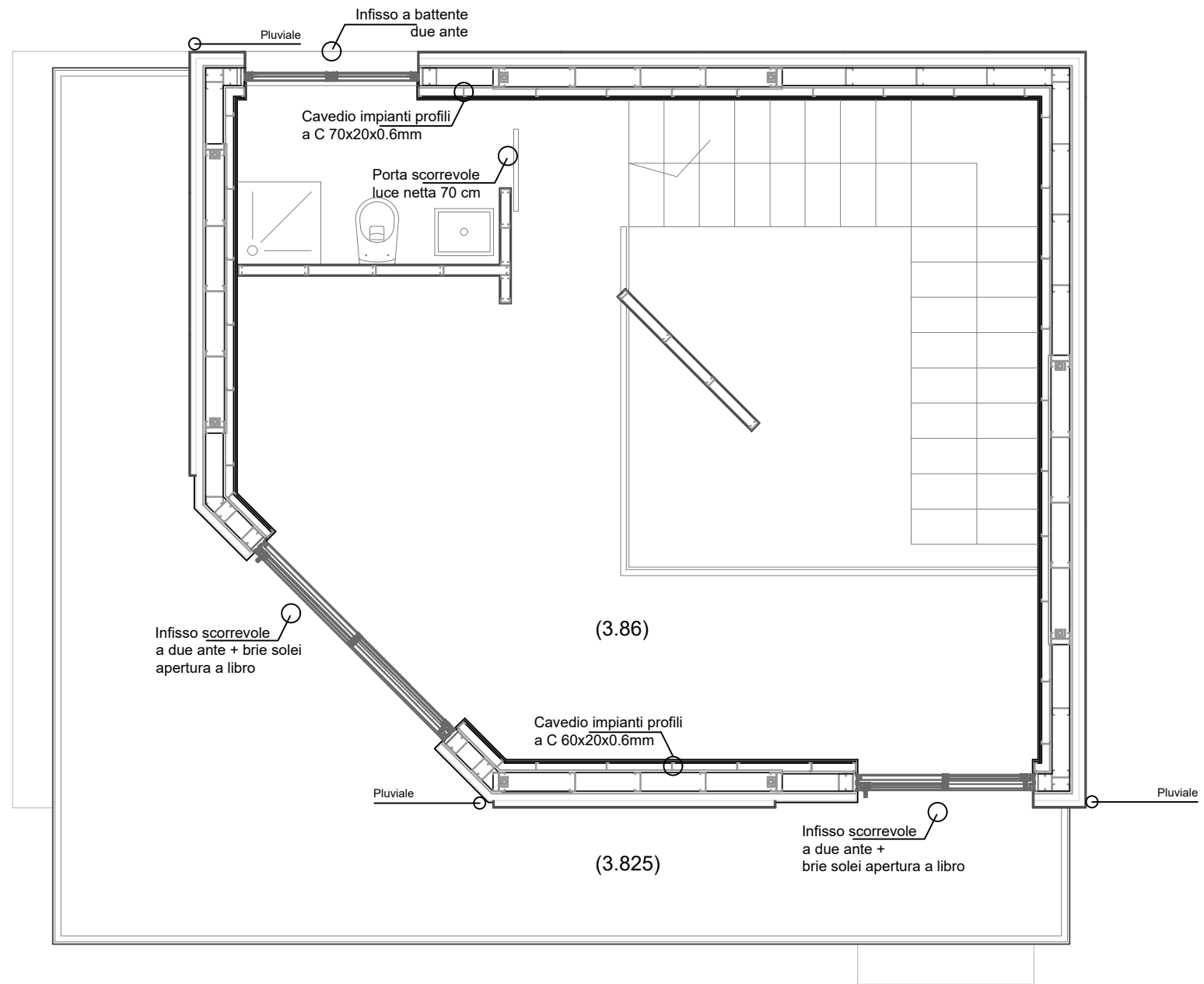
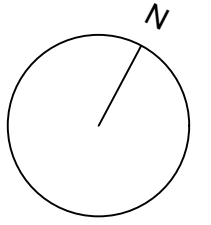
A-A'



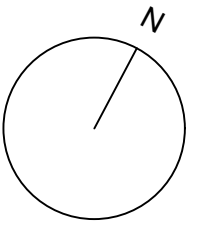
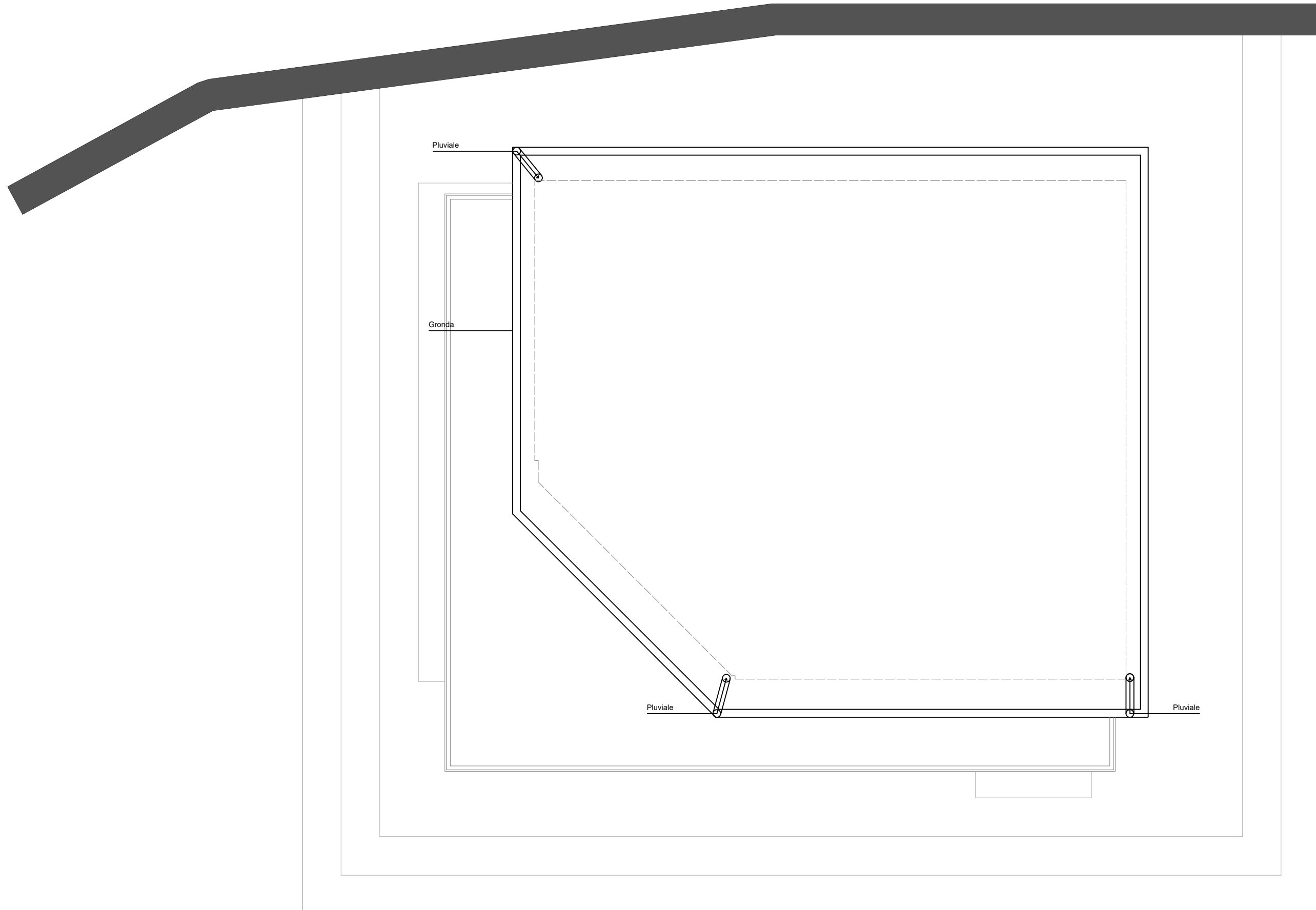
Pianta piano terra



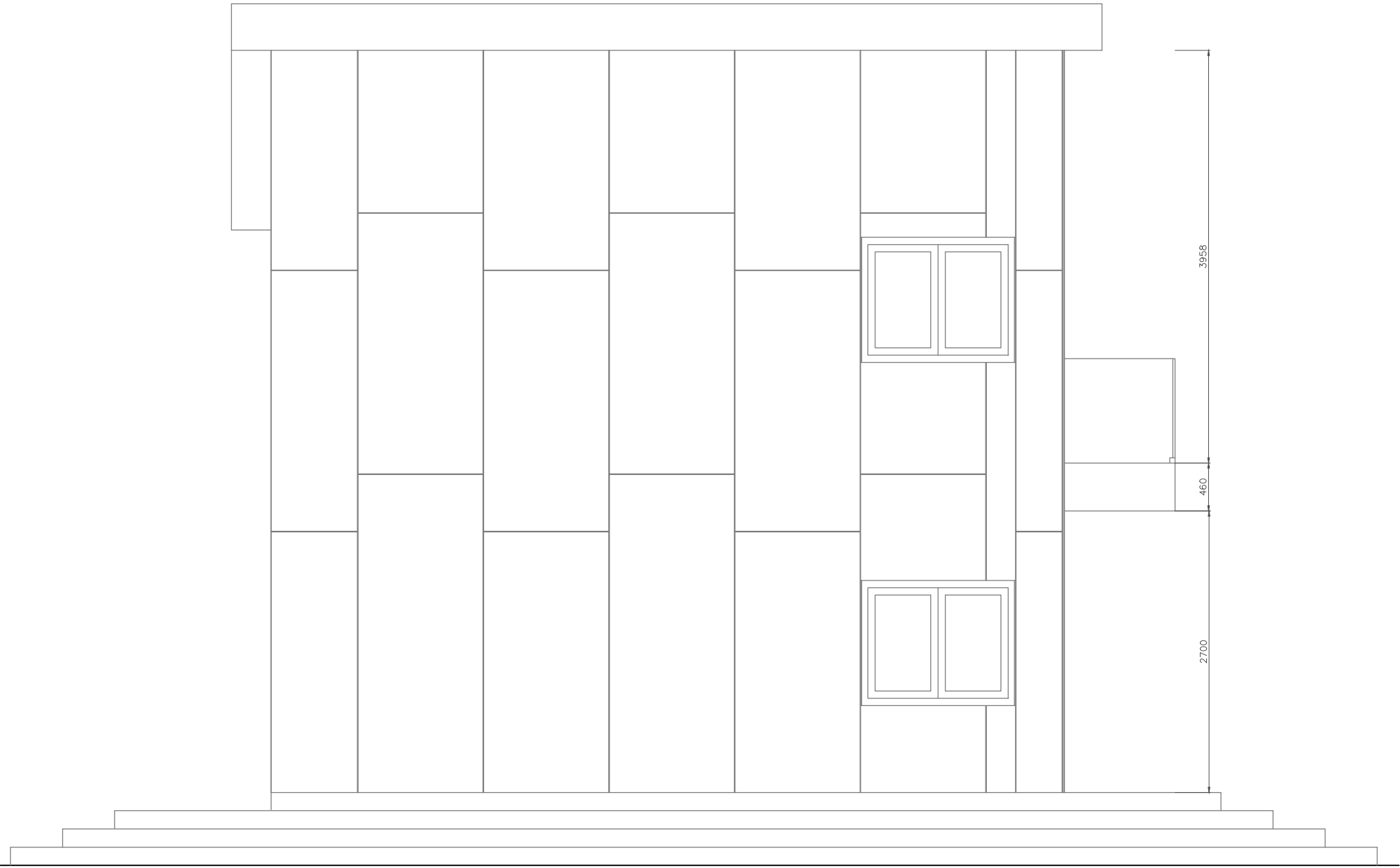
Pianta piano primo



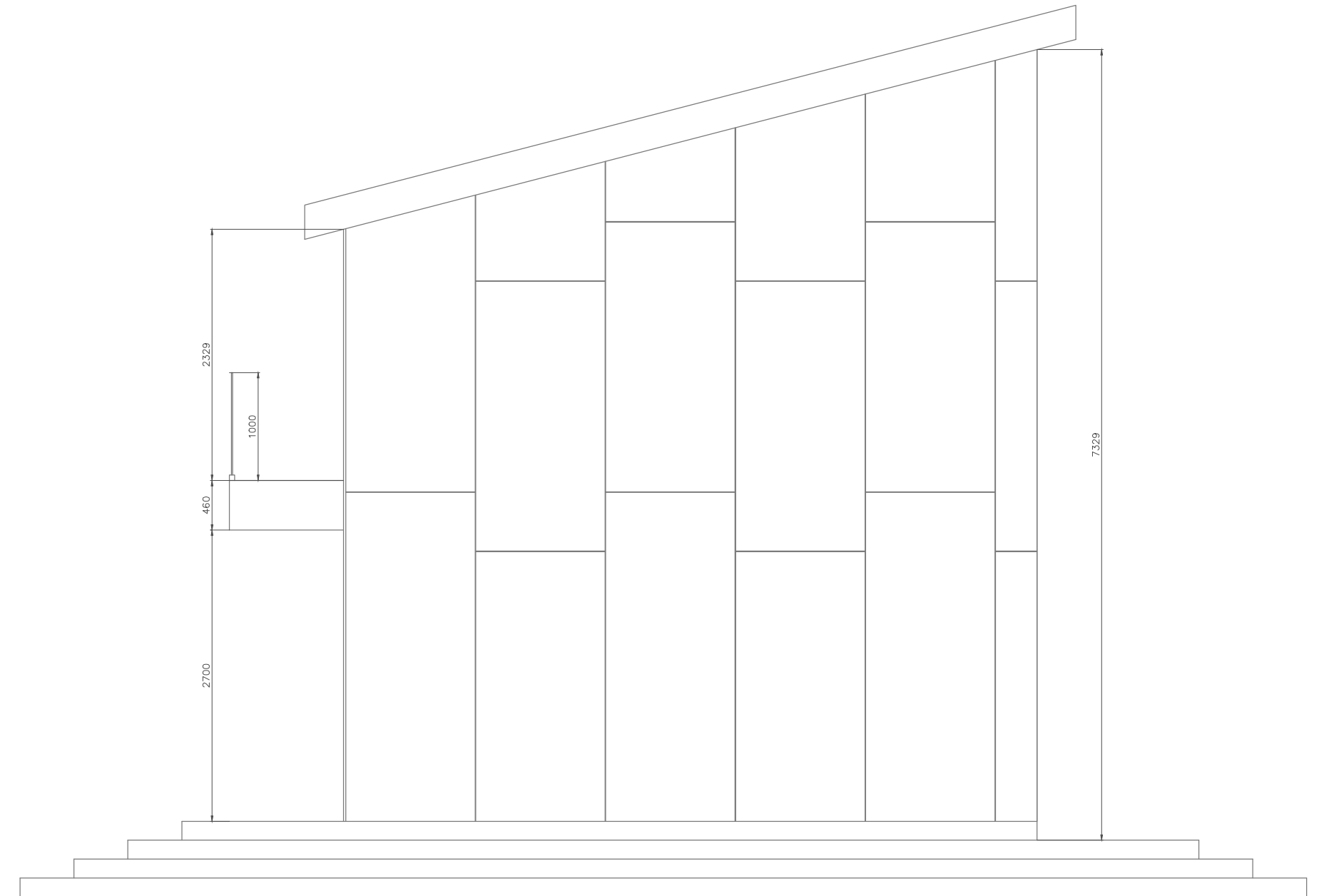
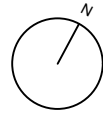
Pianta copertura



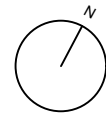
Prospetto Nord-ovest



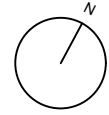
Prospetto Sud-est



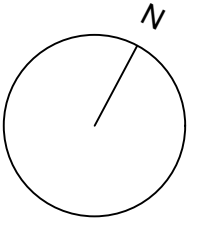
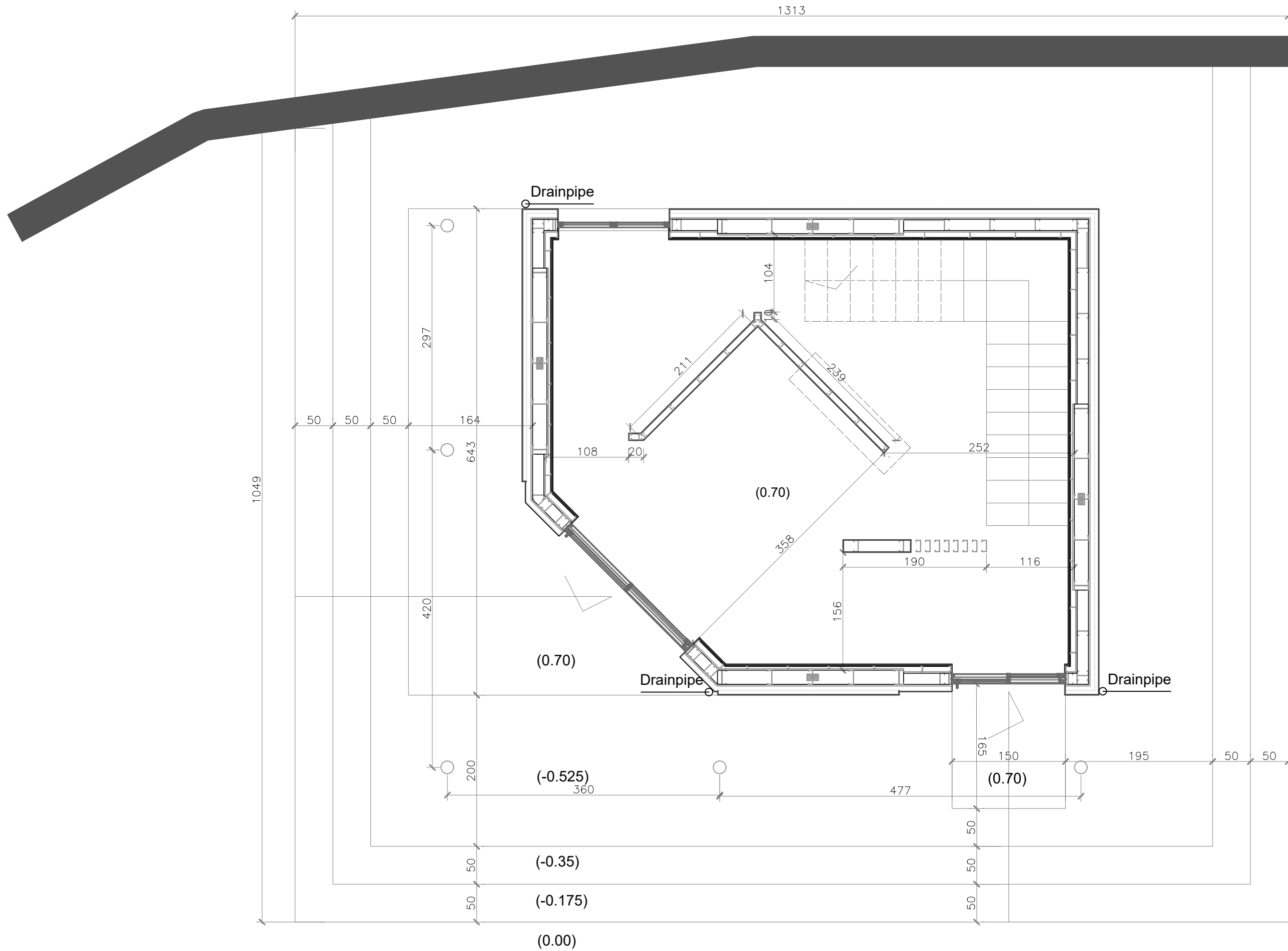
Prospetto Nord-est



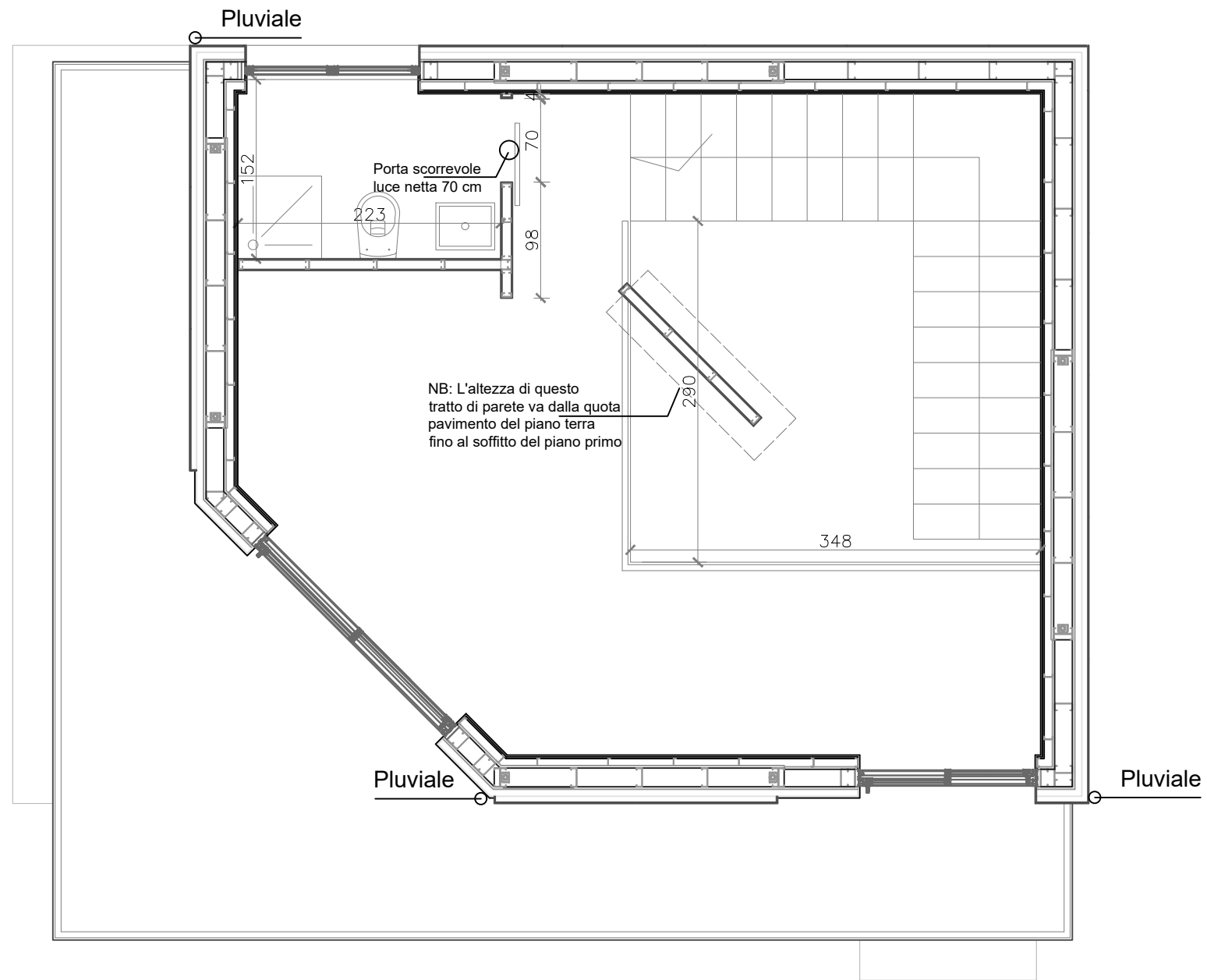
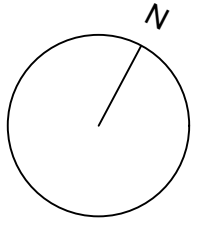
Prospetto Sud-Ovest



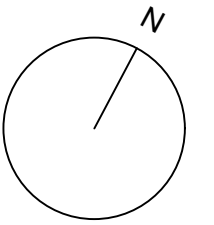
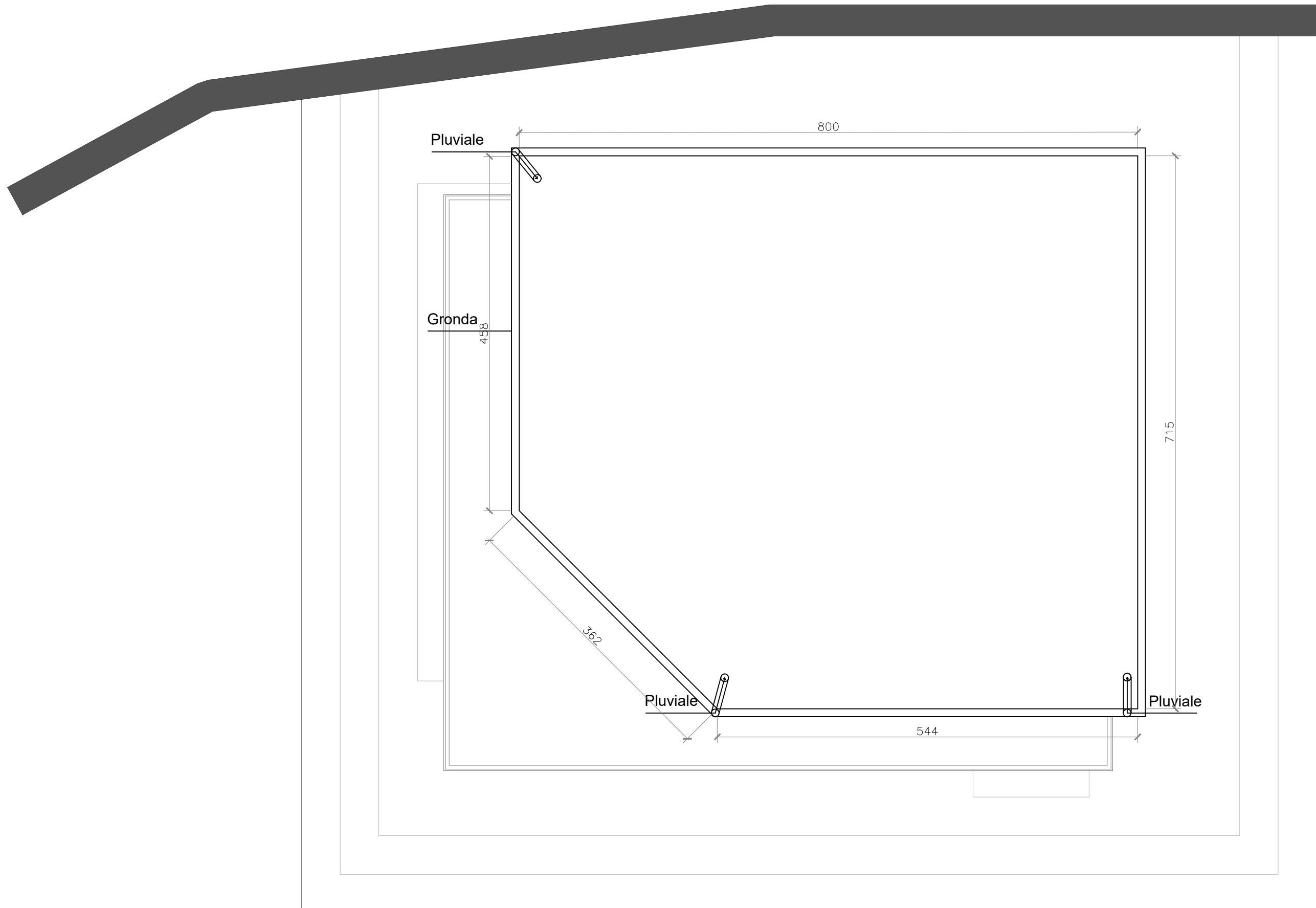
Ground floor



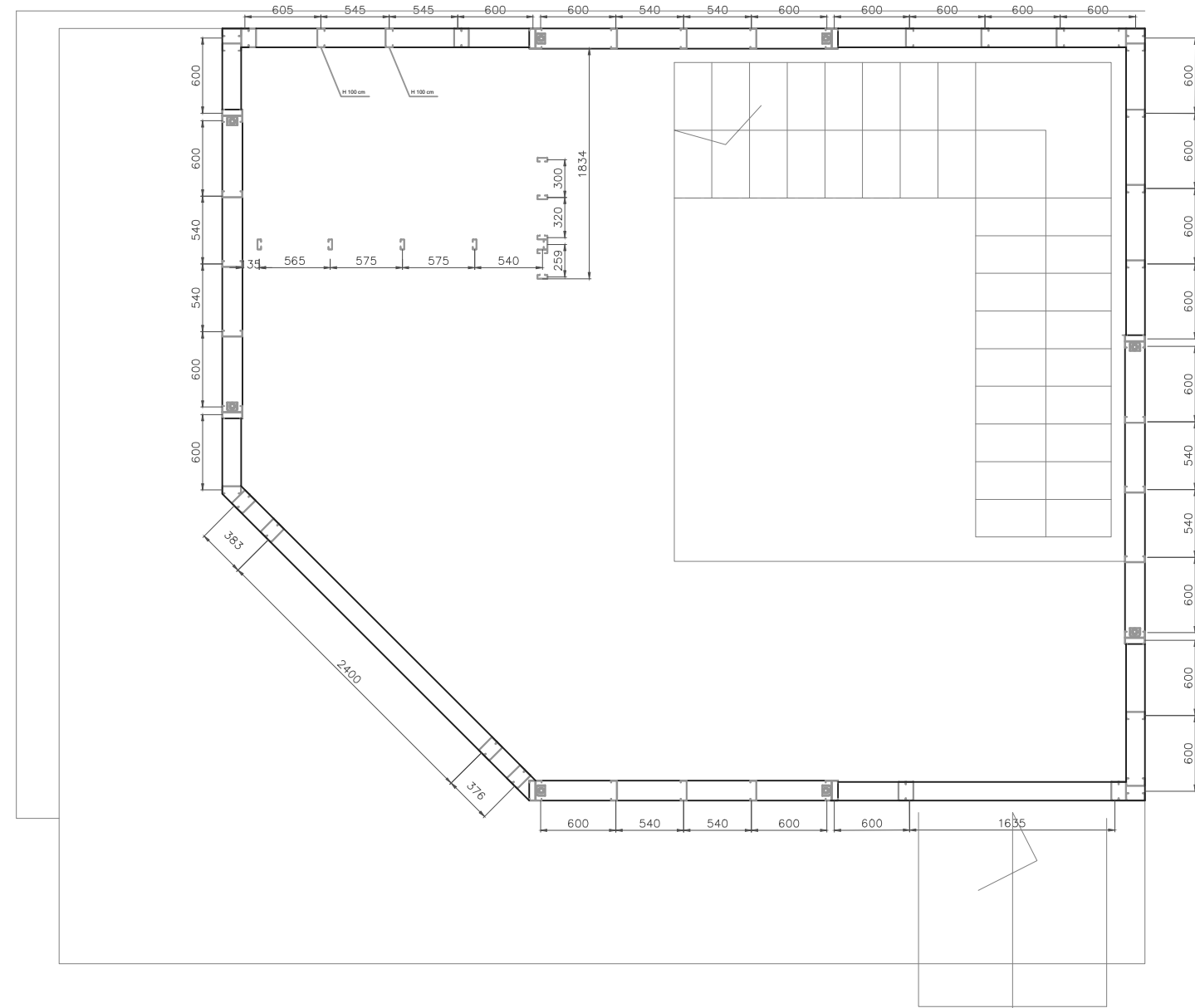
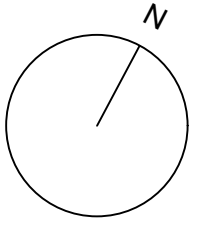
Pianta piano primo spiccato



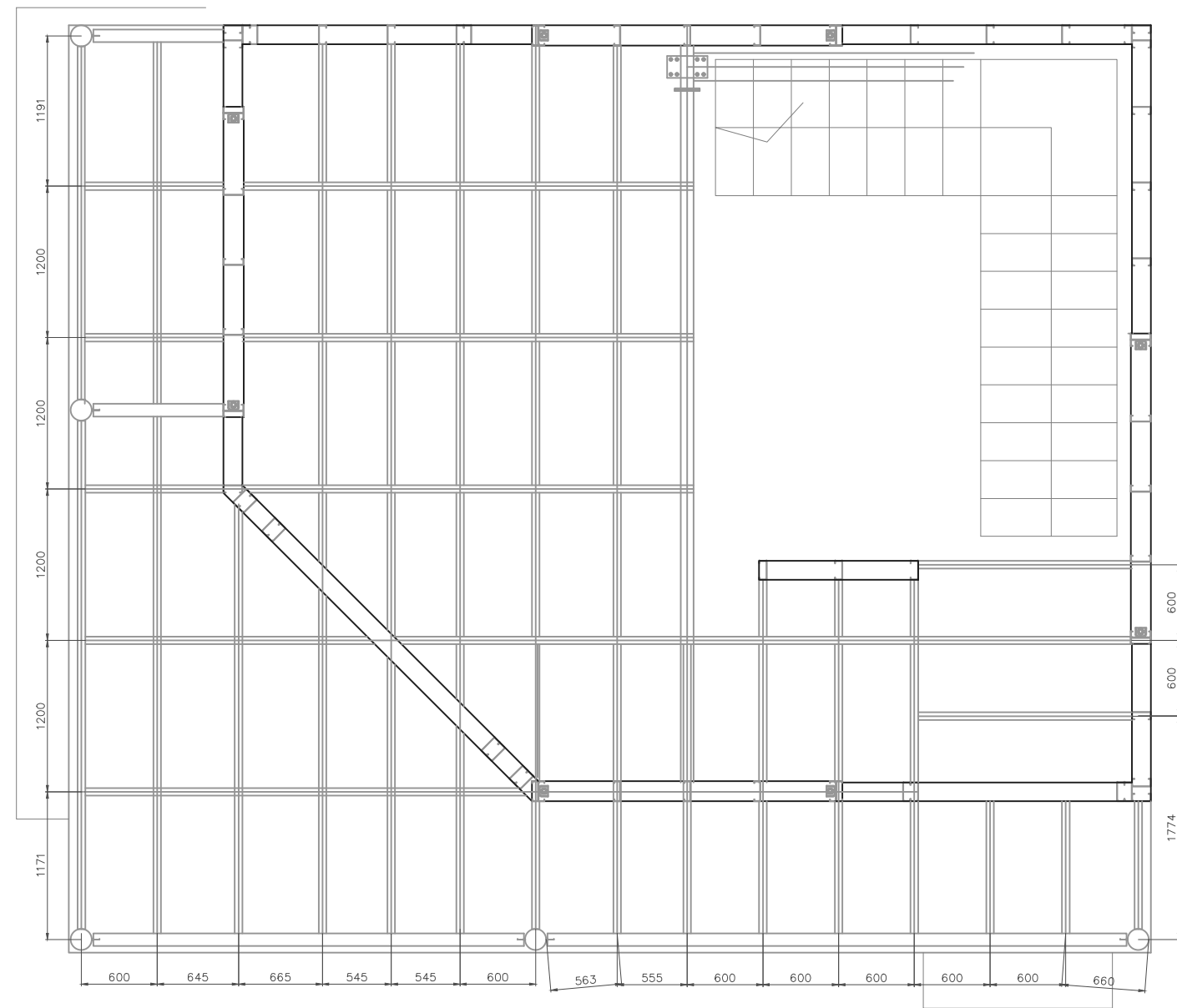
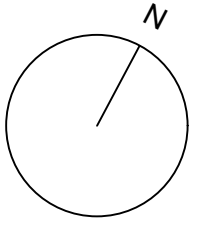
Pianta copertura

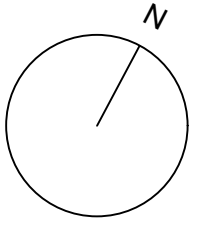


Pianta piano primo pareti perimetrali e tramezzi

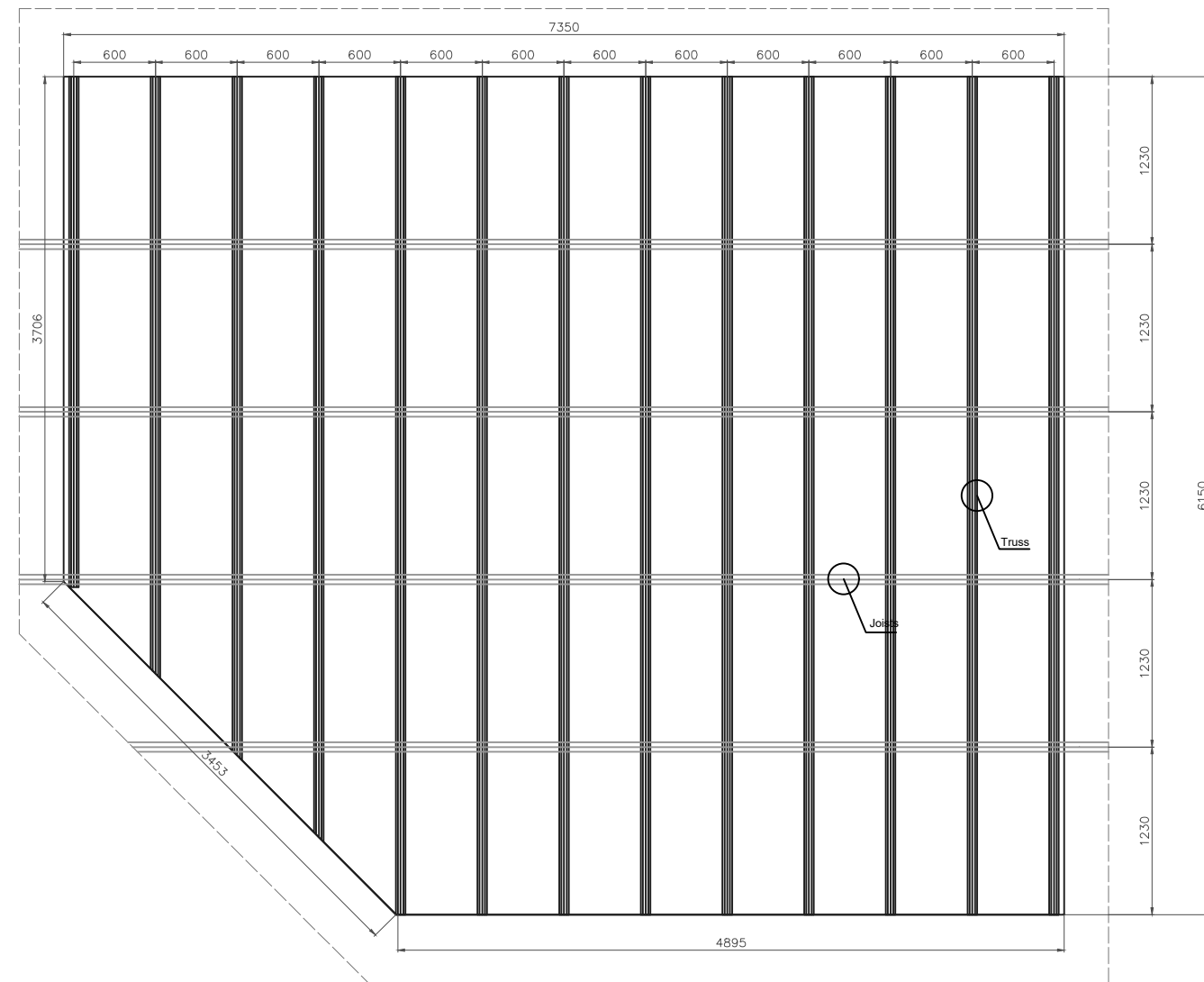


First floor plan

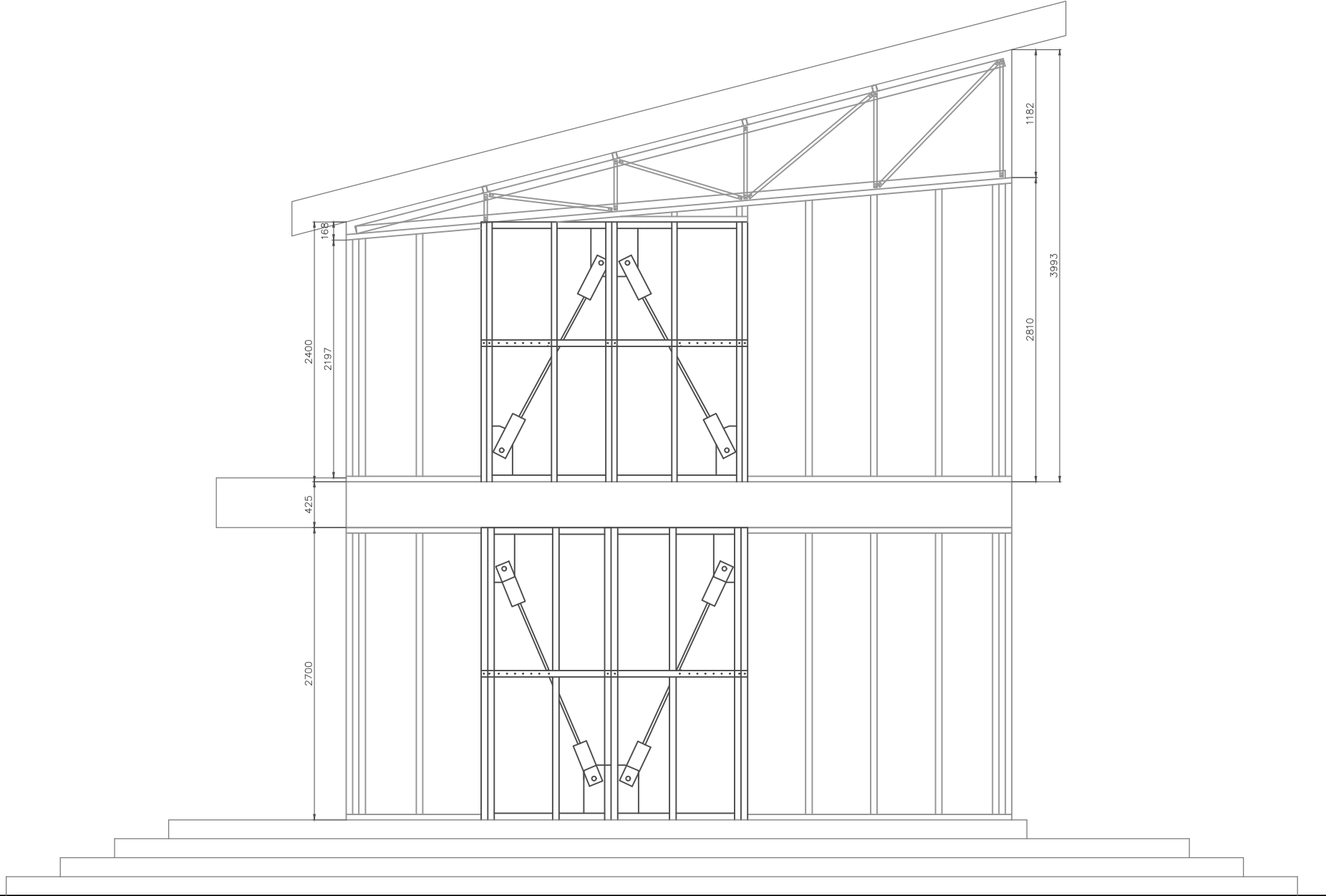
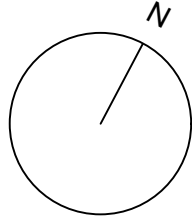




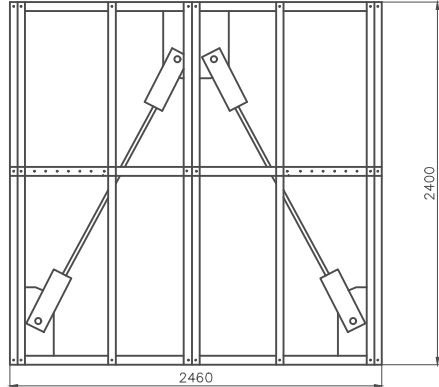
Roof plan



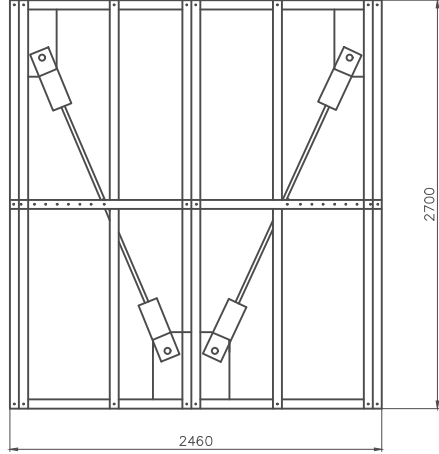
Prospetto Sud-Ovest



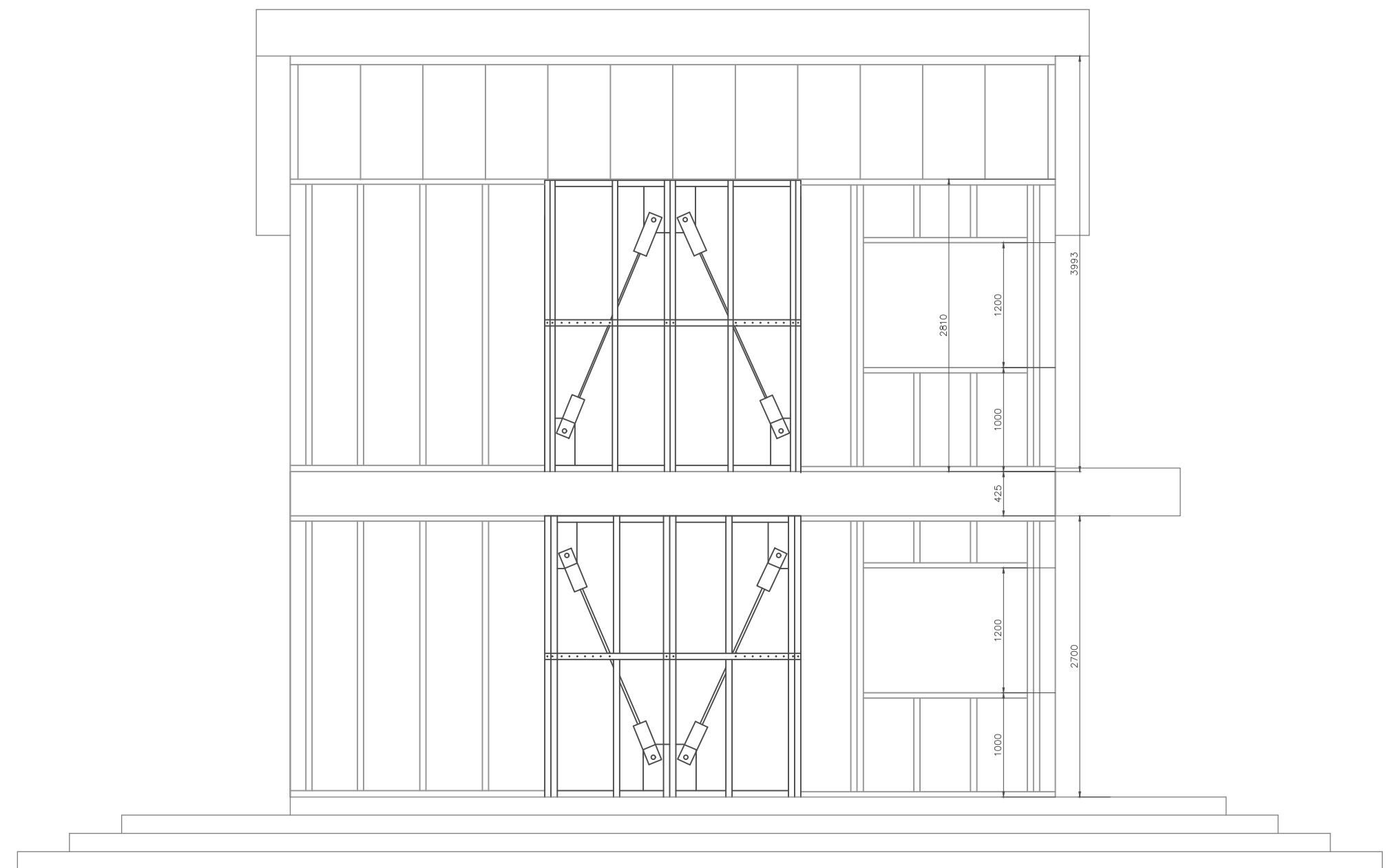
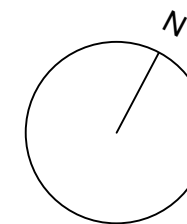
Parete Leggera



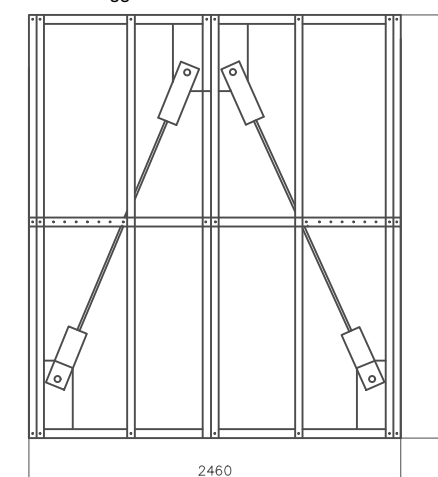
Parete Pesante



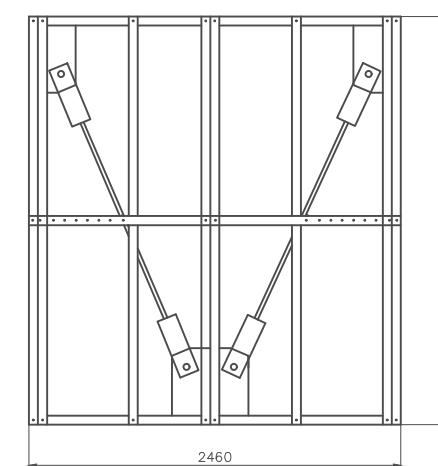
Prospetto Sud-Est



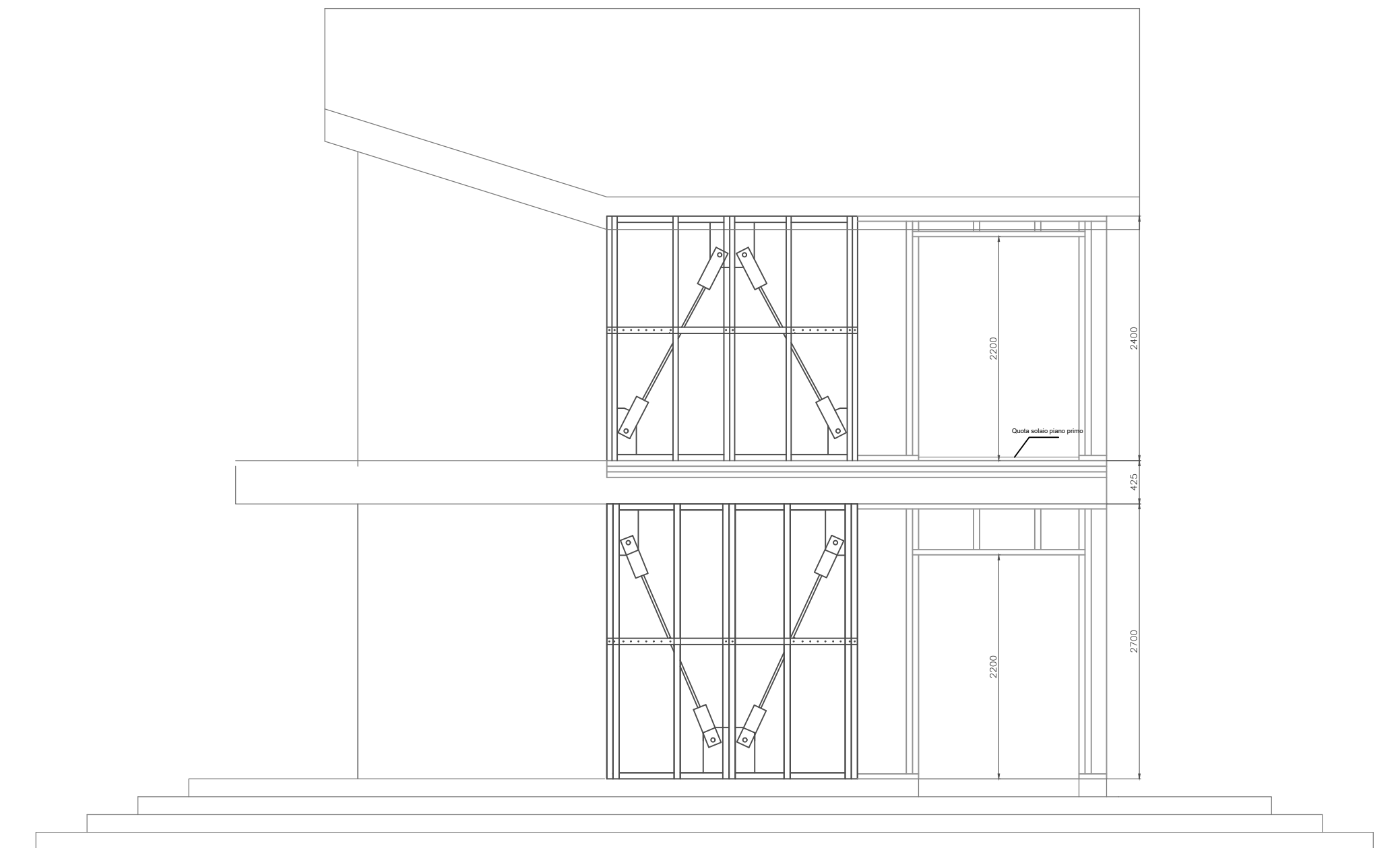
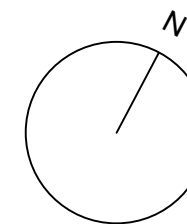
Parete Leggera



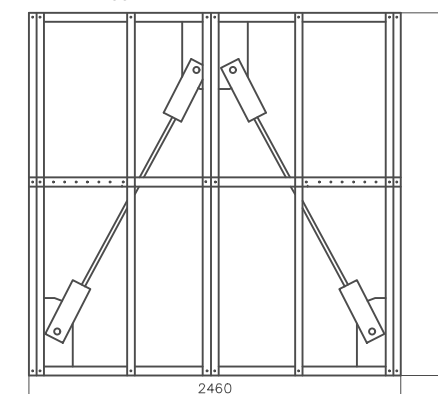
Parete Pesante



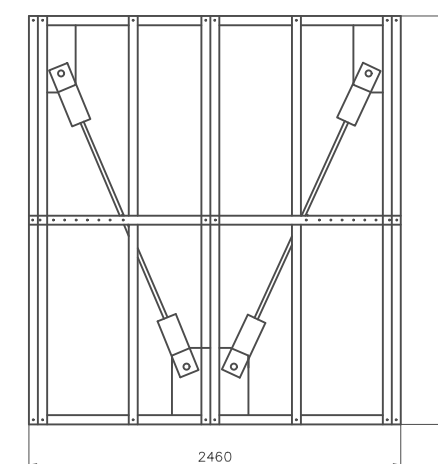
Prospetto Nord-Est



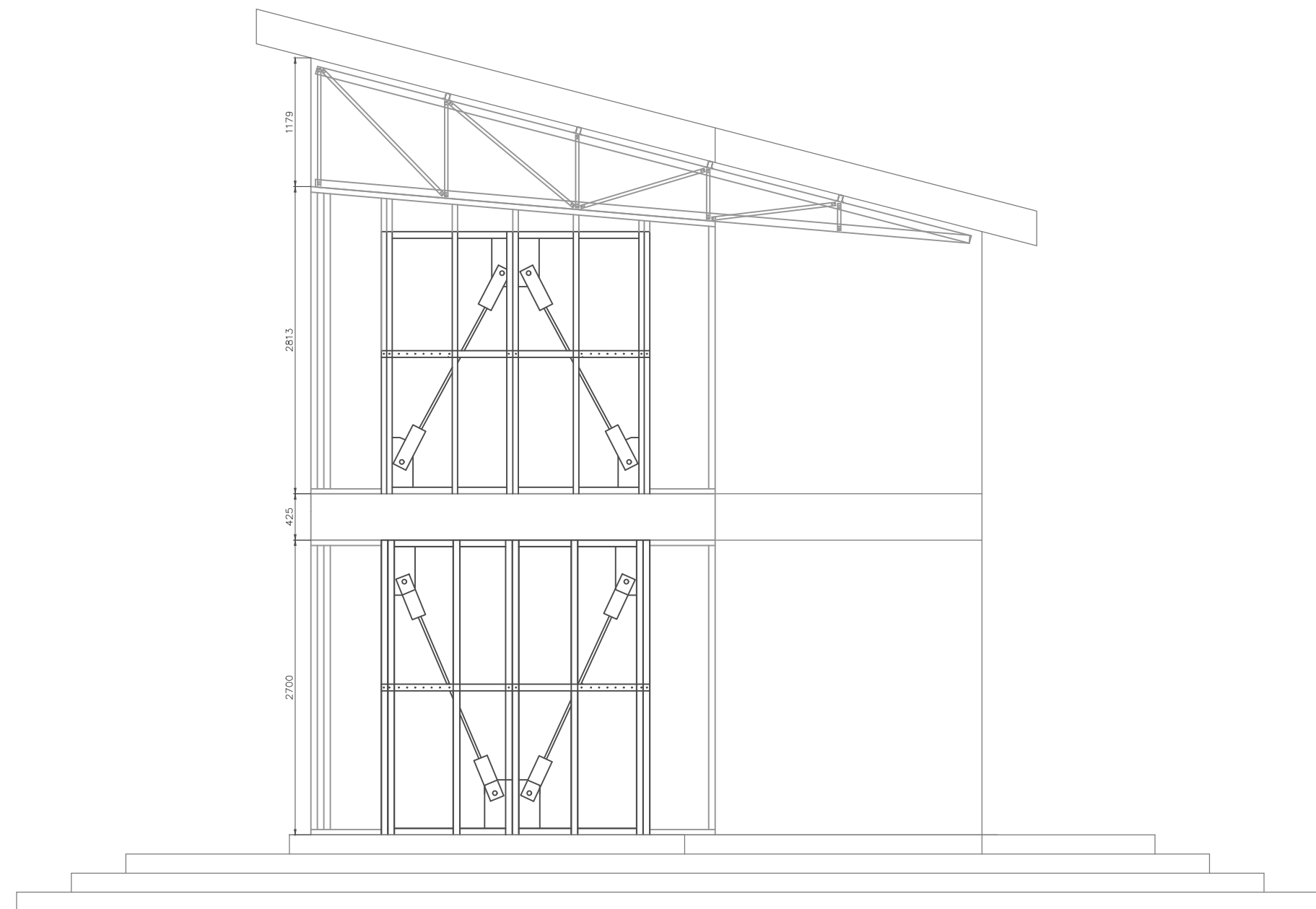
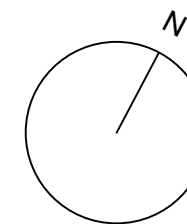
Parete Leggera



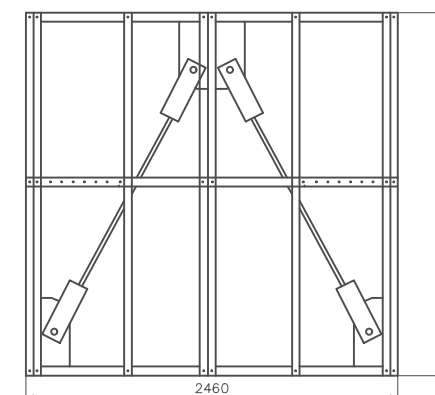
Parete Pesante



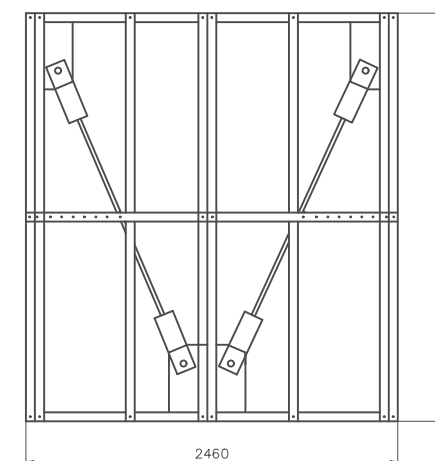
Prospetto Nord-Ovest



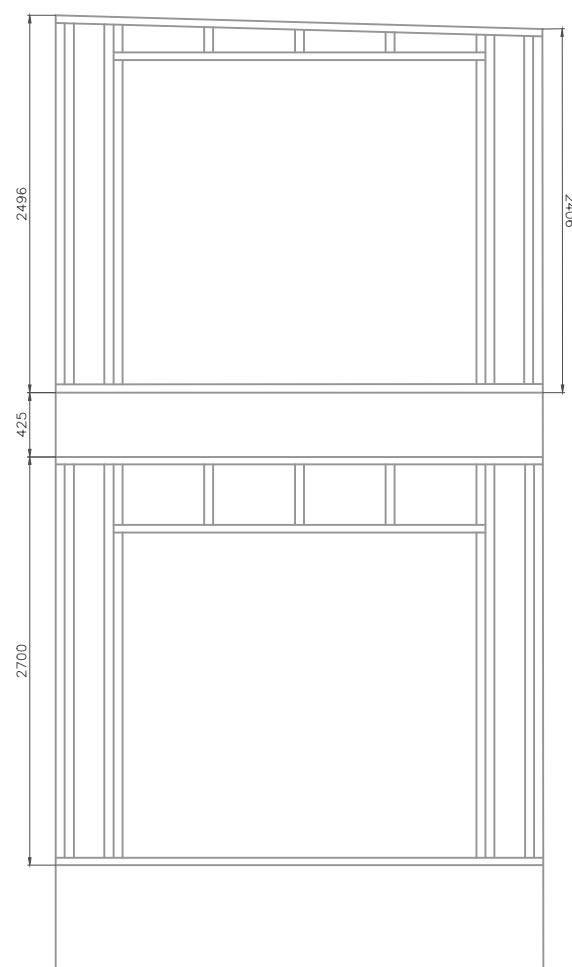
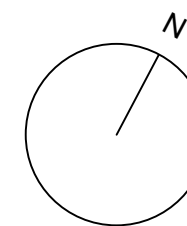
Parete Leggera



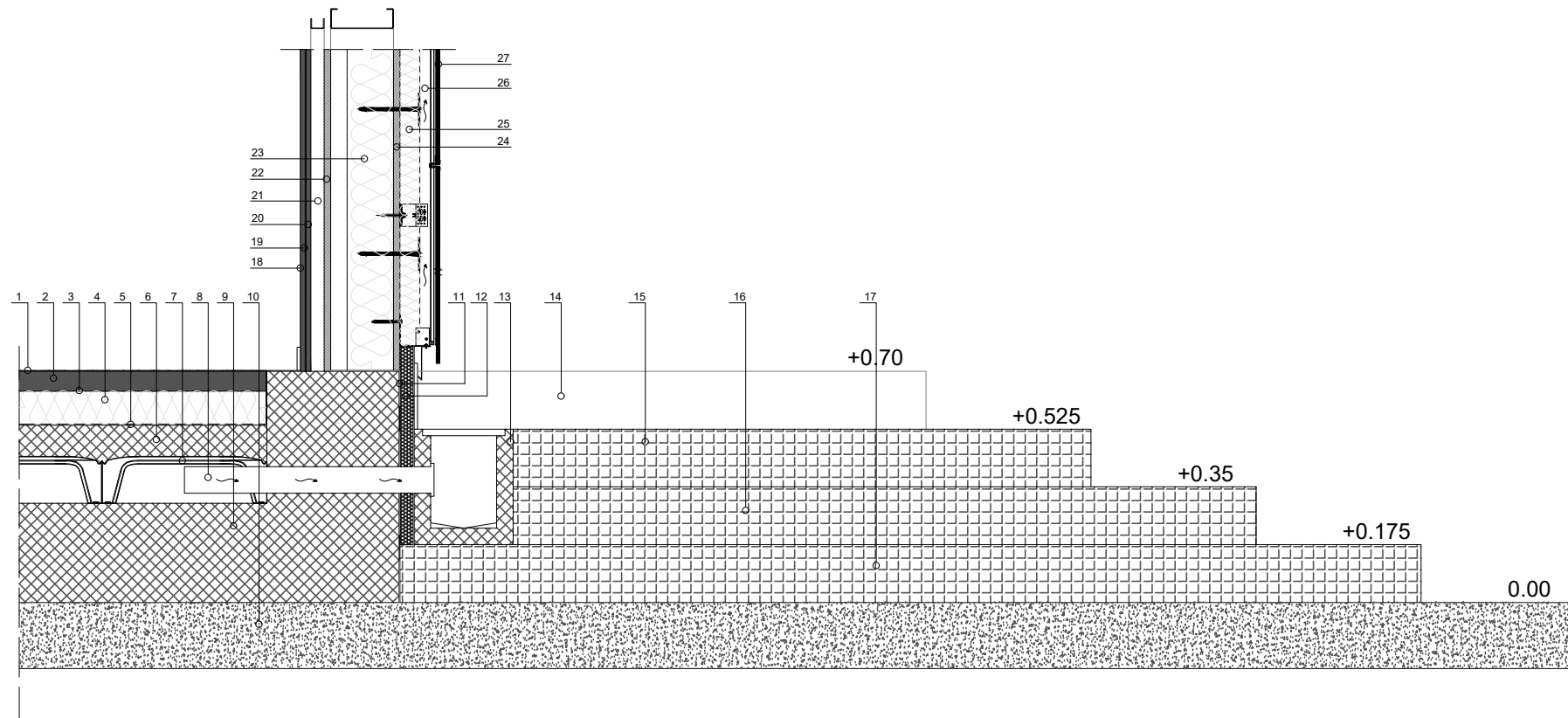
Parete Pesante



Prospetto Sud-Ovest



Dettaglio I solaio

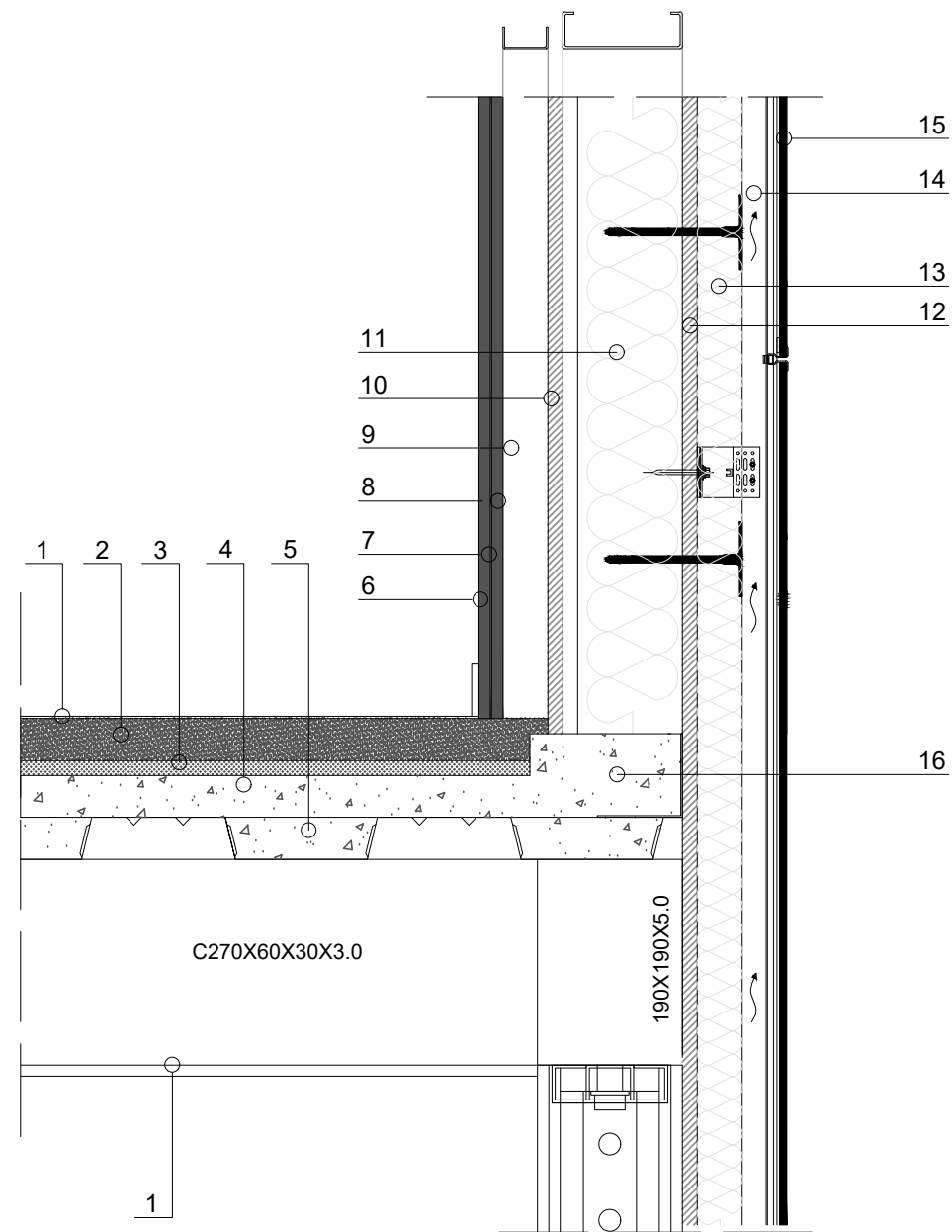


1. Gres porcellanato sp 3 mm
2. Massetto sp 60 mm
3. Foglio in polietilene
4. Durock energy sp 100
5. Membrana impermeabile
6. Caldana in cls
7. Vespaio Areato tipo iglù
8. Tubo di ventilazione
9. Fondazione a platea + cordolo armato
10. Massetto esistente
11. Guaina impermeabile
12. Pannello in XPS sp 40 mm
13. Canale di ventilazione
14. IV gradino
15. III gradino
16. II gradino
17. I gradino
18. Lastra in fibrogesso
19. Freno al vapore
20. Lastra in fibrogesso
21. Cavedio impianti
22. Pannello in OSB sp 20 mm
23. Acoustic Plus 225 sp 140 mm
24. Pannello in OSB sp 20 mm
25. Frontrock casa sp 60 mm
26. Intercapedine sp 50 mm
27. Rockpanel Natural sp 10 mm

Struttura:

Profilo C 190x60x15x4 mm (parete pesante)

Dettaglio solaio piano primo

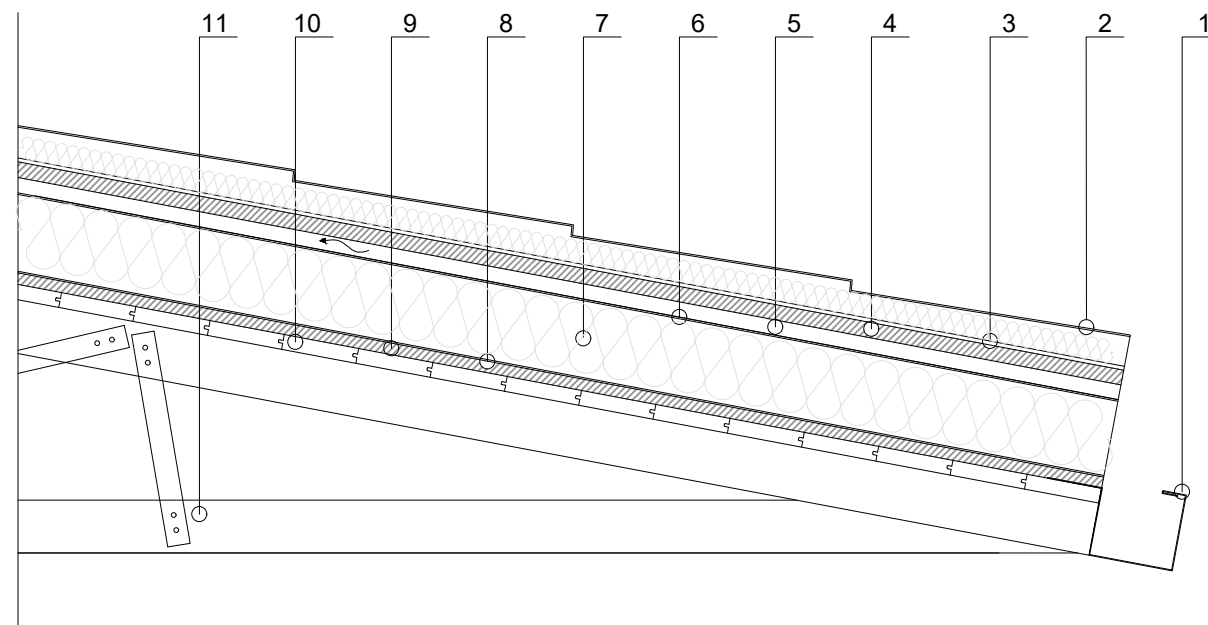


1. Gres porcellanato sp 3 mm
2. Massetto sp 55 mm
3. Pannello fonoisolante sp 20 mm
4. Getto in cls 50 mm
5. Lamira Grecata 55 mm
6. Lastra in fibrogesso
7. Freno al vapore
8. Lastra in fibrogesso
9. Cavedio impianti
10. Pannello in OSB sp 20 mm
11. Acoustic Plus 225 sp 140 mm
12. Pannello in OSB sp 20 mm
13. Frontrock casa sp 60 mm
14. Intercapedine sp 50 mm
15. Rockpanel Natural sp 10 mm
16. Cordolo h 50

Struttura:

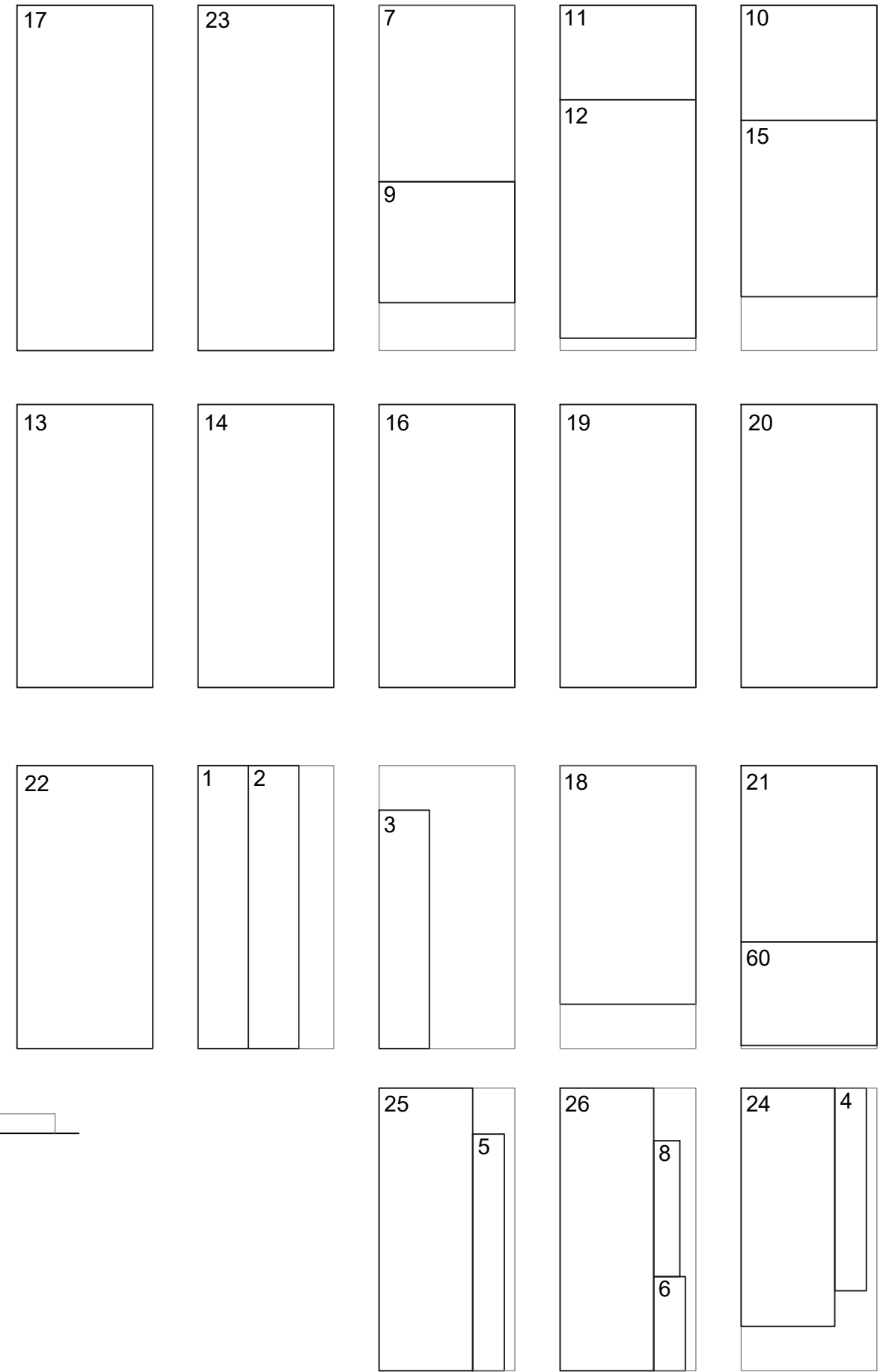
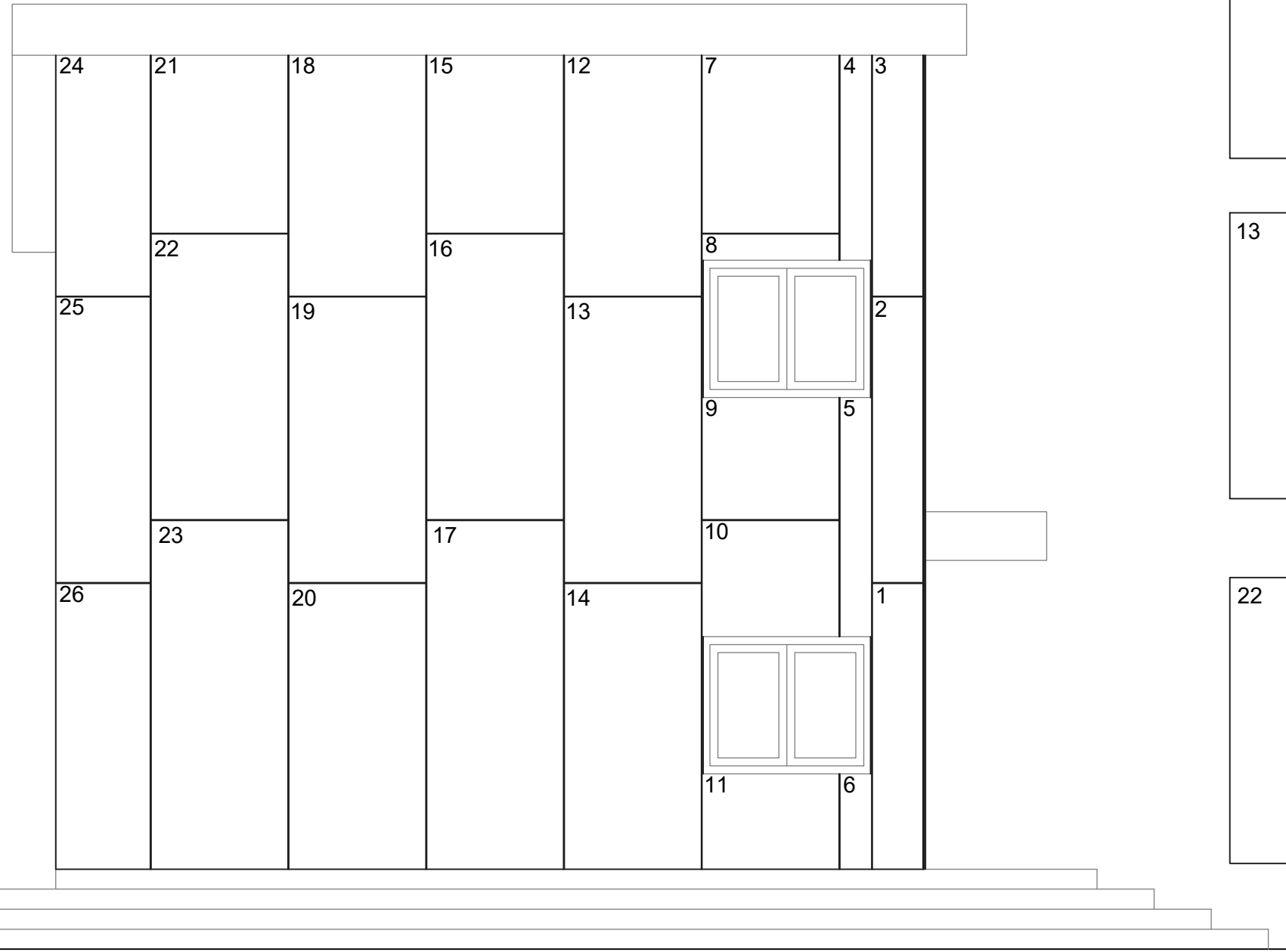
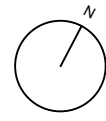
Profilo C 160x60x15x3 mm (parete pesante)

Dettaglio solaio di copertura

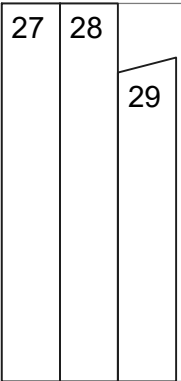
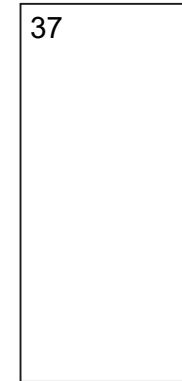
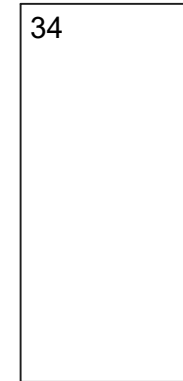
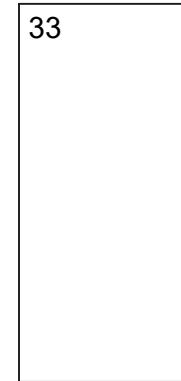
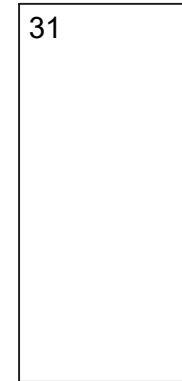
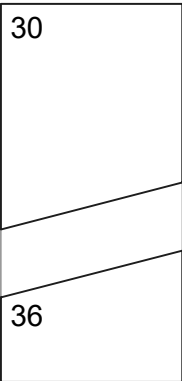
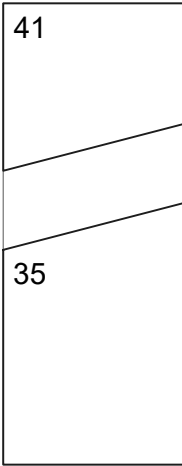
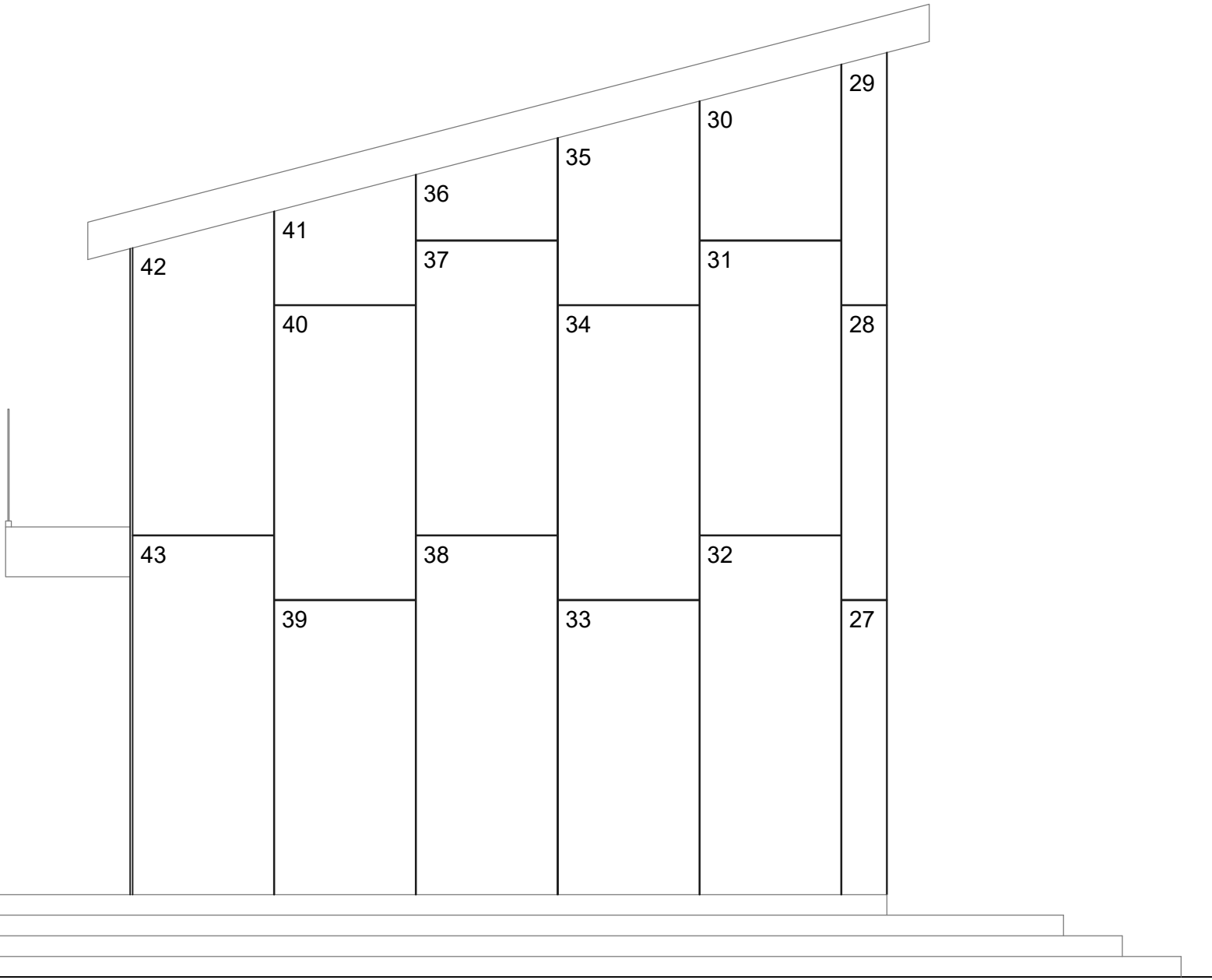
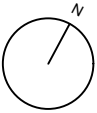


1. Grondaia
2. Pannello coibentato TT COPPO sp 40 mm
3. Membrana Bituminosa
4. Pannello in OSB sp 15 mm
5. Lamiera grecata
6. Telo impermeabile traspirante
7. Durock energy sp 100 sp 100 mm
8. Barriera al vapore
9. Pannello in OSB
10. Assito in legno di abete sp 23 mm
11. Struttura in CFS

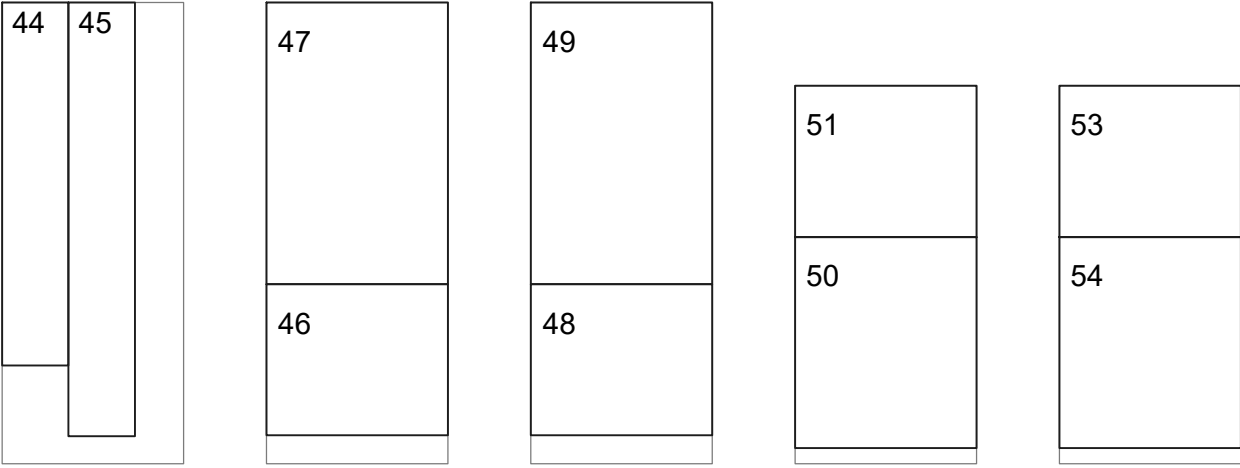
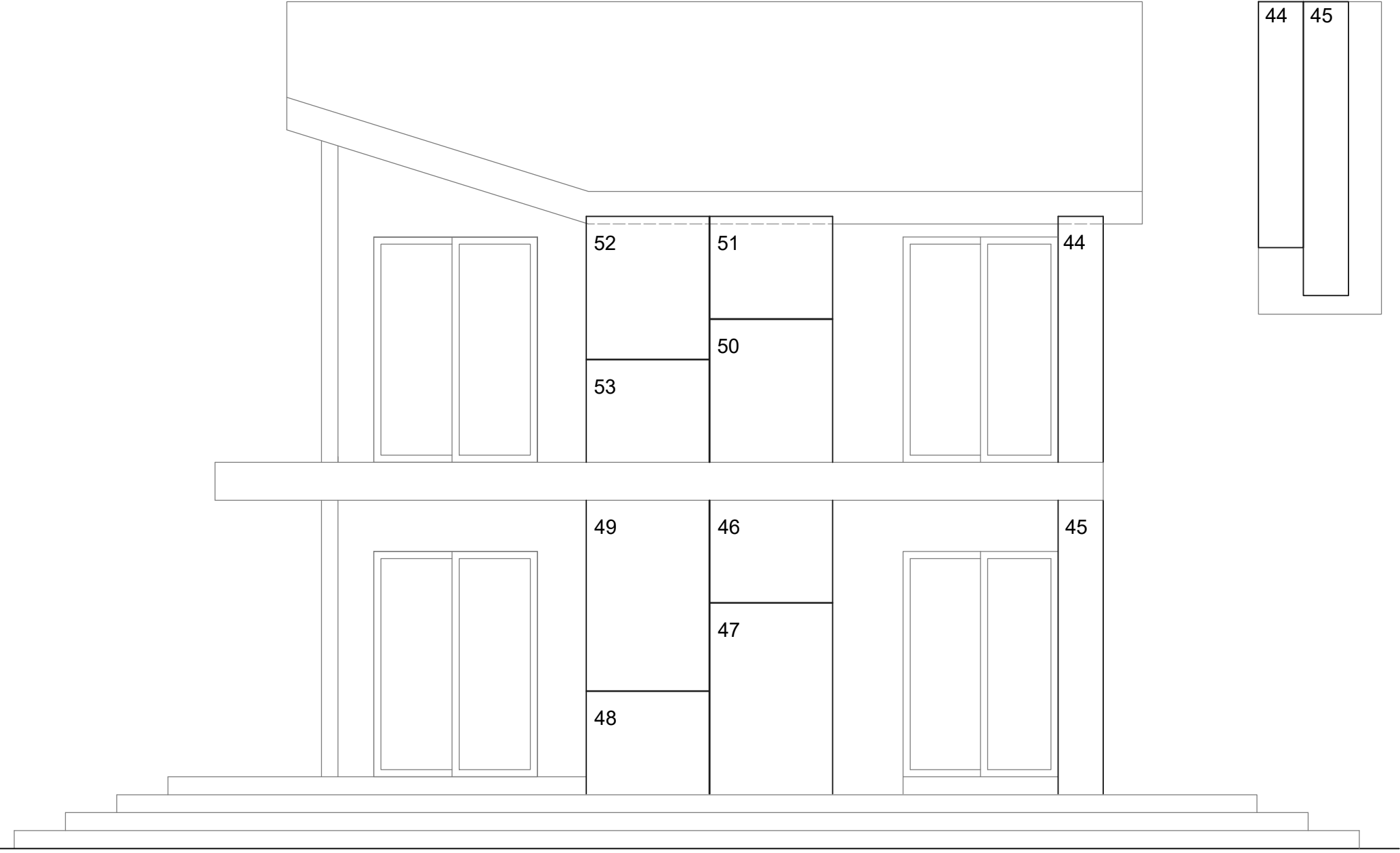
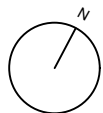
Prospetto Nord-ovest



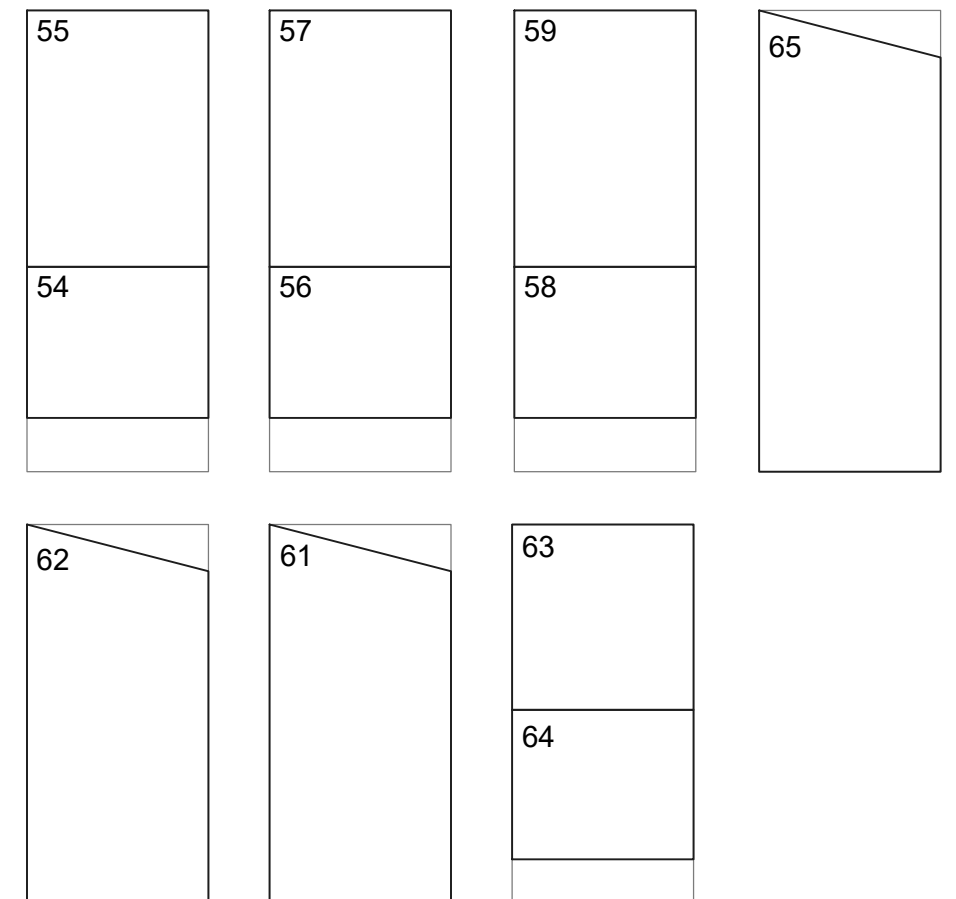
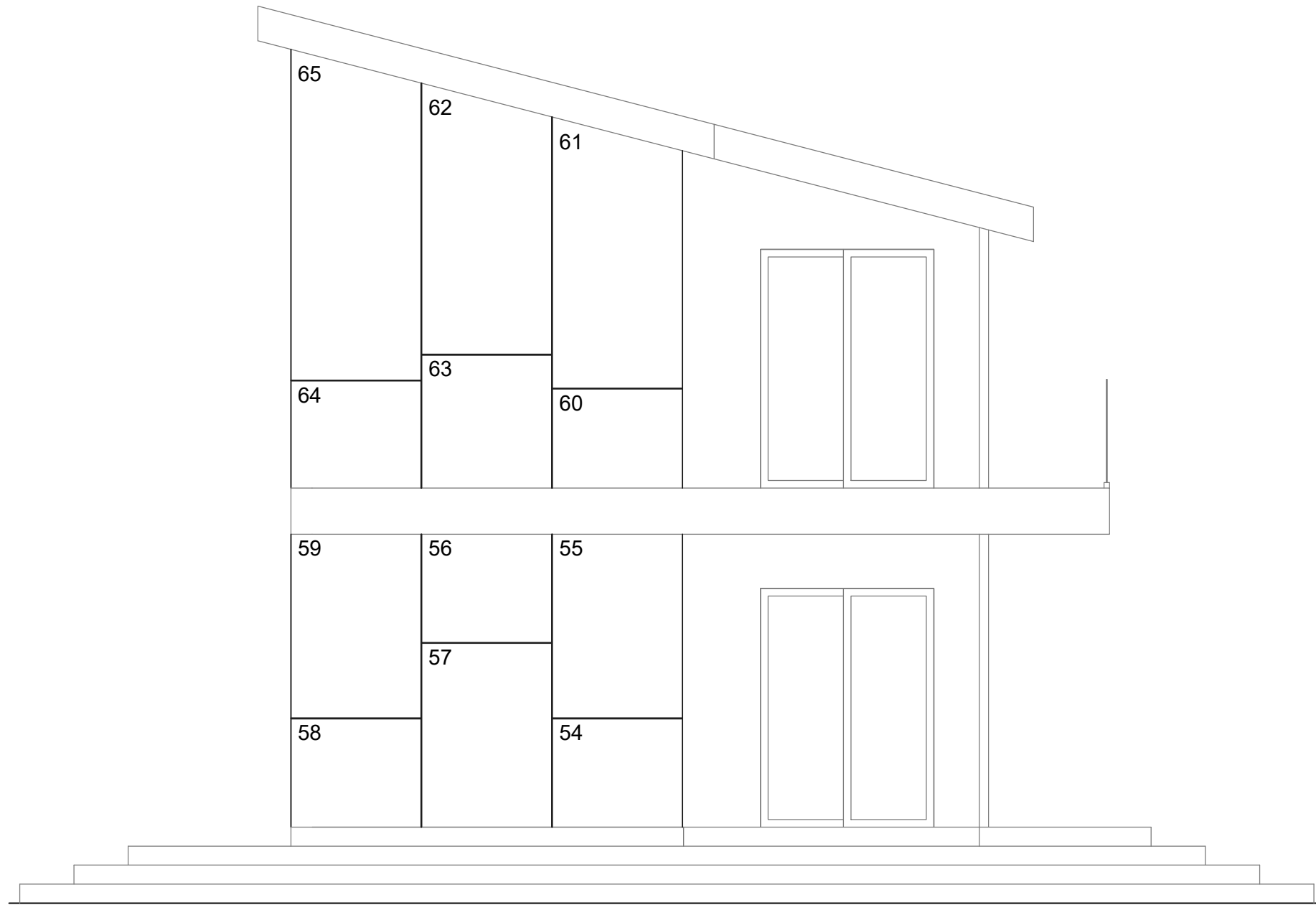
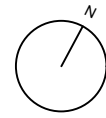
Prospetto Sud-est



Prospetto Sud-est



Prospetto Sud-Ovest



Innovative Lightweight Steel System braced with UHS Steel Bars

A.1.2 Creep tests

DATE	T1	T2
24/02/2020	0	0
02/03/2020	0	0
09/03/2020	0	0
30/04/2020	1	0
25/05/2020	2	0
03/06/2020	2	0
08/06/2020	2	0
18/06/2020	2	0
29/06/2020	2	0
06/07/2020	2	0
13/07/2020	2	0
10/08/2020	2	0
27/08/2020	2	0
31/08/2020	2	0
14/09/2020	2	0
28/09/2020	2.5	0
05/10/2020	2.5	0
12/10/2020	2.9	0
02/11/2020	3	0
09/11/2020	3	0
16/11/2020	3	0
23/11/2020	3	0
30/11/2020	3	0
07/12/2020	3	0
14/12/2020	3	0
11/01/2021	4.5	2
18/01/2021	4.5	2
08/02/2021	4.5	2

Innovative Lightweight Steel System braced with UHS Steel Bars

TEST 1

TEST 2

24/02/2020



02/03/2020



Innovative Lightweight Steel System braced with UHS Steel Bars

TEST 1

TEST 2

09/03/2020



30/04/2020



Innovative Lightweight Steel System braced with UHS Steel Bars

TEST 1

TEST 2

25/05/2020



03/06/2020



Innovative Lightweight Steel System braced with UHS Steel Bars

TEST 1

TEST 2

08/06/2020



18/06/2020



Innovative Lightweight Steel System braced with UHS Steel Bars

TEST 1

TEST 2

29/06/2020



06/07/2020



Innovative Lightweight Steel System braced with UHS Steel Bars

TEST 1

TEST 2

13/07/2020



10/08/2020



Innovative Lightweight Steel System braced with UHS Steel Bars

TEST 1

TEST 2

27/08/2020



31/08/2020



Innovative Lightweight Steel System braced with UHS Steel Bars

TEST 1

TEST 2

14/09/2020



28/09/2020



Innovative Lightweight Steel System braced with UHS Steel Bars

TEST 1

TEST 2

05/10/2020



12/10/2020



Innovative Lightweight Steel System braced with UHS Steel Bars

TEST 1

TEST 2

02/11/2020



09/11/2020



Innovative Lightweight Steel System braced with UHS Steel Bars

TEST 1

TEST 2

16/11/2020



23/11/2020



Innovative Lightweight Steel System braced with UHS Steel Bars

TEST 1

TEST 2

30/11/2020



07/12/2020



Innovative Lightweight Steel System braced with UHS Steel Bars

TEST 1

TEST 2

14/12/2020



11/01/2021



Innovative Lightweight Steel System braced with UHS Steel Bars

TEST 1

TEST 2

18/01/2021



08/02/2021

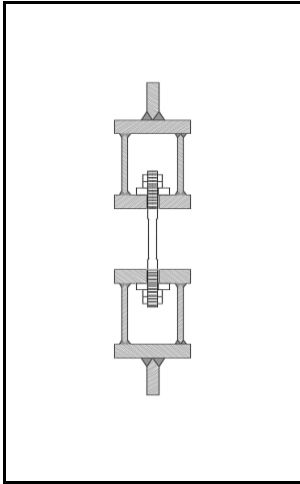


Appendix 2: Bar-nut assembly tests

Innovative Lightweight Steel System braced with UHS Steel Bars

TESTS ON BAR-NUT INTERACTION

GENERAL DATA

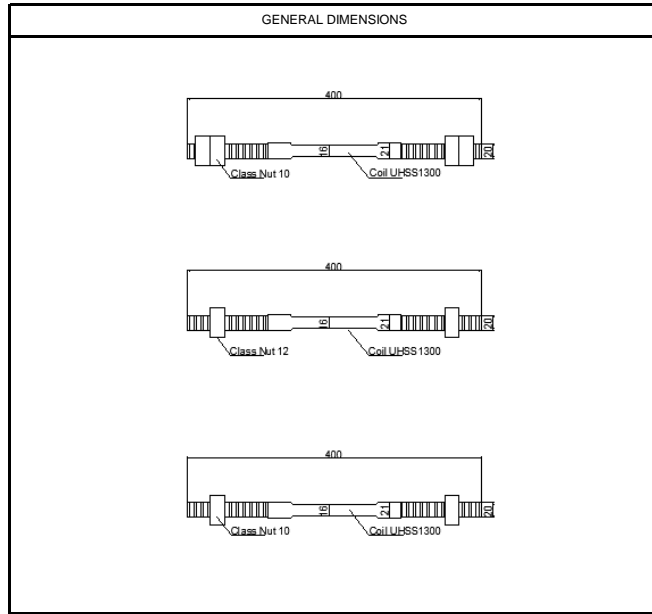


SAMPLE DATA		
BAR DATA	Length (mm)	400
	Dmin (mm)	16
	Dmax (mm)	20
NUT DATA	Material	UHSS1300
	Type 1	DADO CLASSE 10.9
	Type 2	DADO CLASSE 12.8

TESTS DATA		
PARAMETRI	Number of test	8
	Displacement rate(mm/s)	0.05
	Frequency (Hz)	5

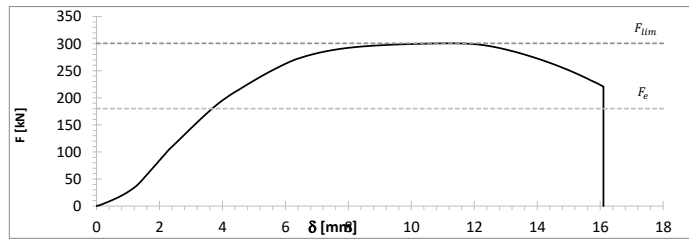


GENERAL DIMENSIONS



F_{lim} : peak load

F_e : yield stress

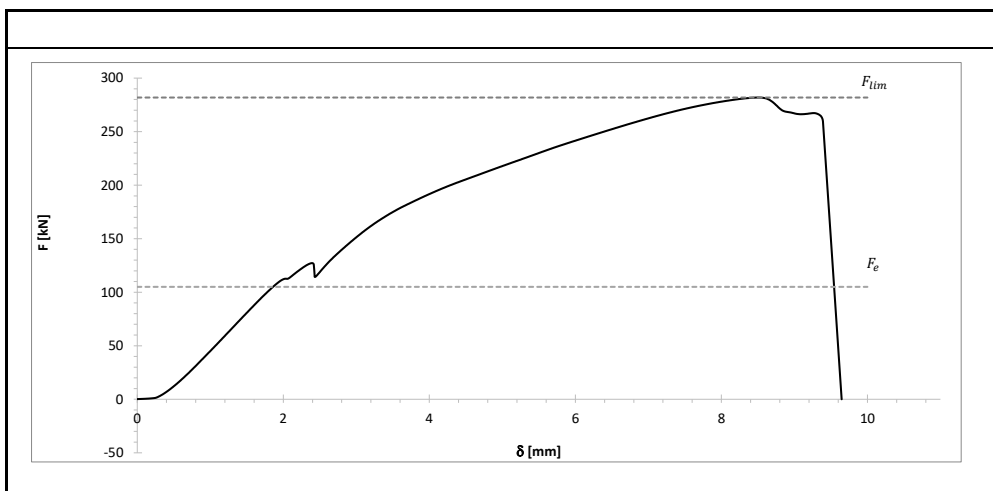


TESTS ON BAR-NUT INTERACTION

TEST RESULTS\ D1-10_01

DATE	04/12/2019
TEAM LEADER	RAFFAELE LANDOLFO
RESEARCH GROUP	LUIGI FIORINO
	ALESSIA CAMPICHE
	SARMAD SHAKELL
STUDENT	FERDINANDO NACLERIO

RESULT VALUES	Peak load (kN) F_{lim}	281,86
	Elastic load (kN) F_e	105,11
COLLAPSE MECHANISM	NUT THREAD PLASTICIZATION	



SAMPLE	BEFORE TEST	AFTER TEST
<p>Technical drawing of the sample showing dimensions: 20, 21, 16, 400, and 'Classe dado 10'. The material is labeled 'Barra UH+SS1300'.</p>	<p>Photograph of the sample in the testing machine before the test.</p>	<p>Photograph of the sample in the testing machine after the test, showing deformation.</p>

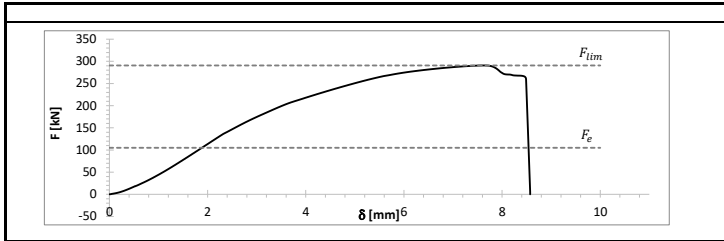
NOTE

TESTS ON BAR-NUT INTERACTION

TEST RESULTS\ D1-10_02

DATE	04/12/2019
TEAM LEADER	RAFFAELE LANDOLFO
RESEARCH GROUP	LUIGI FIORINO
	ALESSIA CAMPICHE
	SARMAD SHAKELL
STUDENT	FERDINANDO NACLERIO

RESULT VALUES	Peak load (kN) F_{lim}	290,76
	Elastic load (kN) F_e	105,22
COLLAPSE MECHANISM	NUT THREAD PLASTICIZATION	



tens.ultima	
x	y
0	290,76
10	290,7556

ten. Snerva	
x	y
0	105,00
10	105

SAMPLE	BEFORE TEST	AFTER TEST
<p>Technical drawing of a bar-nut assembly. The bar has a total length of 400 mm. The nut is 20 mm high. The bar diameter is 10 mm. The material is Coil LHSS1300. The nut is Class Nut 10.</p>		

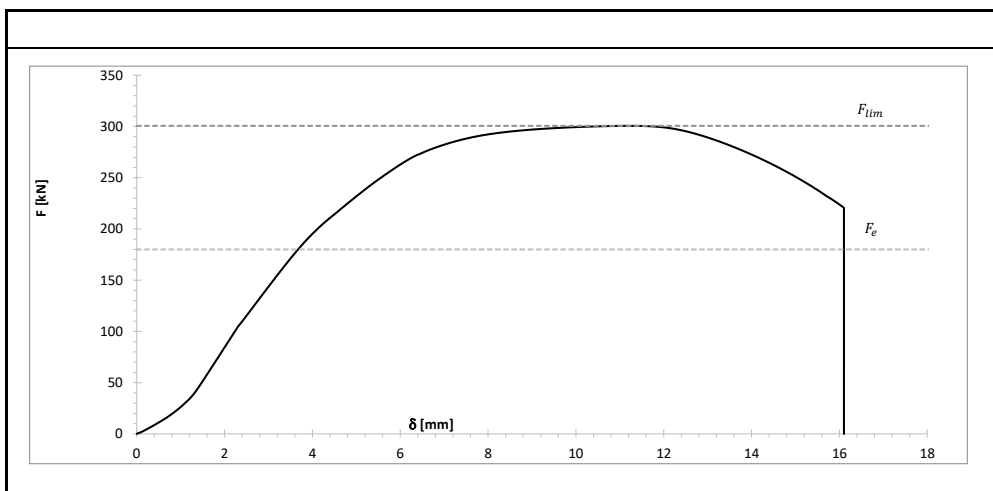
NOTE

TESTS ON BAR-NUT INTERACTION

TEST RESULTS\ D1-12_01

DATE	04/12/2019
TEAM LEADER	RAFFAELE LANDOLFO
RESEARCH GROUP	LUIGI FIORINO
	ALESSIA CAMPICHE
	SARMAD SHAKELL
STUDENT	FERDINANDO NACLERIO

RESULT VALUES	Peak load (kN) F_{lim}	300,61
	Elastic load (kN) F_e	180,00
COLLAPSE MECHANISM	TENSION FAILURE OF THE BAR	



SAMPLE	BEFORE TEST	AFTER TEST

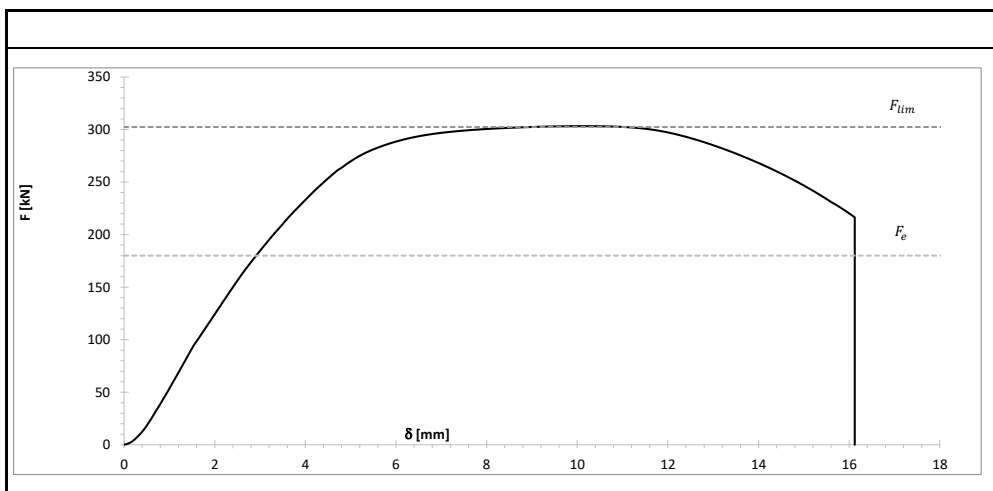
NOTE

TESTS ON BAR-NUT INTERACTION

TEST RESULTS\ D1-12_02

DATE	04/12/2019
TEAM LEADER	RAFFAELE LANDOLFO
RESEARCH GROUP	LUIGI FIORINO
	ALESSIA CAMPICHE
	SARMAD SHAKELL
STUDENT	FERDINANDO NACLERIO

RESULT VALUES	Peak load (kN) F_{lim}	302,42
	Elastic load (kN) F_e	180,00
COLLAPSE MECHANISM	TENSION FAILURE OF THE BAR	



SAMPLE	BEFORE TEST	AFTER TEST

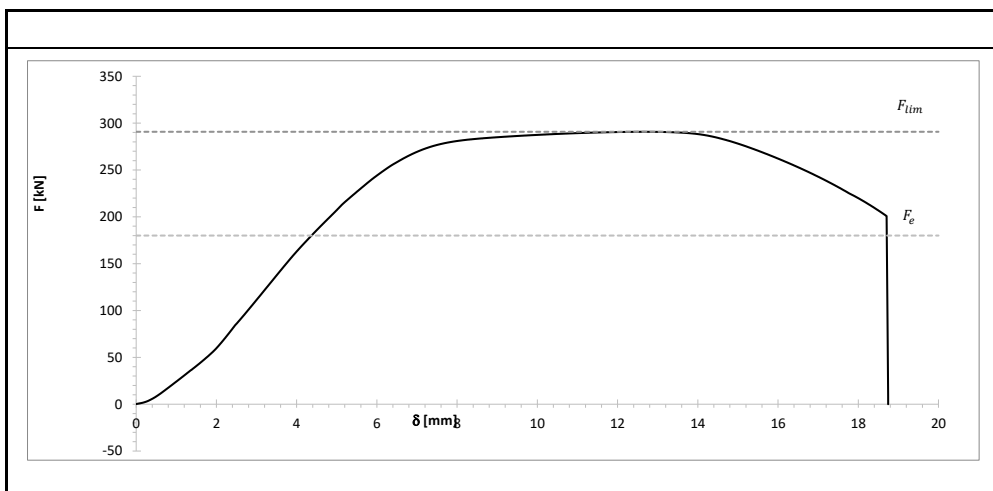
NOTE

TESTS ON BAR-NUT INTERACTION

TEST RESULTS\ D1-12_02

DATE	04/12/2019
TEAM LEADER	RAFFAELE LANDOLFO
RESEARCH GROUP	LUIGI FIORINO
	ALESSIA CAMPICHE
	SARMAD SHAKELL
STUDENT	FERDINANDO NACLERIO

RESULT VALUES	Peak load (kN) F_{lim}	290,77
	Elastic load (kN) F_e	180,00
COLLAPSE MECHANISM	TENSION FAILURE OF THE BAR	



SAMPLE	BEFORE TEST	AFTER TEST
<p>Technical drawing of the sample. It shows a vertical bar with a total length of 400 mm. The top section has a diameter of 20 mm, the middle section has a diameter of 21 mm, and the bottom section has a diameter of 16 mm. The material is specified as Barra LHSS1300 and the thread specification is Classe dado 12.</p>	<p>Photograph of the sample in the testing machine before the test. The sample is vertically oriented and held between two grips of the machine.</p>	<p>Photograph of the sample in the testing machine after the test. The sample has failed, with the lower section broken and the upper section remaining in the grips.</p>

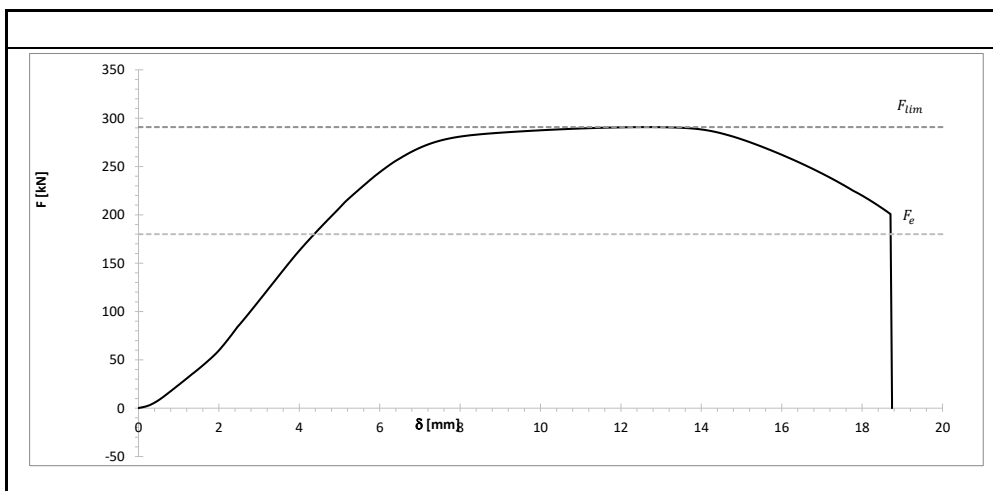
NOTE

TESTS ON BAR-NUT INTERACTION

TEST RESULTS\ D2-10_01

DATE	04/12/2019
TEAM LEADER	RAFFAELE LANDOLFO
RESEARCH GROUP	LUIGI FIORINO
	ALESSIA CAMPICHE
	SARMAD SHAKELL
STUDENT	FERDINANDO NACLERIO

RESULT VALUES	Peak load (kN) F_{lim}	302,42
	Elastic load (kN) F_e	170,50
COLLAPSE MECHANISM	TENSION FAILURE OF THE BAR	



SAMPLE	BEFORE TEST	AFTER TEST

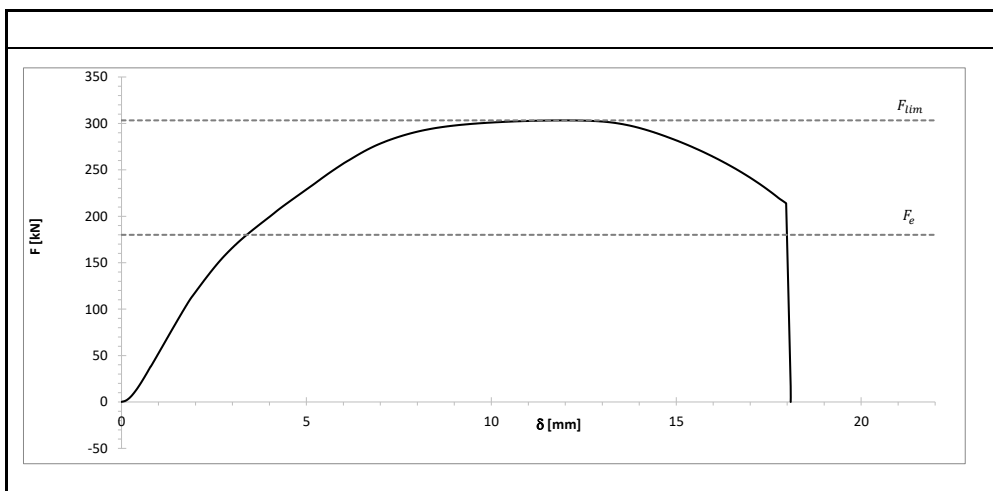
NOTE

TESTS ON BAR-NUT INTERACTION

TEST RESULTS\ D2-10_02

DATE	04/12/2019
TEAM LEADER	RAFFAELE LANDOLFO
RESEARCH GROUP	LUIGI FIORINO
	ALESSIA CAMPICHE
	SARMAD SHAKELL
STUDENT	FERDINANDO NACLERIO

RESULT VALUES	Peak load (kN) F_{lim}	303,30
	Elastic load (kN) F_e	180,25
COLLAPSE MECHANISM	TENSION FAILURE OF THE BAR	



SAMPLE	BEFORE TEST	AFTER TEST
<p>Technical drawing of the sample. It shows a vertical bar with a total length of 400 mm. The top section has a diameter of 20 mm, the middle section has a diameter of 21 mm, and the bottom section has a diameter of 16 mm. The material is specified as Barra UHSS1300 and the thread is Classe dado 10.</p>	<p>Photograph of the sample in the testing machine before the test. The sample is labeled D2_10_2.</p>	<p>Photograph of the sample in the testing machine after the test. The bar has failed, and the remaining part is labeled D2_10_2.</p>

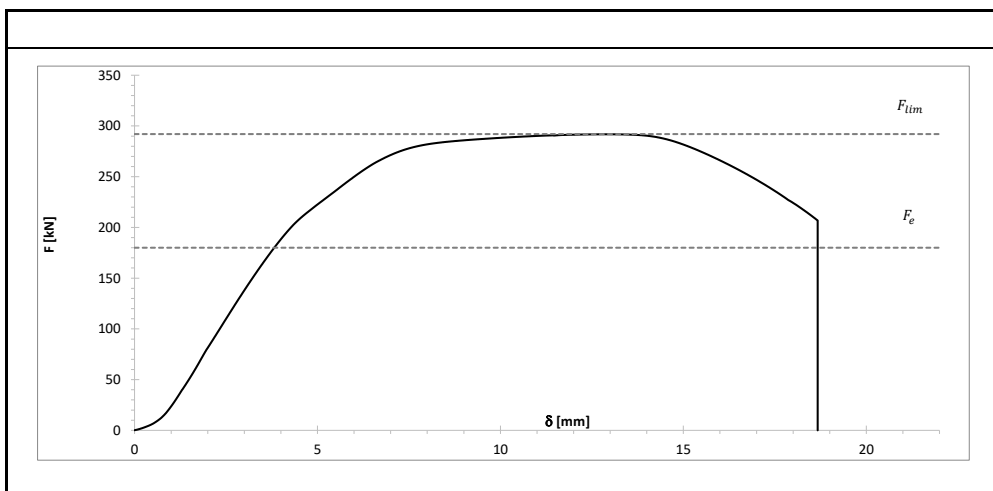
NOTE

TESTS ON BAR-NUT INTERACTION

TEST RESULTS\ D2-10_03

DATE	04/12/2019
TEAM LEADER	RAFFAELE LANDOLFO
RESEARCH GROUP	LUIGI FIORINO
	ALESSIA CAMPICHE
	SARMAD SHAKELL
STUDENT	FERDINANDO NACLERIO

RESULT VALUES	Peak load (kN) F_{lim}	292,00
	Elastic load (kN) F_e	180,25
COLLAPSE MECHANISM	TENSION FAILURE OF THE BAR	



SAMPLE	BEFORE TEST	AFTER TEST
<p>Technical drawing of the sample showing dimensions and labels: 20, 21, Barra UH-HS1300, 16, Classe dado 10, 40,0.</p>	<p>Photograph of the sample in the testing machine before the test.</p>	<p>Photograph of the sample in the testing machine after the test, showing failure.</p>

NOTE